



Determining and predicting the seakeeping performance of ships based on jerk in the ship motions

Master thesis

J.M. Werkman

Determining and predicting the seakeeping performance of ships based on jerk in the ship motions

Master thesis

by

J.M. Werkman

In partial fulfilment of the requirements for the degree of

Master of Science
in Marine Technology

at the Delft University of Technology,
to be defended publicly on Wednesday 31 July 2019 at 13:00.

Project duration: October 2018 – July 2019

Thesis committee:	Prof. dr. ir. J. Westerweel	Delft University of Technology (chairman)
	Dr.-Ing. S. Schreier	Delft University of Technology (supervisor)
	Dr. ir. K. Visser	Delft University of Technology
	Dr. A.J. Böttger	Delft University of Technology
	Dr.-Ing. S. Sigmund	Damen Shipyards Gorinchem (supervisor)

A digital version of this thesis is available at <https://repository.tudelft.nl/>

Abstract

The comfort assessment of ships is based on several criteria. There are for example criteria for motions, noise and vibrations. The criteria for motions are nowadays often defined as comfort limits on the accelerations in the ship motions. However, from other industries it followed that the rate of change of the accelerations, the jerk, can also have an influence on the sense of comfort of passengers and crew. The goal of this thesis is to investigate whether it would be useful to add jerk criteria to the comfort assessment of ships. Jerk cannot be measured directly (yet), so it has to be obtained from acceleration measurements or calculations. For this goal filter and processing procedures are defined. To be able to make comparisons different ways of quantifying the jerk are established. One is aimed at peak values, since these are often determining the limit for comfort and operability. The other is focused on quantifying the non-linearity of the response. Research is performed on what the physics behind jerk are, and what phenomena are likely to cause large jerk values. The prime cause is found in slamming. The jerk following from slamming is influenced mostly by the shape of the bow and the speed of immersion in the water. Using the measurement data of two different hulls from other research the effect of varying conditions on the jerk is investigated. From this research it follows that there can be a difference in seakeeping behaviour when looking at jerk instead of accelerations. Since jerk is the third derivative of displacement to time, the non-linearity in this response is relatively high. Therefore non-linear codes are required to calculate the jerk response correctly. The use of a Reynolds Averaged Navier Stokes (RANS) code proves to be able to predict the jerk behaviour correctly. In this thesis only model test measurements and calculations are used. The scaling of jerk to full scale, and difficulties that it might impose, are only discussed theoretically. The general conclusion is that jerk is worth investigating to compare the seakeeping behaviour of ships. Until quantitative limits are available only qualitative comparisons are possible, but these can already give additional insight.

Preface

After many years of studying in Delft I reached the final piece of my student career: my master thesis. In the year 2010 I started with the bachelor Civil Engineering in Delft. During my bachelor my father and I visited the container ship CMA CGM Marco Polo, at the time the largest container ship in the world. At that moment I realised that my passion laid more in the maritime industry. Therefore I made the switch to the master Marine Technology after my bachelor graduation. To conclude this master I chose to graduate in ship hydromechanics, one of my interest fields within marine technology. Damen Shipyards offered me the possibility to investigate the jerk in ship motions, within the hydromechanics team of their R&D department.

I would like to thank anyone who helped me getting from there to the point where I am now, finishing my final report. Sebastian Sigmund, my daily supervisor at Damen. He helped me with his knowledge and pushed me to think in different directions, of which I had not thought of myself. Sebastian Schreier, my supervisor from the TU Delft. With his questions he was always pushing me to think better about what I was doing and why. Jochem de Jong from Damen, especially in the beginning helping to steer the project in the right direction. Furthermore this thesis would not have been possible without the measurement data from earlier projects. I would like to express my gratitude to Pepijn de Jong, the TU Delft and Damen for providing me with this data. Also I would like to thank Sebastian Sigmund again for his RANS CFD simulation data he allowed me to use in my project. Graduating is not possible without a graduation committee, so I would like to thank Jerry Westerweel, Klaas Visser and Amarante Böttger for making time for me, even though it is the middle of the summer.

The next word of thanks is for my friends. The friends I made in high school, the friends I made in Delft and the friends I made at Broach. They are all nice company and provided the welcome distraction from studying all these years. From the J22 campaign I sailed with Maarten and Daan, to making trips to München and Trondheim. But also smaller things, like eating together and drinking beers or watching a Formula 1 race. But also just the small talks over a coffee at the university. Or in case of the days working on this report in Delft, a somewhat longer coffee talk with Joost. Thank you all.

Family is everything, you grow up with them and they make you in the person you become. From my personal view, although slightly biased, I can say they did a pretty decent job. Therefore I would like to thank my grandparents, my parents Harry and Angelique, my sisters Idske and Karlijn and everyone else. A special word of thanks is reserved for my parents, who made it possible for me to go to the university. No matter the amount of years I kept on going, they always believed in me and supported me.

Finally I want to thank my girlfriend Michelle. You were there when I came home, tired after a long day. You were there when I felt I was stuck and did not make much progress. You were there to celebrate important milestones with me. You are always there for me with your love. I cannot express in words how good that makes me feel.

*Joren Werkman
Delft, July 2019*

Contents

Abstract	v
Preface	vii
1 Introduction	1
1.1 Problem description	1
1.2 Objectives	2
1.3 Research questions	2
1.4 Approach	2
2 Ship motion response	5
2.1 Definitions	6
2.2 Linear approach	7
2.2.1 Assumptions	7
2.2.2 Equations of motion	8
2.2.3 Regular waves	8
2.2.4 Irregular waves	9
2.2.5 Applicability	10
2.3 Non-linear behaviour	10
2.3.1 Large amplitude waves	11
2.3.2 Non-linear waves	12
2.3.3 High forward speed	12
2.3.4 Slamming	12
2.3.5 Viscous forces	13
2.4 Assessing methods	13
2.5 Jerk	15
2.5.1 Physical interpretation	15
2.5.2 Von Karman slamming	15
3 Determining jerk	17
3.1 Filtering	17
3.2 Savitzky-Golay method	20
3.3 Energy spectrum differentiation	21
3.4 Requirements on measurements	22
4 Quantifying ship response	23
4.1 Quantifying response in regular waves	23
4.1.1 Peak values	23
4.1.2 Non-linearity ratio	25
4.1.3 'Ideal' response	26
4.2 Quantifying response in irregular waves	26
4.2.1 Significant value	26
4.2.2 Probability of exceedance	27
4.2.3 Rayleigh plots	28
4.2.4 Non-linearity	29
4.3 Overview of definitions	30
4.4 Uncertainty	31
4.4.1 Uncertainty individual peaks	31
4.4.2 Spread of peak measurements	32

5	Fast models in regular head waves	35
5.1	Introduction	35
5.2	Comparison	37
5.2.1	Hull types	37
5.2.2	Wave steepness	43
5.2.3	Forward speed	43
5.3	Analysis over ship length	46
5.3.1	Decomposition heave and pitch	46
5.3.2	Different cases	48
6	Fast models in irregular head waves	55
6.1	Introduction	55
6.2	Comparison	55
6.2.1	Hull types	56
6.2.2	Significant wave height	59
6.2.3	Forward speed	59
6.3	Analysis over ship length	62
6.3.1	Decomposition heave and pitch	62
6.3.2	Different cases	62
6.4	Non-linearity	65
6.5	Prediction of response	67
6.5.1	Numerical methods	67
6.5.2	Behaviour in regular waves	68
7	Numerical computation of ship motions	69
7.1	Non-linearity of numerical methods	69
7.2	Regular waves tests - RANS CFD	71
7.2.1	Peak values	71
7.2.2	Non-linearity	73
7.2.3	Time traces	73
7.2.4	Analysis of wave encounter	75
7.3	Summary	78
8	Upscaling	81
8.1	Theory of scaling	81
8.1.1	Similarities	81
8.1.2	Froude scaling	81
8.1.3	Scaling of jerk	82
8.1.4	Overview of scaling factors	83
8.2	Difficulties	83
8.2.1	Different scaling parameters	83
8.2.2	Scaling of slamming	84
9	Conclusions and recommendations	85
9.1	Conclusions	85
9.2	Recommendations	88
	Bibliography	89
	Appendices	
A	Link between sine fit & non-linearity ratio	95
B	Filter comparison	101
C	Time traces regular waves	127

Introduction

To start this research first the problem description will be given in section 1.1. The research objectives for this problem are defined in section 1.2. To reach this objectives several research questions have been established in section 1.3. The approach to answer this questions is given in section 1.4.

1.1 Problem description

Damen, a Dutch family-owned shipyard, is always looking to improve the comfort of their ships. Comfort is currently being assessed using for example criteria for motions, noise, vibrations and exhaust gasses. The comfort criteria for ship motions are now mostly based on accelerations. There are however more aspects to consider. From research in the aerospace industry [17, 20], the public transport industry [6, 10, 33, 44] and the elevator industry [23] it follows that the rate of change of acceleration of a motion, the jerk, might have an influence on the motion perception and thus the sense of (dis)comfort of passengers.

According to the Oxford Dictionaries, jerk is "a quick, sharp, sudden movement" [42]. Jerk is however also the name of the derivative of acceleration. Although both these phenomena are definitely connected, they are not physically the same. In this thesis the term jerk will be used for the derivative of the acceleration.

Jerk is thus the derivative of acceleration, the third derivative of position with respect to time. This means that every ship in seaway experiences jerk in its six degrees of freedom: surge, sway, heave, roll, pitch and yaw. For example if a ship is sailing in relatively calm regular waves, the heave acceleration will be harmonic, and thus the heave jerk will be as well. The jerk is thus always there, but this kind of jerk is not likely to cause discomfort. However, when the ship slams into a wave there are probably large peak values in the jerk which can cause discomfort. Contrary to other industries jerk has not yet been investigated in the motions of ships. To improve comfort, a design criterion based on the jerk could be implemented in the future. For this a measure of the 'severeness' of jerk is required.

The prediction of jerks in ship motions is however more difficult than the definition would suggest. In ship motion calculations jerk has up until now not been considered, so it is not clear how well the available tools predict this motion characteristic. For ship motion calculations different computational fluid dynamics (CFD) tools are available. There are tools based on the potential theory: 2D strip theory and 3D panel methods. There are also tools based on the Reynolds Averaged Navier-Stokes (RANS) equations. These tools are generally increasingly accurate, but the computational costs are also increasing. The ability of these tools to correctly predict jerks in the motions is still unknown.

As mentioned slamming causes a very sudden change in acceleration and thus a significant jerk in certain ship motions. The effects of slamming on the ship motions are however difficult to predict, especially with the more linearised prediction tools such as the strip theory and the panel method. Slamming is a highly non-linear effect, which is not captured by these linearised tools. There are ways to include non-linear effects in the linearised tools, but the accuracy of this regarding the jerks in the motions it causes is unknown and should be investigated.

Another way to predict ship motions is using model tests. In these tests the motions and accelerations can be measured. Jerk can however not be measured directly, since there are not yet (commercially) available jerk sensors [46]. Therefore the jerk in the motions should be determined by differentiating the acceleration signal. But in these measurements noise is always present and it is unknown how this affects the possibility to accurately determine jerk.

1.2 Objectives

The main objective of this research is to assess whether jerk could be a good parameter to assess the motion comfort of ships, besides the accelerations. There are two ways in which the jerk assessment of a ship can be performed. The first one is in a qualitative manner, for example when two different ships are compared on their seakeeping performance. If the accelerations are larger at one ship, but the jerk is larger at the other, jerk can thus give additional information. If the jerk is always larger at the ship that also has the larger accelerations, the assessment of jerk does not have to be necessary to compare the ships.

The second way is with a quantitative comparison. If there are limits on comfort for both acceleration and jerk, it could be that a ship is below the comfort limit for accelerations but exceeds the limit of jerk. In this case the jerk can also be a valuable addition to assessing the seakeeping performance. For this method there are however comfort limits required, which need to be determined in physiological tests. With these tests limits for comfort and workability are determined, just like the limits that are already available for accelerations.

Since no limits are available yet, this research will mainly focus on the qualitative comparison of jerk. For this procedures for quantifying the jerk are required, which can later be used in the quantitative research as well to find which method has the best correlation with for example the comfort of passengers. Two different procedures will be investigated.

Another objective is gaining insight in the most important physics behind jerk and what causes ships to experience large jerk values. When this is known ships can be optimised with these physics in mind, to minimise the jerks and/or accelerations.

1.3 Research questions

To reach the objectives as defined in the previous section, the following research questions are defined.

What is the influence of different physical phenomena on jerk?

One of the first steps is to determine which physical phenomena have the biggest influence on jerk and/or cause the largest jerks. These phenomena can then be investigated using measurement data from model tests.

How can the jerk in ship motions be determined from model tests and/or full scale tests?

For this question the type of data, the quality of the data and filtering of the measurement signal has to be investigated. Noise in the signal makes determining the jerk in the acceleration signal more difficult. This question also covers requirements on the measurement data (for example sampling rate) to accurately determine jerk.

How can the severeness of jerks in the ship motions be quantified?

As mentioned in the problem description jerk is always present in the ship motions, it does not have to be bad for the sense of comfort. Therefore a method to quantify the severeness of the jerk should be determined.

How can the jerk in ship motions be predicted with sufficient accuracy?

Sufficient accuracy is a variable concept. It can mean that the calculation method should be able to predict the order of magnitude of the jerks and the peaks in the jerk correctly. But another meaning can be that the number of large jerk peaks that can be expected is predicted, not necessarily the magnitude of the peaks.

1.4 Approach

Jerk is a response of the ship to the seaway it is sailing in. It is therefore important to understand the physics of ship motion response. The drivers behind ship motions and the different approaches to describe ship motions are discussed in chapter 2. Special attention will be given on the physical interpretation of jerk. Also one of the most likely phenomena to cause large jerk values, slamming, will be analysed theoretically to understand what the influence of different parameters is and what implications this has on jerk.

As mentioned in the problem description the jerk cannot be measured directly. It therefore has to be determined from the differentiated acceleration signal. In these measurements usually noise is present, so the effect of this on the ability to numerically differentiate the signal to determine the time trace of the jerk has to be investigated. This will be done in chapter 3. The uncertainty in the measurement signals and the implications it has on the ability to make comparisons are discussed in chapter 4.

No full scale data was available for this research, so the link between model scale and full scale could only be investigated theoretically. In chapter 3 the requirements on model test measurements, and the implications this has on full scale measurements will be discussed. The theoretical description of scaling, the implications on the jerk and the difficulties that this might impose are described in chapter 8.

To be able to compare the jerk several procedures of quantifying the jerk have to be investigated. From the literature mentioned in the problem description it became clear that often peak values are used for this, so this will have the primary focus. However also a different quantifying method for the severeness of the ship motions based on jerk will be investigated. This is done in chapter 4. Since the comparisons that will be made are primarily qualitative, the main goal is to see whether comparing the jerk of ships gives a different perspective than comparing the accelerations. Therefore also the quantification of acceleration is described.

In chapter 5 model test data is processed and the jerk is quantified according to the previously determined procedures. The data is analysed on both the accelerations and the jerk. With this good comparisons can be made to determine the influence of several phenomena on the jerk and determine whether jerk would give a different perspective compared to accelerations. The data from model tests using the same models but in irregular waves is analysed in chapter 6. The focus here is first on analysing the difference between the hulls and the influence of several parameters again. The behaviour is also linked to the behaviour of the models in regular waves.

An important step in the design of a ship is the prediction of the motions using numerical methods. These are usually cheaper to perform than model tests and can thus give a first indication of the sea-keeping behaviour of a ship. There are different types of methods. Their difference and the impact it has on the ability to correctly predict jerk is analysed in chapter 7. Results from numerical simulations using the same conditions as the model tests in regular waves are compared with the measurement data. In this thesis the correct prediction of the order of magnitude of the jerk will be investigated. The differences between the calculations and measurements are then analysed as well.

By performing all these steps the research questions defined in the previous section can be answered. This will be done in chapter 9. Some additional questions that came up, which are beyond the scope of this thesis, are recommended for further research in this chapter as well.

2

Ship motion response

All ships move in the seaway they are sailing in. The different motions are defined in section 2.1. Due to the response of a ship to the sea, it not only experiences velocity and acceleration in its degrees of freedom, but also jerk. The first step in determining jerk is to investigate how a ship responds in seaway and what the physics behind these responses are. All the responses of a ship in seaway are in the basis non-linear with respect to the disturbant waves. However, in some cases the responses of a ship can be described well with a linear approach. The distinction between the linear approach and non-linear behaviour will be explained in this chapter.

In figure 2.1 two (partial) time traces of vertical acceleration (a_z) of a model are shown. These time traces are the result of a RANS (Reynolds Averaged Navier-Stokes) calculation for the same model, but in different regular wave conditions. In the first time trace, figure 2.1a, the wave length is longer than in the second time trace, 2.1b. In both time traces also a sine fit determined by the least squares method [21] is plotted. This is a sine function with an according amplitude and frequency that leads to the least difference with the time trace of the acceleration. The similarity between the acceleration data and the sine fit is described with the coefficient of determination (r^2). This is the square of the coefficient of correlation [41], and indicates how strong the linear correlation between two data sets is. The value of this coefficient can be between 0 and 1, where a r^2 -value of 1 indicates that there is a perfect similarity between the data sets. The data sets are then identical. Time trace 1 has a r^2 -value of 0.993. This means that the acceleration can for 99.3% be correctly described with a single sine function. Time trace 2 has a r^2 -value of 0.791, or 79.1%. The time traces of the jerk, corresponding with the time traces in figure 2.1, are plotted in figure 2.2. The jerk in time trace 1 can be described for 93.2% with a sine function, the jerk of time trace 2 only for 37.5%.

As will be explained in this chapter, a sine function is the response to a regular wave that would be described by the linear response theory. For time trace 1 this is sufficient, the sine function can almost perfectly describe the accelerations and the jerk of the ship. The shape of the acceleration of time trace 2 has less similarity with a sine function. Especially the (negative) peaks and the gradient of the acceleration are not well described. The jerk corresponding to time trace 2 is not described well at all with a sine function. All the peaks are several factors higher than described by the sine function. This thus illustrates that the non-linearity of the response is important when investigating the jerk. The amount of non-linearity grows exponentially with increasing derivatives, as will be further discussed in chapter 4.

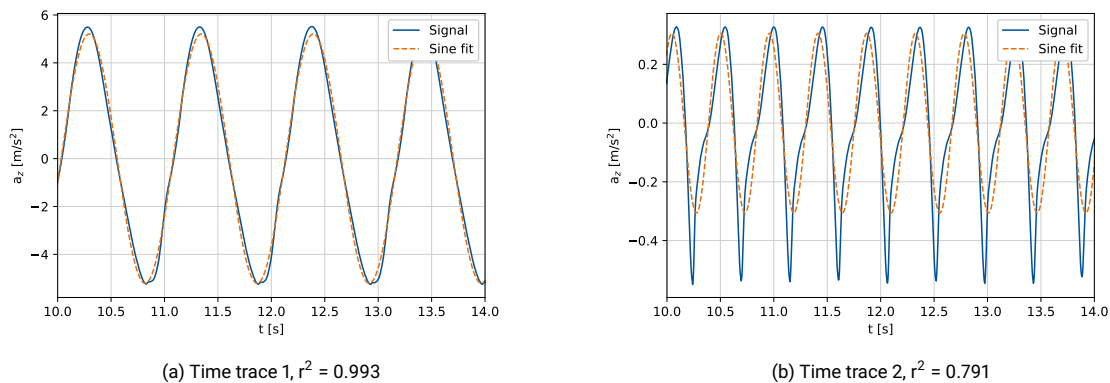


Figure 2.1: Examples of time traces of vertical acceleration in ship motions

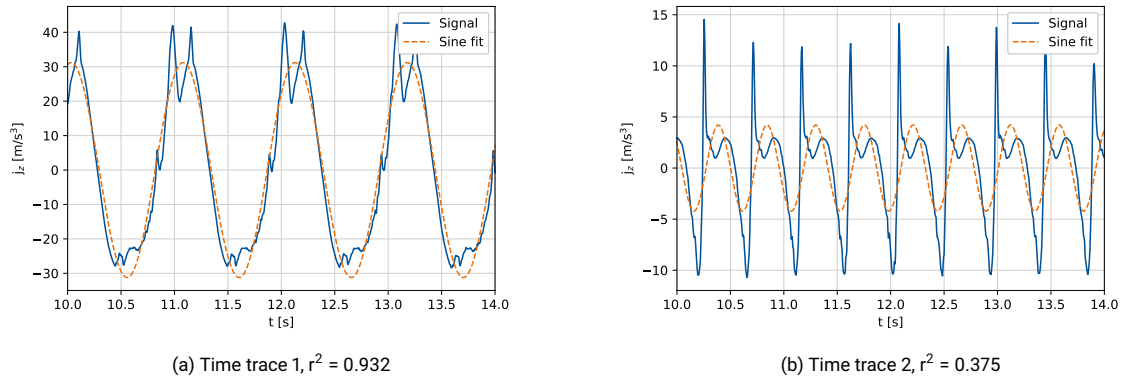


Figure 2.2: Examples of time traces of vertical jerk in ship motions

The linear approach, and the assumptions this is based on, will be described in section 2.2. There are several phenomena that drive the ship to more non-linear behaviour. These will be discussed in section 2.3. In section 2.4 the different assessing methods of ship response will be described. Finally in section 2.5 the physical interpretation of jerk and a derivation of the most important factors in jerk caused by slamming will be given.

2.1 Definitions

The motions of an unrestrained ship are defined in six degrees of freedom: three translational motions and three rotational motions. The ship-bound right-handed coordinate system has its origin in the centre of gravity of the steady-state position of the ship. In case the ship is moving with steady forward speed, the coordinate system is steadily moving forward as well. The motions along respectively the x -, y -, and z -axis are called surge, sway and heave; the rotations roll, pitch and yaw [39]. See also figure 2.3. The positive direction of each degree of freedom is indicated with the arrows. In table 2.1 the axis and units of all degrees of freedom are defined.

Table 2.1: Definition motions and units

Name	Axis	Displacement	Velocity	Acceleration	Jerk
Surge	x	m	m/s	m/s^2	m/s^3
Sway	y	m	m/s	m/s^2	m/s^3
Heave	z	m	m/s	m/s^2	m/s^3
Roll	ϕ	rad	rad/s	rad/s^2	rad/s^3
Pitch	θ	rad	rad/s	rad/s^2	rad/s^3
Yaw	ψ	rad	rad/s	rad/s^2	rad/s^3

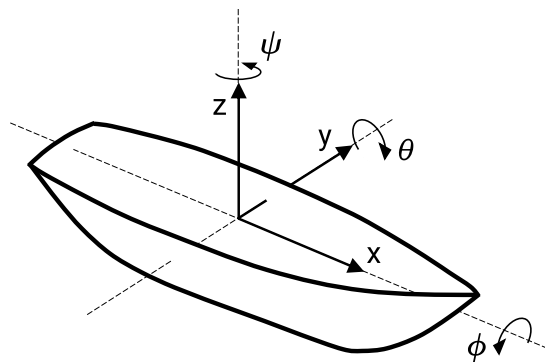


Figure 2.3: Degrees of freedom of an unrestrained ship, recreated from Journée et al. [27]

2.2 Linear approach

The response (displacement, velocity, acceleration or jerk) of a ship is linear if the response can be described with a linear differential equation. The amplitude of the response is then proportional to the amplitude of the incoming wave. The groundwork for the widely used linearised approach to the response of a ship in seaway is laid by the paper of St. Denis and Pierson [54]. The most important result of the linearisation is that the principle of superposition can be applied: the total response of a ship can be determined from the summation of the forces of the restrained ship in waves plus the free motion of the ship in still water. For a heaving ship model this is visualised in figure 2.4. Also the response to different wave components can be superpositioned. The assumptions made in the linear approach and the resulting approach will be discussed in this section.

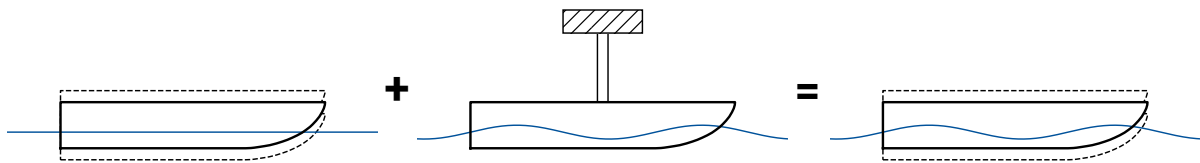


Figure 2.4: Superposition principle, recreated from Journée et al. [27]

2.2.1 Assumptions

In this section the assumptions of the linear ship motion theory are discussed. These assumptions are necessary to justify the superposition principle. The information is obtained from St. Denis and Pierson [54], Ogilvie [40], Lloyd [31] and Journée et al. [27].

Small disturbance

In order for the linearisation to be valid, the disturbance that the ship causes must be small [40]. In this case the wave diffraction can be approximated from the restrained body [37].

Small amplitude waves

Since the forces of the wave on the ship are calculated as if the body is restrained, the forces are calculated on the still water underwater geometry. This is only valid if the amplitude of the waves is small compared to the geometry of the ship. In large amplitude waves the changing geometry above and below the waterline would introduce nonlinear forces on the body [54]. In small amplitude waves the change in geometry is assumed to be negligible and the forces are thus linearly correlated with the wave amplitude.

No non-linear coupling between degrees of freedom

There can be coupling between different degrees of freedom of the ship, for example heave and pitch. This is dependent on (amongst other things) symmetry of the hull of the ship. These coupling effects can however be non-linear. If the coupling effects are non-linear superposition cannot be applied anymore. The non-linear coupling effects are generally assumed to be small, so they are neglected in the linear approach. Only the linear coupling effects are included.

Low to moderate velocity

If the velocity of the ship is low to moderate, the lifting effects of the hull are considered small and can be neglected. Lifting effects due to forward speed are non-linear, so should be neglected to get a linear approach. Also the mass and inertia are assumed to be unaffected by the forward speed [54].

No viscous forces

The assumption that viscous forces, which are non-linear, are neglected, means that the damping in the system is completely accounted for by wave generation. For most degrees of freedom this assumption is valid, since especially in vertical motions (heave and pitch) the viscous damping is very small [27]. Only the roll damping near the resonance frequency is largely underestimated due to the lack of viscous forces [50]. Neglecting the viscous forces enables the use of potential theory to determine ship motions.

2.2.2 Equations of motion

The linearised motions of a ship can be captured in the equations of motion. This starts with Newton's second law of motion, which states that the forces applied on a body are equal to the mass of the body times the acceleration. For a ship the equations of motions for the six degrees of freedom are described in equation 2.1 [37]. In theory each degree of freedom can have coupling terms with other degrees of freedom, following from the asymmetry of the hull. A different shape of the fore and aft body can for example cause an heave motion when the ship is pitching. Therefore \mathbf{M} is a 6x6 matrix.

$$\mathbf{M} \cdot \ddot{\mathbf{x}} = \underline{\mathbf{F}} \quad (2.1)$$

In this equation $\ddot{\mathbf{x}}$ is the acceleration vector (second derivative of motion \mathbf{x} with respect to time) for each of the six degrees of freedom. The elements on the diagonal of the matrix \mathbf{M} represent the mass term (for translational motions) or moment of inertia term (for rotational motions). The off-diagonal elements provide the coupling terms between the different degrees of freedom. The force vector includes all the forces that work on the ship in each degree of freedom. These forces are defined in Journ e et al. [27] as:

- F_r : Radiation forces. These are the hydrodynamic forces caused by the movement of the ship. It consists of the added mass matrix \mathbf{A} (which introduces additional inertia in the system) and the damping term matrix \mathbf{B} : $\underline{\mathbf{F}}_r = -\mathbf{A} \cdot \ddot{\mathbf{x}} - \mathbf{B} \cdot \dot{\mathbf{x}}$
- F_s : Hydrostatic restoring forces: $\underline{\mathbf{F}}_s = -\mathbf{C} \cdot \mathbf{x}$
- F_w : Wave force of the incoming wave. This is calculated using the method of Froude-Krylov [55]. This method assumes that the pressure of the wave is not influenced by the presence of the ship.
- F_d : Diffraction forces. The force due to the disturbance of the incoming wave by the presence of the ship.

Substituting and rearranging the terms in equation 2.1 leads to the equation of motion as in equation 2.2. The mass \mathbf{M} , the added mass \mathbf{A} , the damping \mathbf{B} and the restoring term \mathbf{C} are all matrices. The remaining terms are all vectors to represent each degree of freedom.

$$(\mathbf{M} + \mathbf{A}) \cdot \ddot{\mathbf{x}} + \mathbf{B} \cdot \dot{\mathbf{x}} + \mathbf{C} \cdot \mathbf{x} = \underline{\mathbf{F}}_w + \underline{\mathbf{F}}_d \quad (2.2)$$

This equation of motion is a second order linear differential equation, and is the base for the linear approach to ship motions. In the linear case the added mass \mathbf{A} , the damping term \mathbf{B} and the restoring term \mathbf{C} in the equation of motion are independent of the wave amplitude. The use of this linear approach to determine the response of the ship in regular and irregular waves is described in the next sections.

2.2.3 Regular waves

A regular (two-dimensional) wave ζ propagating in negative y direction is described by equation 2.3. In this equation ζ_a is the amplitude, k is the wave number and y is a spatial term. Furthermore ω is the frequency (or encounter frequency) and t is the time. The wave equation describes the wave at any location at any time instant. In the following equations the response is observed in the origin of the system and the spatial term is thus zero.

$$\zeta(y, t) = \zeta_a \cdot \sin(k \cdot y + \omega \cdot t) \quad (2.3)$$

The solution to the equation of motion in equation 2.2 is then also a sinusoidal, see equation 2.4. In this equation x is the response in the i -th degree of freedom, $x_{i,a}$ is the amplitude of the response and $\epsilon_{i\zeta}$ is the phase difference between the response and the wave.

$$x_i(t) = x_{i,a} \cdot \sin(\omega \cdot t + \epsilon_{i\zeta}) \quad (2.4)$$

$$\frac{x_{i,a}}{\zeta_a} = \text{constant} \quad (2.5)$$

Since the system is linear, the response is proportional to the wave amplitude, see equation 2.5. This transfer function is called the response amplitude operator (RAO). RAOs are only dependent on (encounter) frequency and direction with respect to the sailing direction of the vessel [31]. The RAOs can also be superpositioned to calculate the response at any location of the ship.

2.2.4 Irregular waves

In the previous section the response of a ship in regular waves is described. However, real seas are seldom regular. To be able to describe the motions of a ship in irregular waves an appropriate method is needed. The generally accepted method of describing an irregular sea is the assumption that the elevation is a superposition of different waves with a certain frequency, amplitude and (random) phase angle, see equation 2.6. This is called a Fourier series [19]. An example time series of an irregular sea can be seen in figure 2.5.

$$\zeta(t) = \sum_{j=1}^N \zeta_{a,j} \cdot \sin(\omega_j \cdot t + \epsilon_j) \quad (2.6)$$

Frequency spectrum

The principle of Fast Fourier Transform can be used to decompose the irregular sea into a number of harmonic components with different frequencies and amplitudes. For each of these frequency intervals the amplitude is determined. When plotted this gives the amplitude spectrum. More widely used is the variance density spectrum or energy density spectrum. This spectrum is based on the variance of the amplitude. Linear wave theory shows that the variance of the wave spectrum is proportional to the energy in the wave spectrum [19]. An example of an energy density spectrum, based on a JONSWAP wave spectrum, can be seen in figure 2.6a.

Transfer functions

The linear approach allows also for the superposition principle to be applied in irregular seas. The response to all the individual wave components can be combined to the total response. When the energy density spectrum of a sea is known, a response spectrum (see figure 2.6c) can be determined using a (frequency dependent) transfer function, see equation 2.7. In this equation $S_{x_i}(\omega)$ is the energy density spectrum of the motion response of i-th degree of freedom and $S_{\zeta}(\omega)$ is the energy density spectrum of the irregular waves. The transfer function is the square of the RAO of each frequency component.

$$S_{x_i}(\omega) = \left| \frac{x_{i,a}}{\zeta_a}(\omega) \right|^2 \cdot S_{\zeta}(\omega) \quad (2.7)$$

The transfer function is plotted in figure 2.6b. This transfer function only relates the components of the energy density spectrum of the waves to the response spectrum, thus the amplitude of each wave

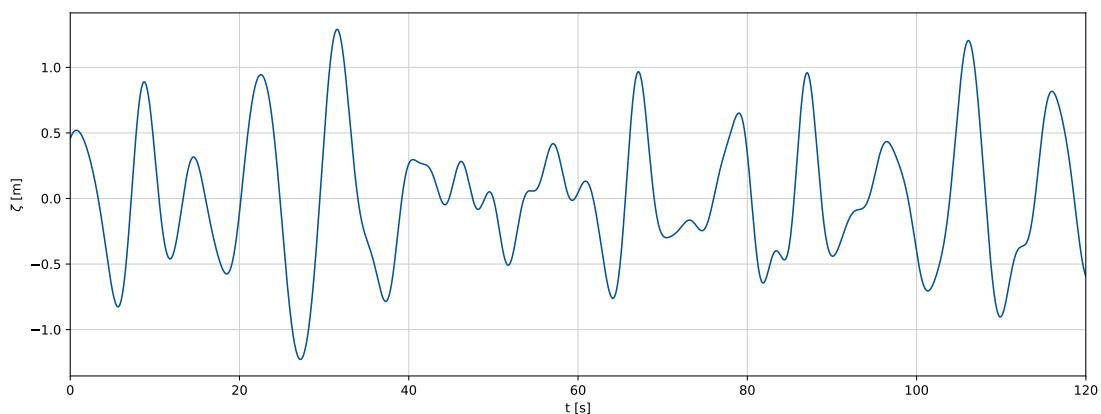


Figure 2.5: Example of a time trace of an irregular sea

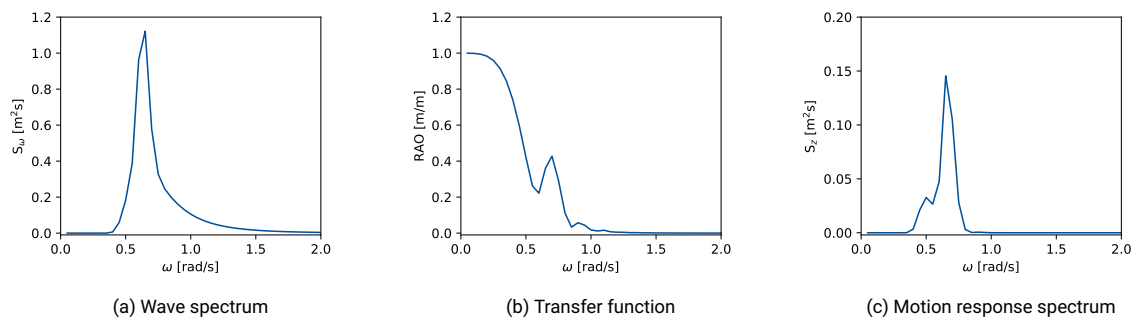


Figure 2.6: Example of energy density spectra and transfer function

component to the amplitude of each response component. To describe the full response and determine a time trace of the response also a spectrum containing the phase difference between each frequency component of the waves and the response is required. This spectrum is not plotted here.

2.2.5 Applicability

The linear method described here is the most simplified method possible to describe the motion response of a ship in waves. Nevertheless many computational tools are based on this linear approach. These tools will be discussed further in chapter 7. The tools often include more (linearised) physics, for example artificial roll damping to compensate for the missing viscous roll damping. Although all this is linearised and thus a simplification of the reality, this method has been validated many times in the last decades to give good predictions of ship motions, especially when the ship speed is relatively low and the disturbances are small [3, 16, 27, 50]. Figure 2.1a in the introduction of this chapter also shows that the linear approximation can in certain cases give a very good approximation of the ship motion. The sine fit in this figure is the response that can be described by the linear theory.

2.3 Non-linear behaviour

Non-linear behaviour of a ship to incoming waves can be described as a response which is not described well with a linear differential equation, and thus the response is not proportionally dependent on the incoming wave. An example of non-linear behaviour can be seen in figure 2.7, recreated with data from de Jong [7]. In this figure the filtered vertical acceleration signal of a model in regular wave conditions is plotted. The least squares sine fit is also plotted, as was also done with the time traces in the introduction of this chapter. If the response to the regular wave would be linear, the sine fit would be the same as the measured response. However, the r^2 -value of this time trace is 0.668 and it can thus not be described well by a sine function. It can be seen clearly that the measured response is not

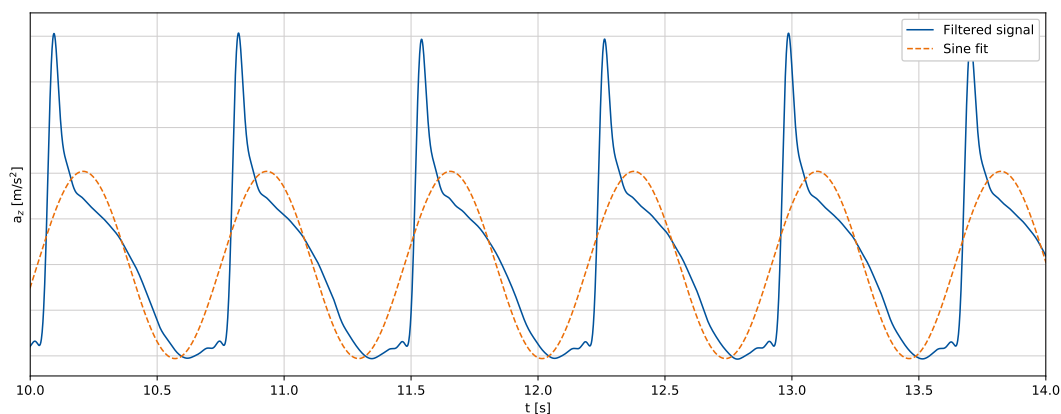


Figure 2.7: Example of non-linear response, from de Jong [7]

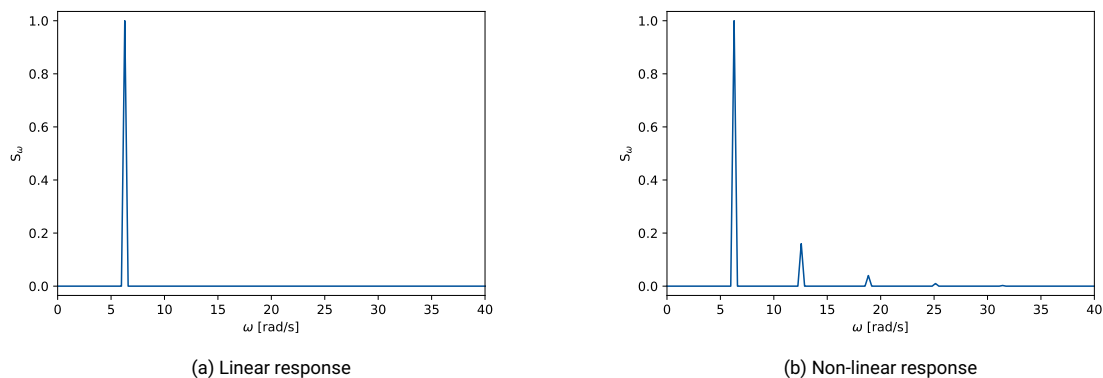


Figure 2.8: Comparison of energy density spectra from linear and non-linear response in regular waves

proportional to the incoming wave and thus non-linear: the positive acceleration peaks are higher much higher than the sine fit. Also the steepness of the acceleration signal from the trough to the crest is higher than the sine fit.

The non-linear response of a ship to regular waves in one of the degrees of freedom can be defined as given in equation 2.8. In this equation ω is the encounter frequency (in rad/s) of the ship with the waves. The first part of the equation is the first order (linear) response, with amplitude A_1 and phase ϵ_1 . The higher order responses are defined in the sum in the right part of the equation. These responses are at multiples of the encounter frequency and have their own amplitudes and phases [15]. Only the first order (linear) response can be linked with a RAO to the disturbant wave, which is the sine fit as plotted in figure 2.7. It is also directly clear that this does not represent all the aspects of the motion signal. No transfer function can be defined between the regular wave and the entire non-linear response.

$$x_i = A_1 \cdot \sin(\omega \cdot t + \epsilon_1) + \sum_{n=2}^N A_n \cdot \sin(n\omega \cdot t + \epsilon_n) \quad (2.8)$$

Non-linear response is thus a response that consists of multiple harmonics: the first order response and higher order responses at multiples of the first order. In figure 2.8 an example of the difference in the energy density spectrum of linear and non-linear response in regular waves can be seen. In figure 2.8a only the peak at the excitation frequency is visible, while in figure 2.8b besides the peak at the excitation frequency also peaks at multiples of the excitation frequency can be seen. These energy density spectra are examples and are not linked to the time trace in figure 2.7. In section 2.4 more explanation about the energy density spectrum will be given.

2.3.1 Large amplitude waves

One of the assumptions of the linear response was that the amplitude of the incoming wave was small compared to the geometry of the ship [27]. When a ship sails in relatively large waves, the motions also increase. The assumption that the hydrodynamic forces can be calculated on the still water geometry is no longer valid. The instantaneous submerged body should be used for calculations, because large changes in the hydrodynamic forces or the distribution of these forces along the hull can be caused by large amplitude waves. If for example part of the hull emerges above the water, the hydrodynamic forces disappear here until it re-enters the water. According to Keuning [29] especially the vertical accelerations become increasingly non-linear with increasing wave amplitude and forward speed.

Also the (normally) above water geometry, for example the bow flare, becomes important. This part of the hull might be submerged in a large amplitude wave, which will then result in a non-linear hydrodynamic radiation and restoring force. In research performed on this topic it was found that the shape of the bow has little influence on the displacement motions of the ship. There is however a significant influence on vertical accelerations, especially in the bow region [43, 45]. The varying behaviour of ships with different bow shapes also becomes clear from the research of de Jong [7], where was found that

a ship with an axe bow (which is optimised for head waves) has significantly lower accelerations in the bow section. This will also be further analysed in chapter 5 and chapter 6.

2.3.2 Non-linear waves

In the previous sections the assumption was made that the waves the ship responds to are described with a single sine function in case of regular waves, or a superposition of different sine functions in case of irregular waves. This is known as the linear wave theory. In reality this is however not always the case. Especially steep waves and waves in shallow water are non-linear, and cannot be described accurately with the linear wave theory anymore [19]. A Stokes wave is a commonly used for describing these non-linear waves, see figure 2.9. The wave plotted here is a 5th order Stokes wave [13]. For reference also a least squares fitted sine wave with the same wave frequency is plotted. It can be seen that the crests of the Stokes waves are higher and the troughs are less deep. The wave is also steeper than a regular sine wave. Since these waves cannot be fully described anymore with a single sine function, the response of a ship to non-linear waves will therefore not be linear in the way it is described in section 2.2.

Wave breaking

If waves become too steep, they can break. This is a very non-linear hydrodynamic phenomenon, of which many details are still unknown [19]. Energy is dissipated in breaking waves, and their effective height reduces. Therefore the ship response to a breaking wave might be lower than would be assumed in linear theory. The ship response might also be larger due to the possible high impact loading of breaking waves.

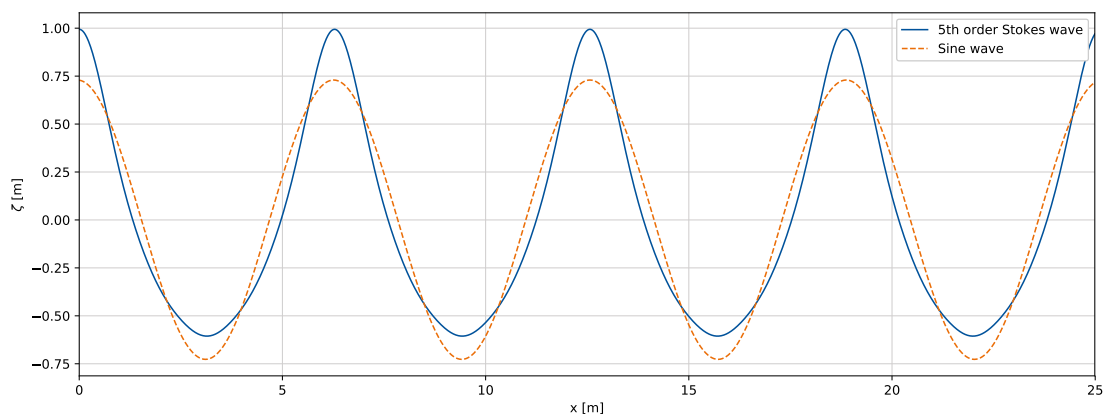


Figure 2.9: Example of 5th order Stokes wave

2.3.3 High forward speed

In the extensive research into non-linear (seakeeping) behaviour of ships performed by Keuning [29] and de Jong [7], the definition for a high-speed ship is a ship with Froude numbers ranging from 0.7 to 0.9. Ships are not in the fully planing regime with these speeds. For a monohull of 30-50 meters, these Froude numbers result in a sailing speed of around 30 knots.

As already mentioned in section 2.3.1, Keuning [29] states that especially the vertical accelerations become increasingly non-linear with increasing wave amplitude and forward speed. At high forward speeds part of the weight of the ship is compensated by hydrodynamic lift. The submerged volume of the ship becomes different, and also the sinkage and trim are affected. Therefore the underwater geometry at high speeds will become different and this (non-linear) effect has a significant influence on the motion response of a ship to the waves [29].

2.3.4 Slamming

The motions of a ship can become so large that there are violent impacts between the hull and the water, a phenomenon called slamming. There are different types of slamming: bottom slamming, bow flare slamming, and stern slamming [5]. Catamarans can also experience wet deck slamming. Bottom slamming happens when the entire bow section emerges from the water in a wave. When the keel then

re-enters the water, large impact loads occur. The magnitude of these impact loads is highly dependent on the deadrise angle [58, 60]. Bow flare slamming occurs at ships with a significant bow flare. When the ship enters the water with speed, there is an impact at the side plating of the bow [2]. Slamming in the bow area is most critical in head waves. Stern slamming happens when the stern of the ship emerges from the water in a wave, and violently enters the water again. Stern slamming occurs most in ships with a large overhanging or a flat stern area, for example container carriers or liquefied gas carriers [2]. Wet deck slamming occurs when large waves impact the bottom of the structure between the two hulls of a catamaran (the wet deck).

Slamming locally leads to large impact pressures. In large ships this leads to substantial structural loads and vibrations, called whipping [31]. In smaller ships slamming causes peaks in the acceleration. The occurrence of slamming is now often considered as the limit of operability of a ship in heavy sea states [29].

The first researches into predicting the large impact pressures of slamming were performed by Von Karman [58] and Wagner [60]. A theoretical slamming pressure coefficient was derived, based on a 2D wedge entering the water. The coefficient is mainly dependent on the deadrise angle of the hull. The smaller the angle between the hull surface and the fluid surface, the larger the impact pressure. Still a big challenge with slamming is the problems with scaling. Slamming, especially with low relative angles between the hull and the fluid, involves trapping and compressing of air. The normally used scaling laws, mostly Froude scaling, do not apply anymore in these cases. It is therefore not possible to accurately predict the impact pressures of slamming using model experiments [28]. Scaling and the impact of slamming on the accuracy of scaling will be discussed more in chapter 8.

2.3.5 Viscous forces

As mentioned in section 2.2.1 viscous forces are neglected in most motion computations, since the major part of damping is caused by wave damping. Only in roll and surge the viscous forces are of greater importance [27]. There these forces can cause non-linear responses. In calculations the non-linear forces in the roll damping are usually linearised at a certain roll angle.

2.4 Assessing methods

There are generally two methods to assess the motion responses of a ship, will be described in this section.

Time domain

The first assessing method is the time domain. This is the most intuitive method, since the response is plotted against time. See for example figure 2.10a. In this figure the fictive non-linear response z of a ship in regular waves (thus a single sine wave) is plotted, see equation 2.9.

$$z = A_1 \cdot \sin(\omega \cdot t) + A_2 \cdot \sin(2\omega \cdot t) \quad (2.9)$$

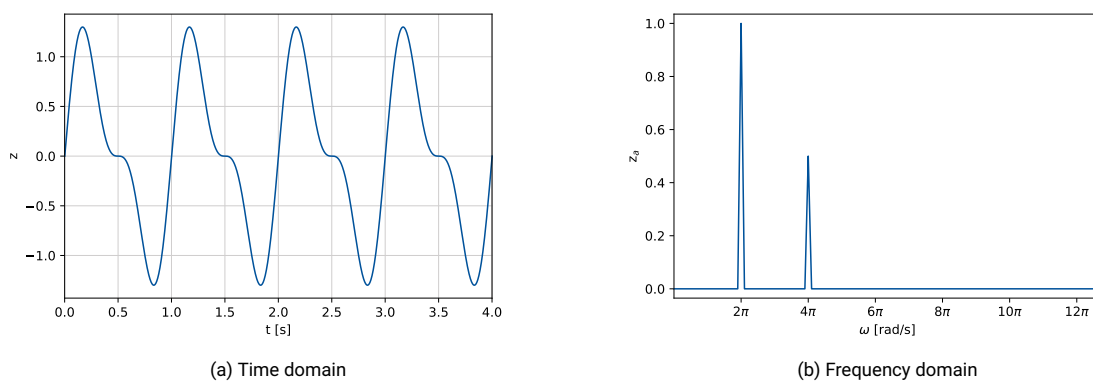


Figure 2.10: Assessing methods for ship motion response

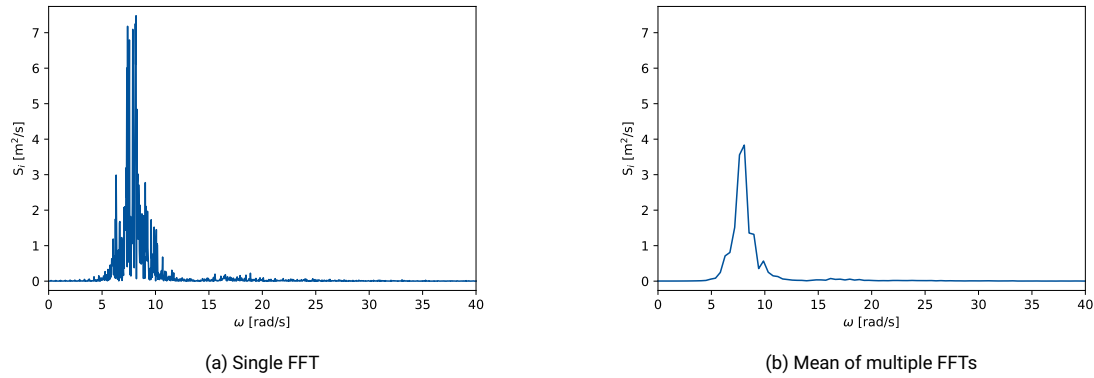


Figure 2.11: Comparison of single FFT and mean of multiple FFTs for response in irregular waves

The response is non-linear because it is not a single sine function as would be expected by the linear approach. Instead multiple sine functions are superpositioned to describe the response. In figure 2.10a the response is plotted for frequency $\omega = 2\pi$ rad/s and amplitudes $A_1 = 1$ and $A_2 = 0.5$.

Frequency domain

Another way of assessing the ship motion response is to convert the response in the time domain to the frequency domain. This is done using the Fast Fourier Transform (FFT) [4]. The FFT transforms the signal in the time domain to a two sided amplitude spectrum with complex numbers which indicate the amplitude and phase of each frequency component. In the analysis of ship motions usually a one-sided spectrum without phase information is used. In figure 2.10b the Fast Fourier Transform of the time trace in figure 2.10a is shown. It can be seen that in the amplitude spectrum the harmonic components of the original function (equation 2.9) can be determined again. One component with a frequency of 2π rad/s with amplitude 1, the other component with a frequency of 4π rad/s and an amplitude of 0.5. In this case the function was known beforehand, but this method is especially valuable when this is not the case.

The frequency spectrum can also be converted to an energy density spectrum, using equation 2.10. Each amplitude A_i of harmonic component i is converted to a component S_i of the energy density spectrum [27].

$$S_i = \frac{A_i^2}{2 \cdot d\omega} \quad (2.10)$$

The use of the energy density spectrum instead of the amplitude spectrum has several advantages. The first is that in irregular waves the amplitude of each harmonic component in the amplitude spectrum is dependent on the frequency interval $d\omega$. The smaller the frequency interval, the smaller the amplitude of each harmonic component. By converting it to an energy density spectrum the dependency on the frequency interval is taken out. The second advantage is that the energy density spectrum has an analogy with the amount of energy of each frequency component. When used for the analysis of a wave spectrum, the amount of energy in each frequency component is the value from the energy density spectrum multiplied by the water density ρ and the gravitational acceleration g [19]. The amount of energy in the spectrum can be determined by integrating the energy density spectrum, see equation 2.11. This is also called the zeroth order moment of the spectrum.

$$m_0 = \int_{\omega=0}^{\infty} S_i(\omega) d\omega \quad (2.11)$$

When making the FFT of an irregular wave response, this is usually done by cutting the time trace in a number of blocks and making the FFT of each block. The mean of the FFTs is then the FFT of the complete time trace. If this would not be done, the spectrum would look like figure 2.11a. This is because the time traces have a finite length, with random components within the spectrum. By taking the mean of the FFTs of several blocks the spectrum looks like figure 2.11b. The amount of energy in the spectra is the same, only the shape is easier to analyse.

2.5 Jerk

In this section a short description of the physical interpretation of jerk will be given. This will be linked to ship hydromechanics with an example of Von Karman slamming theory [1, 58].

2.5.1 Physical interpretation

Newton's second law states that the sum of forces (in a certain direction) on an object is equal to the mass of the object times the acceleration of the object (in the same direction). This is defined in equation 2.12.

$$\vec{F} = m \cdot \vec{a} \quad (2.12)$$

The jerk is defined as the rate of change of the acceleration, see equation 2.13. Combining that with equation 2.12 gives equation 2.14, assuming the mass does not change. The jerk is then the result of the change of the force on a mass. The case where the (added) mass does change is discussed in the next section.

$$\frac{d\vec{a}}{dt} = \vec{j} \quad (2.13)$$

$$\frac{d\vec{F}}{dt} = m \cdot \vec{j} \quad (2.14)$$

The largest jerk in ship motions can thus be expected in situations where the forces on the hull change rapidly. The best known phenomena where this happens is slamming. As already mentioned in section 2.3.4, the impact pressures in slamming can become very large, which thus results in large forces on the hull of a ship. Furthermore the time scale of a typical slam is very small. The rate of change of the force in a slam event must thus be large. It is thus likely to find large jerk in slamming.

2.5.2 Von Karman slamming

To illustrate that a difference in jerk can come from a different hull shape in the same slamming conditions, the approach of Von Karman [1, 58] is used to derive the parametric difference in slamming forces following from different hull shapes. This is a simplified approach, but it identifies some factors influencing the jerk following from slamming.

The Von Karman theory is based on a 2D wedge entering the water with a vertical velocity V_z , see figure 2.12a. This can be seen as a part of the hull that slams into the water due to a heave or pitch motion, or a part of the bow that slams forward into a wave due to the forward speed of the boat. The force on this wedge is then following from equation 2.15. This equation has the same basis as equation 2.12. The chain rule is applied to determine the derivative, as can be seen in equation 2.16.

$$F = \frac{d}{dt}(m \cdot V_z) \quad (2.15)$$

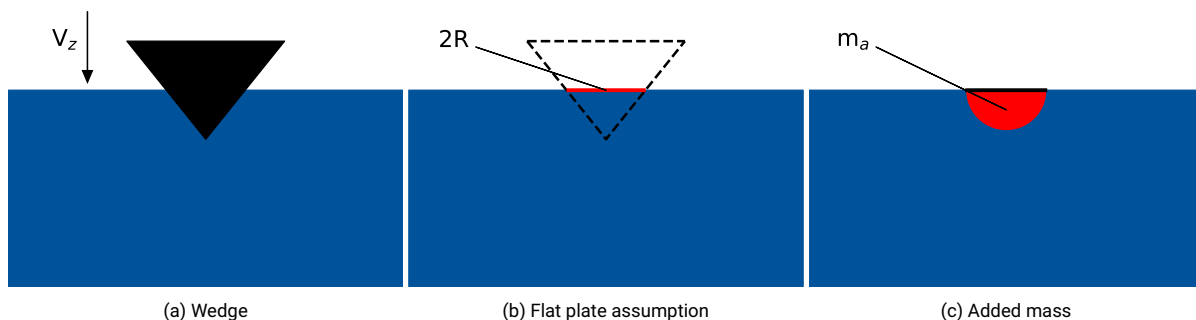


Figure 2.12: Von Karman wedge slamming force approximation

$$F = m \cdot \dot{V}_z + \dot{m} \cdot V_z \quad (2.16)$$

To simplify the approach in this case the vertical velocity of the wedge into the water is assumed to be constant, and the derivative \dot{V} is thus zero. The other term in the equation for the force follows from the change of mass. Usually this term is zero, but in hydromechanics added mass is present, which changes with the submersion of the wedge. In this case this term is thus not zero and is called the Von Karman force F_{VK} , see equation 2.17. In the Von Karman approach the added mass of the wedge at any moment is approximated to be the added mass of a flat plate, with the length $2R$ equal to the submerged horizontal dimension of the wedge, see figure 2.12b. The added mass of a flat plate is defined as given in equation 2.18 [1].

$$F_{VK} = \dot{m}_a \cdot V_z \quad (2.17)$$

$$m_a = \rho \cdot \frac{\pi \cdot R^2}{2} \quad (2.18)$$

In this equation ρ is the density of the water and R is the radius of the plate. The rate of change of the added mass is determined by the square of the rate of change of the radius R . The radius R is a function of time, determined by the shape of the hull and the submersion speed V_z . In figure 2.12b the wedge is displayed as a triangle, but the wedge can also have different shapes. Without knowing the exact function for the hull shape, the rate of change of R^2 is given in equation 2.19. The rate of change of the added mass becomes then as defined in equation 2.20.

$$\frac{d}{dt}R(t)^2 = 2 \cdot R(t) \cdot \frac{d}{dt}R(t) = 2 \cdot R \cdot \dot{R} \quad (2.19)$$

$$\frac{dm_a}{dt} = \rho \cdot \frac{\pi}{2} \cdot \frac{d}{dt}R(t)^2 = \rho \cdot \pi \cdot R \cdot \dot{R} \quad (2.20)$$

Combining equation 2.17 and equation 2.20 leads to the expression for the Von Karman force as given in equation 2.21.

$$F_{VK} = \rho \cdot \pi \cdot R \cdot \dot{R} \cdot V_z \quad (2.21)$$

In section 2.5.1 the jerk was linked to the rate of change of the force on a mass. The jerk following from slamming is thus the rate of change of the Von Karman force, see equation 2.22. The second derivative of the added mass in this equation is defined in equation 2.23.

$$\frac{dF_{VK}}{dt} = \dot{m}_a \cdot V_z \quad (2.22)$$

$$\frac{d^2m_a}{dt^2} = \rho \cdot \frac{\pi}{2} \cdot \frac{d^2}{dt^2}R(t)^2 \quad (2.23)$$

$$\frac{d^2}{dt^2}R(t)^2 = 2 \cdot R(t) \cdot \frac{d^2}{dt^2}R(t) + 2 \cdot \left(\frac{d}{dt}R(t) \right)^2 \quad (2.24)$$

The second derivative of the square of the shape function R is given in equation 2.23. From this equation it becomes clear that two factors play an important role in the jerk following from slamming. The first one is the width of the wedge times the second derivative of R . The second derivative of R is the curvature of the wedge. When the wedge is a triangle as in figure 2.12a, the curvature is zero thus the jerk is constant. When the curvature is not zero the jerk is thus not constant. Also the wider the wedge, the higher the jerk. The second factor is the square of the first derivative of the shape function. The faster the wedge is submerged, the higher the jerk. An optimised bow, like the AXE described in chapter 5, has a smaller pitch velocity and a smaller rate of change of the geometry. The jerk from slamming is thus expected to be significantly lower.

3

Determining jerk

To be able to use the jerk for quantifying seakeeping characteristics of a vessel, first the jerk should be determined. Since there are no commercially available jerk sensors (yet), it cannot be measured directly. The methods explained in this chapter are for the case that the acceleration is calculated or measured, so the data only has to be differentiated once.

As explained in Vuik et al. [59] the errors in numerical differentiation come from rounding/measurement errors and truncation errors. The effect on the total error of rounding and/or measurement errors decrease with increasing step size. On the contrary the effect of truncation errors on the total error decrease with decreasing step size. The numerical derivative of the acceleration signal is calculated in this thesis using the central difference method (see equation 3.1). Both function values have a measurement error ϵ . The error estimate E is then given by equation 3.2.

$$f'(x) \approx \frac{f(x + \Delta t) - f(x - \Delta t)}{2 \cdot \Delta t} \quad (3.1)$$

$$E \leq \frac{\epsilon}{\Delta t} \quad (3.2)$$

Measurements are usually performed at high frequencies, so the time steps are small. This means that the total error when differentiating this signal could be large. Increasing the time steps is not desirable since this lowers the accuracy of the measurement. Therefore the signal first has to be filtered, as explained in this chapter. In section 3.1 several digital filters will be analysed. A special filter, the Savitzky-Golay filter which filters and differentiates the signal at the same time, is analysed in section 3.2. After that in section 3.3 a method of directly differentiating an energy density spectrum is given. Finally in section 3.4 some requirements on measurements will be described.

3.1 Filtering

In model tests and sea trials the acceleration is measured using accelerometers. However, the signal contains the accelerations due to rigid body motions, accelerations due to vibrations and measurement noise. Since in seakeeping analysis generally only the rigid body motions are desired, the vibrations and noise have to be filtered from the signal. If the signal is free from vibrations and noise, which is the case in numerical simulations, numerical differentiation can be applied without filtering.

In the literature it is generally agreed that accurate, repeatable acceleration measurements of the rigid body motions are hard to perform [35, 49, 61]. Accelerometers are sensitive measurement instruments, the smallest accelerations from vibrations are measured as well. This can affect the peak values of rigid body motions significantly. As mentioned above the vibrations and noise therefore have to be filtered from the measurement data. However, the choice of filter type and filter settings like the cut-off frequency have significant influence on the peak values of the acceleration. Therefore the cited literature does not advise one certain filter or filter setting, but recommends to investigate several filters and filter setting and choose the one best usable for the desired goal.

For the purpose of this thesis it is required to separate the rigid body motions in the measurement signals from noise and vibrations. Rigid body motions are relatively low frequency, while vibrations and noise are at higher frequencies. In general terms (digital) filters separate and remove parts of the signals with a certain frequency, while maintaining others. For example, an ideal low-pass filter will remove all the frequencies higher than the cut-off frequency (the stopband) while letting the frequencies lower than the cut-off frequency through (the passband). Filters are however never ideal, they have a

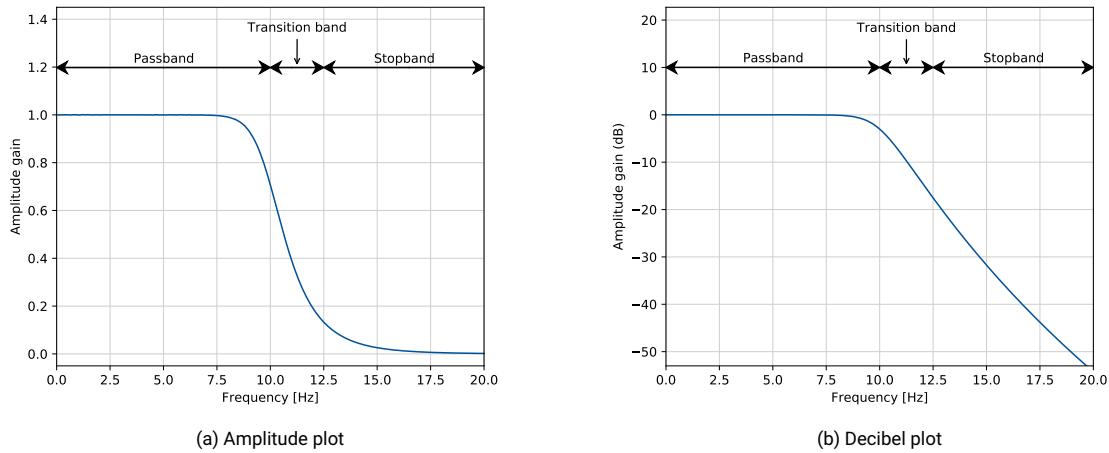


Figure 3.1: Frequency response of 9th order Butterworth low-pass filter with cut-off frequency of 10 Hz

transition from the passband to the stopband (the transition band). This transition is called the roll-off [53]. The higher the roll-off, the smaller the transition band. These bands can be represented in frequency response plots [38], see figure 3.1. The frequency response plots indicate how much the amplitude of a certain frequency is attenuated. This can be done with a linear (unity) scale (figure 3.1a) or as more practice in the field of signal processing using a decibel scale (figure 3.1b). The decibel gain is the logarithm of the attenuation, see equation 3.3 [53].

$$dB = 20 \cdot \log \left(\frac{A_{\text{filtered}}}{A_{\text{original}}} \right) \quad (3.3)$$

In this equation A_{filtered} is the amplitude of a certain frequency component in the filtered signal and A_{original} is the amplitude of that same frequency component in the unfiltered signal. Every gain of -20 dB means that the amplitude has reduced by a factor 10. So -20 dB means the amplitude gain is 0.1, -40 dB means the amplitude gain is 0.01. The cut-off frequency is often defined as the frequency where the amplitude gain first passes -3 dB, which translates to an unity amplitude gain of 0.707. For more information about digital filtering refer to National Instruments Corporation [38] or Smith [53].

As mentioned above the literature states that filtering has a significant influence on the peak values of the acceleration. However, for this research the gradient of the acceleration (the jerk), not necessarily the peaks values of the acceleration are important. Therefore the influence of filtering on the jerk is investigated as well. In appendix B an extensive comparison is made between different filter types, filter orders and cut-off frequencies. The findings of these comparison will be presented here. In this comparison the following aspects are investigated:

- The smoothness of the signal after filtering
- The sensitivity of acceleration peaks and jerk peaks to varying filter settings
- The effect of filtering on the energy density spectrum

Filter type

The compared filter types are the Butterworth filter, the Chebyshev I filter and the Chebyshev II filter. These filters are infinite impulse response filters (IIR filters). The Savitzky-Golay filter, a finite impulse response (FIR) filter, will be discussed separately in section 3.2. The main difference between these types of filtering is that the output of an IIR filter is based on previous output values as well as input values, while the output of a FIR filter is only dependent on input values [38].

The Butterworth filter has the smoothest frequency response, but a slow roll-off. The performance of the filter is however good, since the filtered data does not differ much with varying settings. The Chebyshev I filter has a faster roll-off, but has ripples in the passband. That means that frequencies lower than the cut-off frequency are affected as well. This effect is undesirable, since the data from the rigid body motions is in this frequency region. Also the energy density spectra of the jerk seem

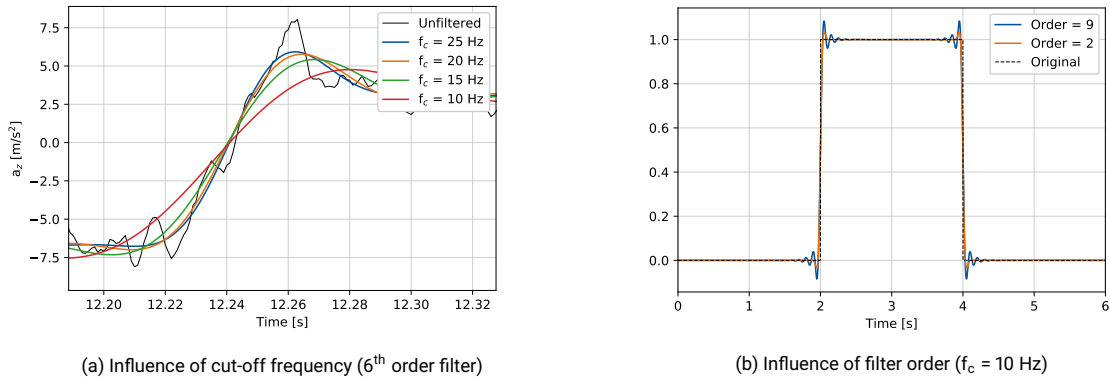


Figure 3.2: Influence of Butterworth filter cut-off frequency and filter order on signals

to be affected more than with other filters. The Chebyshev II filter also has a faster roll-off than the Butterworth filter, but has ripples in the stopband. This is more desirable than ripples in the passband. However, the cut-off frequency cannot be directly used as input for the filter settings. The settings (minimum attenuation in the stopband, critical frequency and order) do however have a big influence on the effective cut-off frequency. The output from the Butterworth filter was least sensitive for small variations in filter settings. Compared to the other filters the peak values observed in the signal changed the least with these small variations in settings. For these reasons the Butterworth filter is chosen as the best suitable filter.

Cut-off frequency

The cut-off frequency should be chosen such that the time scale of the most important events in the time trace is covered [47]. In the time traces used in the appendix to make the comparison the slamming of the model is the event with the shortest duration of approximately 0.05 seconds. This means that the cut-off frequency should not be lower than 20 Hz. In figure 3.2a an acceleration signal of the model in regular waves is shown. The used filter here is a 6th order Butterworth filter, with varying cut-off frequency. It can be seen that indeed the unfiltered signal is represented good with cut-off frequencies of 20 Hz and higher. This can also be seen in figure 3.3. In this figure the mean of the peak values of either acceleration or jerk are plotted for four data sets from chapter 5, determined with varying cut-off frequency. The data sets are not the same in the different figures, but are chosen to show different trends. It can be seen that some data sets (example 2 in figure 3.3a) are already well represented with a cut-off frequency of 5 Hz. Others are increasing until higher frequencies. In some data sets the mean of the peaks is stable, but at higher frequencies the noise is not filtered out entirely anymore, so the peak values increase again (see example 1 in figure 3.3a). The influence on the mean of the jerk peaks can be seen in figure 3.3b. The influence on the non-linearity ratio of the acceleration and the jerk (defined in chapter 4) can be seen in respectively figure 3.4a and figure 3.4b. Ideally all different parameters

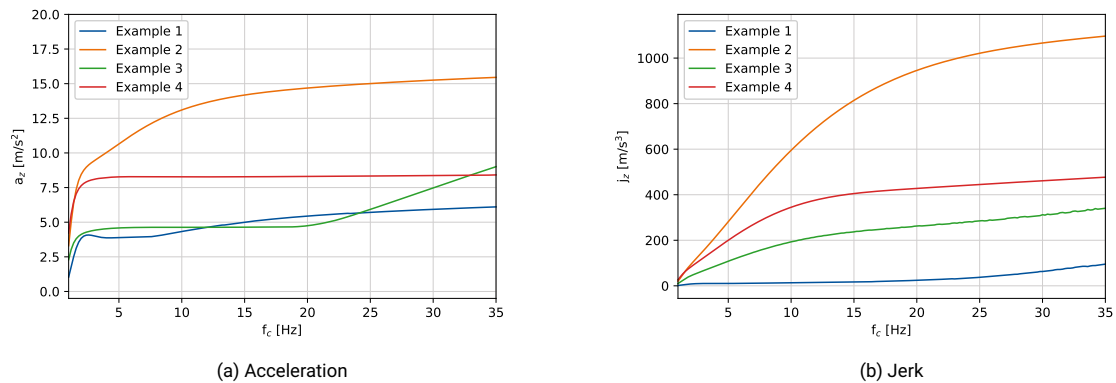


Figure 3.3: Influence of cut-off frequency on mean of peak values (6th order Butterworth filter)

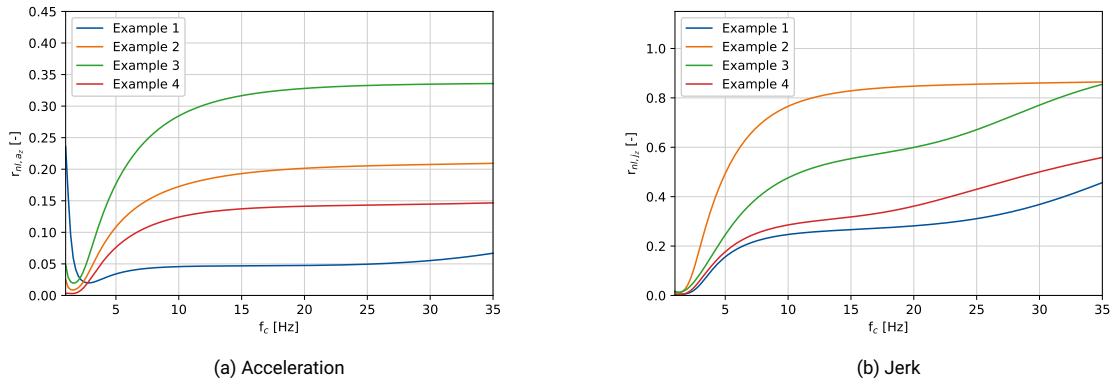


Figure 3.4: Influence of cut-off frequency on non-linearity ratio (6th order Butterworth filter)

from all different runs would be stable around a certain frequency, this then would be the ideal cut-off frequency. This is however not the case, so 20 Hz is chosen as best compromise between the different parameters. All the data sets are processed with this same cut-off frequency.

Order

The order of filtering can increase the smoothness of the filtered signal, since the roll-off in the frequency response becomes steeper. So with increasing order the amount of frequencies above the cut-off frequency in the filtered signal are decreasing. Increasing the order however also increases an effect called ringing [35]. Ringing is the presence of oscillations around a step in the response. An example of ringing with a block signal, and the increase of ringing with increasing filter order can be seen in figure 3.2b. From the comparisons of filter order in appendix B for the acceleration data it can be seen that the occurrence of ringing in the filtered measurement data is however limited. The peak values for acceleration and jerk are, except for the 2nd order filter, within a margin less than one percent. Besides that the signal becomes smoother with increasing filter order. However, increasing the order increases the energy in the energy density spectra of jerk at higher frequencies. This can be expected since the attenuation just before the cut-off frequency is less with higher filter orders. In combination with a correctly chosen cut-off frequency this effect can be limited. In this thesis a 6th order Butterworth filter will be used.

3.2 Savitzky-Golay method

In the work of Savitzky and Golay [51] a method is derived for differentiating noisy data. By calculating a least squares polynomial using a certain window length, the data is differentiated and smoothed. In Luo et al. [32] the effectiveness of this method to accurately calculate the derivative of noisy data is demonstrated. Concluded is that this method has a low noise amplification factor, especially when using higher order differentiation filters. This means that the amplification of the noise compared to the amplification of the desired signal in the derivative is low. Details in the data are well preserved, but are smoothed out more as the window length of the filter increases.

Since in this thesis the derivative of measurement data with noise has to be determined, this method of filtering and differentiating is worth investigating. The behaviour of the Savitzky-Golay method can be described as that of a finite impulse response filter (FIR filter) [52], contrary to the filters investigated in section 3.1, which are infinite impulse response filters (IIR filters).

In figure 3.6 an example of the frequency response plots of the Savitzky-Golay filter can be seen. Cut-off frequency is no input for the Savitzky-Golay method, only the order and the window length. To be able to compare the Savitzky-Golay method with the other filters, combinations of orders and window lengths are determined that are found to have certain cut-off frequencies. This is also dependent on the sampling frequency of the data set. As mentioned above the cut-off frequency is defined as the frequency where the amplitude gain first passes -3 dB, or 0.707 (unity) amplitude gain. In figure 3.6 the frequency response of a 6th order Savitzky-Golay filter with a window length of 235 is shown. With the sampling frequency of 1000 Hz, the cut-off frequency of this combination of settings is approximately 10 Hz. A full overview of cut-off frequencies can be found in table B.4 in appendix B.

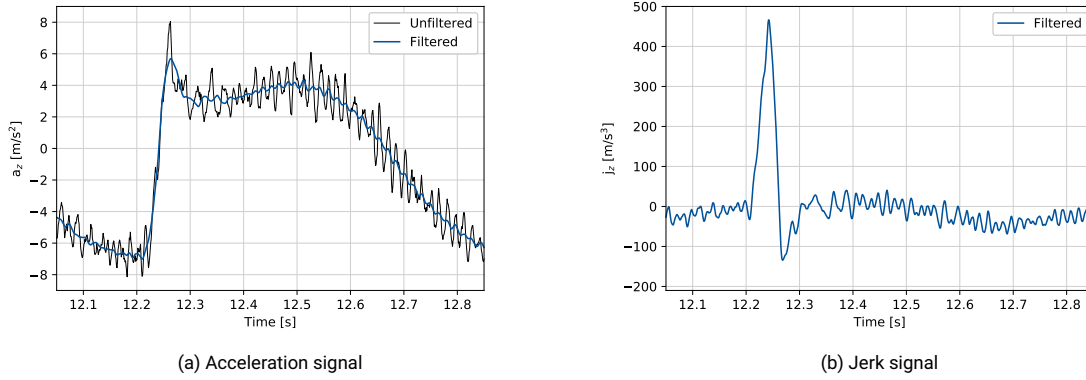


Figure 3.5: Example of signals ($f_s = 1000$ Hz) filtered with 3rd order, Savitzky-Golay filter with window length of 53

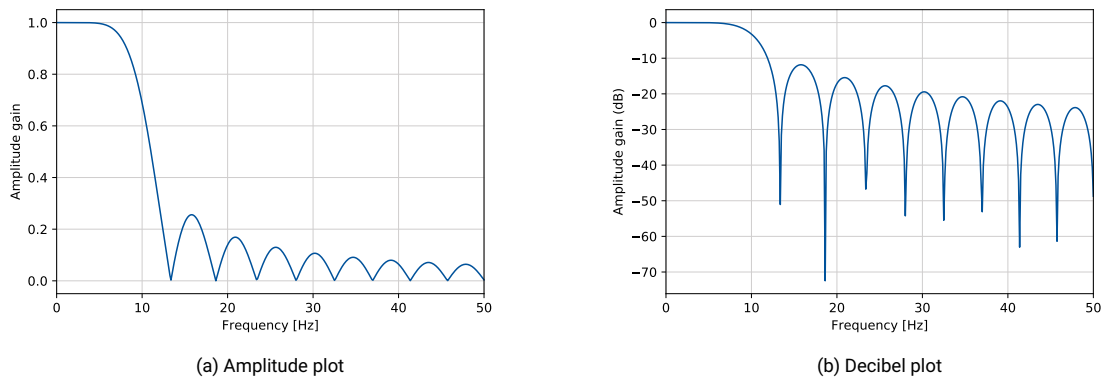


Figure 3.6: Frequency response of 6th order Savitzky-Golay filter with window length of 235 for $f_s = 1000$ Hz

From the comparison in appendix B it becomes clear that the Savitzky-Golay method shows no improvement compared to the previously discussed filters in combination with numerical differentiation. Frequencies above the cut-off frequency remain visible in the filtered and differentiated signals, see figure 3.5. This is due to the large ripples in the stopband of the frequency response of this filter, see figure 3.6. Also the peak values are affected just as much as with other methods of filtering. Another disadvantage of this method is the difficulty to determine the cut-off frequency. Since this is dependent on the sampling frequency of the data set, order of filtering and chosen window length, the method is not practical to use for the goals of this research.

3.3 Energy spectrum differentiation

The energy density spectrum of the jerk can be determined directly from the energy density spectrum of an acceleration signal, following and extending the method described in Mercer [36]. The acceleration signal is build up of a number of harmonic components. Each of these components can be represented as given in equation 3.4. The derivative of each component is calculated with equation 3.5. The change of the sine to a cosine and a possibly neglected phase lag are not important, since only the amplitude and frequency are part of the amplitude spectrum, as defined in section 2.4.

$$x_i = A_i \cdot \sin(\omega_i \cdot t) \quad (3.4)$$

$$\frac{dx_i}{dt} = A_i \cdot \omega_i \cdot \cos(\omega_i \cdot t) \quad (3.5)$$

In these equations x_i is the i -th harmonic component of the acceleration signal and dx_i/dt is the i -th harmonic component of the jerk signal. For each component A_i is the amplitude of the acceleration

and ω_i is the frequency in rad/s. This can also be represented in an amplitude spectrum for the signals. The amplitude spectrum for the acceleration can be converted to energy density spectrum of the acceleration with equation 3.6 and the energy density spectrum for the jerk with equation 3.7.

$$S_{i,acc} = \frac{A_i^2}{2 \cdot d\omega} \quad (3.6)$$

$$S_{i,jerk} = \frac{(A_i \cdot \omega_i)^2}{2 \cdot d\omega} \quad (3.7)$$

In these equations $S_{i,acc}$ is the spectral density of the i -th component of the energy density spectrum of the acceleration and $S_{i,jerk}$ is the spectral density of the i -th component of the energy density spectrum of the jerk. Furthermore $d\omega$ is the step size in the frequency range of the spectrum. Combining these equations gives the equation to directly calculate the energy density spectrum components of the jerk from the energy density spectrum components of the acceleration, see equation 3.8.

$$S_{i,jerk} = \omega_i^2 \cdot S_{i,acc} \quad (3.8)$$

In this equation ω_i is again the frequency of the i -th component in rad/s. If the spectra are in Hertz, equation 3.9 should be used.

$$S_{i,jerk} = (2\pi \cdot \omega_i)^2 \cdot S_{i,acc} \quad (3.9)$$

The advantage of this method is that the energy density spectrum of the jerk can be directly determined from the energy density spectrum of the acceleration. There are however disadvantages. Since the harmonic components, especially at higher frequencies, are multiplied with large values (the square of an high frequency), more noise can become visible than via filtering and differentiating the time signal. Therefore this method is only reliable if the source signal contains (almost) no noise. In theory this method could also be used to determine the jerk spectrum from the energy density spectrum of the velocity or displacement. However since the components then have to be multiplied by respectively ω_i^4 or ω_i^6 , even values which are approximately zero in these spectra become very large in the jerk spectrum. Therefore it is not recommended to use this method.

3.4 Requirements on measurements

The acceleration measurements need to fulfil certain requirements to be able to determine the jerk with sufficient accuracy. Sufficient accuracy here means that the 95% confidence interval of the measured values is small enough to make comparisons. This is ensured by an high signal-to-noise ratio, and the sampling frequency needs to be high enough to capture the important phenomena with a small time scale. The data used in chapter 5 and chapter 6 was measured with a sampling frequency of respectively 1000 Hz and 400 Hz. Furthermore the noise levels of the accelerometers were low enough to extract useful information for the data. No bottom line of sampling frequency or signal-to-noise ratio can be given here, only the statement can be made that the accelerometers used in these experiments provided a small enough 95% confidence interval to be able to make good comparisons between different signals.

In chapter 8 it is shown that the scale factor of time between model experiments and full scale is equal to $\sqrt{\alpha_L}$ in which α_L is the scale factor of the length. Theoretically the sampling frequency of the measurements can be scaled with $1/\sqrt{\alpha_L}$. The sampling frequency to obtain the same amount of information can thus be lower in full scale. The cut-off frequency for filtering needs to be adjusted likewise.

For the full scale measurements it is important to notice that there are likely to be more vibrations in the signal, since a full scale ship can be approximated less as a rigid body compared to a model. When analysing the ship motions it is therefore important to filter out the vibrations due to bending, whipping or other causes. Whether effects like whipping could cause large jerk peaks as well is beyond the scope of this thesis and not investigated.

4

Quantifying ship response

To be able to analyse jerk in the time traces or the jerk energy density spectra of measurements or calculations, procedures for quantifying are necessary. Because it is still unknown which method has the best correlation with for example the sense of comfort, several procedures will be given and described in this chapter.

A distinction will be made in the analysis of the response in regular or irregular waves. The response of a ship in regular waves is suitable for an analysis of the harmonics of the response. Regular waves and thus regular response is however less representative for the actual behaviour of a ship in seaway, since ocean waves are seldom regular. The procedures for quantifying response in regular waves are described in section 4.1. Also the 'ideal' response of a ship will be described in this section.

Measurements of the response of a ship in irregular waves need to be quantified differently. Often the aspects of the incoming waves are not exactly known and are approached using a spectrum. Therefore the usual way of quantifying the response in these waves is with statistics, giving a probability of exceedance for a certain response. The procedures quantifying response in irregular waves are described in section 4.2.

In section 4.3 an overview of all the definitions made in this chapter is given. Finally in section 4.4 a brief analysis on the uncertainty in the measurement values and the propagation of this uncertainty to the jerk values will be made. Also the spread of the peak values of the regular wave tests is analysed, to check if the assumption that the response is the same with each wave encounter is correct.

4.1 Quantifying response in regular waves

Analysis of the response in regular waves can be performed in a number of ways. In ship design often the peak values of responses are reviewed to quantify the response of a ship, see section 4.1.1. From preliminary literature research it became clear that non-linear effects have a large effect on the ship response. A way to quantify this non-linearity will be discussed in section 4.1.2.

4.1.1 Peak values

From the preliminary research in chapter 1 it became clear that comfort limits on motions are often defined by peak values. Therefore these will be used to quantify both acceleration and jerk.

Acceleration

Before analysis can take place first the peak values have to be defined. There are maximum values (or crests) and minimum values (or troughs). For accelerations often the crest values are investigated, since the trough values are often dominated by gravity effects [7]. The maximum values in acceleration often occur where slamming is happening and are therefore often higher and thus more limiting.

The values of acceleration for translational motions can be investigated dimensional, or can be made dimensionless using equation 4.1 as recommended by the International Towing Tank Conference [26]. In this equation L_{pp} is the length between the perpendiculars of the ship, and ζ_a is the amplitude of the wave.

$$\ddot{z}_{\text{non-dimensional}} = \frac{\ddot{z}_{\text{dimensional}} \cdot L_{pp}}{g \cdot \zeta_a} \quad (4.1)$$

The values of acceleration for rotational motions can be made dimensionless with equation 4.2. In this equation the dimensional rotational acceleration $\ddot{\theta}$ is in rad/s^2 and k is the wave number in rad/m .

$$\ddot{\theta}_{\text{non-dimensional}} = \frac{\ddot{\theta}_{\text{dimensional}} \cdot L_{pp}}{k \cdot g \cdot \zeta_a} \quad (4.2)$$

Jerk

Similar to acceleration the peak values in jerk can also be separated in maximum values (or crests) and minimum values (or troughs). Since slamming often means a rapid change in acceleration from a negative value to a positive value, maximum jerk values are to be expected at a slamming event. The negative jerk values can however not be directly linked to the presence of gravity, since gravity is a constant acceleration and thus causes no jerk.

There are no guidelines yet on obtaining a non-dimensional jerk value. Therefore the non-dimensional acceleration in equation 4.1 is expanded with the wave frequency ω . This parameter is chosen to make the jerk non-dimensional, since in a regular sinusoidal acceleration signal the amplitude of the corresponding jerk signal would be dependent on the amplitude of the acceleration and the excitation frequency. This can also be seen in equation 3.5. The definition of the non-dimensional jerk for a translational motion is given in equation 4.3, and the units that make up this dimensionless number in equation 4.4.

$$\ddot{z}_{\text{non-dimensional}} = \frac{\ddot{z}_{\text{dimensional}} \cdot L_{pp}}{g \cdot \zeta_a \cdot \omega} \quad (4.3)$$

$$\ddot{z}_{\text{non-dimensional}} = \frac{[m/s^3] \cdot [m]}{[m/s^2] \cdot [m] \cdot [1/s]} = [-] \quad (4.4)$$

The non-dimensional jerk for a rotational motion is given in equation 4.5, and the units that make up this dimensionless number are given in equation 4.6.

$$\ddot{\theta}_{\text{non-dimensional}} = \frac{\ddot{\theta}_{\text{dimensional}} \cdot L_{pp}}{k \cdot g \cdot \zeta_a \cdot \omega} \quad (4.5)$$

$$\ddot{\theta}_{\text{non-dimensional}} = \frac{[rad/s^3] \cdot [m]}{[rad/m] \cdot [m/s^2] \cdot [m] \cdot [1/s]} = [-] \quad (4.6)$$

Jerk-to-acceleration ratio

The ratio between the maximum value in the jerk and the maximum value in the acceleration is also investigated. The ratio $r_{\text{jerk-acc}}$ is defined as given in equation 4.7, and by substituting equations 4.1 and 4.3 in this equation this results in equation 4.4.

$$r_{\text{jerk-acc}} = \frac{j_{\text{non-dimensional}}}{a_{\text{non-dimensional}}} \quad (4.7)$$

$$r_{\text{jerk-acc}} = \frac{j_{\text{dimensional}}}{a_{\text{dimensional}} \cdot \omega} \quad (4.8)$$

If the system would be linear, the response functions of acceleration and jerk would be as given in respectively equations 4.9 and 4.10.

$$a = A \cdot \sin(\omega \cdot t + \epsilon) \quad (4.9)$$

$$j = \frac{da}{dt} = \omega \cdot A \cdot \cos(\omega \cdot t + \epsilon) \quad (4.10)$$

The maximum values of these response functions are the amplitudes of the harmonic, so A for the acceleration and $\omega \cdot A$ for the jerk. Filling in these values in the ratio $r_{\text{jerk-acc}}$ in equation 4.8 leads to the conclusion that this ratio will always be 1, if the ship response to a regular wave is linear. Therefore this ratio might be an indication of how non-linear the response is. The importance of this will be explained more in section 4.1.2.

4.1.2 Non-linearity ratio

From the researches of Keuning [29] and de Jong [7] it follows that the motions become increasingly non-linear with increasing speed and wave height. Especially the accelerations are found to be highly non-linear. This is because of the exponential growth of all higher order responses. To demonstrate this the amplitudes of the harmonic components of the derivatives of equation 4.11 are given in table 4.1. Only the amplitudes of the harmonic components are given. The phase difference, and thus the difference between sine and cosine in the derivatives is left out since this has no effect on the amplitude.

$$x_i(t) = A_1 \cdot \sin(\omega \cdot t) + A_2 \cdot \sin(2\omega \cdot t) + A_3 \cdot \sin(3\omega \cdot t) \quad (4.11)$$

Table 4.1: Exponential growth of amplitudes of higher order components

Derivative	First order	Second order	Third order
0 (displacement)	A_1	A_2	A_3
1 (velocity)	$\omega \cdot A_1$	$2\omega \cdot A_2$	$3\omega \cdot A_3$
2 (acceleration)	$\omega^2 \cdot A_1$	$4\omega^2 \cdot A_2$	$9\omega^2 \cdot A_3$
3 (jerk)	$\omega^3 \cdot A_1$	$8\omega^3 \cdot A_2$	$27\omega^3 \cdot A_3$

As can be seen all the higher order components of the response increase exponentially over the derivatives. Therefore the total amount of energy of the non-linear response (called 'non-linear energy' here) also follows an exponentially growing trend. Therefore a procedure of quantifying the amount of non-linear behaviour has been investigated in the scope of this thesis. This is defined in the non-linearity ratio r_{nl} , see equation 4.12, equation 4.13 and equation 4.14.

$$r_{nl} = \frac{m_{0,non\ linear}}{m_{0,total}} \quad (4.12)$$

With:

$$m_{0,non\ linear} = \int_{1.5 \cdot \omega_e}^{\infty} S_{x_i}(\omega_e) d\omega \quad (4.13)$$

$$m_{0,total} = \int_0^{\infty} S_{x_i}(\omega_e) d\omega \quad (4.14)$$

In this equation ω_e is the excitation frequency, so the encounter frequency of the ship with the waves. The value $m_{0,non\ linear}$ is the integral of the energy density spectrum starting from 1.5 times the excitation frequency. This integral is thus the amount of energy in the energy density spectrum that is in higher orders than the first order, the non-linear energy. The split between linear and non-linear energy at 1.5 times the excitation frequency is chosen because it is halfway between the first order response and the second order response. Therefore if the encounter frequency is slightly off or there is small variation in the encounter frequency and the energy in the spectrum is thus slightly spread to surrounding frequencies, the energy is still captured as linear or non-linear. For an example see figure 2.8b, where the split would thus be made just below 10 rad/s.

The non-linearity ratio can be determined for both the acceleration and the jerk. It is a dimensionless number, but does not give an indication on the magnitude of the response. The response can be highly non-linear, but very small and thus not very uncomfortable. It is therefore not expected that the non-linearity ratio in itself is a good indicator for the comfort on a ship, but it might be a useful addition to the acceleration or jerk values.

In appendix A it is mathematically proven that the non-linearity ratio is a measure how much the time trace of the response does not fit a sine function. Also it is proven that this is the opposite of the r^2 -value (the coefficient of determination), see equation 4.15. The coefficient of determination is thus a measure of how linear the time trace of a response is.

$$r_{nl} = 1 - r^2 \quad (4.15)$$

4.1.3 'Ideal' response

From the research of Keuning [29] it follows that the impact of the bow in waves and the accelerations coming from that are severely affecting the comfort on board of ships. These events are highly non-linear. Now often acceleration levels are used to assess the comfort on ships, but following from the above statement the assumption can be made that the amount in which the ship responses are non-linear might also have an influence on the experience of (dis)comfort in a ship.

The linear response of a ship is the result of the geometric parameters (for example length, breadth and draft) and hydrostatic parameters (for example displacement and longitudinal position of the centre of gravity) [27], and is therefore always present. The ship responses cannot be altered much without drastically changing the properties of a ship. The non-linear response of a ship, the higher order responses, can however be minimised. It is therefore also stated in de Jong [7] that the more optimised a ship is, the more linear the response is. This also supports the investigation of the non-linearity ratio defined in section 4.1.2 as a measure of the comfort of a ship. If the ship response would be completely linear, the non-linearity ratio would be zero. The coefficient of determination r^2 would be 1, since the linear response of the ship to a regular wave is also a sine function.

4.2 Quantifying response in irregular waves

If the ship is in irregular waves, quantifying the response is not so straightforward anymore. Since the wave pattern and thus the response spectrum is assumed to be a superposition of a number of regular waves, there is not one peak value anymore. The linear response of a ship in irregular waves has been described in section 2.2.4. In the case of linear response the response can be represented with significant values, as described in section 4.2.1.

The behaviour of a ship in irregular waves can however also be non-linear, for example with fast, planing boats. The extensive research of Fridsma [14] into the behaviour of fast boats in irregular waves lead to the conclusion that the vertical accelerations are random and highly non-linear in relation to the wave elevation [7, 18]. In these cases the only way described in literature to investigate the behaviour of a ship is with statistics, using for example probability plots and values for probability of exceedance of a certain value. This will be discussed in section 4.2.2.

4.2.1 Significant value

In the analysis of irregular seas usually the assumption can be made that the wave elevation is Gaussian distributed along a zero mean level [27]. In this case all the statistical properties of the wave elevation can be derived from the energy density spectrum of the waves [19]. If the response of a ship is linear, this means that the response spectrum (see section 2.2.4) has these same statistical properties.

The standard deviation σ (or root mean square) can be determined, see equation 4.16. The root mean square can also be determined from the zeroth order moment of the energy spectrum m_0 , see equation 4.17 and equation 4.18.

$$\sigma = \sqrt{\frac{1}{N-1} \cdot \sum_{n=1}^N \zeta_n^2} \quad (4.16)$$

$$m_0 = \int_0^{\infty} S_{\zeta}(\omega) d\omega \quad (4.17)$$

$$\sigma = \sqrt{m_0} \quad (4.18)$$

In wave statistics the significant wave height is the mean value of the highest one-third of waves [19]. The significant wave height is four times the root mean square, see equation 4.19. The significant value for a ship response can be found likewise. This is the mean of the one-third highest maximum to minimum (crest to trough) values, the significant double amplitude (SDA) value.

If the surface elevation or ship response is described as a Gaussian distribution, the amplitudes of the waves or the amplitudes of the motion response can be described using a Rayleigh distribution. Using

this Rayleigh distribution the maximum wave height or maximum response can then be determined. Theoretically this would be infinity, but usually the maximum is defined as the once every 1000 peak value [27]. This is approximately twice the significant value, see equation 4.20.

$$H_{1/3} = 4 \cdot \sigma = 4 \cdot \sqrt{m_0} \quad (4.19)$$

$$H_{\max} = 1.86 \cdot H_{1/3} \approx 2 \cdot H_{1/3} \quad (4.20)$$

4.2.2 Probability of exceedance

If the response of a ship becomes non-linear with respect to the wave spectrum, the statistical values described in section 4.2.1 are not representative anymore for the behaviour of the ship. This is because the amplitudes of the non-linear ship response are not Rayleigh distributed anymore. The occurrence of peaks can also not be predicted anymore by applying the superposition principle on the response to regular wave components [7].

The non-linear (random) character of the ship responses makes it necessary to analyse sufficient data to come to a valid representation of the ship behaviour in terms in probabilities of exceedance. In the case of model tests this might mean that multiple runs are necessary to obtain a sufficient amount of data. The recommendation of the International Towing Tank Conference [26] is to have at least 200 wave encounters.

When sufficient data is available the crests (or troughs) can be analysed. The probability of exceedance of a the value of a certain crest is calculated with equation 4.21. In this equation X is a data set with N values for the crest values, sorted from small to large. The calculated probability $P(X_i)$ is the chance that the i-th element of the data set is exceeded.

$$P(X_i) = \frac{i}{N+1} \quad (4.21)$$

An important factor in calculating the distributions is determining a method for identifying the crests or troughs in measurement data. In de Jong [7] two different methods were proposed. The first one made the assumption that between two zero-crossing there could only be one crest or trough, and the crest or trough should exceed a certain threshold value based on the standard deviation of the data. The second method stated that the time lag between two crests or troughs should be at least 0.5 seconds. It was assumed that the relevant rigid body motions that were studied would not appear in a higher frequency than that. In de Jong [7] the second method was chosen. The probabilities in the higher part of the Rayleigh plot were found to be almost identical, while in the lower part the results were less distorted. In section 4.2.3 these methods will be compared to see which if the second method is also the best choice when analysing jerk in the ship motions. A correctly determined distribution of the crests and troughs is also important when trying to fit a certain mathematical distribution through the data [57].

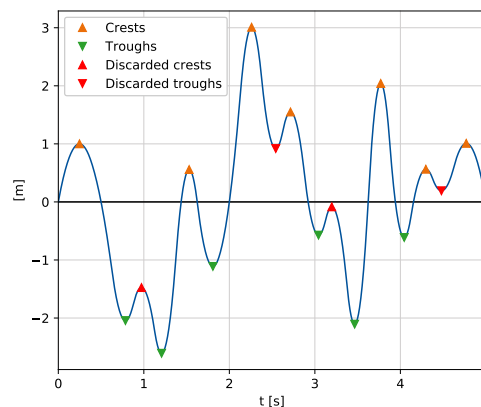


Figure 4.1: Example of crests and troughs

This will not be done in this thesis, so here it is only important that the same procedures are applied to all the data to be able to make a qualitative comparison.

Also a local maximum that is negative, or local minimum which is positive are discarded as respectively crest or trough, see the example time trace in figure 4.1. This means that the assumption is made that each crest should be positive and each trough should be negative.

4.2.3 Rayleigh plots

A useful way to plot the probability of exceedance is in a Rayleigh plot, see figure 4.2. For example, the chance that the amplitude of a crest in the acceleration is higher than 20 m/s², is approximately 15%, as also indicated in the figure. The Rayleigh plot is a plot where the horizontal axis is changed in such a way that a Rayleigh distribution will appear as a straight line in the plot. This is done using equation 4.23. As stated in section 4.2.2 the response of a ship in irregular waves would follow an Rayleigh distribution if approximated well by the linear approach. The crests and troughs would then appear as a straight line in the Rayleigh plot. From the fact that the crests and troughs are far from a straight line in figure 4.2 it can be concluded that the response is highly non-linear.

In figure 4.2 also the probability of exceedance is plotted for a Rayleigh distribution with a significant double amplitude (SDA) calculated with equation 4.19, which would be the response if it was a linear response and the same amount of energy would be in the energy density spectrum. It can clearly be seen that the Rayleigh distribution based on the SDA is not representative for the actual response of the ship. The lower crest values seem to follow the linear response, but especially the higher crest values are significantly higher.

The probability of exceedance of a certain amplitude (with value a) according to a Rayleigh distribution is calculated with equation 4.22 [7]. Inverted, the amplitude that is exceeded with a certain probability as input is calculated using equation 4.23.

$$P(x_a > a) = \exp\left(-\frac{a^2}{2\sigma^2}\right) \quad (4.22)$$

$$a = \sigma \cdot \sqrt{-2 \cdot \ln(P(x_a > a))} \quad (4.23)$$

As mentioned in section 4.2.2 the procedure of identifying the crests and troughs has an influence on the Rayleigh plots. This can be seen in figure 4.3. Method 1 is the first method explained in section 4.2.2 with the threshold value. Method 2 is the method with a minimum time gap between two subsequent crests or troughs. The methods are applied on the vertical jerk corresponding to the data in figure 4.2. Only the crest values are plotted, as a line instead of markers, to better show the difference. In de Jong [7] it was concluded that method 2 worked better. This method is found to be working better for jerk

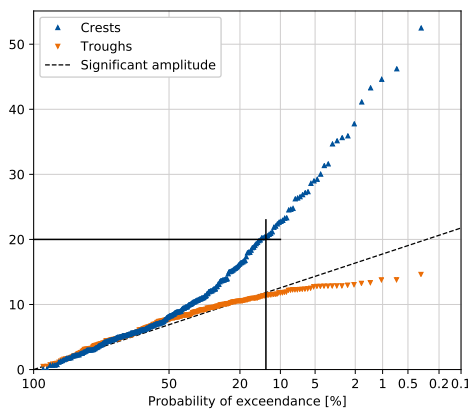


Figure 4.2: Example of Rayleigh plot

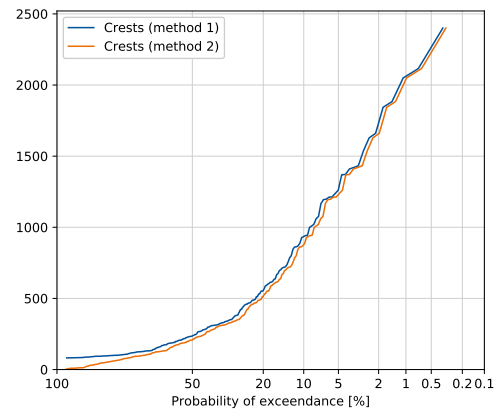


Figure 4.3: Comparison of methods for identifying crests

as well. The methods give the same probabilities in the higher part of the Rayleigh plot. In the lower part method 2 goes to zero at 100% probability of exceedance, while method 1 states the chance that a crest value of 100 m/s^3 is 100%. Therefore method 1 is chosen for this research as well for identifying the peaks and troughs.

The probabilities of exceedance determined in this chapter are sensitive for first the filtering of the measurement data and then applying the method of crest and trough identifying. Therefore there might be a difference between the calculated probability and the actual probability. The calculated values can however be used to qualitatively compare different designs or different conditions, if the same processing is applied to the different data sets. With the qualitative comparison it is possible to say that the probability of exceedance of a certain value is higher for one ship than for the other.

4.2.4 Non-linearity

A different method than using statistics to quantify the non-linear response of a ship in irregular waves is applying the theory of the non-linearity ratio (section 4.1.2). However, there is no analogy with the correlation of a sine fit anymore, since fitting a sine is not possible through irregular waves. It can however be an indication of the non-linearity in the ship response.

Instead of a first order peak and higher order peaks in the energy density spectrum, there is now a response spectrum with higher order energy, see figure 4.4. From the energy density spectrum of the displacement motions it can be determined where the first order roughly ends, since the motion is (almost) completely first order response. For the data sets used in this thesis a good estimation to make the split between first order energy and higher order energy is at 1.7 times the peak frequency of the spectrum. This is an estimation, since there are already higher orders for the low frequencies at the side that is now quantified as first order energy. It is however impossible to separate this any further. The non-linearity ratio is thus for the response in irregular waves an estimation. It might be useful to compare different ships, if determined in the same conditions with the same procedures.

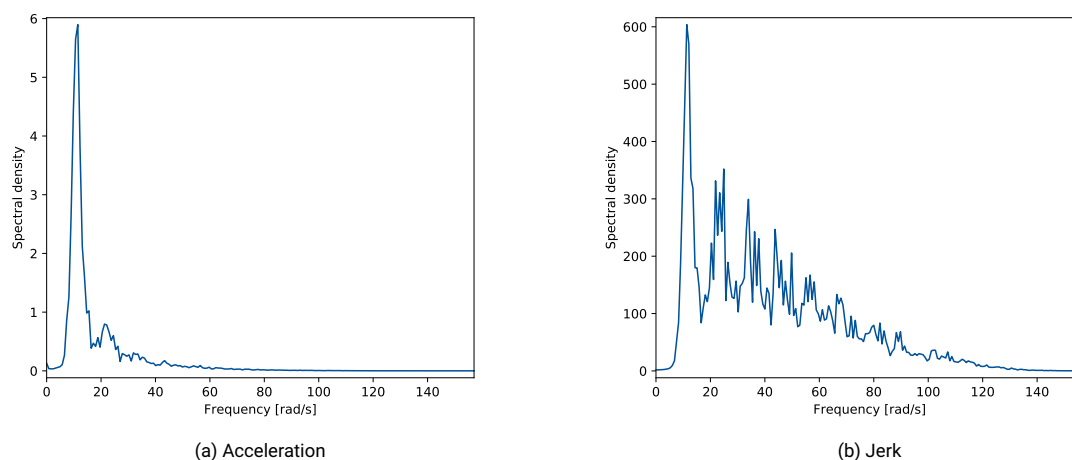


Figure 4.4: Example of energy density spectrum of response in irregular waves

4.3 Overview of definitions

In this chapter a number of definitions and explanations have been given that are crucial for the understanding of the remaining part of this thesis. Therefore a short summary of these definitions is given in table 4.2.

Table 4.2: Overview of the used terms and their definitions

Term	Definition
Linear response	Linear response means that there is only a first order response of a ship to the disturbant waves or wave spectrum. The effect from this is that there is for every wave frequency a linear relation between the wave (spectrum) and the response (spectrum), and the response is thus at the same frequency or in the same frequency spectrum as the wave (spectrum).
Non-linear response	The response of a ship is non-linear if there is a response at the excitation frequency of the waves, and one or more multiples of this frequency. If the disturbant waves are part of a wave spectrum, there can be energy in the response spectrum at multiples of all the frequencies in the wave spectrum.
First order response	The part of the response of the ship that is at the same frequency as the disturbant wave (spectrum), is the first order response. A response that is (mainly) first order can be slightly non-linear, but is dominated by the first order response. Therefore the response is very similar to a response determined with the linear assumption.
Higher order response	The part of the response of the ship that is at multiples of the frequency of the disturbant wave (spectrum).
First order energy	The amount of energy in the energy density spectrum that is at the frequency or frequency spectrum of the disturbant wave or wave spectrum.
Higher order energy	The amount of energy in the energy density spectrum that is at multiple(s) of the excitation frequency (spectrum). Since there is no energy in the wave spectrum at these frequencies, it must come from non-linear response of the ship to the wave (spectrum).
Sine fit	The sine fit is a single harmonic function, fitted with a least squares method the response time trace. The frequency of this function is equal to the encounter frequency, and the amplitude, phase and offset are determined to have the best correlation with the response time trace. Only applicable in regular waves.
Coefficient of determination (r^2 -value)	The coefficient of determination is a measure for the correlation between the response time trace and the sine fit. As proven in appendix A this is a measure for how linear the response is, which part of the response comes from the first order response. Only applicable in regular waves.
Non-linearity ratio	The non-linearity ratio is the ratio of the higher order energy in the energy density spectrum of the response to the total amount of energy in the energy density spectrum. As proven in appendix A the non-linearity ratio is the opposite of the r^2 -value (in regular waves) and therefore a measure of how non-linear the response is, which part of the response comes from the higher order response(s). In irregular waves a sine fit is not possible, but the non-linearity ratio then gives an indication of how non-linear the response is.

4.4 Uncertainty

In the measurements that are going to be compared in the next chapters there is uncertainty in the measurement data. The total uncertainty is defined as a composition of the precision error and the bias error [7]. The precision error is the spread of a measured value around a certain mean value. The bias is the distance between the true value and the mean value of the measurements. These errors are a result of for example measurement errors, accuracy of instruments and uncertainties in the environment or model. A more detailed assessment of uncertainty can be found in appendix D of de Jong [7] or in the guidelines of the International Towing Tank Conference [24].

For this research the exact values are of less importance, because comparisons are going to be made qualitatively. It is however needed to have an approximation of the uncertainty, since than with certainty can be said if one value is indeed larger than the other. Therefore a simplified uncertainty analysis will be performed in this section.

4.4.1 Uncertainty individual peaks

In the doctoral thesis of de Jong [7] an extensive derivation of the uncertainty in the measurements also used in chapter 5 and chapter 6 is performed, by determining a 95% confidence interval. In this thesis a simplified approach will be used. To determine the same confidence interval for the jerk, the propagation of the uncertainty through differentiation is determined. As already mentioned in the introduction of chapter 3, the error introduced through numerical differentiation consists of the truncation error and the measurement error. In the method used in this report, central differentiation, the truncation error is of order Δt^2 , where Δt is the time step in the measurements [59]. The regular wave experiments used in chapter 5 were performed at 1000 Hz (so a time step of 0.001 seconds), the irregular wave experiments used in chapter 6 at 400 Hz (so a time step of 0.0025 seconds). The truncation error is therefore assumed to be negligible.

The uncertainty as defined by de Jong [7] can be defined as a measurement error and thus propagates through differentiation as defined in equation 4.24.

$$U_{jerk} \leq \frac{U_{acc}}{\Delta t} \quad (4.24)$$

In this equation U_{acc} is the uncertainty in the acceleration value, U_{jerk} is the uncertainty in the jerk value. It can be seen that according to this definition the uncertainty in the jerk would become very large because of the small time steps in the measurements. In chapter 3 it was however argued that the event with the smallest time scale, slamming, was 0.05 seconds and that the data should thus be filtered at 20 Hz. Because of the filtering it is thus not representative anymore to define the time step in equation 4.24 with the inverse of the sampling frequency. Since all events with a time scale smaller than 0.05 seconds are filtered out, this value will be used to determine the propagation of uncertainty through the numerical differentiation.

The uncertainty for individual acceleration peaks at the bow is defined in de Jong [7] as 0.884 m/s² for the ESC and 0.877 m/s² for the AXE. In this report that uncertainty is approximated as 0.88 m/s². Using equation 4.24 and the assumption for the time step the uncertainty in the individual jerk peaks at the bow is then 17.6 m/s³. The uncertainty of individual peaks at the centre of gravity is lower, but not defined. In figure 4.5a and figure 4.5b the mean acceleration and jerk levels with error bars are plotted for the ESC. The error bars indicate the 95% confidence interval. In these figures the results of tests (with model speed $v_s = 2.876$ m/s) in regular waves with varying wave steepness κ are plotted. These tests will be discussed further in chapter 5.

$$U_{acc,bow} = 0.88 \text{ m/s}^2 \quad (4.25)$$

$$U_{jerk,bow} = 17.6 \text{ m/s}^3 \quad (4.26)$$

In the research of de Jong [7] more uncertainties are included. In this report these uncertainties are assumed to be small or constant, and are neglected for simplification reasons. As mentioned before determining the exact value is of less importance, since mostly qualitative comparisons will be made.

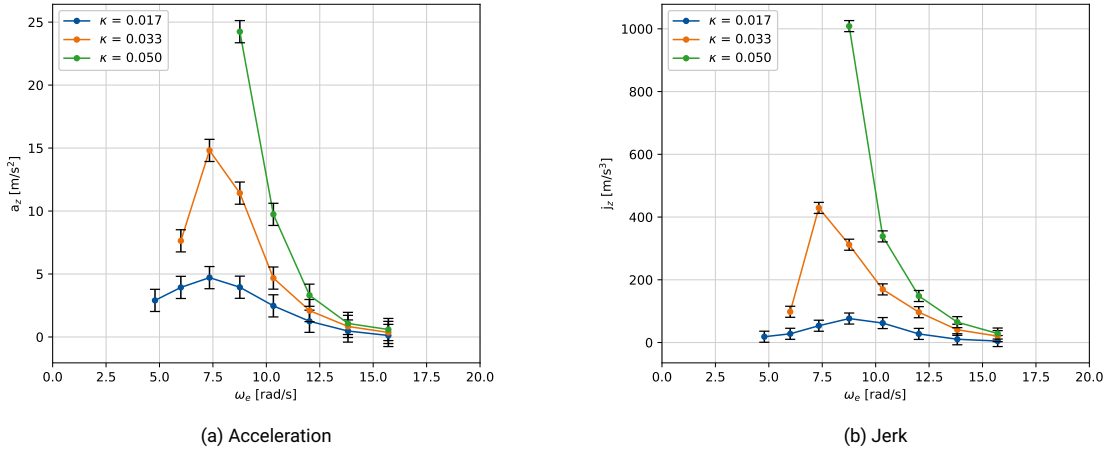


Figure 4.5: Crest values with error bars, ESC, bow, $v_s = 2.876$ m/s

It can be seen that for both the acceleration and the jerk the uncertainty is low enough to make reasonable qualitative conclusions about them. The uncertainty in the measurements will not be treated furthermore in this report, but all the comparisons were made considering this uncertainty. If values fall within the uncertainty window of each other, no statements will be made that one or the other is larger or smaller.

4.4.2 Spread of peak measurements

In the analysis of the regular wave experiments in chapter 5 single values are used as maximum or minimum value in for example the accelerations. It is however important to investigate if this single value is a good representation for the behaviour of the model in an experiment. Theoretically the response should be the same with each wave encounter, so the spread in the maximum or minimum values should be low. All the crest values of the heave acceleration and heave jerk are plotted per wave frequency as a box plot in respectively figure 4.6 and figure 4.7. In these figures the spread of the values can be seen for both models used in the tests, the AXE and the ESC. The trough values of the pitch acceleration and pitch jerk per wave frequency are visualised as box plot in respectively figure 4.8 and figure 4.9. The crest values for the heave and the trough values for the pitch are presented because these are often limiting, as will be explained further in chapter 5.

In all the figures it can be seen that the spread of the values is very low. The assumption that the response is the same with each wave encounter is thus valid. Therefore the mean value of the crests or troughs per measurement is used in chapter 5 to make comparisons.

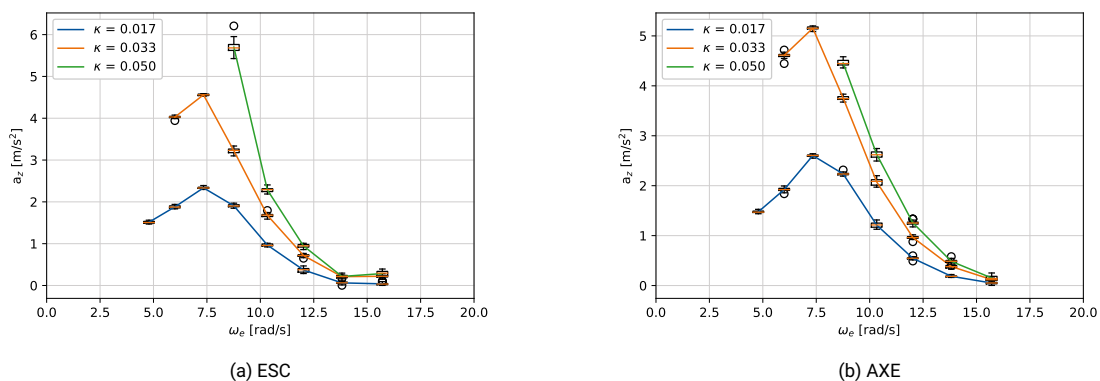


Figure 4.6: Box plots crests heave acceleration, $v_s = 2.876$ m/s

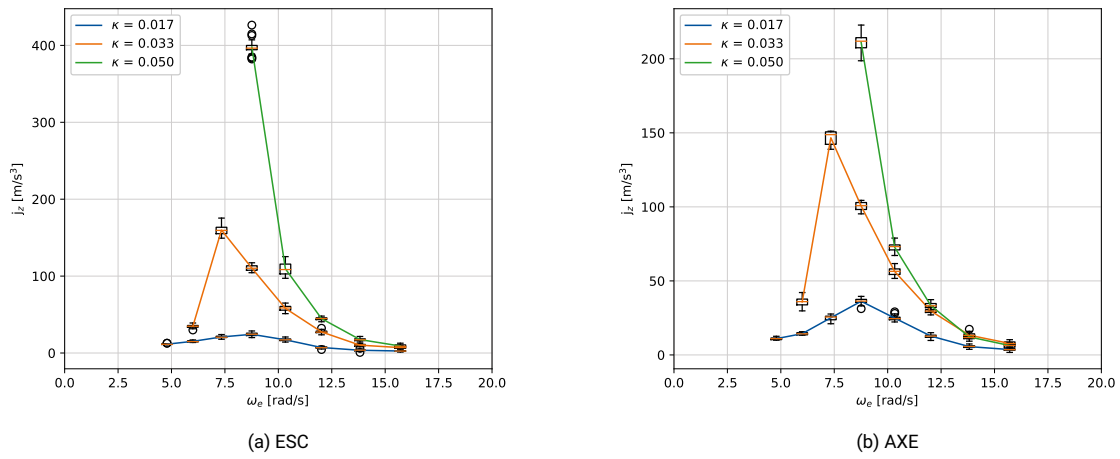


Figure 4.7: Box plots crests heave jerk, $v_s = 2.876$ m/s

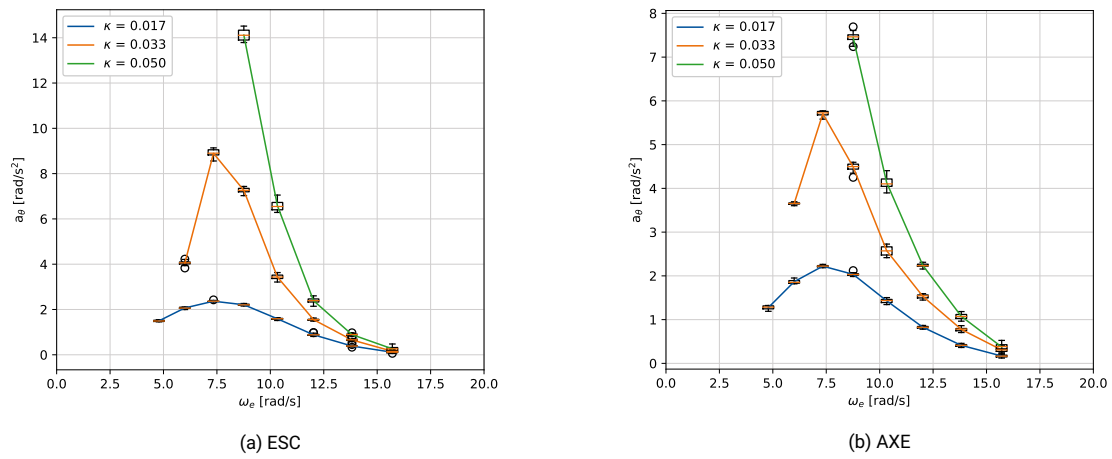


Figure 4.8: Box plots troughs pitch acceleration, $v_s = 2.876$ m/s

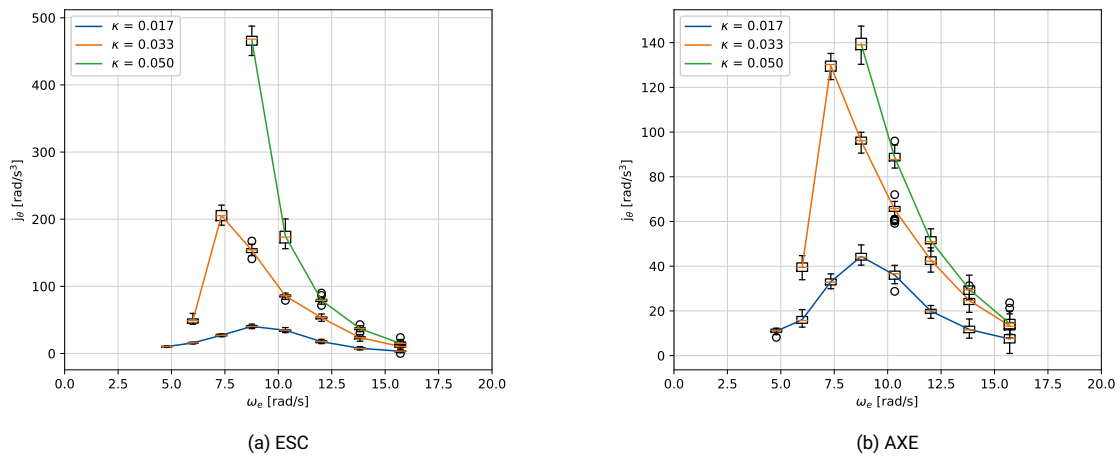


Figure 4.9: Box plots troughs pitch jerk, $v_s = 2.876$ m/s

Fast models in regular head waves

In this chapter the jerk in the response of model tests in regular waves will be investigated. The model tests were performed in the FAST II research project [7]. Tests were performed with two hull types: one with an axe bow, and one based on the enlarged ship concept. In section 5.1 more specifics of the performed tests will be given. Next in section 5.2 comparisons will be made of the two hulls in different conditions to see what the difference of the hulls in terms of jerk behaviour is, and what the influence of different parameters on the jerk response is. These comparison methods will also be used in section 5.3 where the difference in jerk over the length of the ship will be investigated.

5.1 Introduction

The towing tank tests in regular waves were performed with models with a length of 2.75 m, based on the axe bow concept (AXE) and the enlarged ship concept (ESC). A schematic view of the hull shapes of these models can be seen in figure 5.1. The tests were performed in a larger scope to investigate the seakeeping behaviour of fast vessels, see the doctoral thesis of de Jong [7] for more information on this subject. Since the behaviour of fast vessels was investigated, the tests were performed with a (full scale) speed of 25 knots and 35 knots. Converted to the 1:20 model using Froude scaling this means respectively a speed (v_s) of 2.876 m/s and 4.026 m/s. For details on Froude scaling see chapter 8. The Froude numbers associated with these speeds and the length of the model are 0.554 and 0.775. Based on these Froude numbers the ships are in a semi-planing regime [9]. In all the tests the vertical accelerations at the centre of gravity (CoG) and the bow were measured. Also the motions at the centre of gravity were measured.

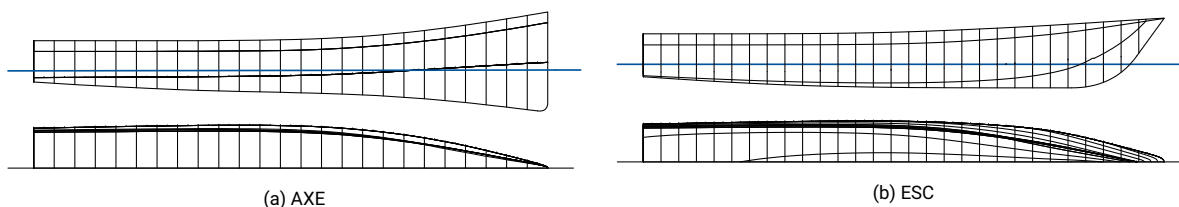


Figure 5.1: Schematic view of the models used in the tests, from de Jong [7]

Wave frequencies

The tests were performed with wave frequencies ranging from 2.68 rad/s to 5.81 rad/s. The encounter frequency ω_e of the models with these waves is calculated with equation 5.1. In this equation ω is the frequency of the waves, v_s is the speed of the ship and g is the gravitational acceleration. This equation is valid for head waves. The non-dimensional frequency ω_{nd} , which can also be used to compare the behaviour of the models, is calculated with equation 5.2. In this equation L_{wl} is the waterline length of the ship. An overview of the different wave frequencies can be seen in table 5.1. In this thesis the dimensional encounter frequency is used, contrary to the report of de Jong [7] where the non-dimensional frequency is used. To be able to compare the different reports the non-dimensional frequencies are also given here.

$$\omega_e = \omega + \frac{\omega^2 \cdot v_s}{g} \quad (5.1)$$

$$\omega_{nd} = \omega \cdot \sqrt{\frac{L_{wl}}{g}} \quad (5.2)$$

Table 5.1: Overview of the wave frequencies used in the model tests

ω [rad/s]	ω_e (2.876 m/s) [rad/s]	ω_e (4.026 m/s) [rad/s]	ω_{nd} [-]
2.68	4.79	5.63	1.42
3.13	6.00	7.15	1.66
3.58	7.34	8.84	1.90
4.02	8.76	10.65	2.13
4.47	10.33	12.67	2.37
4.92	12.02	14.85	2.60
5.37	13.82	17.20	2.84
5.81	15.71	19.66	3.08

Wave steepnesses

The model tests were performed with constant wave steepness ratios κ of 1/60, 1/30 and 1/20. The wave steepness ratio is defined as given in equation 5.3. In this equation ζ_a is the wave amplitude λ is the wave length. An overview of the wave frequencies and the corresponding wave amplitudes are given in table 5.2.

$$\kappa = \frac{2 \cdot \zeta_a}{\lambda} \quad (5.3)$$

The consequence of constant wave steepness is that the wave amplitude is different at each frequency. To compare the responses the measurements have to be corrected for this, using the non-dimensional numbers given in section 4.1. The advantage of constant wave steepness is that the non-linear effects (for example wave breaking) due to increasing wave steepness in a constant wave amplitude test are avoided. The disadvantage is that at high wave frequencies, the wave amplitudes are small. Therefore the signal-to-noise ratio of the measurements decreases, making it harder to accurately process them.

Table 5.2: Overview of the wave amplitudes used in the model tests

ω [rad/s]	ζ_a [mm]		
	$\kappa = 1/60$	$\kappa = 1/30$	$\kappa = 1/20$
2.68	71	130	-
3.13	52	105	-
3.58	40	80	120
4.02	32	63	95
4.47	26	51	77
4.92	21	42	64
5.37	18	36	54
5.81	15	30	46

Time traces and slamming

In this chapter references will be made to time traces. These time traces with the corresponding energy density spectra for the acceleration and jerk can be found in appendix C. Also there will be referred to first order dominated response, or slamming that is visible in the time traces. An example of what is referred to as first order response can be seen in figure 5.2. The acceleration and the corresponding jerk (although noisy) look like a sine function, and are thus dominated by the linear response to the disturbant wave.

An example of slamming can be seen in figure 5.3. The acceleration suddenly changes from negative to positive, and the sine fit is less good than with the first order dominated example. In the jerk it can be seen that part of the time trace follows the sine fit, but there is a sudden impulse due to the slamming. A more detailed analysis of the ship response when slamming occurs can be found in section 7.2.4.

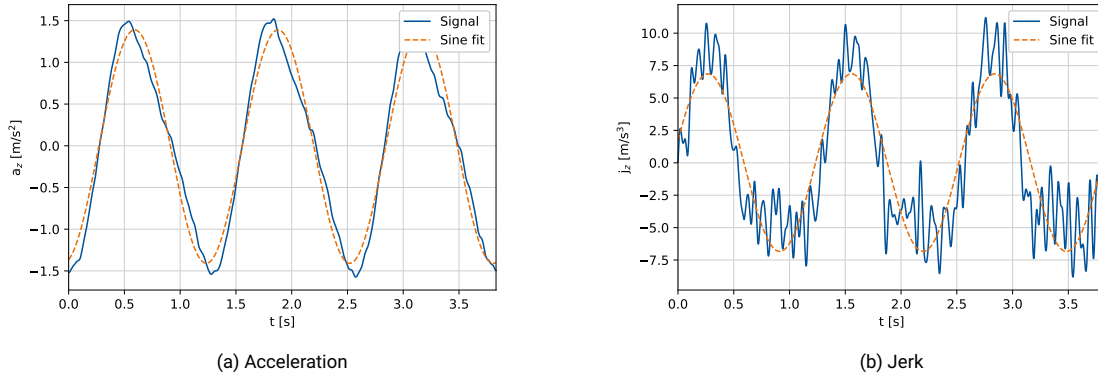


Figure 5.2: Time traces, ESC, centre of gravity, $v_s = 2.876$ m/s, $\omega_e = 4.79$ rad/s, $\kappa = 0.017$

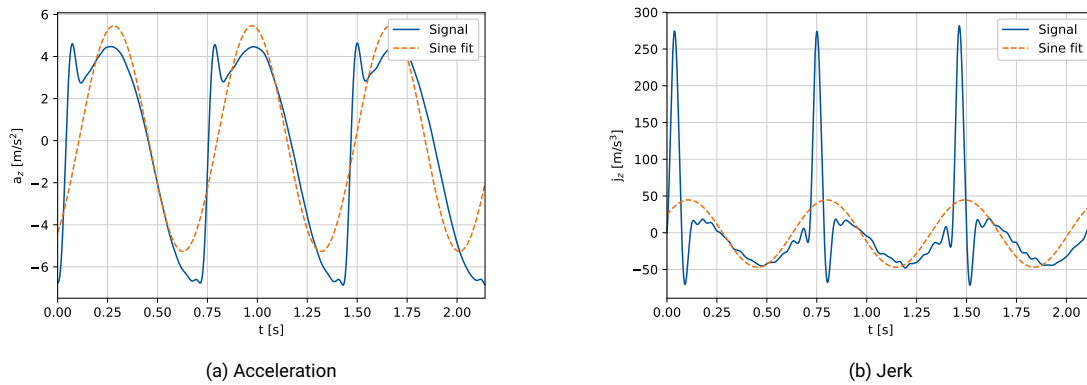


Figure 5.3: Time traces, ESC, centre of gravity, $v_s = 4.026$ m/s, $\omega_e = 8.84$ rad/s, $\kappa = 0.033$

5.2 Comparison

In this section the response of the two different hulls is compared. This will be done on the basis of wave frequency, wave steepness and forward speed. In most of the comparisons the measurements of the 25 knots tests (model speed $v_s = 2.876$ m/s) were used, since more data was available from these tests. Only in the comparison of the influence of forward speed the 35 knots (model speed $v_s = 4.026$ m/s) data will be used. The values that will be compared are the acceleration crests, the jerk crests and the non-linearity ratio. The acceleration crests, although not directly the scope of this thesis, are included to see if a comparison based on the jerk would give different results in terms of which hull performs better at certain conditions.

5.2.1 Hull types

Acceleration peaks

The maximum (non-dimensional) vertical acceleration of both the ESC and the AXE can be seen in respectively figure 5.4a and figure 5.4b. The acceleration crest value is made non-dimensional using equation 4.1. The obtained values are plotted against the encounter frequency of the ship with the waves, for each wave steepness.

For both hull types the natural frequency is clearly visible in the plots, with the peak around 8 rad/s. Most of the tests were performed at frequencies higher than the natural frequency. The values for the acceleration clearly decrease with increasing frequency, for both hull types. The accelerations at the centre of gravity are slightly higher for the AXE than for the ESC. Looking at the time traces of the response it can clearly be seen that the response is mainly first order, see time traces 1 and 2 in appendix C. The first order heave amplitude of the AXE bow is higher than the heave amplitude of the ESC, resulting in higher accelerations, see figure 5.6. In this figure the RAO of the heave displacement

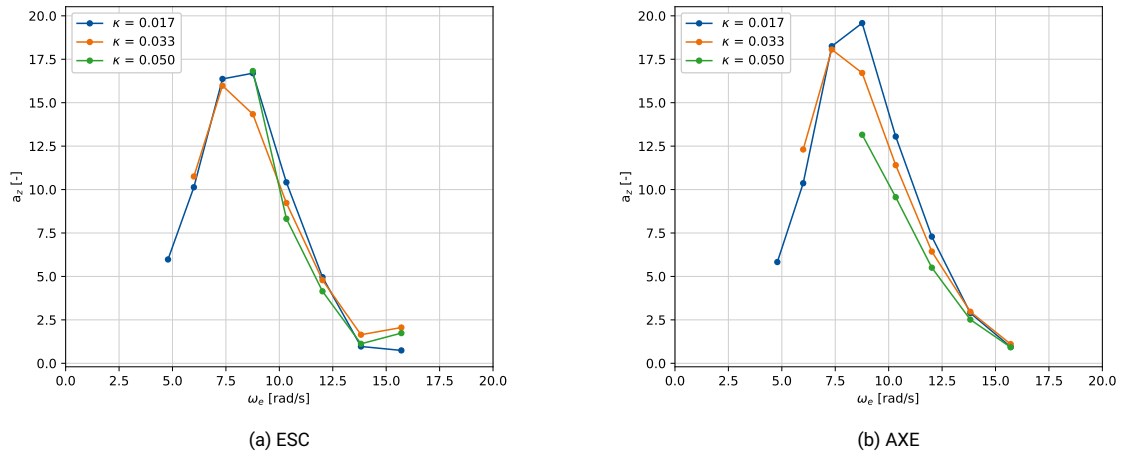


Figure 5.4: Maximum vertical acceleration (non-dimensional), centre of gravity, $v_s = 2.876$ m/s

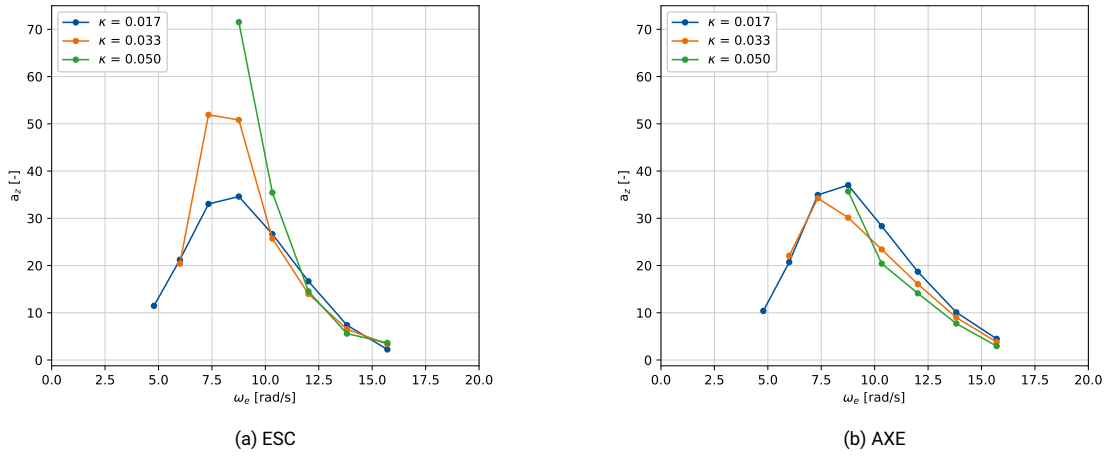


Figure 5.5: Maximum vertical acceleration (non-dimensional), bow, $v_s = 2.876$ m/s

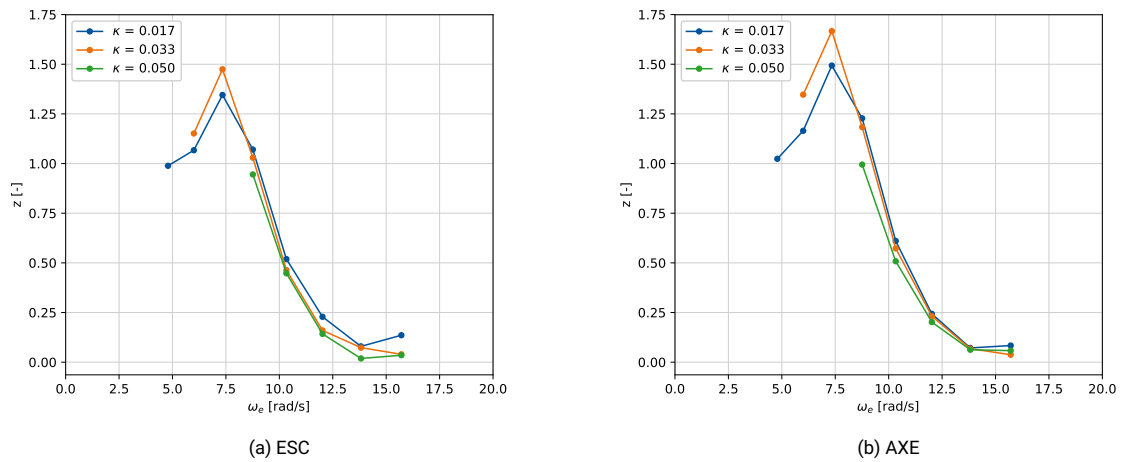


Figure 5.6: Maximum vertical displacement (non-dimensional), centre of gravity, $v_s = 2.876$ m/s

(z_a/ζ_a) is plotted. The larger vertical accelerations at the centre of gravity of the AXE thus come from a larger heave displacement at the same frequency waves. The only exception is the response in waves with a steepness of $\kappa = 0.050$ at a frequency of $\omega_e = 8.76$ rad/s. The time traces (time traces 3 and 4 in appendix C) show contrary to the other points a more severe slam. In this case the response of the AXE is lower than the response of the ESC.

Looking at the accelerations at the bow there are certain differences, see figure 5.5a and figure 5.5b for the non-dimensional amplitude of the vertical acceleration at the bow of respectively the ESC and the AXE. Contrary to the accelerations at the centre of gravity, here only the response in wave steepness $\kappa = 0.017$ is dominated by the first order response. The accelerations are then again slightly larger at the AXE. For the other wave steepnesses the response of the ESC is larger than the response of the AXE. In the time traces of these cases more distinct slamming is visible, see time traces 5 and 6 in appendix C. The AXE bow is more optimised for this slamming [7], and therefore the response of the AXE is smaller than the response of the ESC.

The vertical accelerations at the bow are a superposition of the vertical acceleration at the centre of gravity and the pitch acceleration. As mentioned above the accelerations at the centre of gravity are mainly dominated by the first order response. The distinct slamming in the accelerations at the bow are thus originating from the pitch accelerations, this will be analysed further in section 5.3.

Jerk peaks

The maximum (non-dimensional) values for the vertical jerk of the ESC and the AXE, at the centre of gravity, are plotted in respectively figure 5.7a and figure 5.7b. The jerk is made non-dimensional with equation 4.3. The obtained values are again plotted against the encounter frequency.

From the graphs it becomes clear that the jerk behaviour of the hulls is different from the accelerations. Where the values of the accelerations of the AXE were generally larger at the centre of gravity than those of the ESC, the jerk values of the ESC are mostly larger than those of the AXE, especially around the natural frequency. The only exception is the tests with wave steepness $\kappa = 0.017$. The time traces (see again time traces 1 and 2 in appendix C) show that the jerk values in these results are still dominated by the first order response, and are thus slightly higher on the AXE. In the waves with higher steepnesses the accelerations of the ESC are smaller than the AXE, but the ESC shows a more distinct slam in the waves. This results in a higher jerk value. At higher encounter frequencies the response of both hull types becomes more first order, there is no real slamming visible anymore. The response values therefore become more first order.

In figure 5.8a and figure 5.8b the maximum non-dimensional jerk at the bow is plotted. The trend of the lines looks the same as with the jerk in the centre of gravity. The difference between the jerk at the bow of the ESC and the AXE is slightly larger than at the centre of gravity, indicating that the bow of the AXE is indeed optimised for these conditions.

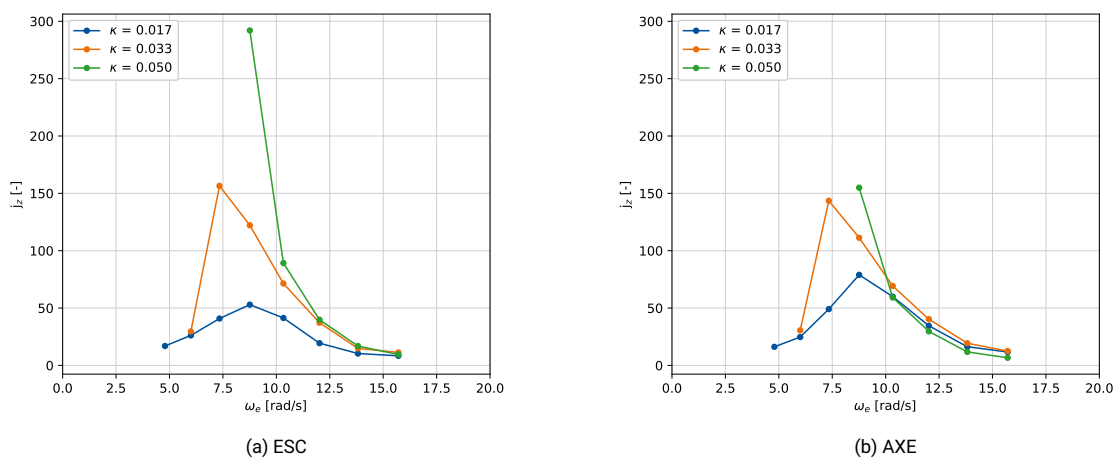


Figure 5.7: Maximum vertical jerk (non-dimensional), centre of gravity, $v_s = 2.876$ m/s

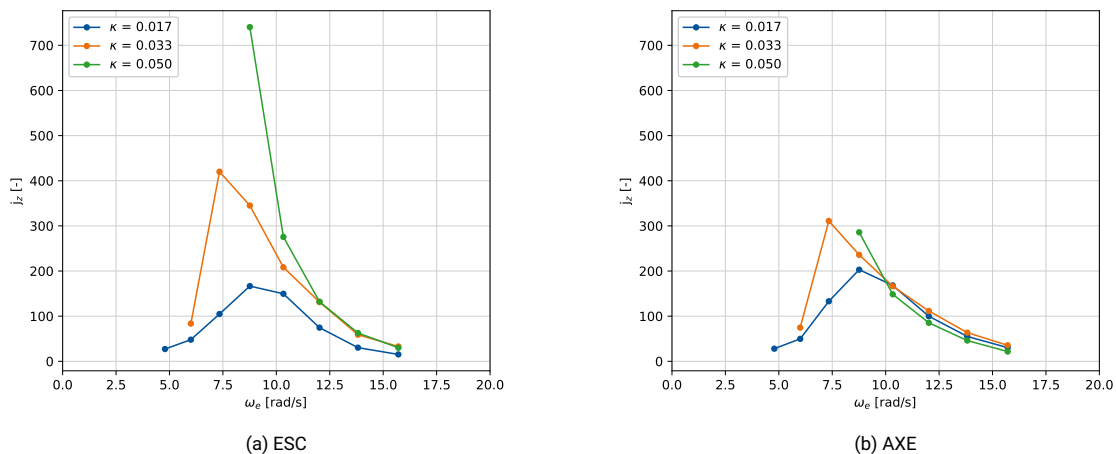


Figure 5.8: Maximum vertical jerk (non-dimensional), bow, $v_s = 2.876$ m/s

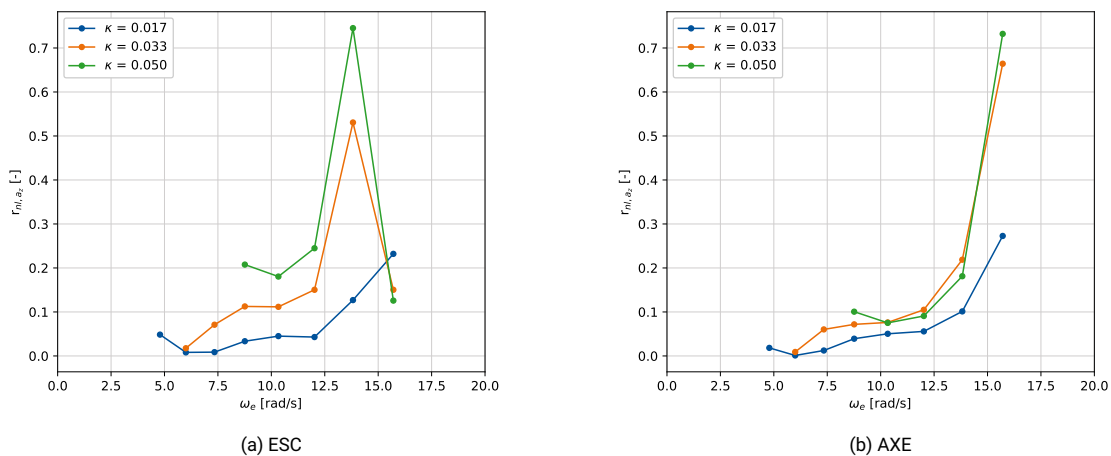


Figure 5.9: Non-linearity ratio vertical acceleration, centre of gravity, $v_s = 2.876$ m/s

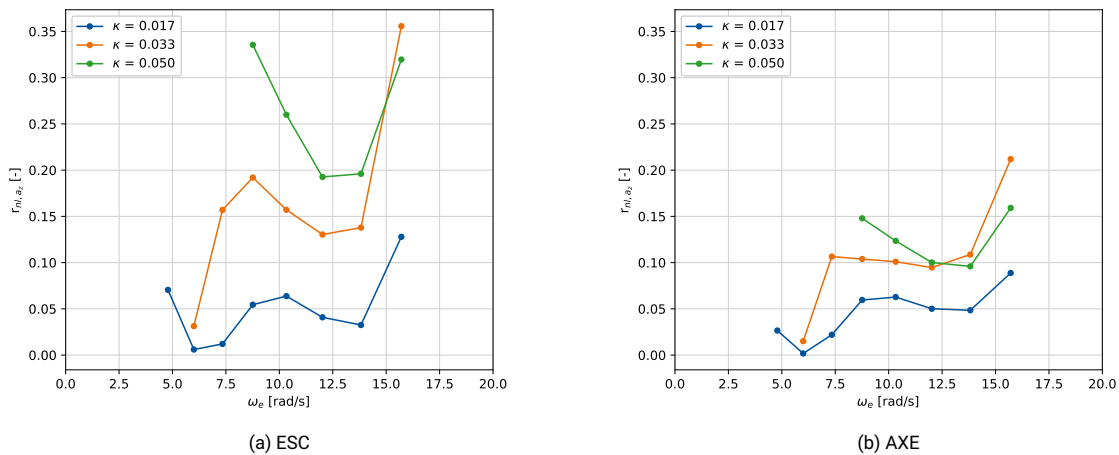
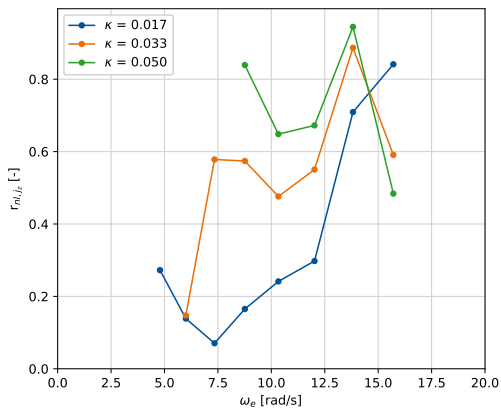
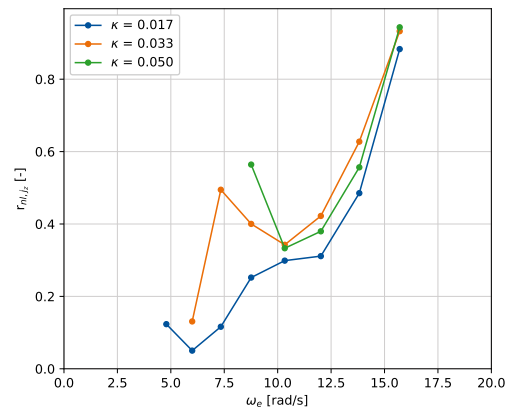


Figure 5.10: Non-linearity ratio vertical acceleration, bow, $v_s = 2.876$ m/s

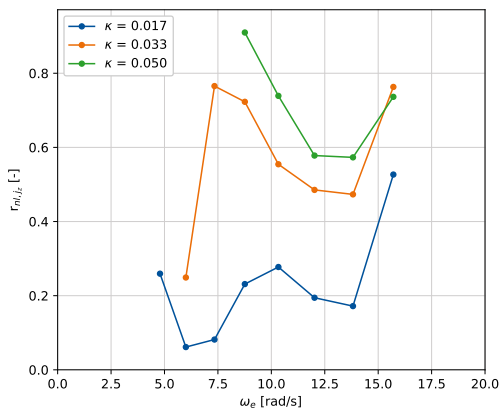


(a) ESC

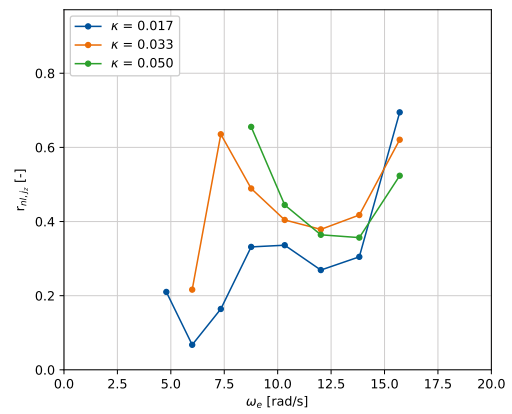


(b) AXE

Figure 5.11: Non-linearity ratio vertical jerk, centre of gravity, $v_s = 2.876$ m/s

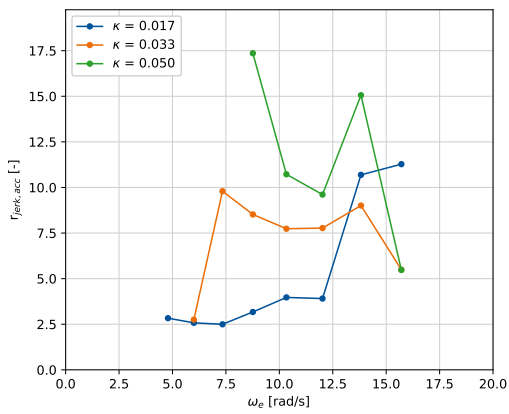


(a) ESC

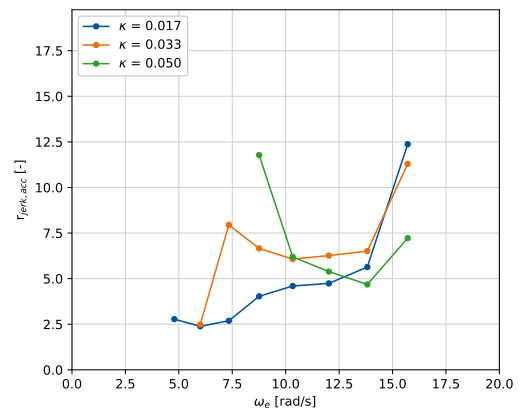


(b) AXE

Figure 5.12: Non-linearity ratio vertical jerk, bow, $v_s = 2.876$ m/s



(a) ESC



(b) AXE

Figure 5.13: Jerk-to-acceleration ratio, centre of gravity, $v_s = 2.876$ m/s

Non-linearity ratio

In chapter 4 also a procedure to quantify the amount which the response is non-linear was proposed, the non-linearity ratio. This ratio can be determined for either the acceleration or the jerk. In figure 5.9a and figure 5.9b the non-linearity ratio for the acceleration at the centre of gravity for the ESC and the AXE have been plotted. The ratios are relatively constant at the lower encounter frequencies, and become larger at higher encounter frequencies. This means that, although the responses are small at the high frequencies, they are largely non-linear. It can also be seen that the response of the AXE in general is less non-linear than the ESC. This also illustrates that the non-linearity ratio has no (direct) link with the value of the response, since prior in this section it was concluded that the acceleration peaks are higher for the AXE. There is no clear peak visible near the natural frequency. This can be explained by the fact that most of the acceleration responses at the centre of gravity were dominated by the first order response, as concluded earlier in this section.

The peak that is visible in the non-linearity of the ESC (figure 5.9a) at $\omega_e = 13.82$ rad/s and at the AXE (figure 5.9a) at $\omega_e = 15.71$ rad/s is coming from the fact that the second order response (the peak in the energy density spectrum at two times the encounter frequency) is (almost) equal to or larger than the peak of the first order response. This will be analysed further in section 5.3.2. Here also an example of the energy density spectra where this phenomenon happens can be seen, see figure 5.32a and figure 5.32b.

The non-linearity ratio of the acceleration at the bow can be seen in figure 5.10a and figure 5.10b. Contrary to the non-linearity ratio at the centre of gravity, there is a more distinct peak visible at the natural frequency of the ESC. This is because of the slamming that happened in these tests, which is a non-linear event. The optimisation of the bow of the AXE is again visible here, with a relatively less non-linear response.

The non-linearity ratio can also be determined for the jerk, see figure 5.11a and figure 5.11b. As expected from the explanation in chapter 4 the jerk is more non-linear than the acceleration, which is the trend in both figures. It can be seen that the non-linearity is generally higher around the natural frequency and at the higher frequencies. The only exception are the tests with $\kappa = 0.017$, here the non-linearity ratio seems to drop around the natural frequency. This can be explained by the fact that there is no distinct slamming visible in the time traces of these tests, while that is the case in the time traces of the higher wave steepnesses. Since the slamming is highly non-linear, this explains the different trend in non-linearity ratio.

The non-linearity ratio of the jerk at the bow is plotted in figure 5.12a and figure 5.12b for respectively the ESC and the AXE. The non-linearity generally follows the same trend as the non-linearity at the centre of gravity. However, the ratio is relatively higher around the natural frequency and lower at higher frequencies. Also there is no second normal mode visible.

Jerk-to-acceleration ratio

In chapter 4 also the jerk-to-acceleration ratio has been defined, see equation 4.7. This ratio, determined at the centre of gravity, has been plotted in figure 5.13a and figure 5.13b. Although the figures show similarity with the figures of the non-linearity ratio for the jerk, they are less clear and it is harder to distinguish trends in them. This method of quantifying will therefore not be used furthermore.

5.2.2 Wave steepness

In all the figures in section 5.2 the response is plotted for different values of the wave steepness. In this section the effect of wave steepness on the response of the ship is discussed. In time traces 7, 8 and 9 in appendix C the response at the bow of the ESC in the same wave frequency but varying wave steepness values can be seen.

Acceleration peaks

In figure 5.4 it can be seen that there is a general decreasing trend of the non-dimensional acceleration peaks with increasing wave steepness at the centre of gravity. This also shows that although it was concluded in the previous section that the responses are dominated by the first order response, they are still non-linear to the disturbant wave. If the response would be linear and the response would thus be proportional to the wave amplitude, the non-dimensional response should be the same. This effect is also visible in the heave displacement, see figure 5.6.

Contrary to the accelerations at the centre of gravity, the acceleration peaks at the bow of the ESC have an increasing trend with increasing wave steepness as seen in figure 5.5. This is mainly due to the increased slamming in these conditions. The AXE and the ESC at higher frequencies show the same trend as the accelerations at the centre of gravity, decreasing with increasing wave steepness.

Jerk peaks

In figure 5.7 and figure 5.8 the jerk peaks at respectively the centre of gravity and the bow can be seen for the ESC and the AXE. It can be seen that the maximum value of the jerk increases with increasing wave steepness. This is especially visible around the natural frequency of the ship, where the slamming is occurring. The severity of slamming, which increases with increasing wave steepness, seems to be the main cause for the largest jerk peaks in the ship model. The jerk behaviour is dominated by slamming at both the centre of gravity and the bow, contrary to the acceleration peaks. These were mainly dominated by the first order response in the centre of gravity. In the jerk in time traces 7, 8 and 9 in appendix C it is clearly visible that the impulse from the slamming significantly increases with increasing wave steepness.

Non-linearity ratio

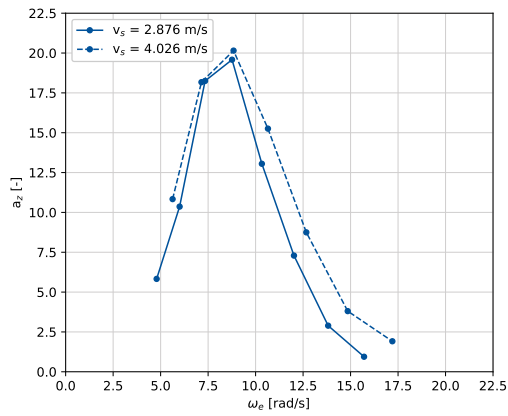
The non-linearity for acceleration and jerk, for the centre of gravity and the bow can be seen in figures 5.9 to 5.12. The general trend is an increasing non-linearity ratio for increasing wave steepness. The difference between no occurrence of slamming for wave steepness $\kappa = 0.017$ and the occurrence of slamming for higher wave steepness values can be seen clearly. Since the slamming is a highly non-linear event, the non-linearity ratios of the higher wave steepness values are relatively high around the natural frequency. This is contrary to the response to waves with a wave steepness of $\kappa = 0.017$, which has a decreasing non-linearity ratio around this frequency.

5.2.3 Forward speed

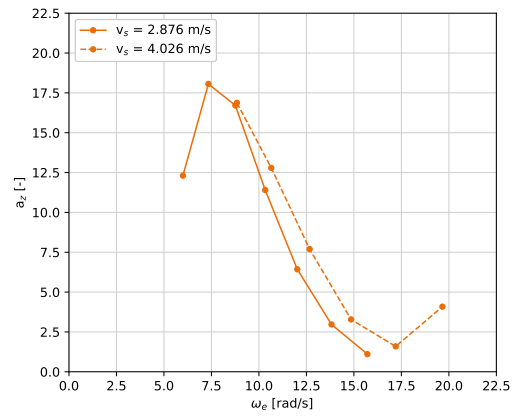
To compare the influence of increasing forward speed the data of the tests with $v_s = 2.876$ m/s and the data from the tests with $v_s = 4.026$ m/s are compared. This will only be done for a selection of the results the AXE, since the ESC shows very similar trends. Also only the results from the tests with wave steepness values of $\kappa = 0.017$ and $\kappa = 0.033$ will be compared, since these are tests that were mainly dominated by first order response and tests where slamming occurred. This way the effect of increasing ship speed can be compared for both these conditions.

Acceleration peaks

In figure 5.14 and figure 5.15 the maximum values for the acceleration are given at respectively the centre of gravity and the bow. For the wave steepness of $\kappa = 0.017$ it can be seen that the acceleration response at the centre of gravity near the natural frequency is slightly higher, but the response at the bow around the natural frequency is lower. Since the response at this wave steepness is still dominated by the first order response, this comes from increased heave response and decreased pitch response. The influence of heave and pitch in the total ship response will be investigated further in section 5.3. At higher frequencies the general trend is increased acceleration response with increasing speed. With higher wave steepnesses the difference around the natural frequency is not visible anymore, because the maximum values for the acceleration are dominated by slamming here. The slamming increases with increasing forward speed.

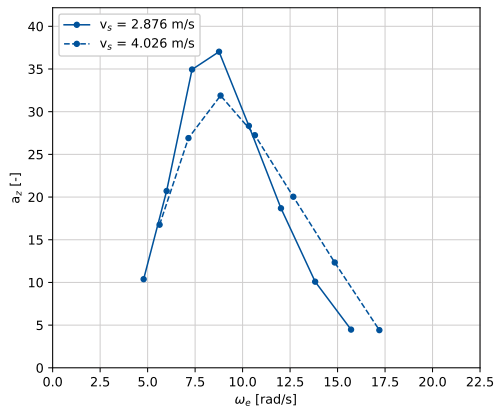


(a) $\kappa = 0.017$

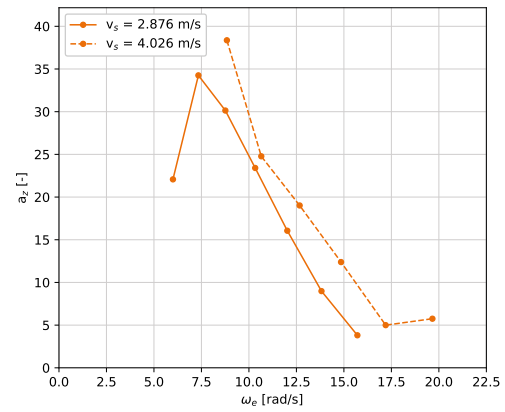


(b) $\kappa = 0.033$

Figure 5.14: Maximum vertical acceleration (non-dimensional), AXE, centre of gravity

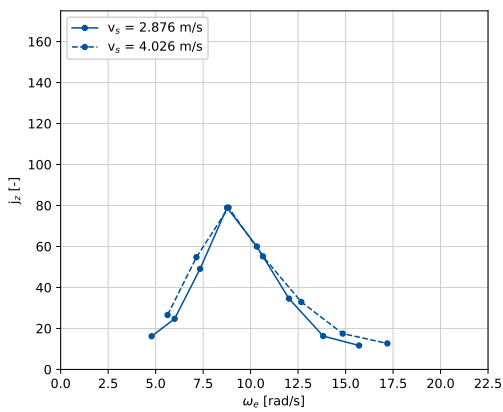


(a) $\kappa = 0.017$

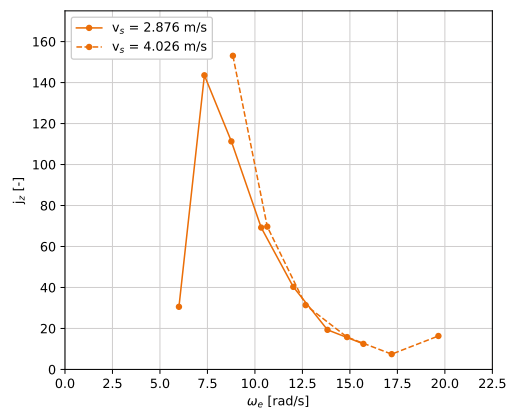


(b) $\kappa = 0.033$

Figure 5.15: Maximum vertical acceleration (non-dimensional), AXE, bow

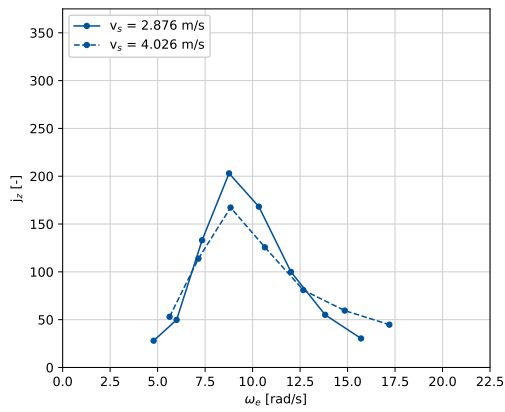


(a) $\kappa = 0.017$

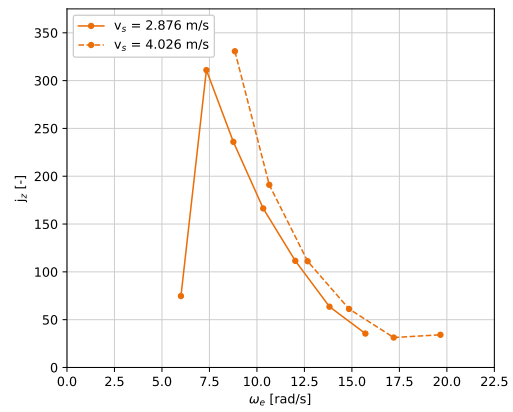


(b) $\kappa = 0.033$

Figure 5.16: Maximum vertical jerk (non-dimensional), AXE, centre of gravity

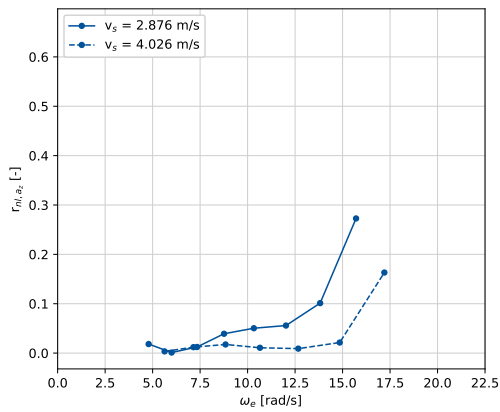


(a) $\kappa = 0.017$

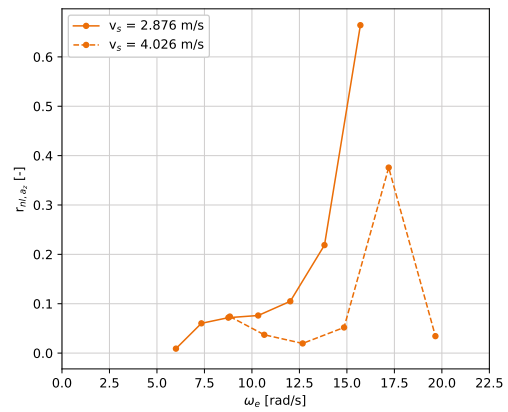


(b) $\kappa = 0.033$

Figure 5.17: Maximum vertical jerk (non-dimensional), AXE, bow

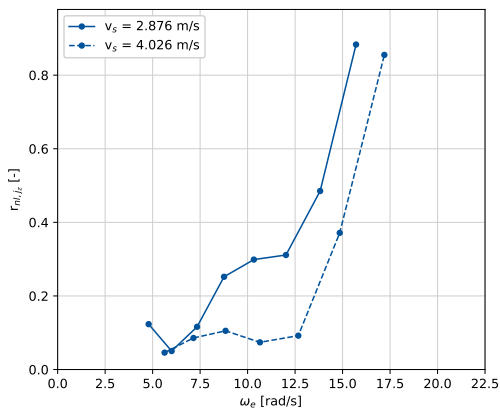


(a) $\kappa = 0.017$

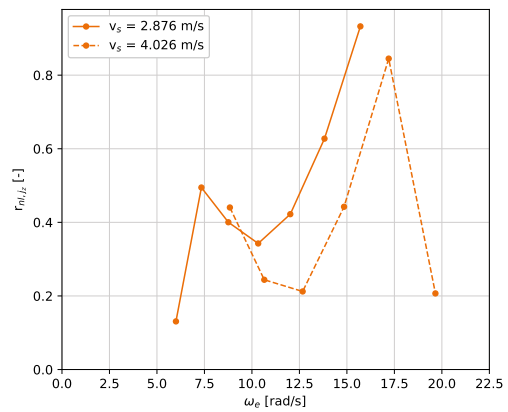


(b) $\kappa = 0.033$

Figure 5.18: Non-linearity vertical acceleration, AXE, centre of gravity



(a) $\kappa = 0.017$



(b) $\kappa = 0.033$

Figure 5.19: Non-linearity vertical jerk, AXE, centre of gravity

Jerk peaks

With the jerk peaks a similar trend as in the acceleration peaks is visible, as can be seen in figure 5.16 and figure 5.17. In these figures the maximum values of the jerk at the centre of gravity and the bow are plotted. With the wave steepness $\kappa = 0.017$ the jerk is lower around the natural frequency at the centre of gravity with increasing speed, and higher at the bow. This is an expected consequence because the response is mainly first order. Also the peak values are increasing with increasing speed at higher frequencies. At the higher values for the wave steepness an increase of the jerk values is also visible around the natural frequency, since the slamming in these region increases with increasing forward speed.

Non-linearity

In figure 5.18 and figure 5.19 the non-linearity ratio at the centre of gravity for the acceleration and the jerk can be seen. The general trend in these figures is that the response of the model is less non-linear at increasing speeds. This mainly comes from an higher first order response, see for example time traces 10 and 11 in appendix C. The higher order components, which are mainly a result of the impact with the waves, remain the same order of magnitude. Therefore the maximum values of the acceleration and the jerk only slightly increase, as concluded in the previous sections.

At higher frequencies the non-linearity ratios increase, but since the amplitude of the disturbant wave and thus the amplitude of the motion response is very small, it is hard to see what this has for implications on the time traces.

5.3 Analysis over ship length

In the previous section the vertical accelerations and jerk at the centre of gravity and the bow have been compared. In this section the influence of heave and pitch on the acceleration and jerk are investigated, to see if one has more effect than the other. With this also the maximum values of the vertical acceleration and vertical jerk as well as the non-linearity ratio at any longitudinal position of the ship can be determined. As was described in chapter 4, the maximum values are often limiting for the operability and comfort of the ship. With an analysis of these values over the length of a ship the operability and comfort can be assessed at different important locations, for example the wheelhouse, crew accommodations and working areas.

5.3.1 Decomposition heave and pitch

The vertical acceleration at any part of the ship along the centerline is a result of the heave acceleration and the pitch acceleration. The vertical acceleration at any longitudinal position x (along the centerline) can be calculated as given in equation 5.4. In this equation the assumption is made that motions can be linearly superpositioned to calculate the motions at any point on the ship. For this assumption to be valid two conditions have to be met. One is that the model is rigid so that there is no bending of the hull. This is assumed to be the case. The other is that the rotations are small, so that equation 5.5 is valid. The maximum pitch displacement observed in all the tests is approximately 0.15 radians, which is 8.6 degrees. This is small enough to make the assumption valid. The positive x -direction and positive θ -rotation are as defined in section 2.1.

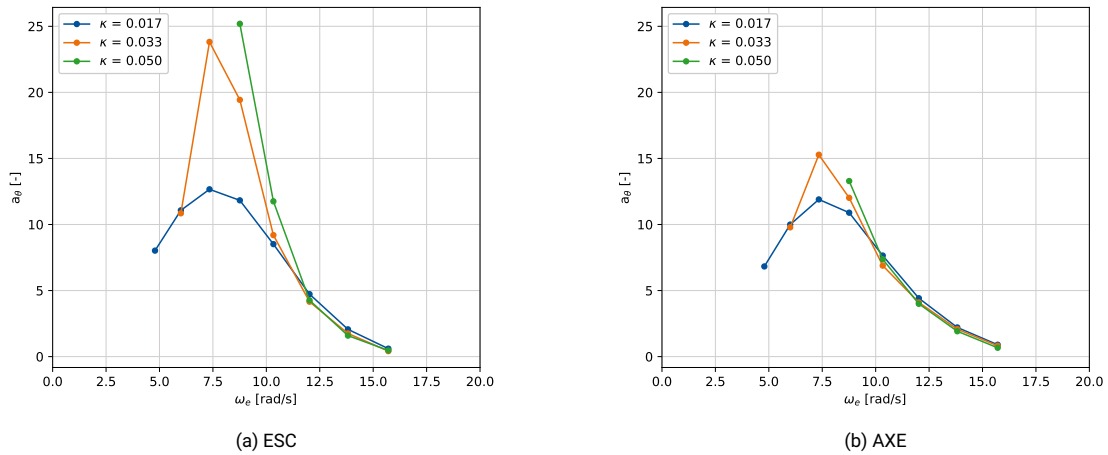
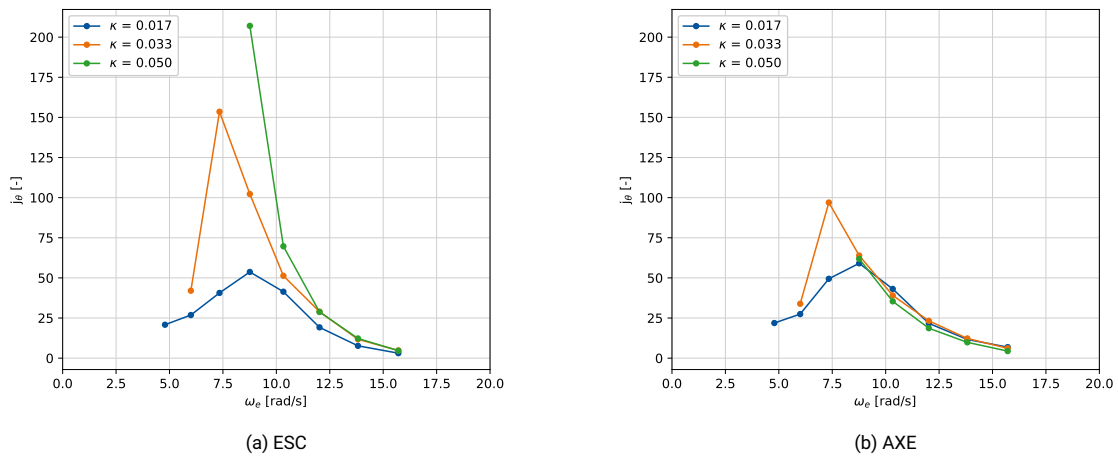
$$a_{z,x} = a_{z,CoG} - a_{\theta} \cdot x \quad (5.4)$$

Assuming that:

$$\sin(\theta) \approx \theta \quad (5.5)$$

The acceleration terms in these equation are the full time traces, not only the amplitude. Phase differences between different degrees of freedom are then automatically included. Since the acceleration at the centre of gravity and the bow are known, as well as their longitudinal positions, the pitch acceleration can be calculated using equation 5.4. With the pitch acceleration and the pitch jerk the vertical acceleration and vertical jerk at any longitudinal position of the ship can be determined.

In figure 5.20 the maximum values for the pitch acceleration of the ESC and the AXE are plotted. Note that the trough value is in most cases the largest pitch acceleration value. This is because the bow pitching upward is, according to the definitions in section 2.1, a negative value. Slamming, which is

Figure 5.20: Maximum pitch acceleration (non-dimensional), $v_s = 2.876$ m/sFigure 5.21: Maximum pitch jerk (non-dimensional), $v_s = 2.876$ m/s

the cause of the largest values in most cases, causes a bow upward acceleration. It can be seen that the pitch accelerations of the AXE are lower than the pitch accelerations of the ESC. This is contrary to the heave accelerations, which are higher at the AXE. Since the vertical acceleration at the bow is a superposition of the heave acceleration and the pitch acceleration, this explains the lower vertical accelerations at the bow of the AXE, compared to the bow of the ESC.

The maximum values of the pitch jerk for the ESC and the AXE are plotted in figure 5.21. These values have a similar trend as the pitch accelerations. The jerk values for the AXE are lower than the ESC in the same conditions.

The difference in the pitch acceleration and pitch jerk between the ESC and the AXE can also clearly be seen in respectively time traces 12 and 13 in appendix C. In these time traces the acceleration and jerk of both the heave and the pitch are plotted. There are some differences in the heave acceleration and heave jerk, but the main difference in the behaviour between the two hulls comes from the pitch acceleration and the pitch jerk.

When looking at the non-linearity of the pitch acceleration (figure 5.22) and the non-linearity of the pitch jerk (figure 5.23) it can be seen that the pitch response of the AXE is in almost all wave conditions less non-linear than the ESC. This is where the optimisation of the AXE bow can be observed well. Especially in the higher wave steepness tests the relative difference is large.

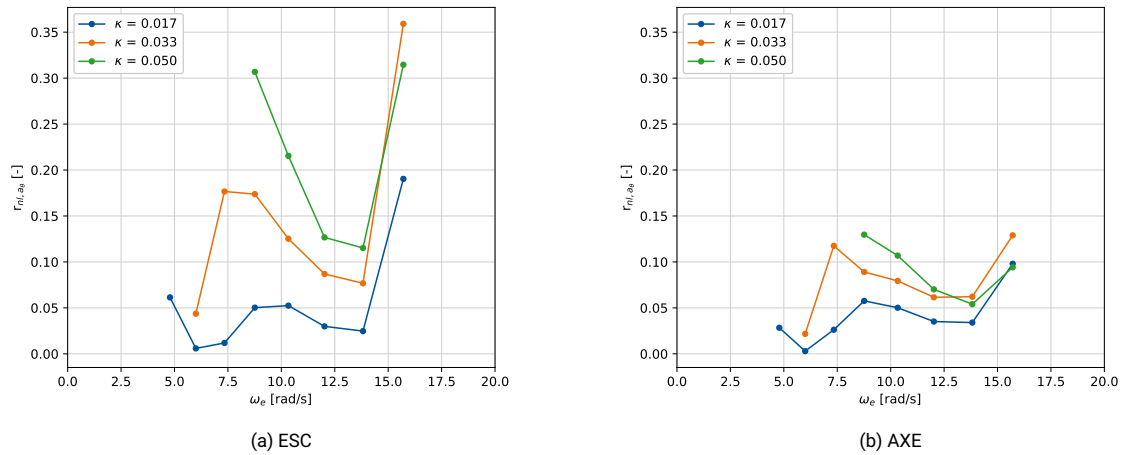


Figure 5.22: Non-linearity pitch acceleration, v_s = 2.876 m/s

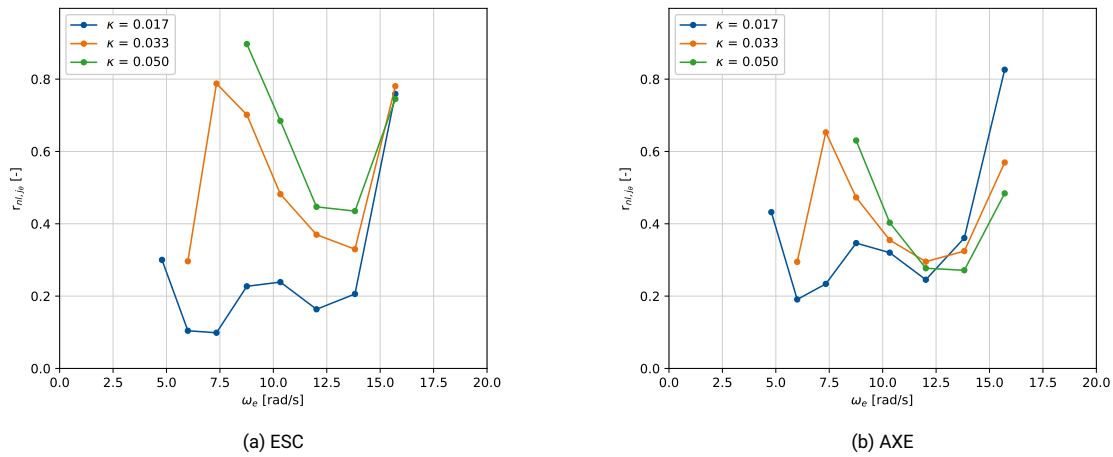


Figure 5.23: Non-linearity pitch jerk, v_s = 2.876 m/s

5.3.2 Different cases

In this section for a number of different conditions the maximum values along the ship length for both models will be analysed. Since not every test run can be analysed here, these cases have been selected to illustrate the different types of behaviour. The other test runs behaved in similar ways, but that is not documented here.

Linear response

For this case the results from the model tests with speed v_s = 2.876 m/s and an encounter frequency of ω_e = 7.34 rad/s in waves with steepness κ = 0.017 are used. This test was already dominated by the first order response and thus quite linear, but to best illustrate how the linear distribution of the maximum values along a ship would look like the measurements for this case have been filtered with a lower cutoff frequency.

The phase difference between the heave and the pitch is an important parameter in the way the maximum values over the length of the ship look like. In figure 5.24 the maximum values for the vertical acceleration and vertical jerk along the length of the model can be seen. These values have the shape of a parabola. As expected in case of only linear response, the shape of the plot of the jerk looks the same as the shape of the plot of the accelerations.

To better illustrate the importance of the phase difference between the heave and the pitch a theoretical case of combined heave and pitch acceleration over the length of the model has been plotted in figure 5.25. The heave and pitch have been assumed as a sine signal. In figure 5.25a there is no phase angle

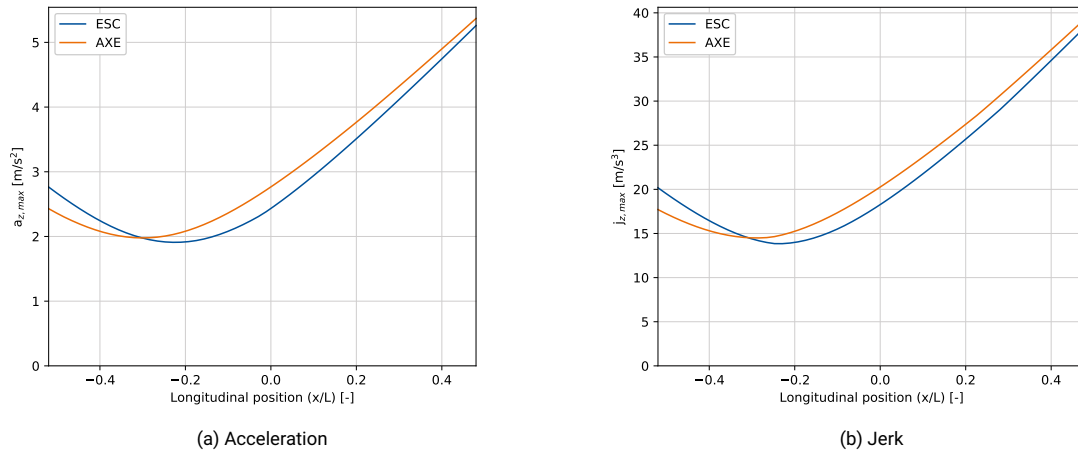


Figure 5.24: Maximum values over ship length (linear response), $v_s = 2.876$ m/s, $\omega_e = 7.34$ rad/s, $\kappa = 0.017$

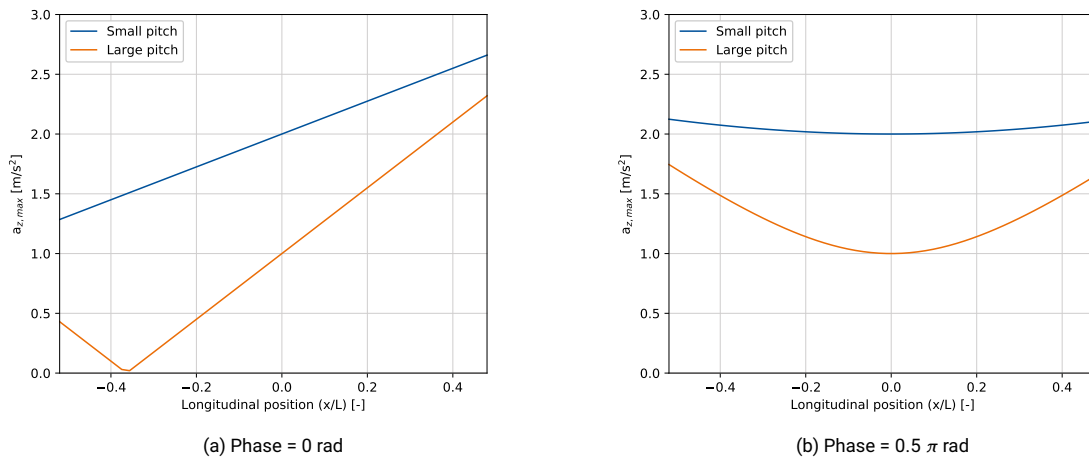


Figure 5.25: Maximum acceleration values over ship length, theoretical linear response

between the heave and the pitch. This results in straight lines. If the pitch is small compared to the heave, the vertical accelerations are increasing towards the bow (positive x/L values) and decreasing towards the stern (negative x/L). This also happens when the pitch is large compared to the heave, but in this case there is a point where the vertical acceleration resulting from the pitch completely cancels out the vertical acceleration from the heave. Behind this point there is a negative amplitude, but since the maximum (absolute) value is plotted in the figure this shows as a bend in the line. In this longitudinal part the vertical accelerations are in anti-phase (phase = π rad) with the accelerations at other longitudinal parts of the model.

In figure 5.25b the maximum value for the vertical acceleration over the length of the ship has been plotted in case the phase difference between the heave and the pitch is π rad. This means that in this case the heave is a sine function and the pitch is a cosine function. It can be seen that the maximum values for the vertical acceleration now are shaped like a parabola, with the lowest value in the centre of gravity ($x/L = 0$). The larger the pitch motions, the more the maximum acceleration value increases towards the bow and stern of the model.

The plots of the maximum values from the model tests in figure 5.24 are neither a straight line nor a parabola originating in the centre of gravity. This means that the (absolute value) of the phase difference between the heave and pitch is in between 0 rad and 0.5π rad.

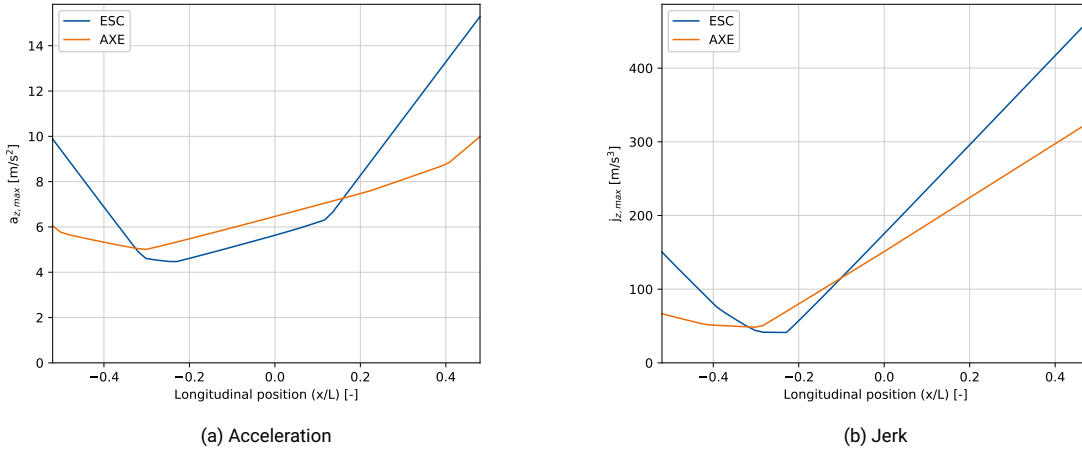


Figure 5.26: Maximum values over ship length, $v_s = 2.876$ m/s, $\omega_e = 7.34$ rad/s, $\kappa = 0.033$

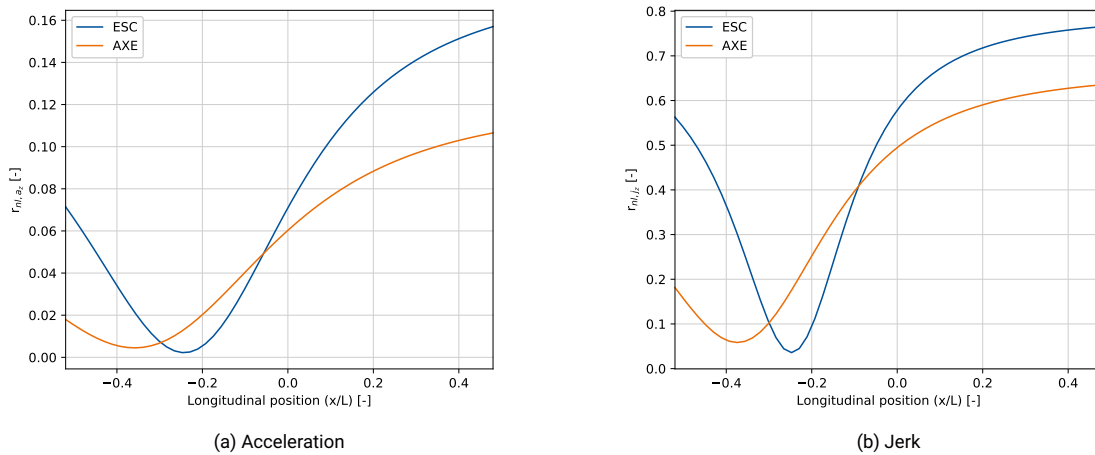


Figure 5.27: Non-linearity over ship length, $v_s = 2.876$ m/s, $\omega_e = 7.34$ rad/s, $\kappa = 0.033$

Around natural frequency

To see the effect of slamming on the maximum values along the length of the ship, the results from the model tests with speed $v_s = 2.876$ m/s and an encounter frequency of $\omega_e = 7.34$ rad/s in waves with steepness $\kappa = 0.033$ are analysed. Both the ESC and the AXE experience slamming in these conditions.

In figure 5.26a the accelerations over the length of the model is plotted for the ESC and the AXE. There are several bends visible in the plots of the maximum values. Around the natural frequency the maximum value comes from the heave acceleration. More forward to the bow of the ship there is a bend in the line, where the pitch acceleration due to the slamming becomes larger than the heave acceleration. The slamming causes a crest in the acceleration. At the stern this effect is also visible, here the slamming causes a trough in the acceleration. It can be seen that at the AXE the heave acceleration is the cause for the maximum value of the acceleration at a larger part of the ship. Only close to the bow, and a small section at the stern are dominated by the slamming. It is also visible that the heave acceleration of the AXE is slightly higher than the ESC around the centre of gravity.

The maximum jerk values for this case are visible in figure 5.26b. At almost every section of the ESC the maximum value for the jerk is originating from the slamming, not from the heave. So this is different compared to the accelerations. At the AXE this is also the case, but the values are in general lower than the ESC. At the stern of the AXE there is a section which is dominated by the heave jerk. It can be seen that the optimisation of the AXE is even more pronounced in the jerk, there is only a small section where the jerk at the ESC is lower.

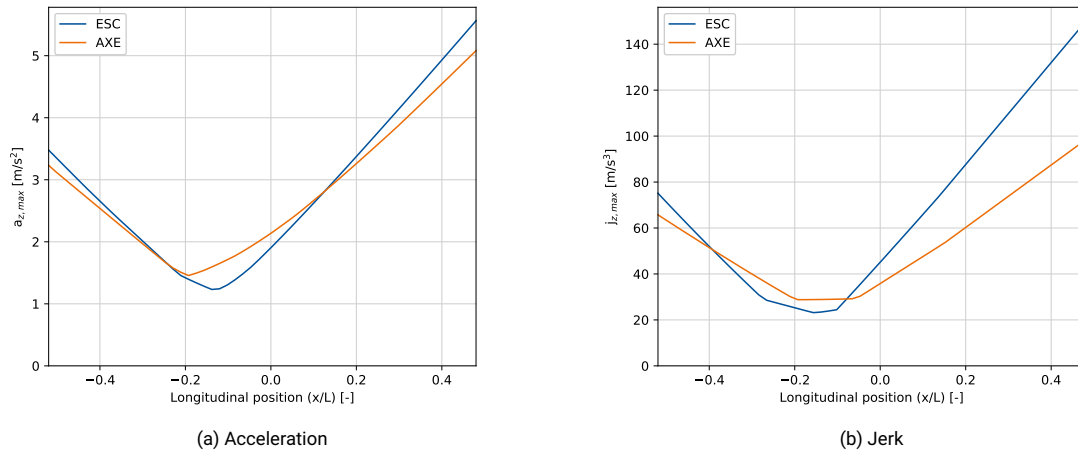


Figure 5.28: Maximum values over ship length, $v_s = 2.876$ m/s, $\omega_e = 12.02$ rad/s, $\kappa = 0.050$

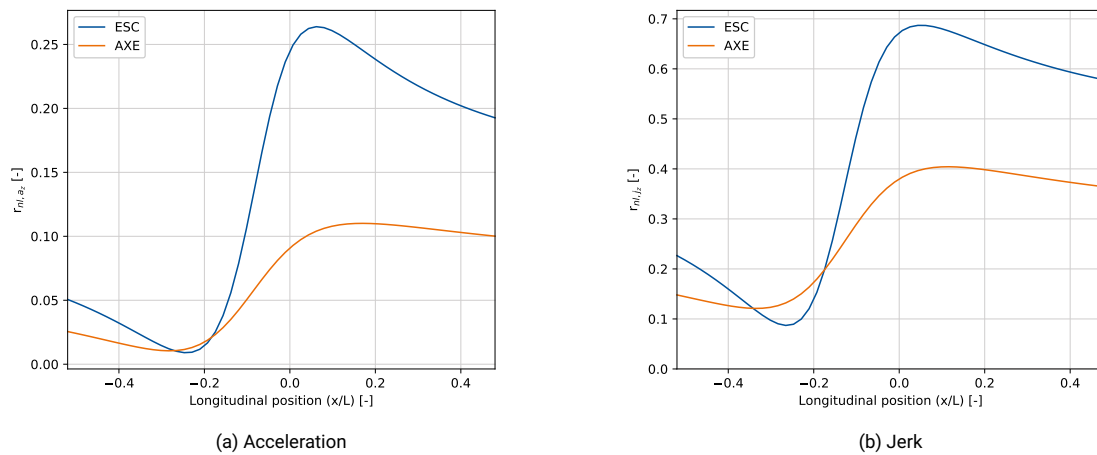


Figure 5.29: Non-linearity over ship length, $v_s = 2.876$ m/s, $\omega_e = 12.02$ rad/s, $\kappa = 0.050$

The non-linearity in respectively the accelerations and the jerk are plotted in figure 5.27. Both the graphs have similar trends, only the values are different. The response of the AXE is in general less non-linear than the response of the ESC. There is trough visible in the non-linearity. The longitudinal location of this trough coincides with the location of the lowest accelerations and troughs.

Higher encounter frequencies

To analyse the behaviour over the ship length in higher encounter frequencies the results from the model tests with speed $v_s = 2.876$ m/s and an encounter frequency of $\omega_e = 12.02$ rad/s in waves with steepness $\kappa = 0.050$ are analysed.

In figure 5.28a the accelerations over the length of the AXE and ESC model are plotted. The behaviour is very similar, although at the ESC there is small slamming visible in the forward part, where the response of the AXE more looks like first order response.

In the jerk behaviour over the ship length, visible in figure 5.28b, a more distinct difference is visible. At both models there is a peak in the jerk due to slamming visible in the forward part. The peak is however significantly lower at the AXE than at the ESC.

The non-linearity of the acceleration and the jerk is plotted in figure 5.29. It can be seen that at these high encounter frequency the non-linearity of the response is lower at almost every section of the AXE model, compared to the ESC.

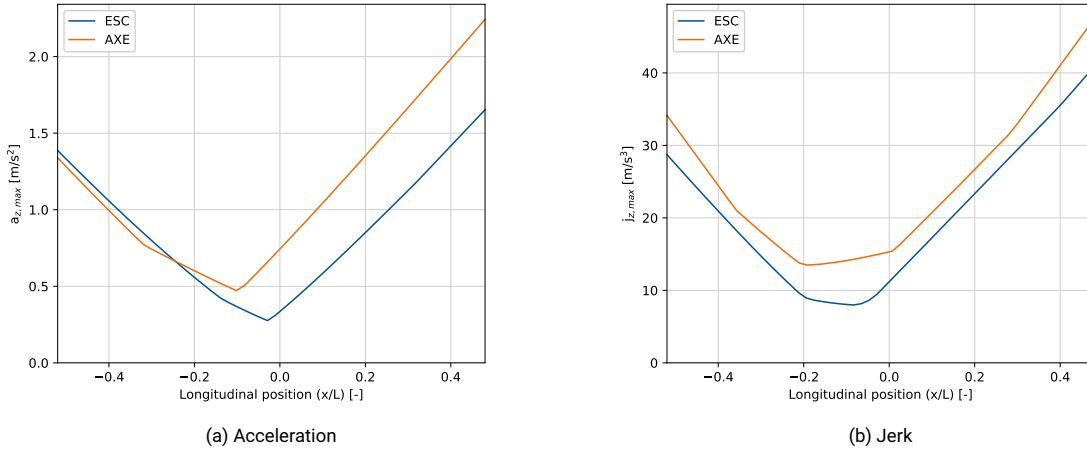


Figure 5.30: Maximum values over ship length, $v_s = 2.876$ m/s, $\omega_e = 13.82$ rad/s, $\kappa = 0.033$

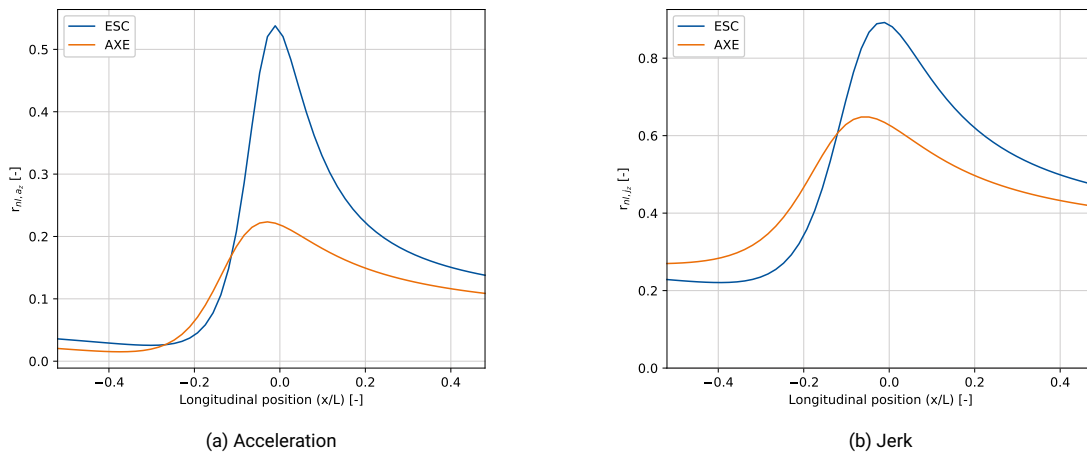


Figure 5.31: Non-linearity over ship length, $v_s = 2.876$ m/s, $\omega_e = 13.82$ rad/s, $\kappa = 0.033$

Large non-linearity

In section 5.2 it was already mentioned that at some (high) encounter frequencies there was a peak in the non-linearity ratio, see for example figure 5.9a. To more deeply analyse this behaviour the results from the model tests with speed $v_s = 2.876$ m/s and an encounter frequency of $\omega_e = 13.82$ rad/s in waves with steepness $\kappa = 0.033$ are used. In general the motion response is very small in these cases because of the low wave amplitude at this encounter frequency. Therefore this case will not be limiting to the seakeeping behaviour of the ship. The accelerations (figure 5.30a) and jerk (figure 5.30b) show a behaviour that is similar to previously described cases. In this case the behaviour of the ESC is slightly better than the behaviour of the AXE, but the response in general is thus very low.

In the non-linearity, especially the non-linearity of the accelerations of the ESC, a relatively large peak is visible. This peak comes from the way the non-linearity ratio is defined and the superposition of the heave and pitch acceleration. In this case the peak in the heave acceleration and the peak in the pitch acceleration are out of phase. The phase difference in combination with the peaks being the same order of (small) magnitude leads to a time trace of the acceleration which looks more like a harmonic function with twice the excitation frequency. This can be seen in figure 5.33b. In the energy density spectrum the component at twice the encounter frequency is then larger than the component at the encounter frequency. The way how the non-linearity ratio is defined (see section 4.1.2) results in a large value here. Some length before and after this point the acceleration signal (visible in respectively figure 5.33a and figure 5.33c) the pitch acceleration has a larger contribution to the vertical acceleration and is then the main component.

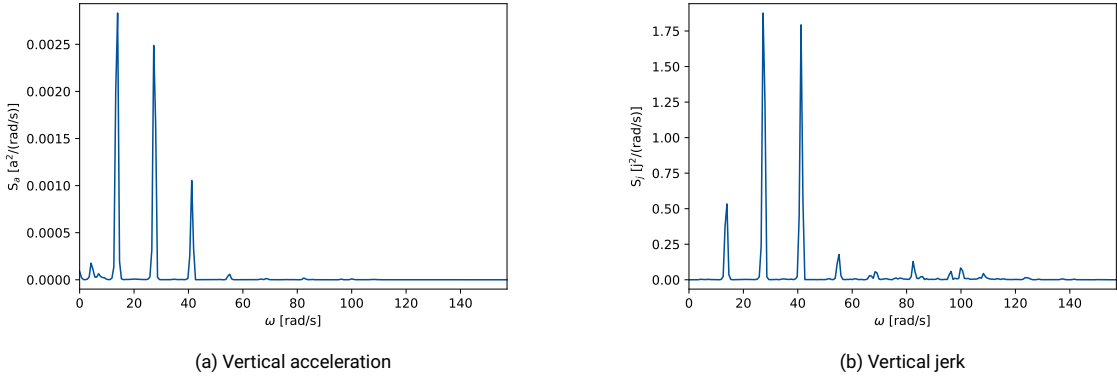


Figure 5.32: Energy density spectra, ESC, centre of gravity, $v_s = 2.876$ m/s, $\omega_e = 13.82$ rad/s, $\kappa = 0.033$

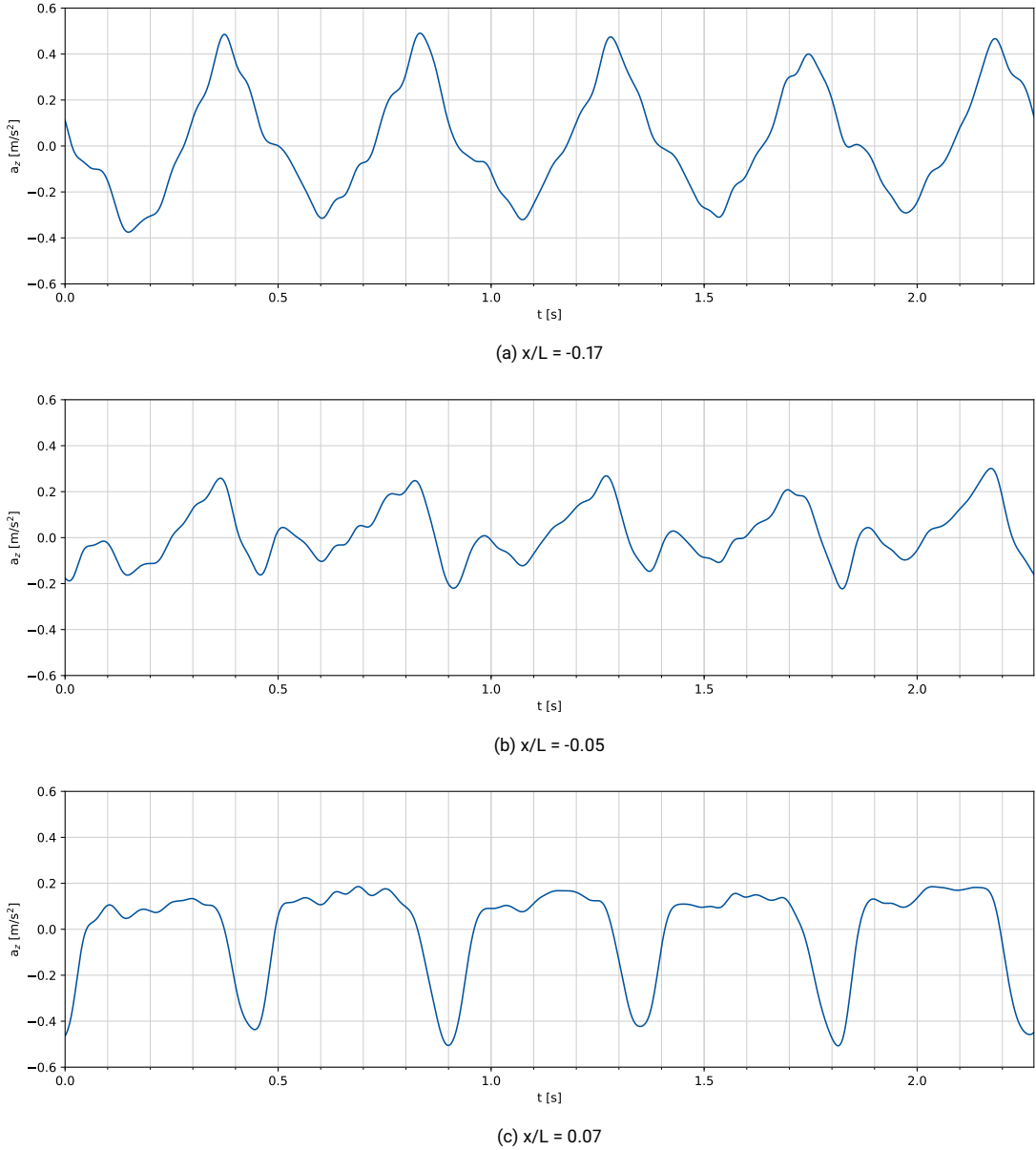


Figure 5.33: Acceleration signal at different longitudinal positions, ESC, $v_s = 2.876$ m/s, $\omega_e = 13.82$ rad/s, $\kappa = 0.033$

6

Fast models in irregular head waves

Prior to the FAST II project where the model tests in regular head waves have been performed, irregular wave tests with the same models have been performed in the FAST project [7, 30]. The behaviour of a model in irregular waves is more relevant since the seas a ship is going to sail in are never regular. However, as already mentioned in chapter 4, especially the non-linear response of a ship to the wave elevation in irregular seas is a highly random process.

In section 6.1 an introduction will be given to the performed tests. Next in section 6.2 different comparisons will be made on the performed tests. This will be extended in section 6.3 with an analysis of maximum values over the length of the ship again. In section 6.4 the non-linearity of the response will be discussed. Finally in section 6.5 the prediction of the behaviour in irregular waves will be treated.

6.1 Introduction

The tests in irregular waves were performed with the same 1:20 scale models of the AXE (axe bow concept) and the ESC (enlarged ship concept) as the tests in regular waves discussed in chapter 5. The tests were performed at full scale speeds of 25 knots, 35 knots and 50 knots. Converted to model scale using Froude scaling this is respectively 2.876 m/s, 4.026 m/s and 5.752 m/s. For details on Froude scaling see chapter 8. Not all wave conditions have been tested at all speeds.

The irregular waves were generated according to a JONSWAP wave spectrum. There are a number of relevant parameters to describe this wave spectrum: the significant wave height (H_s), the mean zero crossing period (T_z), the peak period (T_p) and the peak enhancement factor (γ) [19]. The wave spectrum parameters for the different wave conditions can be seen in table 6.1 [30]. The values at model scale are calculated using Froude scaling.

Table 6.1: Overview of the wave spectrum parameters, from Keuning and Vermeulen [30]

	Full scale				Model scale			
	H_s [m]	T_z [s]	T_p [s]	γ [-]	H_s [m]	T_z [s]	T_p [s]	γ [-]
1	2.0	6	7.8	3.3	0.100	1.34	1.74	3.3
2	2.5	6	7.8	3.3	0.125	1.34	1.74	3.3
3	3.0	6	7.8	3.3	0.150	1.34	1.74	3.3
4	3.5	6	7.8	3.3	0.175	1.34	1.74	3.3
5	4.0	6	7.8	3.3	0.200	1.34	1.74	3.3

6.2 Comparison

The behaviour of the models will be compared on a number of different aspects. First the vertical acceleration and vertical jerk peak values of the different models in similar wave conditions will be compared. This will be done using the Rayleigh plots introduced in chapter 4. It is not possible to compare the time traces, since the wave trains the models are subject to in the tests are not identically alike. Only there spectral aspects, as described in section 6.1, are similar. Other comparisons will be made to see the influence on the response when the significant wave height of the waves is increased, or the speed is increased.

6.2.1 Hull types

In this section the behaviour of the different hulls will be compared. This will be done in three different wave conditions. The behaviour in other wave conditions was not very different compared to the conditions presented here, and thus the conclusions from this analysis are also applicable to the other conditions. The comparison will be made based on acceleration values and jerk values. In the Rayleigh plots the crest values and absolute value of the trough values are plotted. Same as in regular waves, the trough values for acceleration are often dominated by gravity effects. The crest values for acceleration and jerk are often following from slamming, and are more likely to be non-linear. Following the explanation in chapter 4 the distribution of crest or trough values will show up as a straight line in a Rayleigh plot if the response is linear with respect to the wave spectrum, which is also (approximately) Rayleigh distributed. In Keuning and Vermeulen [30] all the wave conditions are checked and validated to be corresponding to a JONSWAP spectrum.

In all Rayleigh plots also the linear response line (called Rayleigh line here) is plotted, as a black dashed line. This line is Rayleigh distributed and is thus a straight line in the Rayleigh plot. This line is obtained by calculating the significant value and corresponding Rayleigh distribution according to respectively equation 4.19 and equation 4.23. In these equations the energy density spectrum integral m_0 of the entire spectrum (thus also the non-linear part) is used. The deviation of the actual measured response thus gives an indication of how non-linear the response is. The more the deviation from the Rayleigh line, the more non-linear the response is. To compare the response in this chapter references will be made to the (expected) maximum value of this response. With this the height of the crest or trough that is expected to be exceeded once every 1000 peaks is meant, so a 0.1% probability of exceedance.

Acceleration

In figure 6.1 the Rayleigh plots for the acceleration at the centre of gravity can be seen. The plots for the AXE are in the first row, the plots for the ESC in the same wave condition are in the second row below the corresponding plot for the AXE. As mentioned above the crest and trough values are plotted. It can be seen that the trough values in all conditions follow the linear distribution relatively good. The crest values are however more non-linear. In these cases non-linear response does not always mean that the values are higher than as expected with the linear approach. In almost all conditions the crest values of the AXE are lower than the Rayleigh line, and thus the significant amplitude of the crests is lower than would be expected with a linear approach. At the ESC it can be seen that the crest values at the higher part of the Rayleigh plot increase to a value significantly larger than the Rayleigh line at the higher speeds. The maximum expected value for the acceleration on the Rayleigh lines are higher for the AXE than the ESC in all conditions. This is thus not represented in the actual accelerations, since these were found to be lower.

At the bow section the difference between the AXE and ESC is even more visible, see figure 6.2. The linear significant values are almost identical in all conditions. Also the trough values are almost equal for both models. The big difference is in the crest values of the acceleration. The actual measured response is especially for the ESC highly non-linear with crest values much higher than the AXE. The response of the ESC also shows a strong deviation from the Rayleigh line.

Jerk

In figure 6.3 the Rayleigh plots for the jerk at the centre of gravity can be seen, for the same conditions as used to analyse the accelerations. The Rayleigh line based on the linear determined significant value is by approximation the same for all conditions. Contrary to the accelerations crest values at the centre of gravity, which were lower than the trough values, the crest values of the jerk are higher than the trough values. In general the trough values are parallel to the Rayleigh line longer than the crest values. The trough values are thus more linear than the crest values, which is in line with the explanation given in the previous section that the crest values are more dominated by highly non-linear effects like slamming. The optimisation of the bow of the AXE is clearly visible again in these plots. The crest values of the jerk are up to two times lower at the AXE. Contrary to the accelerations, where the crest or trough values in some conditions deviated below the Rayleigh line, the jerk crest and trough values only deviate to higher values than the Rayleigh line. Non-linear response in jerk thus seems to always lead to higher jerk values than linearly assumed.

The jerk values at the bow are plotted in figure 6.4. The shape of the plots is quite similar to the shape of the plots of the jerk at the centre of gravity, only the values are higher. This is in line with what is

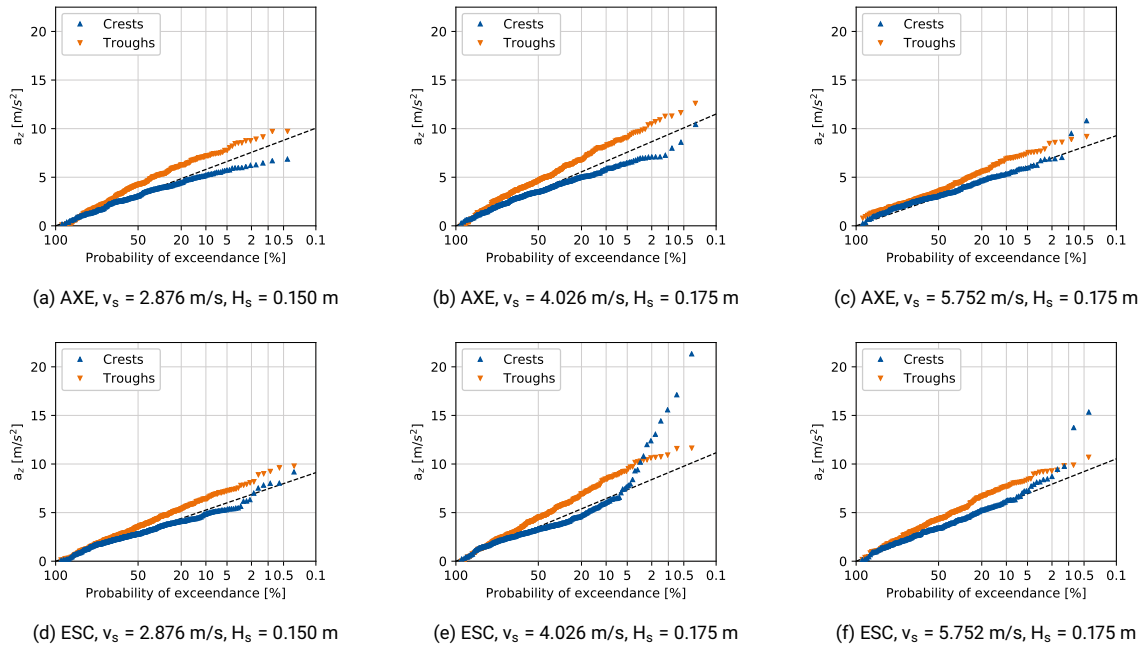


Figure 6.1: Rayleigh plots vertical acceleration, centre of gravity

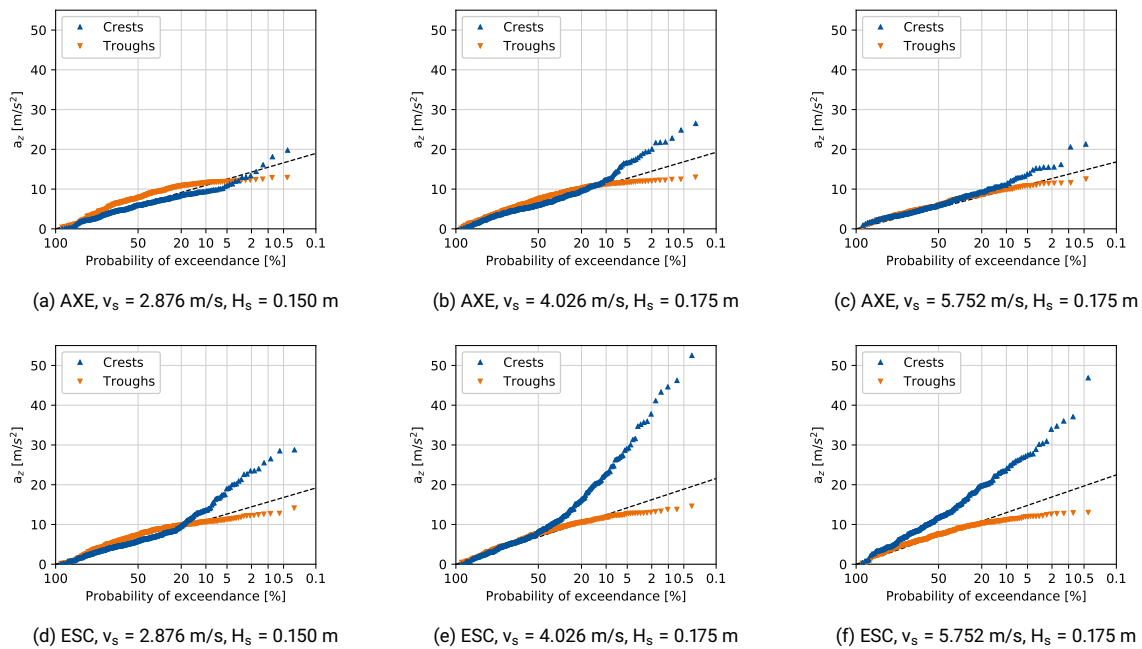


Figure 6.2: Rayleigh plots vertical acceleration, bow

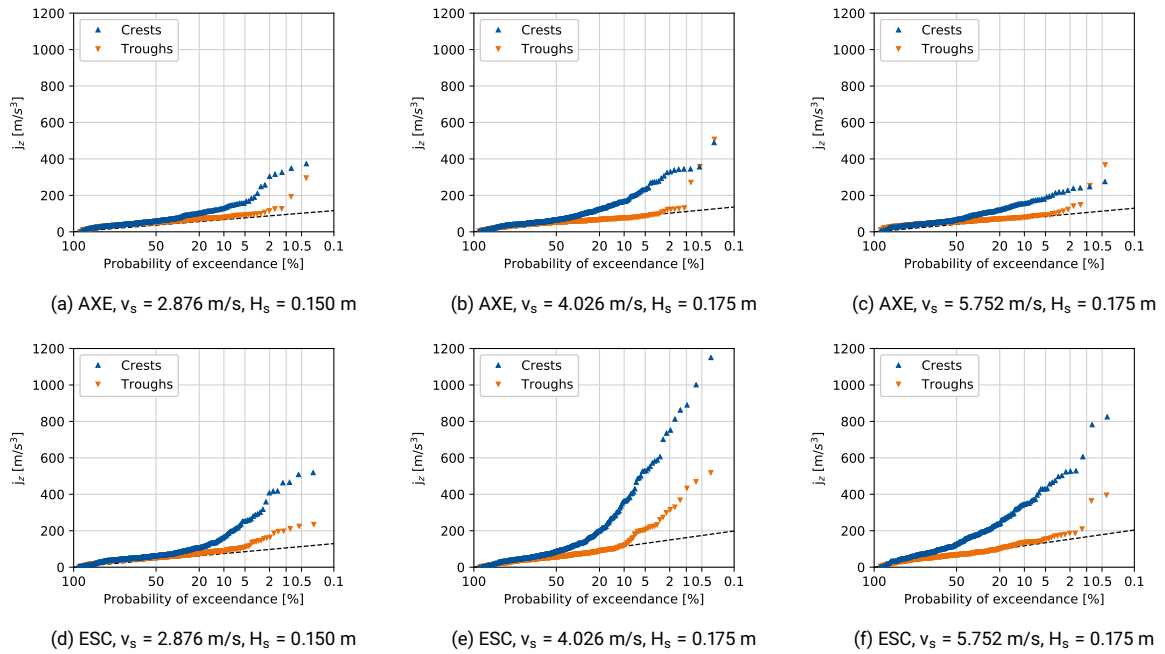


Figure 6.3: Rayleigh plots vertical jerk, centre of gravity

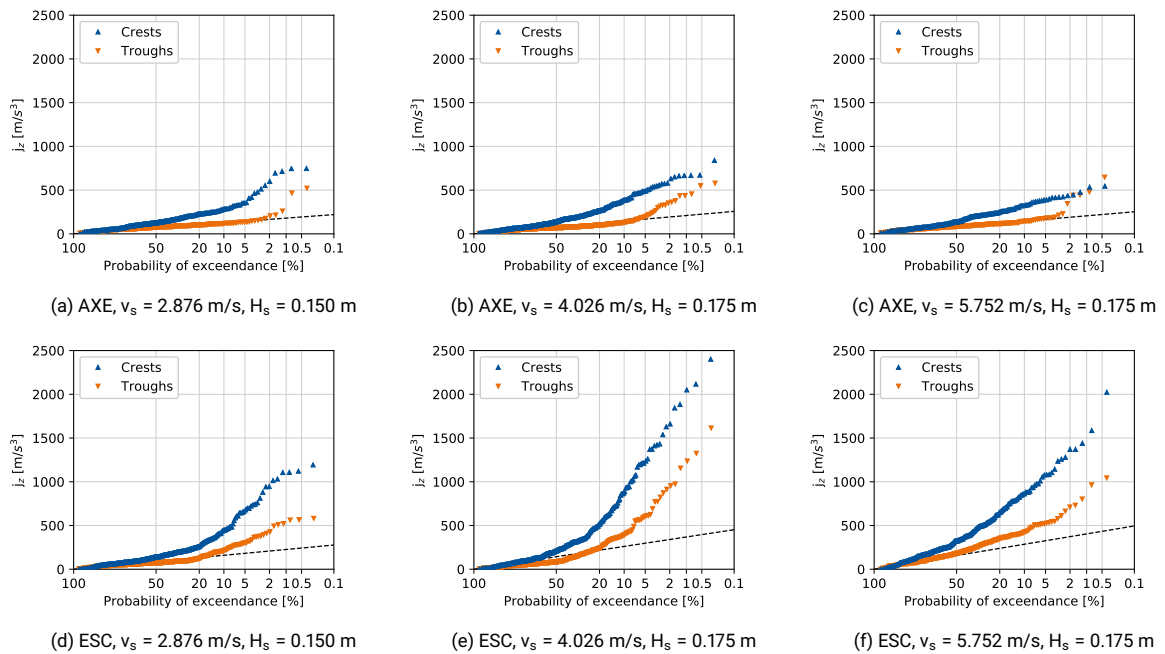


Figure 6.4: Rayleigh plots vertical jerk, bow

found in the analysis of the values over the length of the ship chapter 5. Here was concluded that the maximum jerk value at the bow and at the centre of gravity was dominated by the response following from slamming, contrary to the accelerations. Here the heave acceleration was often the maximum vertical acceleration at the centre of gravity. A more detailed analysis of the behaviour of the maximum values over the length of the ship will be performed in section 6.3.

6.2.2 Significant wave height

To investigate the effect of increasing significant wave height of the irregular waves the response of the ESC in the 25 knots tests is compared for different wave heights. The change in behaviour is similar for the AXE, and the behaviour of the AXE will therefore not be explicitly discussed here.

Acceleration

In figure 6.5 the crest and trough acceleration values are plotted for different significant wave heights. In the first row the response in the centre of gravity is plotted, in the second row the response at the bow. In the plots of the response in the centre of gravity can be seen that the calculated linear response, the Rayleigh line, increases proportionally with the increasing significant wave height. This is as would be expected from the linear approach. The trough values follow this line relatively well, until limited by the gravitational acceleration. The lower part of the crest values is lower than the Rayleigh line but follows the proportional increase. The upper part shows the biggest difference. With increasing wave height the upper part of the acceleration crests become larger than the Rayleigh line and show an increasingly non-linear behaviour. The same phenomena are visible in the acceleration plots at the bow, although the upper part of the crest values increases relatively more. This is what was also seen in the analysis of response in regular waves, large accelerations at the bow in slamming conditions compared to the centre of gravity.

Jerk

The crest and trough values of the jerk are plotted in figure 6.6. The jerk at the centre of gravity is plotted in the first row, the jerk at the bow in the second row. Contrary to the accelerations in the centre of gravity, the jerk shows a strongly increasing non-linear character with increasing significant wave height. The deviation from the Rayleigh line is in all conditions very evident. The maximum jerk value based on the Rayleigh lines is, in these graphs, up to eight times smaller than the actual measured maximum value. The lines of the jerk crest and trough values again look the same as at the centre of gravity, but are higher in value.

6.2.3 Forward speed

In this section the influence of increasing forward speed in the same wave conditions is analysed. For this the response of the AXE in irregular waves with a significant value of 0.175 m (3.5 m full scale) will be analysed, for the speeds 2.876 m/s, 4.026 m/s and 5.752 m/s (respectively 25, 35 and 50 knots full scale).

Acceleration

In figure 6.7 the crest and trough values for the acceleration are plotted. In the first row the values at the centre of gravity can be seen. The values at the bow are in the second row. It can be seen in the response plot of the centre of gravity that the trough values are highest and follow the Rayleigh line. The crest values are lower than the Rayleigh line, but at the highest speed the values are relatively close to this line. The significant value is highest for the tests with ship speed $v_s = 4.026$ m/s. This is because with this speed most of the energy of the wave spectrum is close to the natural frequency of the models [7]. The tests with ship speed $v_s = 5.752$ m/s are thus further away from the natural frequency and the response seems to be less non-linear.

The crest values of the accelerations at the bow are in all conditions higher than at the centre of gravity. At the bow it is more clearly visible that tests with ship speed $v_s = 4.026$ m/s are the most non-linear response, with crest values larger than the Rayleigh line. The crests of the tests with ship speed $v_s = 5.752$ m/s follow to a large extent the Rayleigh line and thus seem to be less non-linear than the other conditions. The non-linearity in the response will be analysed to a further extent in section 6.4.

Jerk

The jerk at the centre of gravity and the bow is shown in respectively the first and second row of figure 6.8. The crest values of the jerk for the tests with ship speed $v_s = 2.876$ m/s and $v_s = 4.026$ m/s follow

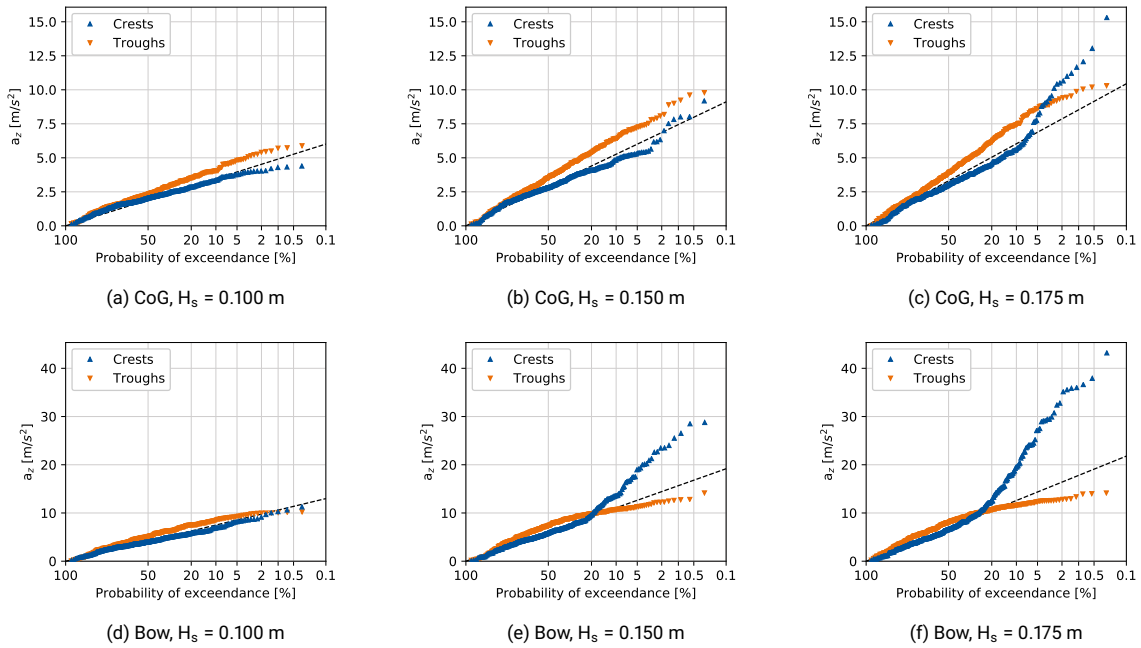


Figure 6.5: Rayleigh plots vertical acceleration, ESC, $v_s = 2.876$ m/s

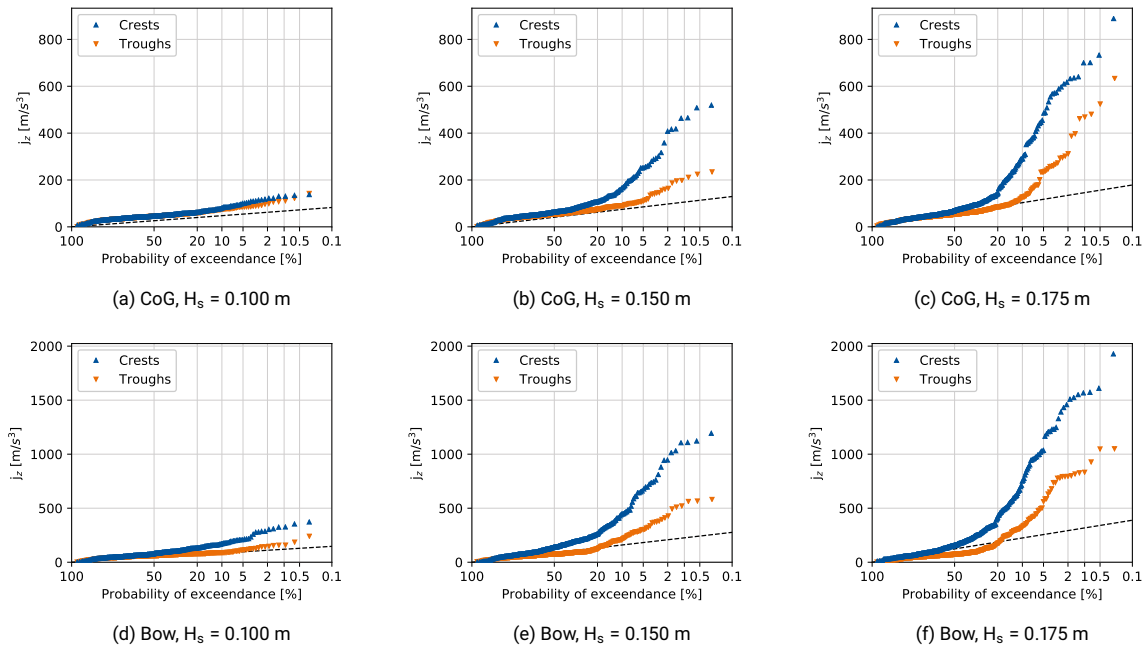


Figure 6.6: Rayleigh plots vertical jerk, ESC, $v_s = 2.876$ m/s

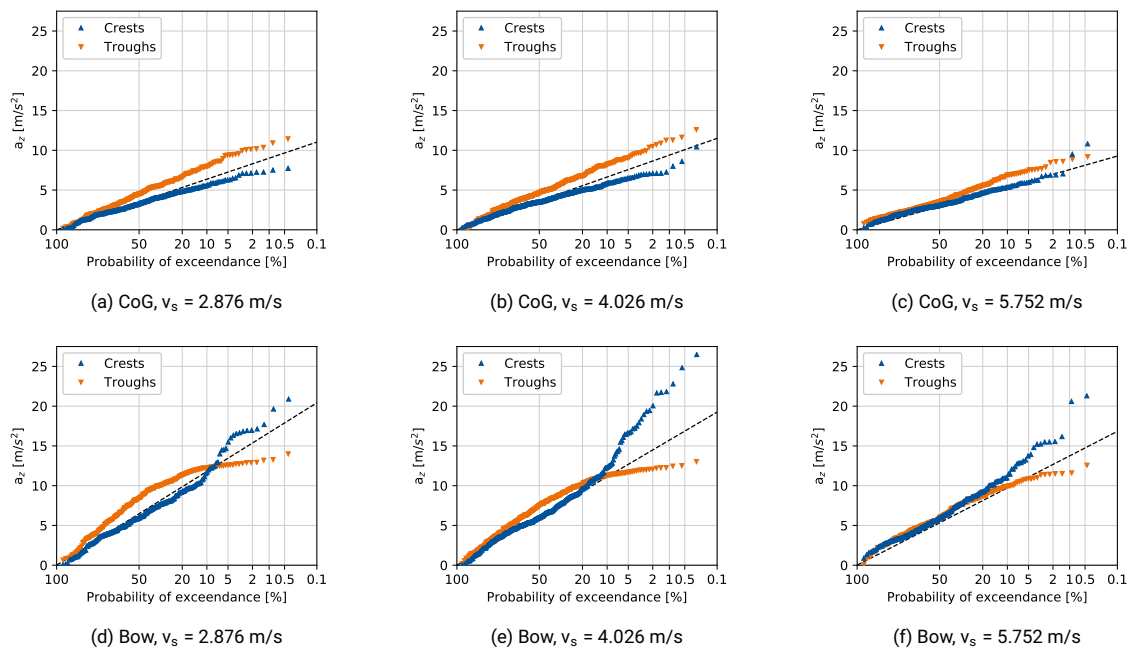


Figure 6.7: Rayleigh plots vertical acceleration, AXE, $H_s = 0.175$ m

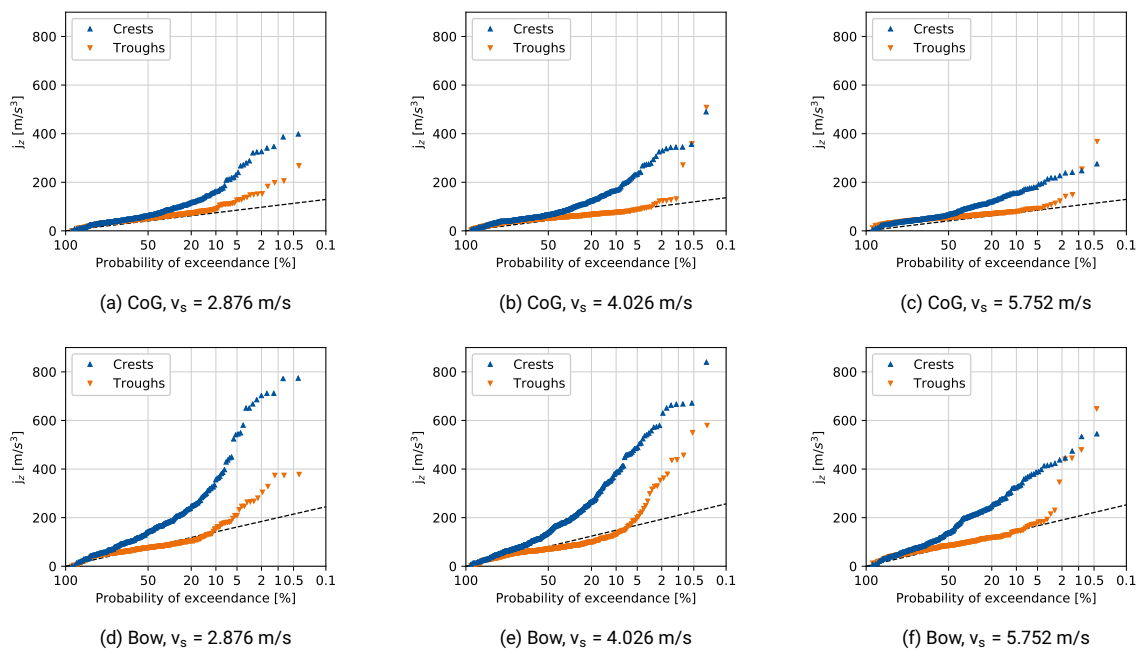


Figure 6.8: Rayleigh plots vertical jerk, AXE, $H_s = 0.175$ m

a quite similar distribution. The crest values for the tests with ship speed $v_s = 5.752$ m/s are lower than the other conditions, again because this speed in combination with the wave conditions is further away from the natural frequency of the models compared to the other speeds.

6.3 Analysis over ship length

To analyse the pitch in the ship motions and the values of acceleration and jerk over the length of the ship, the same procedures as determined in section 5.3 have been applied to the measurement data of the irregular waves. With the measurements of accelerations at the centre of gravity and the bow the pitch acceleration can be determined. From this the pitch jerk can then be derived. For both these data sets Rayleigh plots can then be determined, to analyse the part of the response following from pitch.

6.3.1 Decomposition heave and pitch

In figure 6.9 the pitch accelerations of the same conditions as analysed in section 6.2.1 are plotted. As defined in section 2.1 the pitch acceleration is positive when the bow moves down. The bow up movements from slamming result thus in large trough values. This can also be seen in figure 6.9. In this figure the pitch accelerations of the AXE are plotted in the first row, and the pitch accelerations of the ESC are plotted in the second row. It can be seen that the crest values are quite similar for both hulls in all conditions, while the trough values of the ESC are significantly higher than the AXE. This corresponds with the conclusion of chapter 5 that the AXE is optimised to minimise pitching. The reduced pitching is also the main reason the accelerations at the bow of the AXE are lower than at the bow of the ESC.

In the figures also the Rayleigh lines are plotted. Although the distribution of the pitch acceleration seems to be relatively straight in the Rayleigh plot in most cases, these are not significant values that would follow from linear approach. However, the assumption can be made that the pitch acceleration is not very non-linear. This will be further analysed in section 6.4.

The optimisation of the bow of the AXE is also clearly visible in the Rayleigh plots of the pitch jerk, as can be seen in figure 6.10. The jerk values at the AXE are in all conditions significantly lower than the ESC. The Rayleigh lines indicate that in all the conditions the pitch jerk is not approximated well by the linear approach.

6.3.2 Different cases

Determining the values of acceleration and jerk over the length of the ship, as performed for the regular waves in section 5.3, works different in irregular waves. This is because the accelerations and jerk at any longitudinal position of the ship at any moment in time are not only determined by the at that moment encountered wave, but they are also influenced by the previously encountered waves. Therefore at any part of the ship there is a certain chance that a certain value is exceeded. To determine this, the time traces of the acceleration and jerk are determined at a number of longitudinal position of the ship. In this analysis 100 longitudinal positions with equal interval are used. The same assumptions as in section 5.3 are applied to justify the use of equation 5.4. These assumptions were that the model is rigid and the rotations are small.

When the time traces of the accelerations and jerk at any longitudinal position are determined, the Rayleigh plots at that position can be determined. Since every longitudinal position has its own Rayleigh distribution, the best way to visualise this is to plot the acceleration or jerk values corresponding to a certain probability of exceedance over the length of a ship. When looking at for example figure 6.11c, the probability is 1% that the accelerations at the AXE at $x/L = 0.2$ exceed approximately 11 m/s^2 . For the ESC this is approximately 16 m/s^2 , in the same wave spectrum. The performance of the AXE is thus better at this point. Similar to the procedure used in chapter 5, the absolute largest value is plotted here. At the forward part of the ship this is often the crest value, more to the stern of the ship this is the trough value.

In some figures there seem to be small outliers from the lines, see for example the jerk at $x/L = -0.1$ at the ESC in figure 6.11f. Since the crests and troughs are a finite number of values, the plotted line is based on the values with a probability of exceedance closest to the target value, in this case 1%. It could however be that due to the superposition of heave and pitch, and the way crests and troughs are

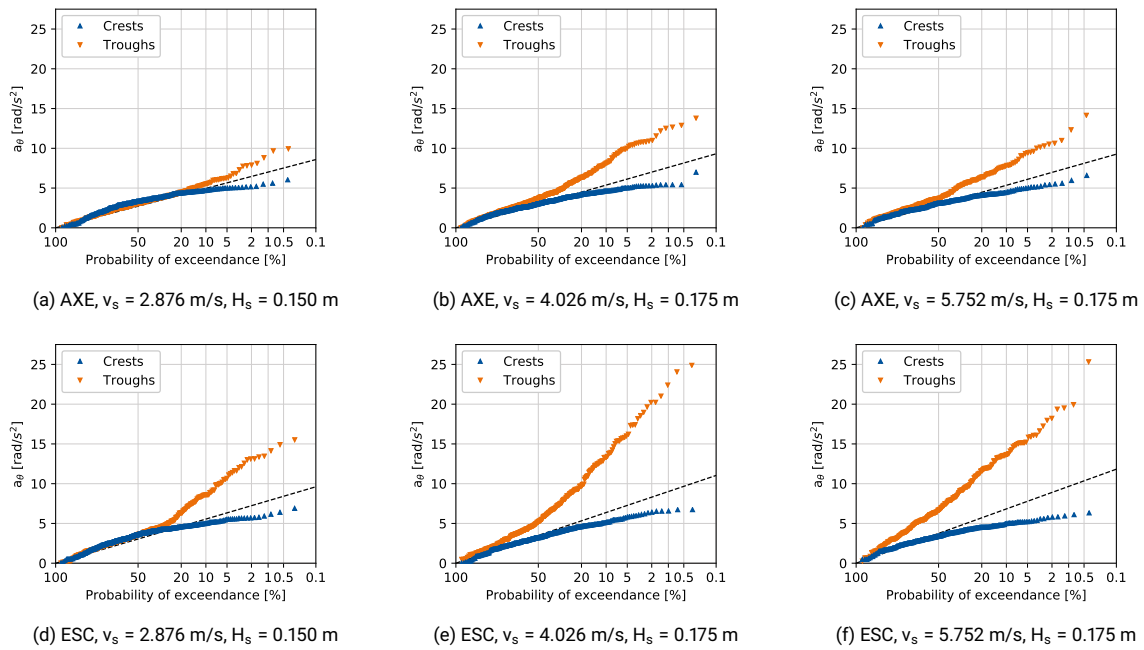


Figure 6.9: Rayleigh plots pitch acceleration

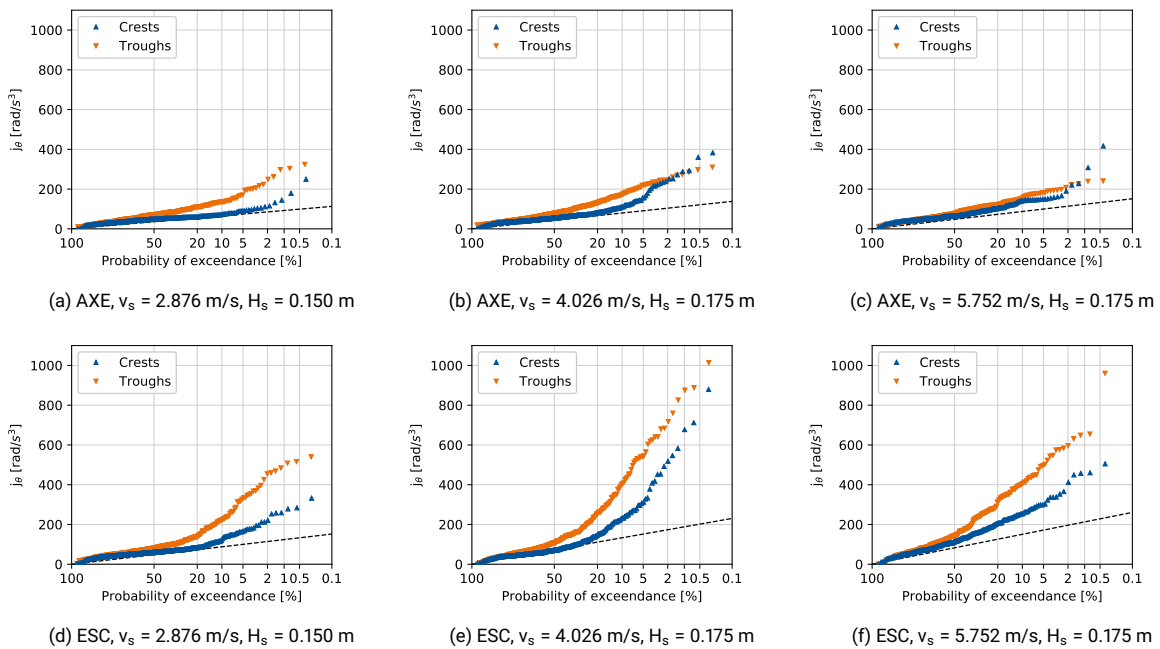


Figure 6.10: Rayleigh plots pitch jerk

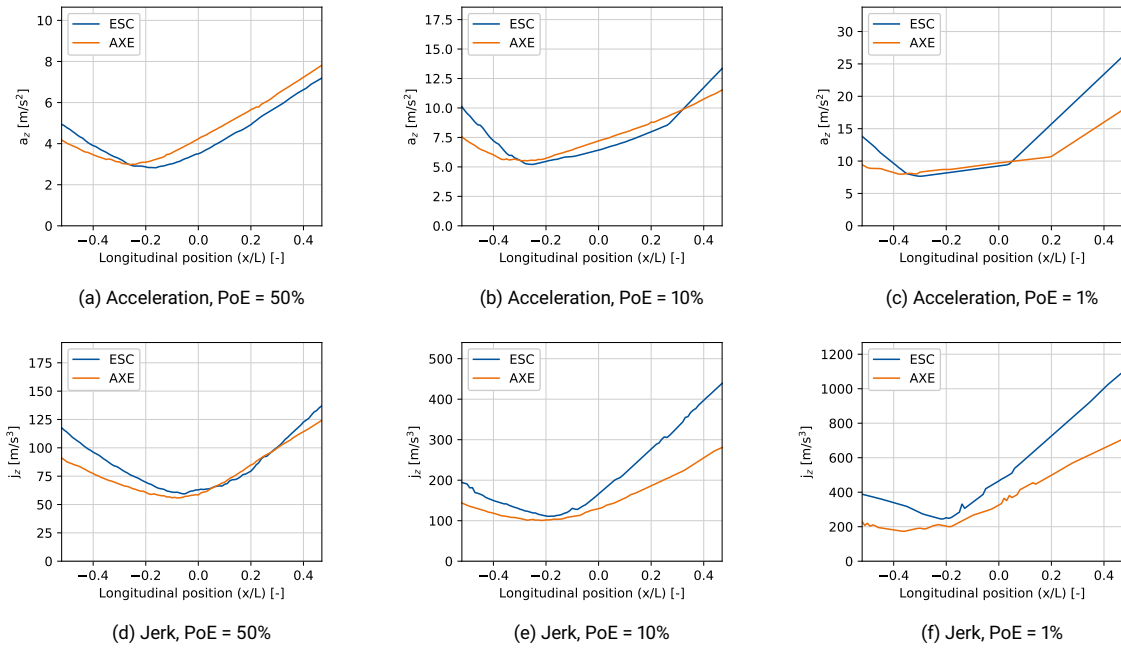


Figure 6.11: Analysis over ship length, $v_s = 2.876$ m/s, $H_s = 0.150$ m

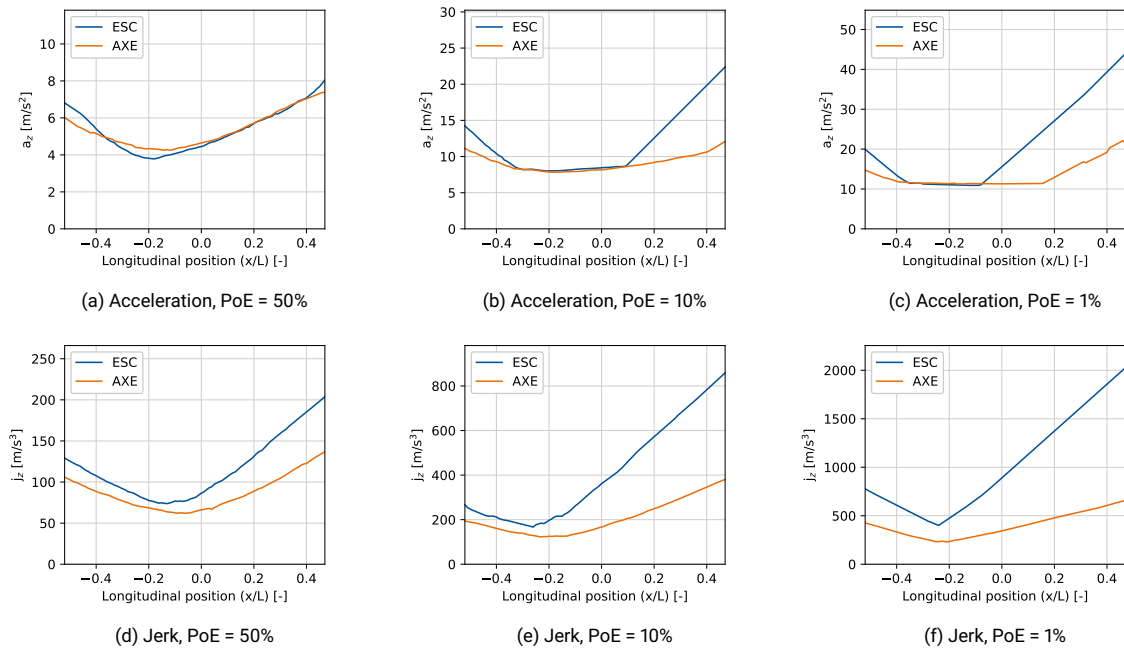


Figure 6.12: Analysis over ship length, $v_s = 4.026$ m/s, $H_s = 0.175$ m

determined, a different number of crests and troughs is found. The probabilities of exceedance then change slightly, which might lead to a different value being closest to that probability of exceedance. This causes a small outlier in the plot.

The values of acceleration and jerk over the length of the ship have been plotted for different probabilities of exceedance (PoE) to illustrate the different behaviours. The plots with probability of exceedance of 50% represent the 'mean' behaviour of the ship in the irregular waves. The plots with a probability of 10% or 1% illustrate the more extreme behaviour. This way the mean behaviour can be compared with the extreme behaviour. The extreme behaviour is often limiting for the operability or comfort in a certain seaway.

Case 1: $v_s = 2.876$ m/s, $H_s = 0.150$ m (full scale 25 knots, $H_s = 3.0$ m)

In figure 6.11 the different plots over the length of the ship can be seen for the case with a ship speed of 2.876 m/s and 0.150 meter significant wave height. The acceleration values are in the first row, the jerk values in the second row. The mean behaviour, with a probability of exceedance of 50%, is relatively equal for both model considering heave and jerk. The ESC is performing slightly better when looking at the accelerations, the AXE is performing better when looking at jerk. This behaviour was also found in the regular waves experiments in moderate wave conditions. The difference in performance becomes bigger when looking at the more extreme conditions, with probability of exceedance of 10% or 1%. The maximum value for the accelerations in these conditions is over the length of the ESC dominated by the pitch accelerations from slamming, as was also observed in the regular waves. This is less at the AXE, and therefore the AXE is also performing better over the whole length when looking at the jerk.

Case 2: $v_s = 4.026$ m/s, $H_s = 0.175$ m (full scale 35 knots, $H_s = 3.5$ m)

The acceleration and jerk plots over the length of the ship for the case with ship speed 4.026 m/s and 0.175 m significant wave height can be seen in figure 6.12. In general the graphs look quite similar to the graphs in figure 6.11. The mean acceleration behaviour is now almost identical. The mean jerk behaviour however shows that the AXE is performing better than the ESC. In the plots of the more extreme conditions it can be seen that the pitching of especially the ESC increased, which leads to larger acceleration and jerk values over the length of the model.

6.4 Non-linearity

In chapter 5 was proven that the non-linear part of the response is important to represent the actual response of the models. To prove that this is also the case for the behaviour in irregular waves, the response of a case is determined with and without the non-linear part. In figure 6.13 the Rayleigh plot for the acceleration can be seen in the first row, and the energy density spectrum in the second row. To get the linear response the data for this specific case has been filtered to not include energy at frequencies anymore at which there is also no (almost) no energy in the wave spectrum. For reference the actual Rayleigh plot and energy density spectrum, which followed from the processing procedure also used in the rest of this report, have been plotted. For the jerk this is done in figure 6.14. It can be seen that in the linear case the crests and troughs are all on the Rayleigh line. The significant value of the Rayleigh lines is lower in the linear case, since there is less energy in the energy density spectrum. The integral of the spectrum m_0 , which is used to determine the significant value, is thus also lower. It can be seen that the maximum values of the acceleration and jerk are significantly underpredicted with the linear approach, up to a factor ten.

The non-linearity ratio, as defined in chapter 4, has in irregular waves a different meaning than in regular waves. The derivation showed that it was the inverse of the coefficient of determination of the sine fit through a regular response. However, it is not possible to fit a sine function through irregular waves, thus there is no coefficient of determination in this case. The definition of the non-linearity ratio (see equation 4.12) can however still be applied to irregular waves. Since there are little test conditions, making plots of the non-linearity as function of speed does not provide much information. Therefore the non-linearity ratios for the different conditions already used multiple times in this chapter are given in table 6.2.

There are no clear trends visible that are valid for both models. For example the vertical jerk at the bow becomes increasingly non-linear for the ESC with increasing speed, but the AXE has a peak in the non-linearity for the condition with ship speed $v_s = 4.026$ m/s. In general it can be seen that the pitch

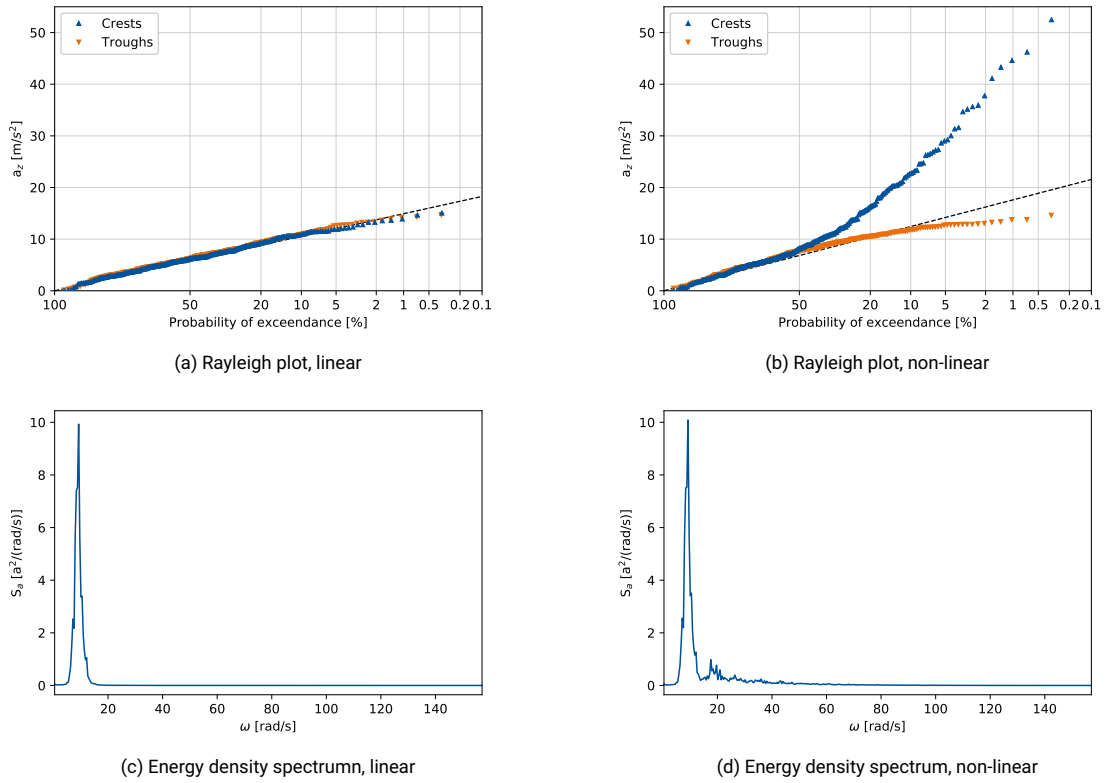


Figure 6.13: Comparison vertical acceleration, ESC, bow, $v_s = 4.026$ m/s, $H_s = 0.175$ m

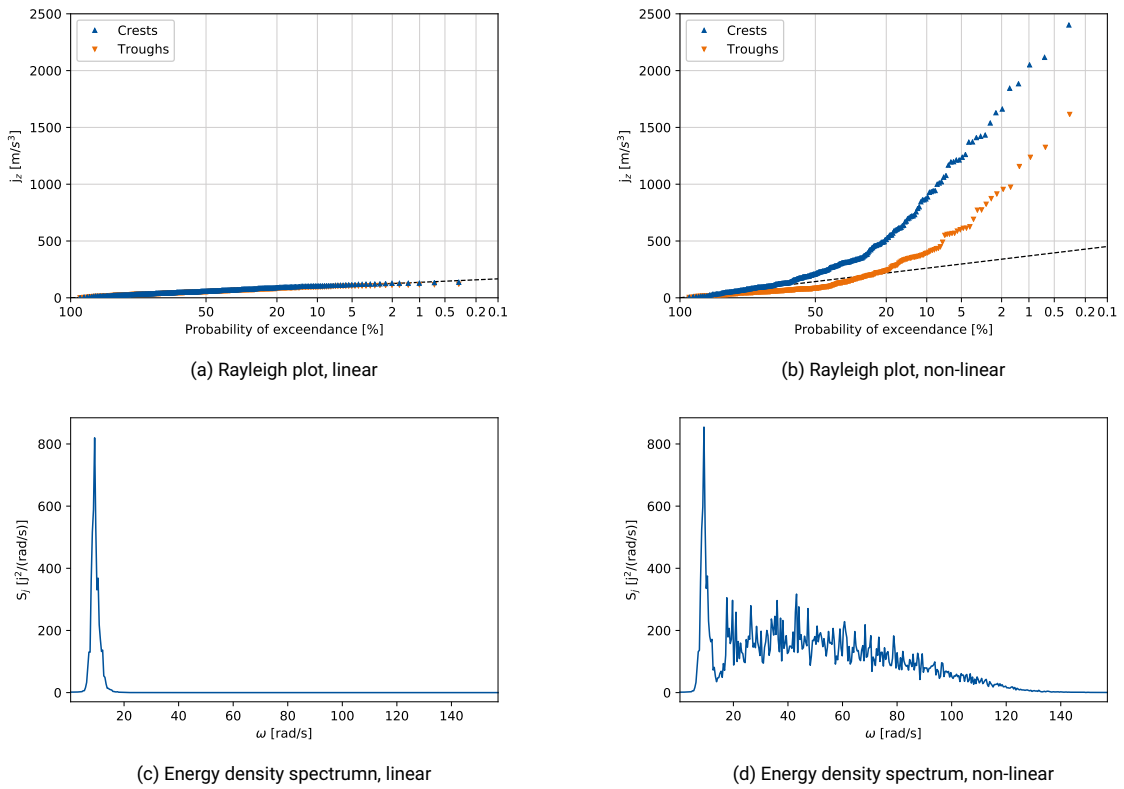
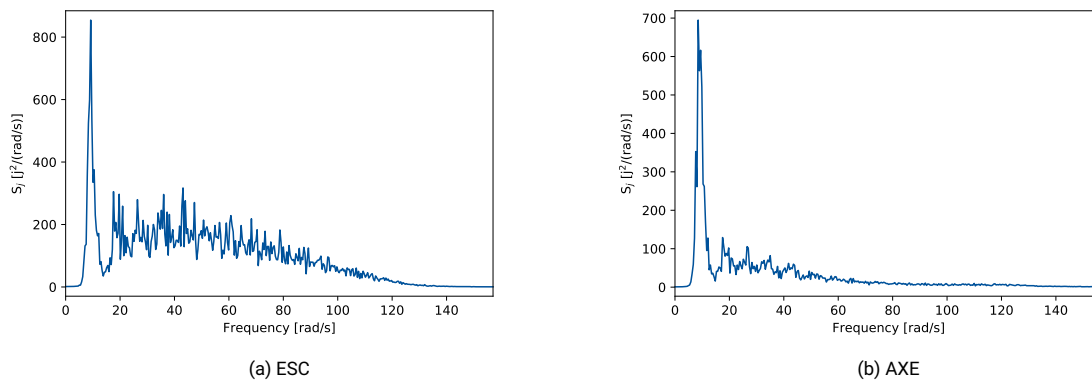


Figure 6.14: Comparison jerk, ESC, bow, $v_s = 4.026$ m/s, $H_s = 0.175$ m

Table 6.2: Non-linearity ratio for different irregular wave conditions

Model	Speed [m/s]	H_s [m]	Centre of gravity				Bow	
			r_{nl,a_z}	r_{nl,j_z}	r_{nl,a_θ}	r_{nl,j_θ}	r_{nl,a_z}	r_{nl,j_z}
AXE	2.876	0.150	0.067	0.544	0.088	0.627	0.087	0.543
ESC	2.876	0.150	0.096	0.716	0.143	0.760	0.141	0.726
AXE	4.026	0.175	0.064	0.482	0.115	0.637	0.110	0.584
ESC	4.026	0.175	0.149	0.786	0.242	0.841	0.260	0.855
AXE	5.752	0.175	0.065	0.472	0.139	0.572	0.131	0.512
ESC	5.752	0.175	0.180	0.745	0.280	0.801	0.294	0.809

Figure 6.15: Energy density spectra of vertical jerk, bow, $v_s = 4.026$ m/s, $H_s = 0.175$ m

acceleration and jerk is more non-linear than the heave acceleration and jerk, which was also concluded in section 6.3 and thus agrees with the behaviour in regular waves. Furthermore the response of the AXE is in general less non-linear than the response of the ESC. This is also clearly visible in figure 6.15. The first peak is the first order response to the wave spectrum, and at higher frequencies the non-linear response is visible. The amount of non-linear energy in the energy density spectrum is significantly lower for the AXE than for the ESC.

6.5 Prediction of response

Predicting the behaviour of a ship in irregular waves is an important step, since the seaway is almost always irregular. As mentioned in chapter 4 and the introduction of this chapter, the non-linear behaviour of a ship in seaway is a highly random process with no direct correlation between wave amplitude and amplitude of the response. Two methods to predict the response will be (briefly) discussed. The first one is the use of numerical methods. The second method is predicting the behaviour based on the response in regular waves.

6.5.1 Numerical methods

The importance to include non-linear behaviour in the response of the ship has been proven multiple times in this report already. Therefore widely used linear numerical methods to predict the response of the ship will not produce useful results in this case. As seen in section 6.2 the linear approach will sometimes lead to overpredictions of the response, but in most cases and especially for jerk the linear approach will lead to extreme underpredictions of the response.

In de Jong [7] the irregular wave tests have also been simulated using a weakly non-linear code, PANSHIP. For more information on non-linearity of numerical methods, see section 7.1. It was found that the results were significantly underpredicted, and looked more like the linear expected behaviour as explained above. When using numerical methods to predict the behaviour of the models in this chapter probably fully non-linear high fidelity codes like Reynolds Averaged Navier Stokes (RANS) are required.

To make a good estimation about the behaviour in irregular waves, at least 200 wave encounters should be simulated [26]. This is however computationally very expensive.

6.5.2 Behaviour in regular waves

Another way to predict the behaviour in irregular waves is linking it to the behaviour in regular waves. Predicting the exact values is difficult because of the highly non-linear behaviour of the models, invalidating the use of transfer functions between the wave spectrum and the response spectrum. The general behaviour can however be predicted. When looking at the heave behaviour in regular waves it was found that the AXE performed better than the ESC especially in higher waves and with higher encounter frequencies, which relates to higher speeds here. At lower speeds and lower wave amplitudes there were conditions where the accelerations of the ESC are lower than the AXE. All this behaviour was also observed in irregular waves. The lower vertical accelerations of the AXE are especially visible at the bow. Looking at jerk the AXE performed better in all conditions, even in the conditions where the accelerations were higher than at the ESC.

Because the vertical acceleration difference is especially visible at the bow, where it is composed of the heave acceleration and the pitch acceleration, it can be concluded that the pitching of a ship is an important contributor to the seakeeping behaviour in irregular seas. The bow of the AXE is optimised for this, which resulted in significantly lower pitch accelerations and pitch jerks.

The main driver in the behaviour as described here is the occurrence of slamming. Since the response in regular tests is (almost) equal each wave encounter, either slamming occurred or there was no slamming at all. This was also concluded by de Jong [7]. When looking at the response values in irregular waves over the length of the ship it can be concluded that in the mean behaviour, which was defined as the values with a probability of exceedance of 50%, no slamming is present and the behaviour is thus similar to the behaviour of regular wave tests where no slamming was observed. In the more extreme behaviour, defined by the probabilities of exceedance of 10% and 1%, the maximum response over the length of the ship was comparable with the slamming behaviour of the models in regular waves. The number of slams in an irregular seaway might thus also be an indicator for the seakeeping behaviour.

The optimisation of the AXE resulted in less non-linear behaviour in the same seaway, compared to the ESC. This validates the assumption made in 4.1.3 that the 'ideal' behaviour of a vessel is completely linear behaviour, and that optimisation should thus be focused on minimising the non-linear behaviour. Improving the non-linear behaviour of a ship in regular waves thus also improves the non-linear behaviour of a ship in irregular waves.

Numerical computation of ship motions

An important step in the process of ship design is predicting the responses of a ship. This can be done using model tests, but these are normally very expensive. Therefore already in 1861 research was performed by Froude in numerical ways to compute and predict the motions of a ship [3]. The methods used nowadays were developed starting from the 1950's [3]. Since then the computational capacities of computers have increased drastically, enabling the use of methods that were not possible before.

In this chapter first an introduction on numerical methods and their non-linearity will be given. This will be done in section 7.1. In section 7.2 the results of the regular wave tests from chapter 5 will be compared to the results of numerical computations of the ship motions in the same conditions using a Reynolds Averaged Navier Stokes (RANS) code. In section 7.3 a short summary will be given.

7.1 Non-linearity of numerical methods

There are three methods of computational fluid dynamics (CFD) which are widely used to numerically calculate the motions of a ship. These are the strip theory, panel methods and RANS. The term CFD is sometimes also used to indicate the RANS method. An important distinction can be made in the non-linearity of the methods. Linear methods make more simplifications in the modelled physics, which makes the calculations less computationally expensive. A consequence of that could be that the calculated response is less representative for the actual response than a response calculated with non-linear methods. In non-linear methods less simplifications are made, but this makes them more computationally expensive.

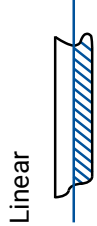
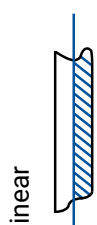
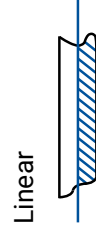

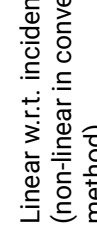

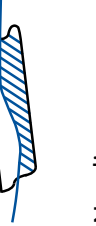

There are different levels of non-linearity in the available numerical methods. In table 7.1, which comes from the International Towing Tank Conference [25], an overview of the different methods is given. The linearisation can be in the incident wave, the disturbance hydrodynamics (added mass and damping terms) and/or the Froude-Krylov and restoring forces (wave forces and buoyancy). As explained in chapter 2, if linearisation is applied, the hydrodynamic terms or forces are calculated for the still water geometry. If the terms are calculated non-linear, the instantaneous submerged geometry is used.

Another factor are the viscous forces. The strip theory and the panel methods are based on the potential theory, and thus do not include viscous forces [27]. For example viscous roll damping can be artificially added to these calculation. RANS CFD calculations can calculate the viscous forces.

Which method should be used is mainly dependent on the level of accuracy required from the results and the test conditions. As explained in section 4.1.2 the amount of non-linear energy in the response grows exponentially with increasing derivative. If thus accurate values for the acceleration or jerk are required, the calculation should be non-linear. If only the heave displacement is required, then linear codes might be sufficient since the displacements of a free sailing ship are usually mostly linear.

The test conditions are also of importance. In section 2.3 phenomena that drive the ship to more non-linear behaviour were described. If the modelled ship is a slow-sailing ship in low to moderate wave conditions, linear codes might be sufficient. If however the speed of the modelled ship is relatively large or the waves amplitudes are large, non-linear codes are required to give accurate results. Especially when slamming is expected, RANS calculations might be required to give accurate results. This is because slamming is a highly non-linear event, as described in section 2.3.4. If however only an indication of the number slams in irregular seas is required, then a weakly non-linear method might be sufficient. The number of slams can than be predicted by the relative keel clearance and the velocity of the re-entry of the hull in the water at any moment. For this the Ochi criterion is defined [27]. This subject will not be discussed further in this thesis.

Table 7.1: Categorisation of numerical methods for ship motion calculation, from International Towing Tank Conference [25]

Non-linearity	Incident wave	Disturbance hydrodynamics	Froude-Krylov and restoring forces	Numerical methods
Linear	Linear	Linear 	Linear 	Strip, Wave Green function, Rankine panel, CFD
Weakly non-linear	Linear	Linear 	Non-linear 	Strip, Impulse-response function, Green function, Rankine panel
Weak scatterer	Linear or non-linear	Linear w.r.t. incident wave (non-linear in conventional method) 	Non-linear 	Rankine panel
Fully non-linear	Non-linear	Non-linear 	Non-linear 	RANS CFD

7.2 Regular waves tests - RANS CFD

For a Damen research project (performed by Sebastian Sigmund from Damen Shipyards Gorinchem) parallel to this graduation project numerical computations using a Reynolds Averaged Navier-Stokes (RANS) CFD code were performed. The simulations have been performed at a model speed of 2.876 m/s with wave conditions equal to the model tests in the wave steepness of $\kappa = 0.033$. The results of these computations could also be used in this thesis. Therefore in this section the results of these simulations will be compared to the measurements of the towing tank tests, to see how well the RANS CFD code predicted the behaviour of the model. For the geometry of the AXE more results were available, so this hull will be used to make the comparisons between the measurements and the calculations. The comparisons will be made based on the peak values of the acceleration and the jerk and the non-linearity. Furthermore the similarity between the time traces will be defined. Finally the behaviour of the vessel over one wave encounter where slamming is occurring will be analysed. Here results for both the AXE and the ESC were available, so these are both used. The procedures for processing the data coming from the RANS calculations is the same as with the measurement data from chapter 5, only no filtering of the data is required. Since the data comes from calculations there is no measurement inaccuracy or measurement noise.

7.2.1 Peak values

In figure 7.1 the heave acceleration and pitch acceleration, determined by the measurements and the RANS CFD calculations, can be seen. The pitch acceleration was a direct output from the calculations, so contrary to the measurements this did not have to be calculated from the acceleration at the centre of gravity and the bow. The plotted heave values are the crest values, since these are often limiting because of slamming. For the pitch this is the trough value, because of the definition of the positive direction of the motions.

Looking at the heave accelerations, the maximum heave acceleration especially at higher frequencies is predicted well. Around the natural frequency the calculated response is higher than the measured response. The latter is also visible in the pitch accelerations. An example of this can be seen in time trace 14 in appendix C. This mainly comes from an overpredicted first order response. In the energy density spectra clearly the first order peak is higher in the calculations than in the measurements. The higher order peaks are generally lower in the calculations than in the measurements.

The heave jerk and pitch jerk are displayed in figure 7.2. Contrary to the heave accelerations, the heave jerk is underpredicted by the RANS CFD code. In the energy density spectra of time trace 14 in appendix C it can be seen that although the first order peak is overpredicted, the higher orders are largely underpredicted for the heave jerk. These higher order peaks are thus the main cause for the height of the peaks of the heave jerk. At higher frequencies, further away from the natural frequency, the calculated values are close to the measured values. Examples of this can be seen in time trace 15 and 16 in appendix C. The calculated peak values of the pitch jerk correspond well with the measured values.

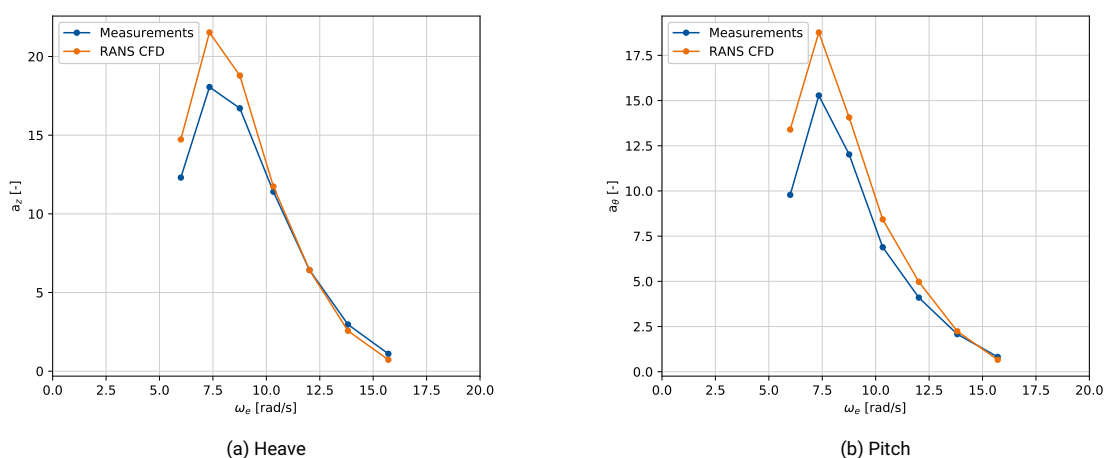


Figure 7.1: Maximum acceleration (non-dimensional), AXE, centre of gravity

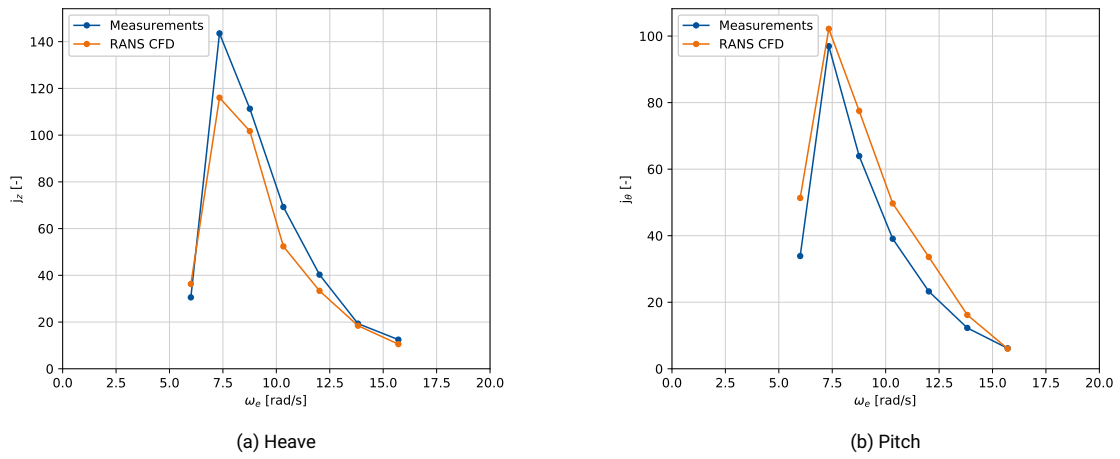


Figure 7.2: Maximum jerk (non-dimensional), AXE, centre of gravity

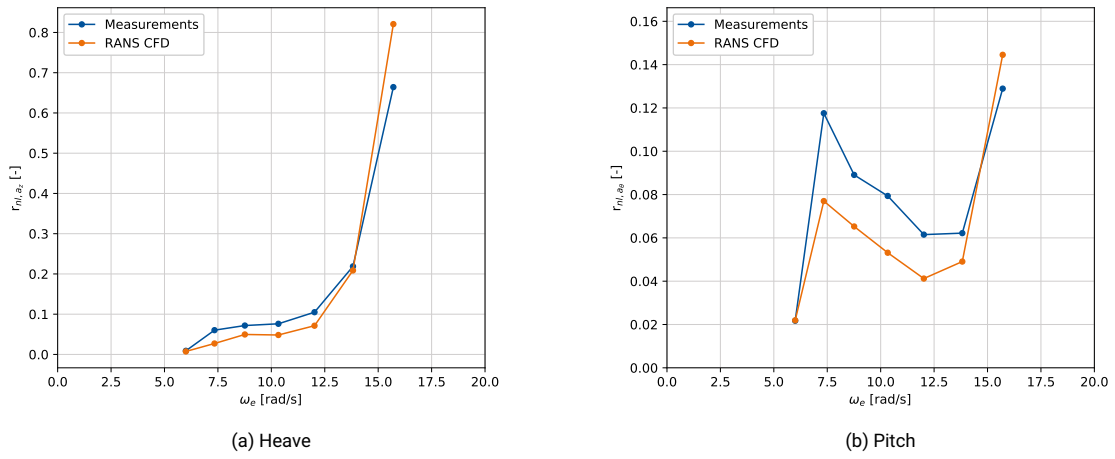


Figure 7.3: Non-linearity ratio acceleration, AXE, centre of gravity

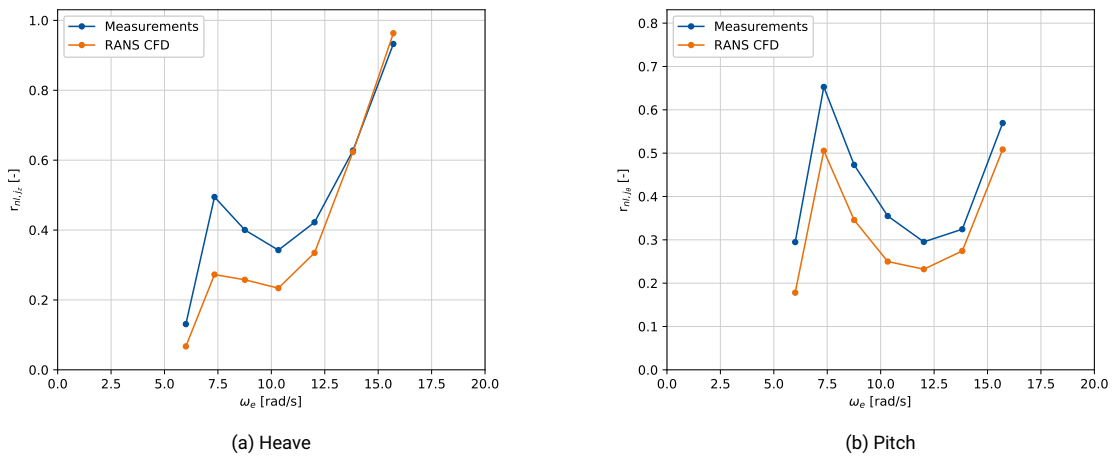


Figure 7.4: Non-linearity ratio jerk, AXE, centre of gravity

From this comparison it can be concluded that the prediction of the response using RANS code is quite accurate. The largest difference is occurring around the natural frequency, where slamming occurs. As mentioned in section 2.3.4 the exact response of slamming is difficult to predict, because of the highly non-linear character of this phenomenon.

7.2.2 Non-linearity

The non-linearity ratio of the accelerations (heave and pitch) is plotted in figure 7.3. The non-linearity ratio for the jerk, also for heave and pitch, is plotted in figure 7.4. From all the figures it becomes clear that the trends with increasing wave frequency are the same for the measurements and the calculations, only the exact value is different. This can be explained by the general tendency of the calculations to overpredict the first order response, and underpredict the higher order responses. The non-linearity ratio is then by definition lower, since it presents the ratio of non-linear energy in the total amount of energy in the energy density spectrum.

7.2.3 Time traces

To analyse the behaviour of a ship it is important that the entire time trace of all the movements is predicted correctly, not only the peak values. This way it can be seen if all the trends are captured by the RANS CFD calculations. In figure 7.6 the time traces of the AXE with encounter frequency $\omega_e = 12.02$ rad/s can be seen. The corresponding energy density spectra for the jerk can be seen in figure 7.7. It can be seen that the similarity between the calculated and measured time traces is generally good. The peak values are predicted well, except the trough values for the pitch jerk. These are overpredicted in this case.

The trends are also predicted well. The only exception is some vibration of approximately 20 Hz which is visible in the heave jerk and especially pitch jerk time traces determined from the measurement data. See for example the pitch jerk between 1.2 and 1.5 seconds. This vibration is not visible in the calculated response. It is unknown what the exact cause of this phenomenon is. In the research of de Jong [7] it is mentioned that in some experiments there is an interaction between the carriage of the towing tank and the model, which might be an explanation. It can also be that other conditions during the experiments, like the generation of the waves or interaction between the waves and the walls of the towing tank, cause this vibration effect. If one of the above mentioned phenomena is the cause of the vibration, this will not show in the calculations since these effects are not there. The exact cause of the vibration cannot be determined, since no additional data like video captures of the experiments are available to see what happens.

In figure 7.5 the best similarity between the time traces of the calculations and the the measurements can be seen. The similarity is defined here with the coefficient of determination (the r^2 -value, see chapter 4 for more information). If the signals are exactly the same the coefficient is 1, if there is no similarity at all the coefficient is 0. This coefficient is determined by taking a period of five wave encounters from

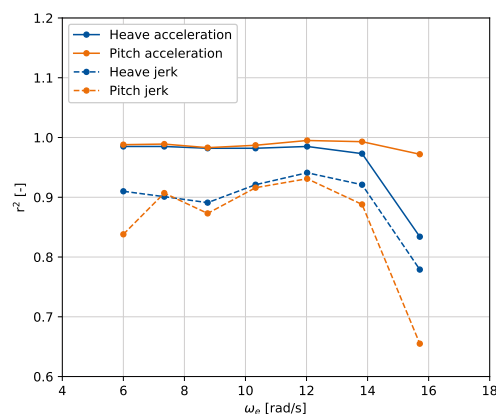


Figure 7.5: Coefficient of determination between calculated and measured response, AXE, centre of gravity

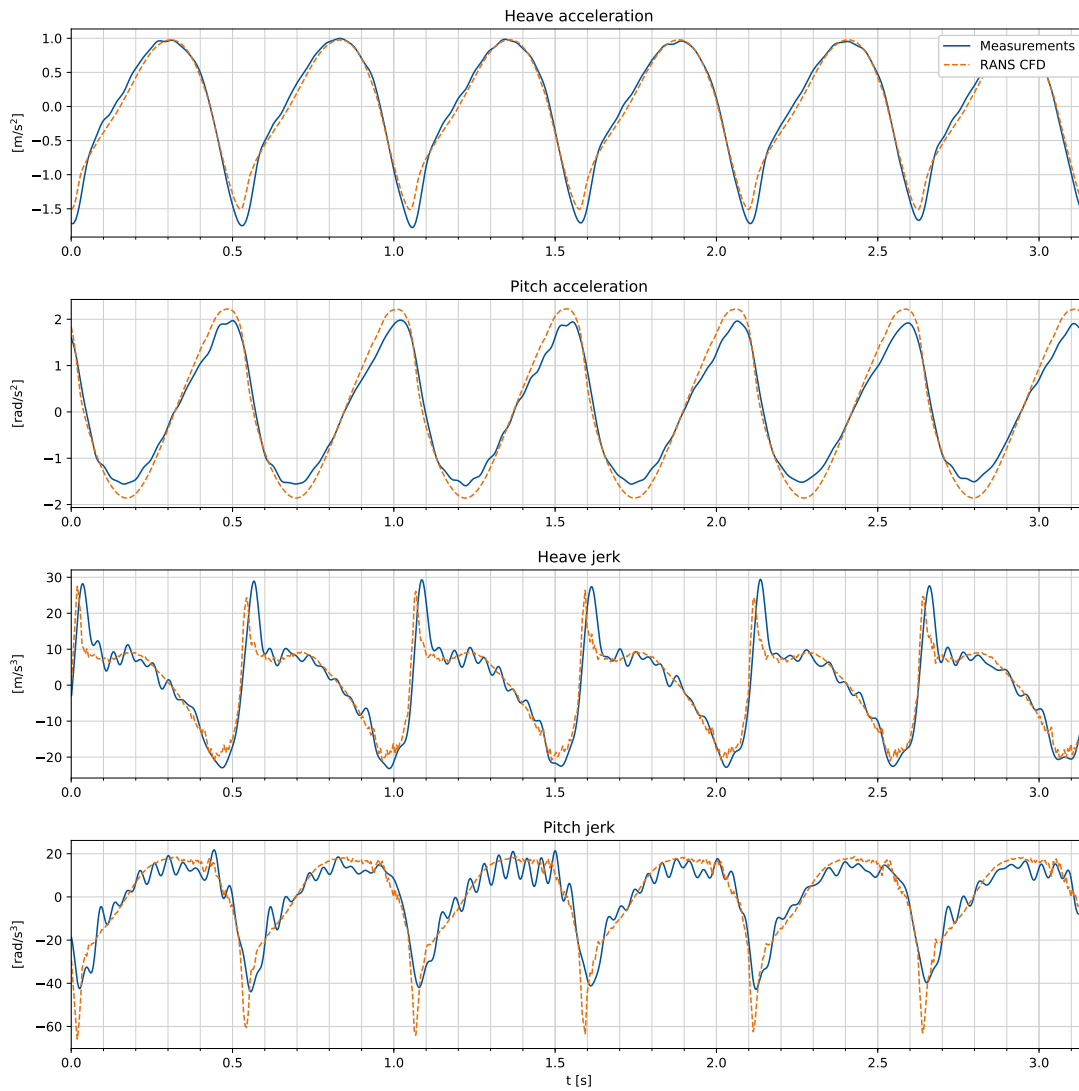


Figure 7.6: Time traces heave and pitch, acceleration and jerk, AXE, centre of gravity, $\omega_e = 12.02$ rad/s, $\kappa = 0.033$

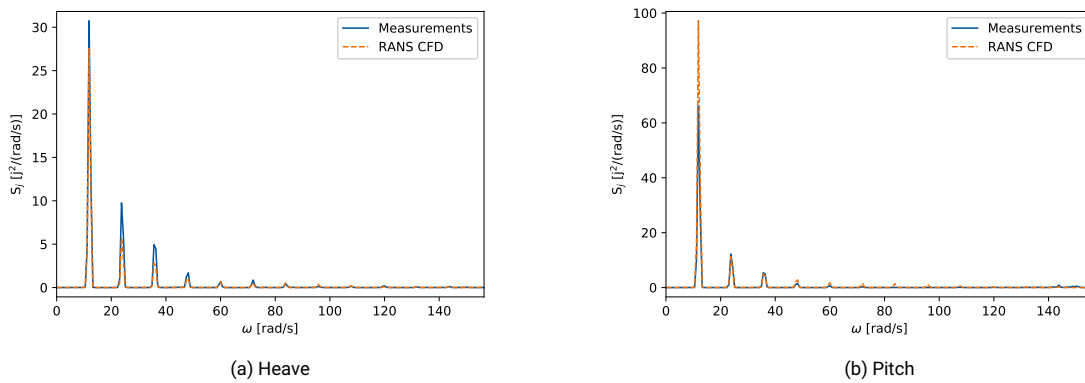


Figure 7.7: Energy density spectra jerk, AXE, centre of gravity, $\omega_e = 12.02$ rad/s, $\kappa = 0.033$

the calculations. From the measurement data then the best fitting period of five wave encounters is determined. Since the phase difference between the wave encounter and the response is not known for both the measurements and the calculations, the assumption is thus that this can be neglected and the best fit is at the same phase difference with the encountered waves.

The similarity of the accelerations is generally good, with values close to 1. Only at higher encounter frequencies the coefficient of determination is low. This is because at these high frequencies the values of the actual response are low. Therefore the signal-to-noise ratio of the measurements is also low, and some noise and measurement inaccuracies are still visible in the time traces. This is the main cause for the lower similarity, even though in the previous section was concluded that the peak values at higher frequencies are in good agreement. An example of this can be seen in time trace 16 in appendix C. The similarity of the jerk is lower than the similarity of the acceleration in all cases.

When looking at a time trace where slamming is occurring, for example time trace 14 in appendix C, it can be seen that the impulse caused by the slamming is visible in the heave acceleration of both the measurements and the calculations. The peak from the slamming is larger in the measurements. In both time traces the peak from the slamming is not the largest measured acceleration, this comes from the first order response. However the largest jerk is caused by the slamming. Since the peak in acceleration due to slamming was underpredicted, the peak in the jerk is also smaller than measured.

7.2.4 Analysis of wave encounter

From the RANS CFD calculations images (captures) are available. Therefore a detailed analysis of a wave encounter where slamming is present will be made in this section [48]. The captures from the AXE, at different time instances, can be seen in figure 7.8. The captures from the ESC at the same time instances can be seen in figure 7.9. The colours in the captures represent mass fractions. Red is a mass fraction of 1 and is water. Blue is a mass fraction of 0 and is air. All the colours in between are a mixture of air and water. For this analysis the difference between water and air is most important, to determine which parts of the hull are submerged and which parts are not. The time traces (vertical displacement to vertical jerk in the centre of gravity) corresponding to the captures are plotted in figure 7.10 for the AXE and figure 7.12 for the ESC. In the time traces the time steps are indicated, to illustrate what the response of the model is at what time step. The time steps in the text below refer to these time steps. Also the time traces for the bow are shown, in figure 7.11 for the AXE and figure 7.13 for the ESC.

Time step 1 - 4: moving upwards from previous encounter

In these time steps the models (both AXE and ESC) are still moving upward from the previous wave encounter. At time step 4 the centre of gravity of the models reached the highest position. Because of the phase difference the bows are already at the highest position at time step 3. The acceleration is already negative and the velocity is thus decreasing towards zero.

Time step 4 - 5: moving downwards

The models start moving downwards by the effects of gravity, and thus the velocity has become negative. The acceleration is still negative. At the centre of gravity the downward movement is only heave displacement, at other positions this is a combination of the heave and pitch.

Time step 5 - 6: slamming

The forward part of the hulls impact the water surface. This results in a sudden change from negative to positive acceleration. This moment is the most important when looking at the jerk. The sudden change of acceleration can only be caused by a large jerk. The velocity reaches its minimum. Because there is now interaction with the water, hydrodynamic restoring forces are decelerating the downward movements of the models.

The AXE already cuts into the water surface with the foremost part of the hull at time step 5, and therefore the submersion of the hull is more gradual and the jerk peak is lower. The ESC hits the water surface with a large part of the hull at the same time (see time step 6 of the ESC), resulting in a large jerk value.

Time step 6 - 9: moving downwards into the water

The momentum of the models still moves them downwards, the velocity is still negative. The hydrodynamic forces are decelerating the models until the velocity is zero. At the end the models are at the

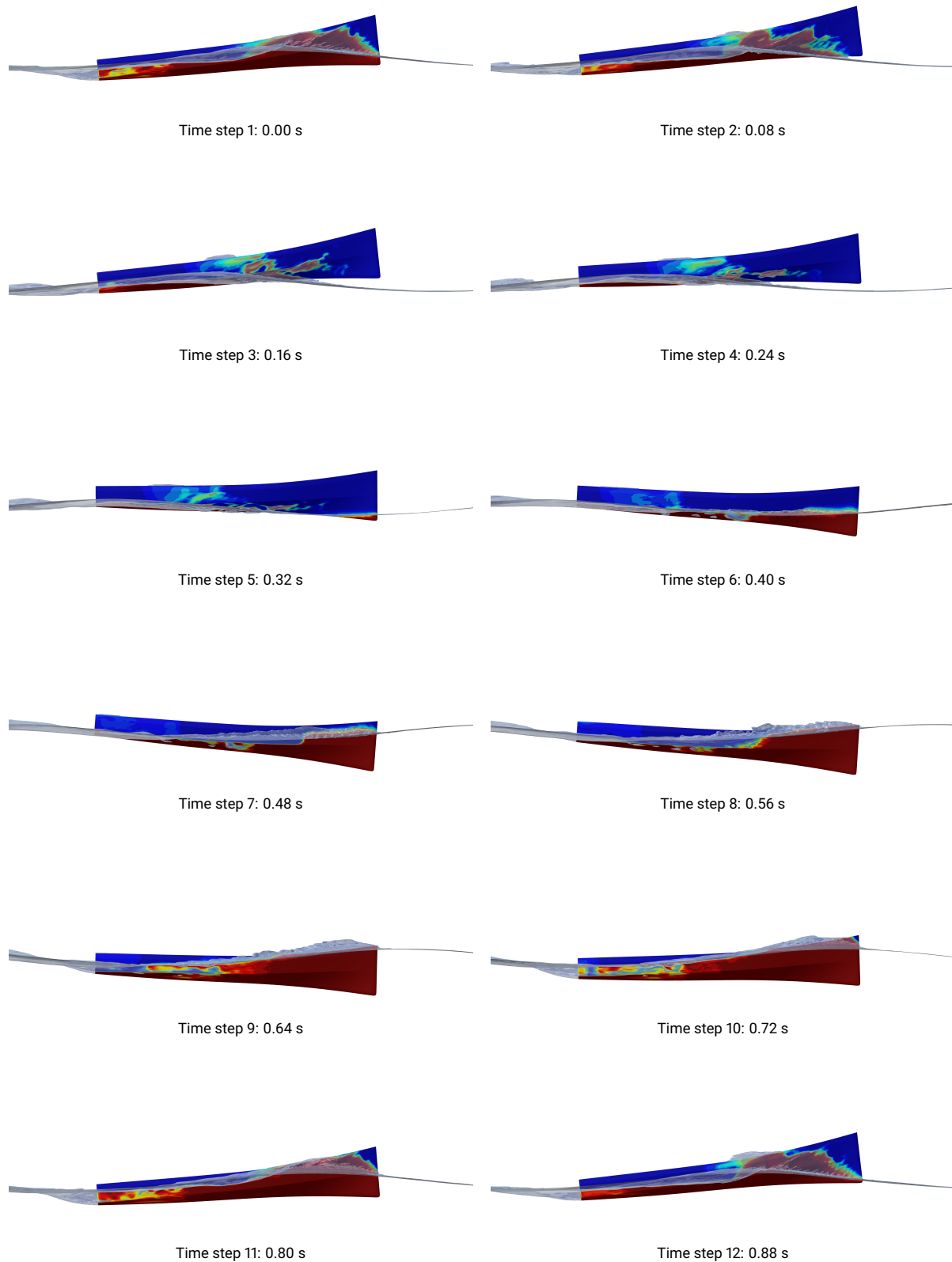


Figure 7.8: Captures from RANS CFD calculation (made by Sebastian Sigmund), AXE, 7.34 rad/s, one wave encounter

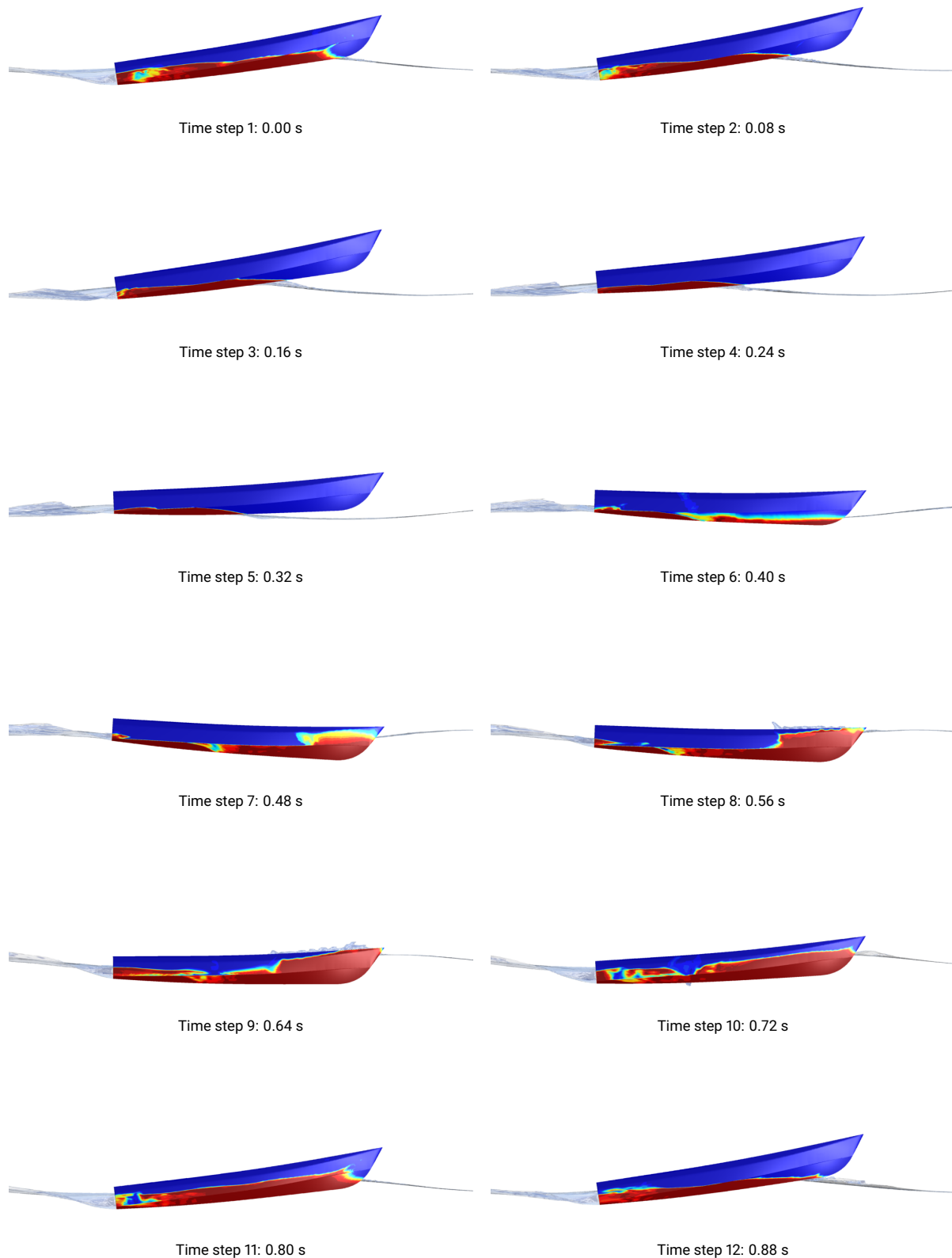


Figure 7.9: Captures from RANS CFD calculation (made by Sebastian Sigmund), ESC, 7.34 rad/s, one wave encounter

lowest position. In the captures of the AXE it can also be seen that there is some shipping of green water because the forward part of the hull is completely submerged. This is contrary to the ESC, where the bow is not completely submerged.

Time step 9 - 12: moving upwards out of the water

The forces due to the weight of the models and the buoyancy are not balanced, there is a net force upwards. The models accelerate upwards out of the water again. One wave cycle is then completed, and it starts again from time step 1.

7.3 Summary

Overall it became clear that the behaviour of the model could be predicted well with the RANS CFD calculations. Although the values did not match exactly, this is almost never the case with calculations. The results are already much better than the results with the weakly non-linear PANSHIP code used in de Jong [7], discussed in chapter 6. There the slamming was not captured at all and the behaviour in irregular seas was drastically underpredicted. From the RANS CFD calculations the slamming could be observed well, and matched the behaviour of the model tests. These calculations are thus a good alternative to model tests to make comparisons between the models.

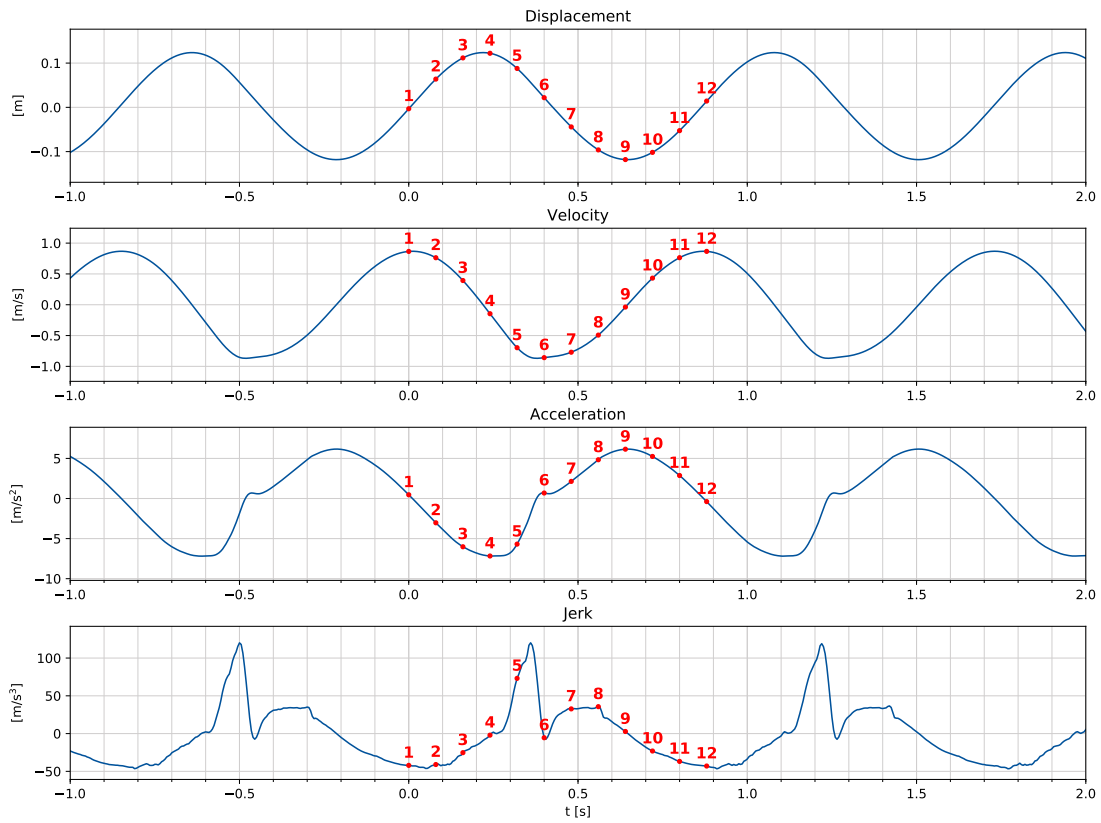


Figure 7.10: Time traces RANS CFD calculation, AXE, centre of gravity, 7.34 rad/s, with time steps of captures

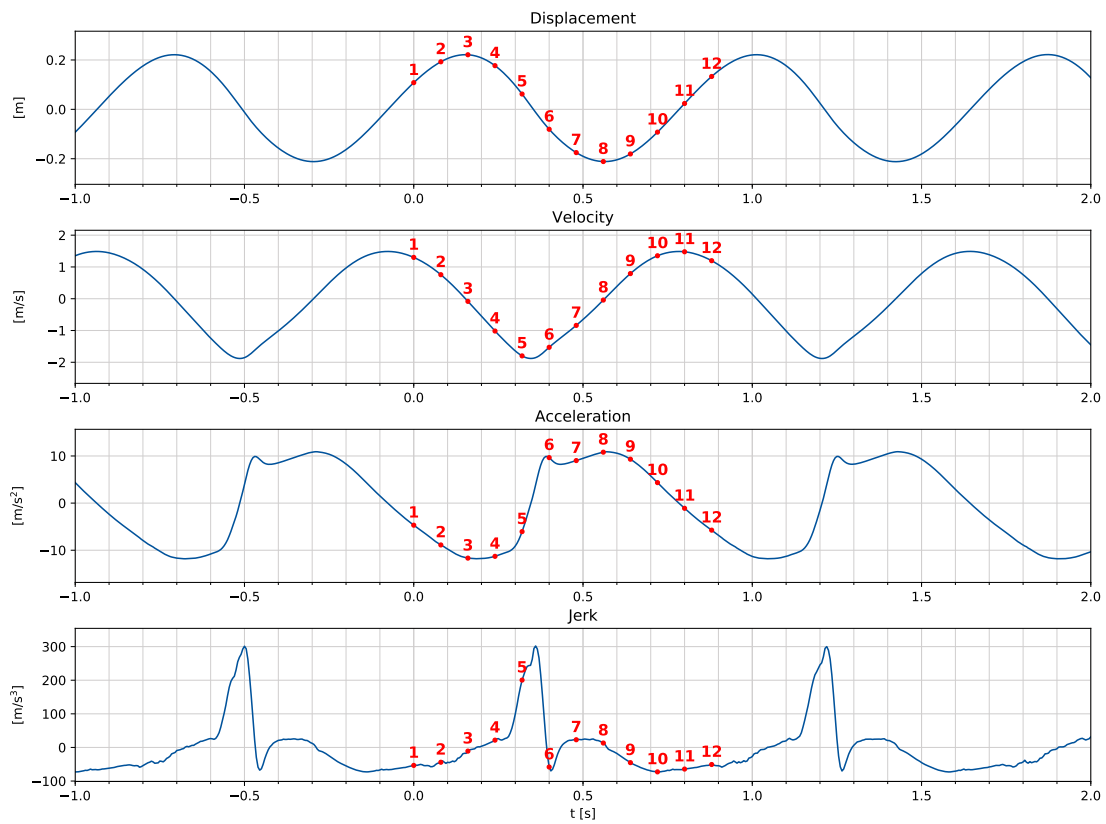


Figure 7.11: Time traces RANS CFD calculation, AXE, bow, 7.34 rad/s, with time steps of captures

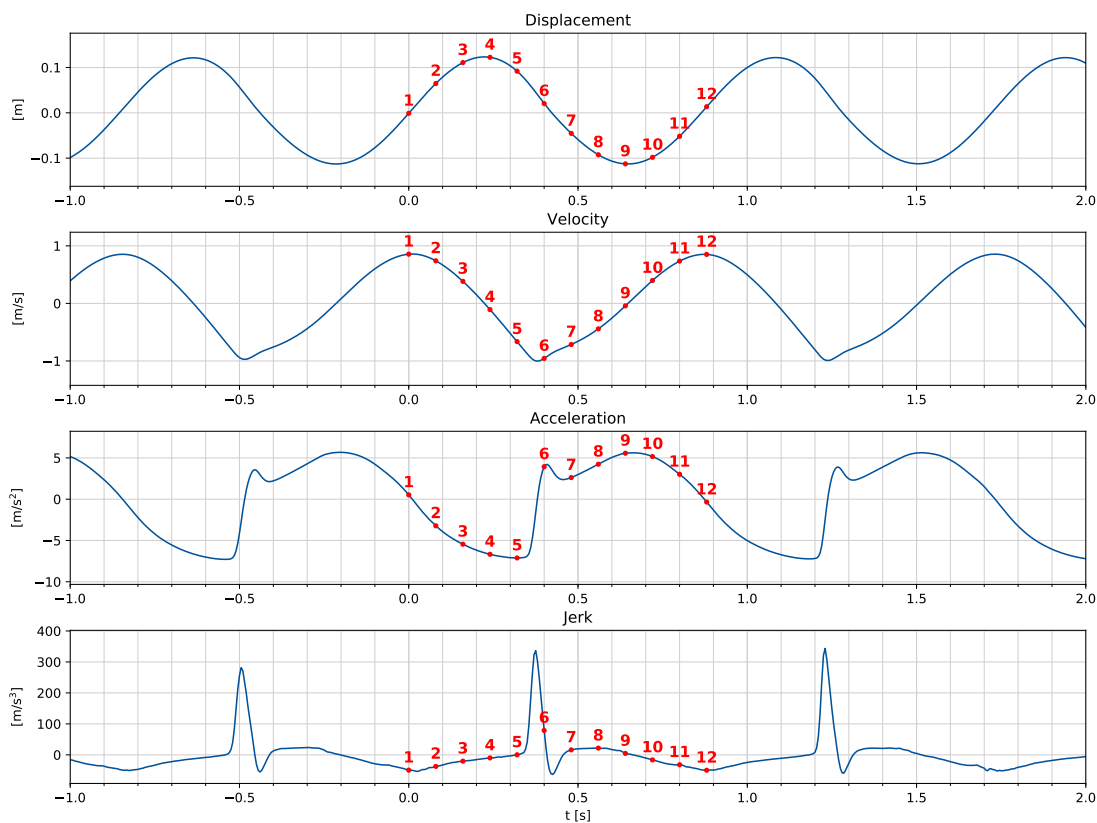


Figure 7.12: Time traces RANS CFD calculation, ESC, centre of gravity, 7.34 rad/s, with time steps of captures

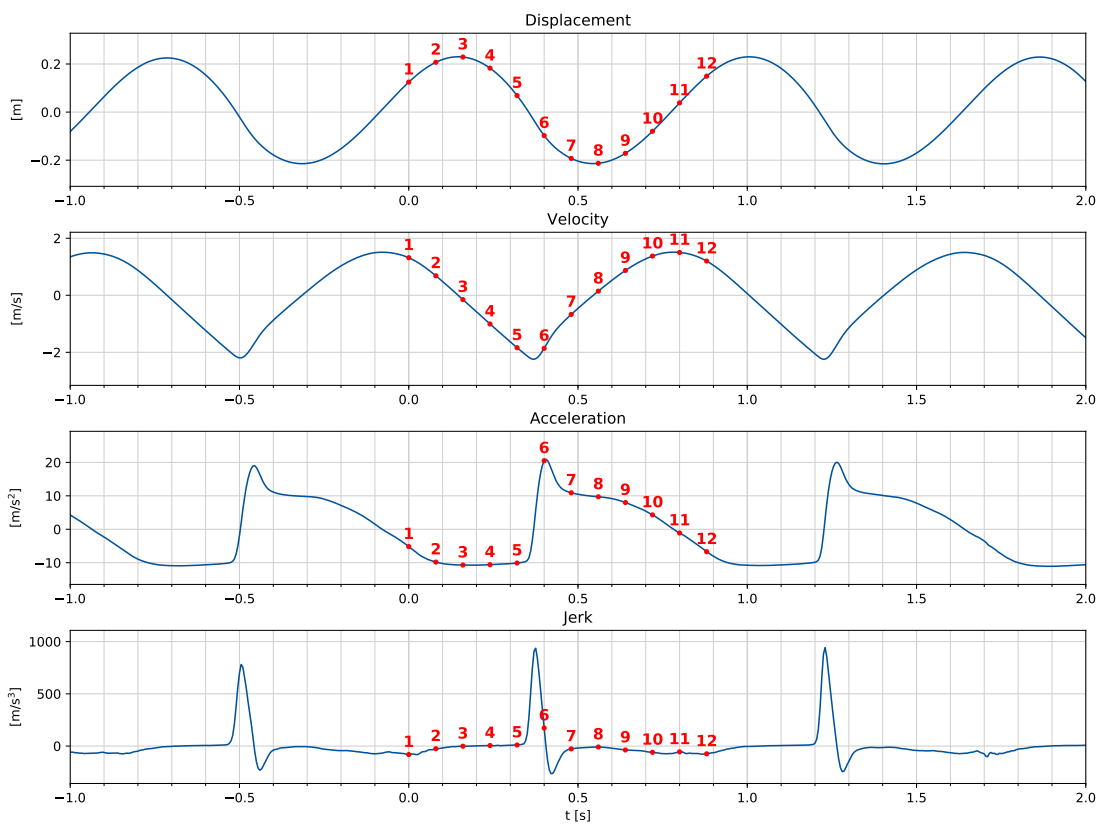


Figure 7.13: Time traces RANS CFD calculation, ESC, bow, 7.34 rad/s, with time steps of captures

8

Upscaling

In this thesis all the data that has been presented originated from model tests, or computations of these models. To be able to predict the jerk behaviour of a ship at full scale, the results of the model scale have to be scaled up. In section 8.1 the generally used scaling laws will be described. Also the implications of these laws on the scaling of jerk will be explained. In section 8.2 the difficulties that might occur in the scaling of jerk will be described.

Unfortunately there was no data available to validate the scaling of jerk. Therefore the contents of this chapter will only be a theoretical description.

8.1 Theory of scaling

To be able to test a ship before actually building it, usually model tests are performed. Model tests are more easy and cheap to perform than full scale tests. Also the test conditions can be controlled relatively easily. The model used in these tests has to be a good representation of the actual ship, called the prototype here. Different similarities can be included to make this representation good. In this section scale factors are used. These scale factors define the ratio between any prototype quantity $X_{\text{prototype}}$ and X_{model} , see equation 8.1.

$$X_{\text{prototype}} = \alpha_X \cdot X_{\text{model}} \quad (8.1)$$

8.1.1 Similarities

In the scaling usually three types of similarities are used [8, 27]: geometric similarity, kinematic similarity and dynamic similarity. Geometric similarity means that all the dimensions of the model are a certain (equal) ratio of the dimensions of the prototype. This ratio for the length, scale factor α_L , is defined in equation 8.2. The way the scale factor is defined means that $\alpha_L \geq 1$.

$$\alpha_L = \frac{L_{\text{prototype}}}{L_{\text{model}}} \quad (8.2)$$

Kinematic similarity means that the velocities and accelerations in the model tests are with a consistent scale factor equal to the prototype. Dynamic similarity is ensured if the forces are scaled with a consistent scale factor.

8.1.2 Froude scaling

To ensure a certain similarity dimensionless numbers are used to derive the scale factors for for example time or the velocity of the model. Dimensionless numbers give a ratio between certain physical processes [8]. Two of the most commonly used dimensionless numbers in hydromechanics are the Froude number and the Reynolds number. The Froude number gives the ratio between inertia forces and gravity forces. The Reynolds number gives the ratio between inertia forces and viscous forces. For ship motions and seakeeping the viscous forces are usually of less importance than inertia and gravity forces. Therefore Froude scaling is used to define the scale factors.

To investigate the physical phenomena in scale, the Froude number should be the same both in prototype scale and model scale. The Froude number is defined as in equation 8.3. In this equation U is a speed relevant for the scaling, for example the forward speed of the ship. Furthermore g is the gravitational acceleration and L is a (relevant) length, for example the waterline length of a ship. The Froude number can also be written as a function of scale factors, see equation 8.4.

$$Fr = \frac{U}{\sqrt{g \cdot L}} \quad (8.3)$$

$$\alpha_{Fr} = \frac{\alpha_U}{\sqrt{\alpha_g \cdot \alpha_L}} \quad (8.4)$$

As mentioned the Froude number should be the same in full scale and model scale, so $\alpha_{Fr} = 1$. Also the gravitational acceleration is the same in both scales ($\alpha_g = 1$). This is because the gravity cannot be altered in the model tests. The scale factor for the velocity is then as derived and defined in equation 8.5 and equation 8.6.

$$1 = \frac{\alpha_U}{\sqrt{1 \cdot \alpha_L}} \quad (8.5)$$

$$\alpha_U = \sqrt{\alpha_L} \quad (8.6)$$

Now that the scaling factor for the velocity and the length are known, the scaling factor of time can be determined, see equation 8.7 and equation 8.8.

$$\alpha_t = \frac{\alpha_L}{\alpha_U} \quad (8.7)$$

$$\alpha_t = \sqrt{\alpha_L} \quad (8.8)$$

Using this method the scale factors for all relevant parameters can be determined. These can be seen in table 8.1 and table 8.2 in section 8.1.4.

8.1.3 Scaling of jerk

The theory applied in the previous section can also be used to determine the scaling factor for jerk. The units of heave jerk are as defined in equation 8.9. This then leads to the scale factor α_{j_z} (according to Froude scaling) in equation 8.10. This scale factor is also valid for surge jerk and sway jerk.

$$j_z = \frac{[m]}{[s^3]} = \frac{z}{t^3} \quad (8.9)$$

$$\alpha_{j_z} = \frac{\alpha_L}{\alpha_t^3} = \frac{1}{\sqrt{\alpha_L}} \quad (8.10)$$

The scale factor for pitch jerk is different. The units of pitch can be seen in equation 8.11. The scale factor for rotations is $\alpha_\theta = 1$. The scale factor for pitch jerk α_{j_θ} (according to Froude scaling) is then defined in equation 8.12. This scale factor is also valid for roll jerk and yaw jerk.

$$j_\theta = \frac{[rad]}{[s^3]} = \frac{\theta}{t^3} \quad (8.11)$$

$$\alpha_{j_\theta} = \frac{\alpha_\theta}{\alpha_t^3} = \frac{1}{\alpha_L \cdot \sqrt{\alpha_L}} \quad (8.12)$$

What can be seen is that both the heave jerk and the pitch jerk are in model scale larger than in full scale. This is contrary to the displacement and velocity, which are smaller in model scale than in full scale. The accelerations are equal in model scale and in full scale.

8.1.4 Overview of scaling factors

In table 8.1 an overview of the basic scaling factors, derived with Froude scaling, can be seen. In table 8.2 the scaling factors, derived with Froude scaling, for the ship motion response can be seen. All the scale factors in these tables have been given as a function of the scale factor for the length α_L . In the tables this factor is abbreviated as α .

Table 8.1: Overview of basic scaling factors according to Froude scaling

Quantity	Scale factor
Length	α
Area	α^2
Volume	α^3
Forward speed	$\sqrt{\alpha}$
Time	$\sqrt{\alpha}$
Frequency	$1/\sqrt{\alpha}$

Table 8.2: Overview of ship response scaling factors according to Froude scaling

Quantity	Scale factor	Quantity	Scale factor
Heave displacement	α	Pitch displacement	1
Heave velocity	$\sqrt{\alpha}$	Pitch velocity	$\frac{1}{\sqrt{\alpha}}$
Heave acceleration	1	Pitch acceleration	$\frac{1}{\alpha}$
Heave jerk	$\frac{1}{\sqrt{\alpha}}$	Pitch jerk	$\frac{1}{\alpha \cdot \sqrt{\alpha}}$

8.2 Difficulties

There are certain difficulties surrounding the principle of scaling. In this section some of these difficulties and their implications on the scaling of jerk are discussed.

8.2.1 Different scaling parameters

As mentioned in the previous section different dimensionless numbers can be used to determine the scale factors. Another example is the Reynolds number, see equation 8.13. In this equation U is a (relevant) speed, L is a (relevant) length and ν is the kinematic viscosity. The scaling factor of the Reynolds number would then be as defined in equation 8.14.

$$Re = \frac{U \cdot L}{\nu} \quad (8.13)$$

$$\alpha_{Re} = \frac{\alpha_U \cdot \alpha_L}{\alpha_\nu} \quad (8.14)$$

Just like the gravitational acceleration, the kinematic viscosity cannot be scaled, since both in model scale and full scale the (model) ship is sailing in the same fluid (water). Therefore $\alpha_\nu = 1$. Although only indirectly present in this equation as part of the kinematic viscosity, another parameter that cannot be scaled is the density ρ . Both full scale and model scale operate in water with roughly the same density, so $\alpha_\rho = 1$. The consequence of these unscalable parameters is that the scale factors, following from different dimensionless numbers, do not match. For example, if the Reynolds number at model scale would be the same as in full scale (thus $\alpha_{Re} = 1$), the scale factor for the velocity would be as derived and defined in equation 8.15 and equation 8.16.

$$1 = \frac{\alpha_U \cdot \alpha_L}{1} \quad (8.15)$$

$$\alpha_U = \frac{1}{\alpha_L} \quad (8.16)$$

The scale factor for velocity according to Reynolds scaling is thus different than the scale factor for velocity according to Froude scaling. This means that the viscous effects are not scaled correctly when Froude scaling is used to determine the scale factors for a model test. Furthermore it is practically very difficult to use correct Reynolds scaling: if the length scale factor is 20, the model ship speed should be 20 times the full scale ship speed. In theory there could be a fluid with properties that ensures correct Froude scaling and correct Reynolds scaling, but this does not exist (yet). To ensure correct Froude scaling and Reynolds scaling simultaneously the scaling factor for the kinematic viscosity would have to be as given in equation 8.17 and equation 8.18, using the scale factors for speed and length following from the Froude scaling.

$$\alpha_v = \alpha_U \cdot \alpha_L = \sqrt{\alpha_L} \cdot \alpha_L \quad (8.17)$$

$$\alpha_v = \alpha_L^{1.5} \quad (8.18)$$

As mentioned in the previous section, the ship motions are mostly dominated by inertia effects. To scale the jerk it would thus probably be best to use the Froude scaling.

8.2.2 Scaling of slamming

In chapter 5 and chapter 6 it was established that slamming is the cause for the largest jerk values. In Faltinsen [11] and in Thomas et al. [56] it is however established that the scaling of slamming is difficult, since this is not purely a hydromechanic phenomenon. Scaling of the slamming forces from model scale to full scale with Froude scaling thus leads to a conservative prediction [11, 56]. This is mainly associated with the fact that in slamming the existence of gas pockets in the fluid has an influence on the slamming pressures [11]. To correctly scale the compressibility of the gas pockets impact loads of these air pockets the dimensionless Euler number must be equal in full scale and model scale [12]. This is not possible in model tests and thus affects the slamming pressure in model scale.

It was concluded that Froude scaling leads to a conservative, thus overprediction, of the forces resulting from slamming. In section 2.5 the forces resulting from slamming were linked to the jerk. So a prediction of the slamming forces in full scale based on Froude scaling from the model scale thus probably leads to an overprediction of the jerk following from slamming. These assumptions can however not be validated in this research.

Conclusions and recommendations

9.1 Conclusions

To finalise this thesis the conclusions to the research questions in chapter 1 are presented. The main goal of was to determine and investigate the jerk in ship motions and see if jerk could give a different perspective compared to accelerations when looking at the comfort and operability of ships. To answer this question several research question were formulated, these will be answered in this section.

What is the influence of different physical phenomena on jerk?

In chapter 2 the ship motion response to waves was analysed in general. All the ship motions are non-linear, but in certain cases the response can be described well by the linear approach. It was concluded that when the response of a ship to the waves is (mostly) linear, the jerk is also a linear consequence of the waves. If a ship then performs better than another ship when looking at the accelerations, it will also perform better when looking at jerk. A difference can only come from non-linear behaviour. Therefore also phenomena were identified that push a ship to more non-linear behaviour. From literature and other research it was concluded that slamming is likely to cause large jerks. This is a highly non-linear phenomenon that causes very sudden changes in acceleration due to the impact with the water. The theoretical analysis of slamming using the Von Karman approach showed that the bow shape and the speed of immersion of the bow are important parameters in the jerk it causes.

To analyse the jerk in ship motions measurement data from fast models in regular head waves was used in chapter 5. Models of two different hull types, the axe bow concept (AXE) and the enlarged ship concept (ESC), were tested in another research. The measurement data could be used in this research. First the difference in response was analysed between the hulls. In most conditions a better performance in accelerations meant the performance in jerk was also better. However in some conditions the performance in accelerations was better at one hull, and the performance in jerk was better at the other hull. It was also found that the non-linearity ratio of the generally better performing hull, the AXE, was in almost all conditions lower than the non-linearity ratio of the ESC.

Also the influence of increasing wave steepness or increasing forward speed on the ship motion response has been investigated. Both the effects increased the jerk responses of the ship. The non-linearity ratio also increased with increasing wave steepness. With increasing forward speed the response became however less non-linear.

Because the vertical accelerations were measured at the centre of gravity and the bow the pitch acceleration and pitch jerk could be determined, under the assumption that the model is rigid and the rotations are relatively small. This way it could be analysed if the jerk behaviour mostly comes from heave or pitch. The pitching of the ship was found to be the largest contributor to the overall jerk behaviour. The optimisation of the bow shape of the AXE also showed up well here, the response was generally much lower and less non-linear.

With the heave and pitch acceleration and jerk known the vertical acceleration and vertical jerk at any longitudinal position on the model could be determined. This showed that in slamming conditions the maximum acceleration around the centre of gravity is for a large extend dominated by the heave acceleration. The maximum jerk at these positions is however mostly following from the pitch jerk due to the slamming. The optimisation of the AXE showed in the fact that pitch acceleration and pitch jerk are smaller and thus are dominating the maximum values at a smaller longitudinal part of the ship.

In chapter 6 the measurement data from the models in irregular waves was used to analyse the behaviour. First the hulls were compared again on their performance looking at accelerations and jerk. The optimisation of the AXE showed well here. Especially in more severe conditions the response was

significantly smaller than the response of the ESC. This was even more visible in the jerk. In chapter 5 was found that the heave response at the centre of gravity was relatively equal for both hulls. The seakeeping behaviour in irregular waves must therefore for an important part be dominated by the pitch motions.

Also the influence of increasing significant wave height and increasing forward speed was investigated. With increasing significant wave height the response became larger and more non-linear. The maximum response thus increased more than proportional to the increase of wave height. For the response to increasing forward speed the natural frequency of the model is most important. If with a certain forward speed the peak of the energy spectrum of the waves is close to the natural frequency, the response is relatively large and non-linear. If the speed increases more and the peak of the energy spectrum of the waves is further away from the natural frequency, the response decreases.

With the acceleration and jerk known for the heave and pitch, the behaviour at any longitudinal position can be determined. Since the behaviour is irregular, contrary to regular waves no single value can be given for a longitudinal position. Therefore the probability of exceedance of a certain value at any position is determined in the analysis over the length of the ship. It could be seen here that the distribution of the moderate values, with 50% probability of exceedance, were comparable with the behaviour of the models in moderate regular wave conditions. The more severe wave encounters with a probability of exceedance of 10% or 1% were comparable with the more severe regular wave conditions where slamming was present. The exact values of acceleration and jerk could not be predicted by comparing it with the regular wave response, but that was also not the goal of this thesis.

The non-linearity ratio in irregular waves does not have the same meaning it has in regular waves. The non-linearity ratio is however analysed, and it was found that the non-linearity of the response has correlation with the severeness of the response in terms of maximum values. Also it could clearly be seen that the optimisation of the AXE meant it responded more linear to the irregular waves. The amount of non-linear energy in the energy density spectrum of the response was significantly lower for the AXE than for the ESC in equal conditions.

How can the jerk in ship motions be determined from model tests and/or full scale tests?

Since there is currently no way to directly measure the jerk, the most viable option found was to differentiate the acceleration measurements from accelerometers. In these measurements noise is present. This noise increases with a factor proportional to the sampling frequency when numerically differentiated, so the signal first has to be filtered. In chapter 3 several methods of filtering were tested on their influence on the measurement signal and the influence on the differentiated signal. The Butterworth filter was chosen because the characteristics of this filter matched the best with the requirements on a filter and the output from this filter was least sensitive for the settings of the filter. From literature it followed that the cut-off frequency had to be chosen accordingly to the time scale of the shortest event in a time series. From the data analysed in chapter 5 it could be estimated that the shortest time scale was 0.05 seconds in certain slamming events, thus the cut-off frequency was set at 20 Hz. For the numerical differentiation the central difference method was used.

To be able to make comparisons with a certain confidence level the uncertainty had to be defined. The exact values of the jerk are not required for this research, since there are no comfort limits in ships based on jerk yet. Therefore a rough approximation of the uncertainty in the maximum jerk values has been made based on the 95% confidence interval from previous research. It was concluded that the jerk values could be determined with enough certainty to be able to make useful qualitative comparisons.

The measurement data used in this thesis had a sampling frequency of 1000 Hz for the regular wave measurements and 400 Hz for the irregular wave measurements. This proved to be more than sufficient to be able to filter the data and determine the jerk. Therefore no exact sampling frequency minimally required to accurately determine the jerk can be given. For full scale measurements the requirements on the sampling frequency are less, since the time scale of all motions of the ship scales with the square root of the scale factor of the length.

An important step in predicting the behaviour of a full scale ship is scaling the results from the model tests to full scale. Since there was no full scale data available to validate the upscaled model test measurements, only a theoretical description of scaling has been given in chapter 8. It was concluded that with the most important scaling method for ship motions, Froude scaling, the jerk values in full

scale would be smaller than in model scale. This is contrary to motions and velocities, which are larger in full scale. Furthermore some difficulties that might occur in the scaling of jerk values have been identified. The most important one is the fact that the largest jerk values come from the slamming of the ship. From other research it followed that the scaling of slamming is difficult, since this is not a purely hydrodynamic phenomenon. In slamming the trapping of air in the water plays an important role. This effect is not scaled correctly when applying Froude scaling. This leads to an overprediction of the slamming pressures in model scale, and might thus lead to an overprediction of the jerk.

How can the severeness of jerks in the ship motions be quantified?

To be able to investigate the jerk in ship motions, different procedures for quantifying the response of a ship have been established in chapter 4. From literature it was found that the acceleration peaks are now used for determining the motion comfort of a ship. Therefore also the peaks in jerk will be used in the comparisons. For both the accelerations and jerk non-dimensional values have been introduced besides the dimensional values. The acceleration and jerk could be observed in a translational motion (surge, sway and heave) or a rotational motion (roll, pitch and yaw).

From other research it followed that the more optimised a ship is for seakeeping, the more linear the response is. It was also shown that the amount of non-linear energy in the response increases exponentially with increasing derivatives from the displacement. Since jerk is the third derivative from the displacement, non-linear behaviour has a large contribution in the jerk. Therefore a way to quantify the non-linearity in the ship response has been established in this thesis, in the form of the non-linearity ratio. This ratio defines the ratio of energy from higher order responses in the energy density spectrum to the total amount of energy in the spectrum. This method was proven to be the inverse of the coefficient of determination of the sine fit through a regular wave response, which indicates how linear the response is.

In regular waves one peak value describes the behaviour of a ship, since the response is the same with every wave encounter. In irregular waves this is not the case, the response to every wave encounter is different, since every wave is different. When the response cannot be approached linearly the response to a wave is also dependent on the preceding wave encounters. In irregular waves the response is therefore described using probabilities of exceedance of a certain value. If the response of the model in a JONSWAP wave spectrum can be approximated well with the linear approach the peaks and troughs in the response will be Rayleigh distributed. The more the response is non-linear, the more it will divert from the Rayleigh distribution. This can be visualised well in a so-called Rayleigh plot, where the axis are altered so that a Rayleigh distribution will show up as a straight line. The non-linearity ratio can also be determined for the response in irregular waves. But since no sine fit can be determined for irregular waves and there is not a single excitation frequency, the ratio does not work according to the definition in regular waves. It does however give an indication of how non-linear the response is.

How can the jerk in ship motions be predicted with sufficient accuracy?

The prediction of jerk in ship motions has been investigated in chapter 7. The distinction has been made in terms of non-linearity of the methods. In previous research it was already found that weakly non-linear methods do not calculate the response in irregular waves well. The linear part of the response was predicted quite accurately, but the non-linear part which is the main cause for the highest peaks in acceleration and jerk was not. Especially since the jerk is highly non-linear in irregular waves, the jerk values were significantly underpredicted when only the linear part of the energy density spectrum was taken into account.

In this research the calculated response of the models in regular waves using RANS CFD calculations was available. The RANS CFD predictions were found to have a very good similarity with the measured response. The values were within the same order of magnitude predicted well. Also the behaviour of the simulated model was similar to the model tests in the towing tank, which was determined by comparing the time traces. Calculations using RANS CFD give thus a highly accurate result, but are computationally expensive. Therefore predicting the behaviour in irregular waves might be costly, since long simulation run times are required to obtain accurate results.

The prediction also depends on how 'sufficient accuracy' is defined. With not fully non-linear codes the values of the maximum jerk might not be predicted well, but there might be a difference in number of slams that can be observed from these calculations. Since slamming was found to be the main cause

for large jerk values, an indication of the amount of large jerk values can be given. This method has not been investigated further in this research.

Overall

The overall conclusion that can be made is that it is valuable to look into the jerk as well when determining the seakeeping behaviour of a ship. In this thesis only qualitative comparisons have been performed to compare the seakeeping behaviour between different hulls or in different wave conditions. In some cases the jerk gave a different perspective compared to a seakeeping analysis performed with accelerations. From this it can thus be concluded that a qualitative comparison is already useful to make. Especially when in the future comfort or workability limits for jerk are available from physiological tests, the jerk in the ship motions can give a different perspective by comparing if the jerk exceeds the comfort limit or not. Next to that the non-linearity can give additional information. In itself this ratio is not a measure for the magnitude of the response, but it can be useful when used parallel to for example peak values of acceleration and jerk. If the response is more non-linear, it might be that the sense of discomfort of passengers is also larger.

The jerk can be determined well from accelerations signals, but is harder to predict using numerical methods because of the highly non-linear nature. Methods with a higher non-linearity are thus required for correct predictions of the jerk. This also applies to the non-linearity ratio.

9.2 Recommendations

Following from this research there are some recommendations for further research. These will be described in this section.

- To be able to optimise a hull form for jerk a systematic series of hulls can be made to investigate the influence of different parameters on the jerk. This will probably align with optimising the ship to behave more linear in waves.
- Physiological research into the limits of what jerk levels are acceptable for passengers in terms of comfort are required to make a real comparison between different hulls. In this research only a qualitative analysis has been performed to assess whether one performed better than the other. If there are limits then a quantitative analysis of the comfort and operability of a vessel can be performed. Especially with the different distributions of maximum values over the length of the ship jerk might give new insights.
- Also physiological research into the link between the non-linearity of motions and comfort levels might give new insights. The non-linearity ratio of a response in itself does not reflect the magnitude of the response, thus a combination with accelerations and/or jerk is required. It might be that a response which is equal in terms of acceleration or jerk values but not equal in terms of non-linearity might give a different comfort experience.
- Because of the highly non-linear nature of jerk the accuracy of determining it might increase when jerk sensors become commercially available. Especially when from physiological research follows that jerk is an important factor in the comfort of passengers on a ship, direct measurements of jerk in model tests might add value to the design of ships.
- Another way of determining the jerk more accurately when quantitative values are needed is improving the uncertainty assessment. For this thesis only qualitative analysis was performed so the exact value of the jerk was of less importance. This might become more important in the future. Determining the uncertainty more accurately can be an alternative to using jerk sensors if these are not available yet, are too expensive, or are too inaccurate.
- In this thesis it has been established that the weakly non-linear methods are not accurate enough to predict the jerk in ship motions well. The RANS CFD method was found to be accurate enough, but is computationally expensive. Investigating if the weak scatterer Rankine panel codes produce accurate results might give an intermediate step between accuracy and computational costs.
- Another way of comparing the seakeeping behaviour of two different hulls is analysing the number of slams using not fully non-linear codes. Since slamming was found to be the primary cause for large jerk values, the number of slams might give an indication of the seakeeping behaviour.

Bibliography

- [1] Ido Akkerman. *Von Karman: Conceptual idea*. Lecture slides, MT44025 - Advanced Course in Ship Hydrodynamics, Delft University of Technology, 2017.
- [2] American Bureau of Shipping. *Guide for Slamming Loads and Strength Assessment for Vessels*. 2016.
- [3] R. Beck and A. Reed. Modern seakeeping computations for ships. In *Twenty-Third Symposium on Naval Hydrodynamics*, pages 1 – 45, Washington, DC, 2001. The National Academies Press.
- [4] Lars Bergdahl. *Wave-Induced Loads and Ship Motions*. Chalmers University of Technology, Göteborg, Sweden, 2009.
- [5] Volker Bertram. *Practical Ship Hydrodynamics*, 2nd edition. Butterworth-Heinemann, Oxford, 2012. ISBN 978-0-08-097150-6.
- [6] J.L. Dais and M. Balachandra. Motion discomfort and transportation guideway form. *Transportation Research*, 8(6):523 – 531, 1974.
- [7] Pepijn de Jong. *Seakeeping behaviour of high speed ships*. PhD thesis, Delft University of Technology, 2011.
- [8] M. de Vries. *Scale models in hydraulic engineering*. International institute for Hydraulic and Environmental engineering, Delft, 1982.
- [9] Manhar R. Dhanak and Nikolas I. Xiros. *Springer Handbook of Ocean Engineering*. Springer International Publishing, 2016.
- [10] David Eager, Ann-Marie Pendrill, and Nina Reistad. Beyond velocity and acceleration: jerk, snap and higher derivatives. *European Journal of Physics*, 37(6), 2016.
- [11] O.M. Faltinsen. *Hydrodynamics of High-Speed Marine Vehicles*. Cambridge University Press, 2006.
- [12] O.M. Faltinsen. Hydrodynamics of marine and offshore structures. *Journal of Hydrodynamics, Ser. B*, 26(6):835 – 847, 2015.
- [13] John D. Fenton. A fifth-order Stokes theory for steady waves. *Journal of Waterway Port Coastal and Ocean Engineering*, 111(2), 1985.
- [14] Gerard Fridsma. *A Systematic Study of the Rough-Water Performance of Planing Boats. Irregular Waves - Part 2*. Davidson Laboratory, Stevens Institute of Technology, 1971.
- [15] Alan Friedman. *An Introduction to Linear and Non Linear Systems And their Relation to Machinery Faults*. 2001.
- [16] J. Gerritsma and W. Beukelman. Analysis of the modified strip theory for the calculation of ship motions and wave bending moments. *International Shipbuilding Progress*, 14(156):319 – 337, 1967.
- [17] Peter R. Grant and Bruce Haycock. Effect of Jerk and Acceleration on the Perception of Motion Strength. *Journal of Aircraft*, 45(4), 2008.
- [18] Jennifer Grimsley, Yu Liu, and Gene Hou. An examination of the statistical behavior of planing craft peak vertical accelerations in irregular waves. In *Proceedings of the 29th American Towing Tank Conference*, 2010.
- [19] Leo H. Holthuijsen. *Waves in Oceanic and Coastal Waters*. Cambridge University Press, 2007. ISBN 978-0-521-86028-4.

- [20] R.J.A.W. Hosman. *Pilot's perception and control of aircraft motions*. PhD thesis, Delft University of Technology, 1996.
- [21] Institute of Electrical and Electronics Engineers. IEEE Trial-Use Standard for Digitizing Waveform Recorders. *IEEE Std 1057*, 1989.
- [22] Institute of Electrical and Electronics Engineers. IEEE Standard for Digitizing Waveform Recorders. *IEEE Std 1057-2017*, 2018.
- [23] International Organization for Standardization. *ISO 18738:2003 - Lifts (elevators) - Measurement of lift ride quality*. Geneva, Switzerland, 2003.
- [24] International Towing Tank Conference. Procedure 7.5-02-01-01 Guide to the Expression of Uncertainty in Experimental Hydrodynamics. *ITTC Recommended Procedures and Guidelines*, 2014.
- [25] International Towing Tank Conference. Procedure 7.5-02-07-02.5 Verification and Validation of Linear and Weakly Nonlinear Seakeeping Computer Codes. *ITTC Recommended Procedures and Guidelines*, 2017.
- [26] International Towing Tank Conference. Procedure 7.5-02-07-02.1 Seakeeping Experiments. *ITTC Recommended Procedures and Guidelines*, 2017.
- [27] J.M.J. Journée, W.W. Massie, and R.H.M. Huijsmans. *Offshore Hydromechanics*, 3rd edition. Delft University of Technology, 2015.
- [28] G.K. Kapsenberg. Slamming of ships: where are we now? *Philosophical Transactions of the Royal Society A: Mathematical, Physical and Engineering Sciences*, 369(1947):2892 – 2919, 2011.
- [29] J.A. Keuning. *Nonlinear Behaviour of Fast Monohulls in Head Waves*. PhD thesis, Delft University of Technology, 1994.
- [30] J.A. Keuning and K.J. Vermeulen. *Model tests with three fast mono-hulls*. Report 1418-M, Delft University of Technology, 2005.
- [31] A.R.J.M. Lloyd. *Seakeeping: Ship Behaviour in Rough Weather*. Ellis Horwood Limited, 1989. ISBN 0-7458-0230-3.
- [32] Jianwen Luo, Kui Ying, Ping He, and Jing Bai. Properties of Savitzky–Golay digital differentiators. *Digital Signal Processing*, 15:122 – 136, 2005.
- [33] Delton L. Martin and Dale H. Litwhiler. An investigation of acceleration and jerk profiles of public transportation vehicles. In *Proceedings of ASEE Annual Conference and Exposition*, 2008.
- [34] MathWorks. *MATLAB documentation*. 2019.
- [35] L. McCue, D. Jacobson, C. Weil, and J. Zselezky. A look at the impact of filter selection on characterization of vertical acceleration peaks. In *Proceedings of the 3rd Chesapeake Power Boat Symposium*, 2012.
- [36] Colin Mercer. *Acceleration, Velocity and Displacement Spectra – Omega Arithmetic*. Prosig, 2006.
- [37] Peter Naaijen. *Engineering approach to Ship / Offshore Hydromechanics*. Course notes, MT44020 - Motions and Loading of Structures in Waves, Delft University of Technology, 2016.
- [38] National Instruments Corporation. *Data Acquisition and Signal Conditioning Course Manual*. 2003.
- [39] J.N. Newman. The theory of ship motions. In *Advances in Applied Mechanics*, volume 18, pages 221 – 283. Elsevier, 1979.
- [40] T. Francis Ogilvie. Recent progress toward the understanding and prediction of ship motions. In *Proceedings of the 5th Symposium on Naval Hydrodynamics*, pages 3 – 80, Bergen, Norway, 1964.
- [41] David J. Olive. *Linear Regression*. Springer International Publishing AG, Cham, Switzerland, 2017. ISBN 978-3-319-55252-1.

- [42] Oxford Dictionaries, 2018. <https://en.oxforddictionaries.com/>.
- [43] J.F O’Dea and D.A. Walden. The effect of bow shape and nonlinearities on the prediction of large amplitude motion and deck wetness. In *Proceedings of the 15th Symposium on Naval Hydrodynamics*, pages 163 – 176, 1984.
- [44] J. P. Powell and R. Palacín. Passenger stability within moving railway vehicles: Limits on maximum longitudinal acceleration. *Urban Rail Transit*, 1(2):95 – 103, 2015.
- [45] Suresh Rajendran, Guillermo Vásquez, and C. Guedes Soares. Effect of bow flare on the vertical ship responses in abnormal waves and extreme seas. *Ocean Engineering*, 124:419 – 436, 2016.
- [46] Jose J. Rangel-Magdaleno, Rene J. Romero-Troncoso, Roque A. Osornio-Rios, and Eduardo Cabal-Yeppez. Novel Oversampling Technique for Improving Signal-to-Quantization Noise Ratio on Accelerometer-Based Smart Jerk Sensors in CNC Applications. *Sensors*, 9(5):3767 – 3789, 2009.
- [47] Mikael Razola, Katrin Olausson, Karl Garne, and Anders Rosén. On high-speed craft acceleration statistics. *Ocean Engineering*, 114:115 – 133, 2016.
- [48] Michael R. Riley, Tim Coats, Kelly Haupt, and Donald Jacobson. The Characterization of Individual Wave Slam Acceleration Responses for High Speed Craft. In *Proceedings of the 29th American Towing Tank Conference*, 2010.
- [49] Michael R. Riley, Kelly D. Haupt, Timothy W. Coats, Neal C. Ganey, and Heidi P. Murphy. *A Guide for Measuring, Analyzing, and Evaluating Accelerations Recorded During Seakeeping Trials of High-Speed Craft*. Naval Surface Warfare Center, West Bethesda, United States, 2016.
- [50] N. Salvesen, E.O. Tuck, and O.M. Faltinsen. *Ship Motions and Sea Loads*. Society of Naval Architects and Marine Engineers, 1970.
- [51] Abraham Savitzky and M. J. E. Golay. Smoothing and Differentiation of Data by Simplified Least Squares Procedures. *Analytical Chemistry*, 36(8):1627 – 1639, 1964.
- [52] Ronald W. Schafer. What Is a Savitzky-Golay Filter? *IEEE Signal Processing Magazine*, 28(4):111 – 117, 2011.
- [53] Steven W. Smith. *The Scientist and Engineer’s Guide to Digital Signal Processing*, Second edition. California Technical Publishing, 1999.
- [54] Manley St. Denis and Willard J. Pierson. On the motions of ships in confused seas. In *Transactions of The Society of Naval Architects and Marine Engineers*, 1953.
- [55] A.H. Techet. *Froude Krylov Excitation Force*. Course notes, 13.42 Design Principles for Ocean Vehicles, Massachusetts Institute of Technology, 2005.
- [56] Giles Thomas, Stefan Winkler, Michael Davis, Damien Holloway, Shinsuke Matsubara, Jason Lavroff, and Ben French. Slam events of high-speed catamarans in irregular waves. *Journal of Marine Science and Technology*, 16(1):8 – 21, 2011.
- [57] Douglas VanDerwerken and Carolyn Judge. Statistical analysis of vertical accelerations of planing craft: Common pitfalls and how to avoid them. *Ocean Engineering*, 139:265 – 274, 2017.
- [58] Th. Von Karman. *The impact on seaplane floats during landing*. National Advisory Committee for Aeronautics, 1929.
- [59] C. Vuik, F.J. Vermolen, M.B. van Gijzen, and M.J. Vuik. *Numerical Methods for Ordinary Differential Equations*. Delft Academic Press, 2015.
- [60] Herbert Wagner. *Landing of Seaplanes*. National Advisory Committee for Aeronautics, Washington, DC, United States, 1932.
- [61] John Zselezky. Behind the scenes of peak acceleration measurements. In *Proceedings of the 3rd Chesapeake Power Boat Symposium*, 2012.

Appendices

Appendix A - Link between sine fit & non-linearity ratio

Appendix B - Filter comparison

Appendix C - Time traces regular waves

A

Link between sine fit & non-linearity ratio

The goal of this appendix is to prove that the non-linearity ratio (r_{nl}), defined in chapter 4 is equal to one minus the correlation between a time trace and the sine fit of this time trace, defined in the coefficient of determination (the r^2 -value), see equation A.1.

$$r_{nl} = 1 - r^2 \quad (\text{A.1})$$

This will be done by first analytically determining the sine fit and the coefficient of determination of this sine fit, see section A.1. Then the non-linearity for the used function is derived in section A.2. The link between the non-linearity and the coefficient of determination of the sine fit is given in section A.3.

A.1 Sine fit

A.1.1 Derivation

For the derivation of the sine fit the three parameter least squares sine fit algorithm described in the guide of Institute of Electrical and Electronics Engineers [21] will be used. This method assumes that the frequency of the sine fit is already known. The method described in the paper is for a discrete data set.

The non-linear response of a ship to regular waves in one of the degrees of freedom (named y_i) can be defined as given in equation A.2. In this equation ω is the encounter frequency (in rad/s) of the ship with the waves. The first part of the equation is the first order (linear) response, with amplitude A_1 and phase ϵ_1 . The higher order responses are defined in the sum in the right part of the equation. These responses are at multiples of the encounter frequency and have their own amplitudes and phases.

$$y_i = A_1 \cdot \sin(\omega \cdot t + \epsilon_1) + \sum_{n=2}^N A_n \cdot \sin(n\omega \cdot t + \epsilon_n) \quad (\text{A.2})$$

The equation used to deliver this proof is a function consisting of two sine functions, see equation A.3. So this is the first order response and one higher order response. For the derivation reported here the phases of the sine components are assumed to be zero. Since the sine fit to the first order response is desired, the required frequency input in the sine fit equations is the encounter frequency.

$$y = A_1 \cdot \sin(\omega \cdot t) + A_2 \cdot \sin(2\omega \cdot t) \quad (\text{A.3})$$

The equations defined in the paper used to determine the sine fit are sums from $n = 1$ to M , the amount of (discrete) data points. These are replaced by an integral from 0 to a time T , see equations A.4 to A.11. In these equations the integration constants are neglected.

$$f_1 = \int_0^T y \, dt = -\frac{2A_1 \cdot \cos(\omega \cdot T) + A_2 \cos(2\omega \cdot T) - 2 \cdot A_1 - A_2}{2\omega} \quad (\text{A.4})$$

$$f_2 = \int_0^T \alpha \, dt = \frac{\sin(\omega \cdot T)}{\omega} \quad (\text{A.5})$$

$$f_3 = \int_0^T \beta \, dt = \frac{-1 + \cos(\omega \cdot T)}{\omega} \quad (\text{A.6})$$

$$f_4 = \int_0^T \alpha \cdot \beta \, dt = \frac{\sin(\omega \cdot T)^2}{2\omega} \quad (\text{A.7})$$

$$f_5 = \int_0^T \alpha^2 \, dt = \frac{\cos(\omega \cdot T) \cdot \sin(\omega \cdot T) + \omega \cdot T}{2\omega} \quad (\text{A.8})$$

$$f_6 = \int_0^T \beta^2 \, dt = -\frac{\cos(\omega \cdot T) \cdot \sin(\omega \cdot T) - \omega \cdot T}{2\omega} \quad (\text{A.9})$$

$$f_7 = \int_0^T y \cdot \alpha \, dt = -\frac{4A_2 \cdot \cos(\omega \cdot T)^3 + 3A_1 \cdot \cos(\omega \cdot T)^2 - 3A_1 - 4A_2}{6\omega} \quad (\text{A.10})$$

$$f_8 = \int_0^T y \cdot \beta \, dt = -\frac{-6A_1 \cdot \omega \cdot T + 3A_1 \cdot \sin(2\omega \cdot T) - 6A_2 \cdot \sin(\omega \cdot T) + 2A_2 \cdot \sin(3\omega \cdot T)}{12\omega} \quad (\text{A.11})$$

With:

$$\alpha = \cos(\omega \cdot t) \quad (\text{A.12})$$

$$\beta = \sin(\omega \cdot t) \quad (\text{A.13})$$

Using these equations the following variables are determined, see equations A.14 to A.17. Because of the size of these equations, they will not be fully displayed anymore.

$$A_N = \frac{f_7 - \bar{y} \cdot f_2}{f_4 - \bar{\beta} \cdot f_2} - \frac{f_8 - \bar{y} \cdot f_3}{f_6 - \bar{\beta} \cdot f_3} \quad (\text{A.14})$$

$$A_D = \frac{f_5 - \bar{\alpha} \cdot f_2}{f_4 - \bar{\beta} \cdot f_2} - \frac{f_4 - \bar{\alpha} \cdot f_3}{f_6 - \bar{\beta} \cdot f_3} \quad (\text{A.15})$$

$$B_N = \frac{f_7 - \bar{y} \cdot f_2}{f_5 - \bar{\alpha} \cdot f_2} - \frac{f_8 - \bar{y} \cdot f_3}{f_4 - \bar{\alpha} \cdot f_3} \quad (\text{A.16})$$

$$B_D = \frac{f_4 - \bar{\beta} \cdot f_2}{f_5 - \bar{\alpha} \cdot f_2} - \frac{f_6 - \bar{\beta} \cdot f_3}{f_4 - \bar{\alpha} \cdot f_3} \quad (\text{A.17})$$

With:

$$\bar{y} = \frac{1}{T} \cdot f_1 = \frac{1}{T} \cdot \int_0^T y \, dt \quad (\text{A.18})$$

$$\bar{\alpha} = \frac{1}{T} \cdot f_2 = \frac{1}{T} \cdot \int_0^T \alpha \, dt \quad (\text{A.19})$$

$$\bar{\beta} = \frac{1}{T} \cdot f_3 = \frac{1}{T} \cdot \int_0^T \beta \, dt \quad (\text{A.20})$$

Then finally the equation of the sine fit to the data is determined using equation A.21. According to Institute of Electrical and Electronics Engineers [22] the most accurate result is obtained when an integer number of full cycles is used to calculate the sine fit, see also section A.1.3. Using this assumption T can be replaced by any multiple of $(2 \cdot \pi)/\omega$. When the equations above are solved, the sine fit in equation A.25 is found. The assumptions were that there is one higher order component and no phases in the harmonic components, but the method is also valid for more higher order components and with non-zero phases.

$$y' = A \cdot \cos(\omega \cdot t) + B \cdot \sin(\omega \cdot t) + C \quad (\text{A.21})$$

With:

$$A = \frac{A_N}{A_D} = 0 \quad (\text{A.22})$$

$$B = \frac{B_N}{B_D} = A_1 \quad (\text{A.23})$$

$$C = \bar{y} - A \cdot \bar{\alpha} - B \cdot \bar{\beta} = 0 \quad (\text{A.24})$$

So finally the equation of the sine fit is:

$$y' = A_1 \cdot \sin(\omega \cdot t) \quad (\text{A.25})$$

It can be concluded that the sine fit with a frequency equal to the encounter frequency results in a response function that is equal to the first order response of the ship. This is true if an integer number of cycles is sampled of all the components of the response function. Since the higher order responses are at a multiple of the encounter frequency, these are always an integer number of higher order responses in one cycle of first order response.

A.1.2 Coefficient of determination

The correlation between the sine fit, which is proven to be the first order of a non-linear response of a ship to regular waves, and the entire non-linear response is expressed in the coefficient of determination. This coefficient is determined with equation A.26, as found in Olive [41].

$$r^2 = \frac{SSR}{SSTO} \quad (\text{A.26})$$

Where SSR is the regression sum of squares, and SSTO is the total sum of squares, see equation A.27 and equation A.28. The equations in the cited book are discrete sums, but are again written as continuous integrals. The same equations as in section A.1.1 are used for the determination of the coefficient of determination.

$$SSR = \int_0^T (y' - \bar{y})^2 dt \quad (\text{A.27})$$

$$SSTO = \int_0^T (y - \bar{y})^2 dt \quad (\text{A.28})$$

Another way to come to the r^2 -value is to use the SSE, the error sum of squares. See equations A.29 and A.30. This clearly shows that the r^2 -value is a measure for how good the correlation between the sine fit and the entire response function is.

$$SSE = \int_0^T (y - y')^2 dt \quad (\text{A.29})$$

$$1 - r^2 = \frac{SSE}{SSTO} \quad (\text{A.30})$$

If equation A.26 is solved for an integer number of cycles, the coefficient of determination in equation A.31 is found. If equation A.30 is solved, the result is equation A.32.

$$r^2 = \frac{A_1^2}{A_1^2 + A_2^2} \quad (\text{A.31})$$

$$1 - r^2 = \frac{A_2^2}{A_1^2 + A_2^2} \quad (\text{A.32})$$

A.1.3 Accuracy sine fit

As stated in section A.1.1 the sine fit is the most accurate if an integer number of cycles is used to determine the sine fit. This is demonstrated in this section with a numerical example. The equation in A.3 is plotted with the values $A_1 = 1\text{ m}$, $A_2 = 0.5\text{ m}$, and $\omega = 2\pi\text{ rad/s}$ ($= 1\text{ Hz}$), see figure A.1. In this figure also the sine fit of this function is plotted.

To prove that the sine fit function is the most accurate when determined from an integer number of cycles, the sine fit has been determined in a range of cycles, including non-integer numbers of cycles. The absolute error from the (analytically) known sine fit amplitude is then calculated as defined in equation A.33. In figure A.2 the absolute error from the known sine fit amplitude (equation A.25) is shown. The vertical dashed lines indicate the full cycles. For example: if 3.3 cycles would be used to calculate the sine fit, the amplitude of this sine fit would have an error of 0.05 compared to the real sine fit.

$$\text{Error} = |A_{\text{calculated}} - A_1| \tag{A.33}$$

From the figure it can be concluded that indeed the accuracy is highest if full cycles are used to calculate the sine fit, since the error is always zero here. Furthermore the errors per cycle decreases if more cycles are used. To obtain the most accurate result it is thus best to calculate the sine fit over a number of integer cycles. In Institute of Electrical and Electronics Engineers [22] a minimum of 5 cycles is advised.

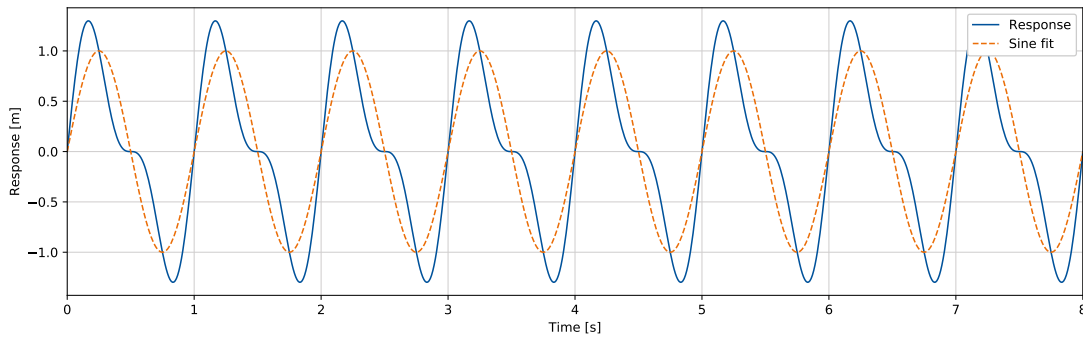


Figure A.1: Plot of the response function

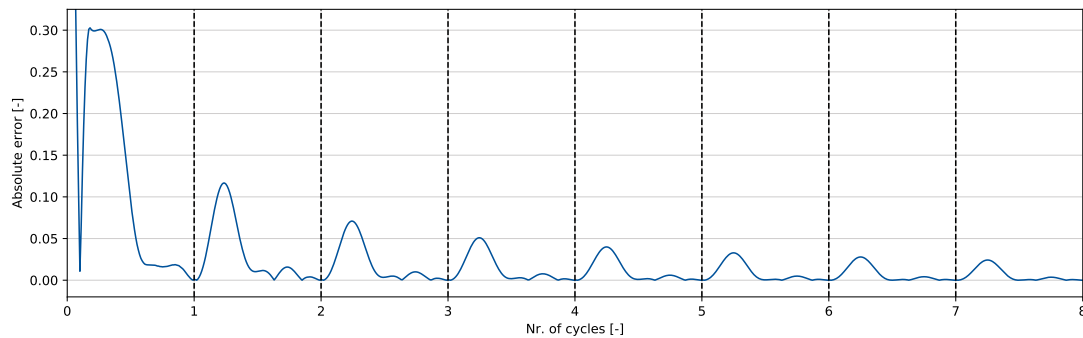


Figure A.2: Absolute error of the calculated sine fit from the real sine fit

A.2 Non-linearity ratio

The definition of the non-linearity ratio r_{nl} is given in chapter 4. For the response function given in equation A.3 the non-linearity ratio is determined. The one-sided amplitude spectrum, obtained with the Fast Fourier Transform, would in this case exist of two peaks: a peak with height A_1 at frequency ω and a peak with height A_2 at frequency 2ω . These peaks are converted to the energy density spectrum with equation 3.6. The total integral of the energy density spectrum $m_{0,\text{total}}$ and the integral of the higher order (non linear) part $m_{0,\text{non linear}}$ are then as given in equations A.34 and A.35.

$$m_{0,\text{total}} = \int \frac{A_1^2}{2 \cdot d\omega} d\omega + \int \frac{A_2^2}{2 \cdot d\omega} d\omega = \frac{A_1^2 + A_2^2}{2} \quad (\text{A.34})$$

$$m_{0,\text{non linear}} = \int \frac{A_2^2}{2 \cdot d\omega} d\omega = \frac{A_2^2}{2} \quad (\text{A.35})$$

The non-linearity ratio is then calculated with equation A.36.

$$r_{nl} = \frac{m_{0,\text{non linear}}}{m_{0,\text{total}}} = \frac{A_2^2}{A_1^2 + A_2^2} \quad (\text{A.36})$$

A.3 Conclusion

After the derivations in this appendix it can be concluded that indeed the link between the non-linearity ratio and the coefficient of determination as given in equation A.1. The non-linearity is equal to SSE as defined in equation A.29. The non-linearity ratio is thus a measure of how non-linear the response is, how different it is from an ideal (linear) response.

The coefficient of determination, r^2 , is then the opposite of the non-linearity ratio. This coefficient can be seen as a measure of how much the response is dominated by the first order (linear) part, so how linear the response is.

B

Filter comparison

As explained in chapter 3 the filtering has a significant influence on the acceleration signal and thus also on the jerk signal. The effect of filtering will be tested on acceleration measurements for a model in regular waves and measurements for a model in irregular waves. Two different data sets from different test programs are used to test whether the effect of the filtering is comparable. For the regular waves test a run from the FAST project phase 2 is used [7]. The run used was a run in head waves with the enlarged ship concept (ESC). The sampling frequency used in this test is 1000 Hz. The model speed is 2.876 m/s, which (with Froude scaling) compares to a full scale speed of 25 knots. The wave amplitude ζ is 95 mm, the wave frequency ω is 4.02 rad/s. This leads to a wave length λ of 3.81 m, and the wave steepness is 0.050. The wave steepness is defined as $2\zeta/\lambda$. In the chosen time frame from the data set a large change in the acceleration due to a slam is visible.

For the irregular waves test a run from the FAST project phase 1 is used [7, 30]. The run used was a run in head waves with the enlarged ship concept (ESC). The sampling frequency used in this test is 400 Hz. The model speed is 2.876 m/s as well. The waves were generated according to a JONSWAP wave spectrum. The full scale wave spectrum parameters are given in the report. The significant wave height H_s is 3 m, the peak period T_p is 6 s. The peak enhancement factor [19] γ is 3.3. The full scale wave spectrum parameters are scaled to the model scale according to Froude scaling. In the chosen time frame from the data set a change in the acceleration due to a slam is visible. Also the irregular character of the acceleration is visible.

In each comparison in this appendix one filter setting will be varied to compare the influence on the data. Each comparison consists of 8 (sub)figures. In subfigures (a) and (b) the frequency response plot (respectively in unity and in decibel scale) will be given. Subfigure (c) shows the acceleration signal of the regular waves data set, including the unfiltered signal. Subfigure (d) shows the acceleration for the irregular waves data set, including the unfiltered signal. In subfigures (e) and (f) the jerk signal is given for respectively the regular waves and the irregular waves data set. This jerk signal is the differentiated acceleration signal, using the central difference formula. Finally in subfigure (g) and (h) the energy density spectrum of the respectively regular and irregular jerk signal is plotted. This energy density spectrum is based on the entire signal, not only the part shown in the subfigures above. For the irregular waves the mean energy density spectrum is used, which is the average spectrum of the energy density spectra of parts of the signal. The y-axis of all the subfigures is the same in all comparisons, except for the decibel frequency response plot. Since the attenuation in decibel is significantly different between different filters and filter settings, it was found that details would be lost if all the plots would have been with the same scale for the y-axis.

To apply the filters below (except the Savitzky-Golay filter) the digital method forward-backward filtering is applied. The data is first passed forward through the filter, and then again in backward direction. The advantage of this is that no phase lag is introduced in the filtered signal, which normally the case when applying a low-pass filter. Since the data is passed through the filter twice, the order of the filter is effectively doubled [34]. The orders documented in this report are the undoubled orders used to determine the filter parameters used for the forward-backward filtering. The Savitsky-Golay filter does not introduce a phase lag by design.

Butterworth filtering

The Butterworth filter is a filter with a smooth transition between passband and stopband, without ripples in each of these bands. The downside is that the roll-off is relatively low, especially at lower order filtering. The transition band can thus be relatively wide. The Butterworth filter has two input parameters: the cut-off frequency and the order of filtering.

In table B.1 the details of the comparisons performed with Butterworth filtering can be found. First, the influence of varying cut-off frequency with constant filter order is compared, then the influence of varying order for a constant cut-off frequency is compared. The Butterworth filter is investigated more than the other filters, since this filter has the smoothest frequency response and showed most promise in early investigations for this thesis.

Table B.1: Overview of Butterworth filter comparisons

Filter details	Cut-off frequencies	Figure	Page
Butterworth, 2 nd order	20 Hz, 25 Hz, 30 Hz	B.1	104
Butterworth, 4 th order	20 Hz, 25 Hz, 30 Hz	B.3	106
Butterworth, 6 th order	20 Hz, 25 Hz, 30 Hz	B.5	108
Butterworth, 8 th order	20 Hz, 25 Hz, 30 Hz	B.7	110
Butterworth, 2 nd order	5 Hz, 10 Hz, 15 Hz	B.2	105
Butterworth, 4 th order	5 Hz, 10 Hz, 15 Hz	B.4	107
Butterworth, 6 th order	5 Hz, 10 Hz, 15 Hz	B.6	109
Butterworth, 8 th order	5 Hz, 10 Hz, 15 Hz	B.8	111
Filter details	Orders	Figure	Page
Butterworth, cut-off frequency 10 Hz	2, 4, 6, 8	B.9	112
Butterworth, cut-off frequency 20 Hz	2, 4, 6, 8	B.10	113

Chebyshev filtering

Chebyshev filters are another type of digital filters. These filters have a smaller transition band than the Butterworth filters, but there are ripples in the passband (Chebyshev I filter) or ripples in the stopband (Chebyshev II filter) [38].

The inputs for the Chebyshev I filter are order of filtering, critical frequency and allowed ripple in the passband. The critical frequency is the frequency in the transition band at which the amplitude gain first drops below the allowed ripple. In table B.2 the details of the comparisons performed with Chebyshev I filtering can be found. The influence of allowed ripple, order of filtering and critical frequency is compared.

The inputs for the Chebyshev II filter are order of filtering, critical frequency and minimum attenuation in the stopband. In this case the critical frequency is the frequency at which the amplitude gain first passes the minimum attenuation value. In table B.2 the details of the comparisons performed with Chebyshev II filtering can be found as well. The influence of minimum attenuation, order of filtering and critical frequency is compared.

Table B.2: Overview of Chebyshev filter comparisons

Filter details	Order	Critical frequency	Allowed ripple in passband	Figure	Page
Chebyshev I	5	20 Hz	0.1 dB, 1 dB, 3dB	B.11	114
Chebyshev I	3, 5, 7	20 Hz	1 dB	B.12	115
Chebyshev I	5	10 Hz, 20 Hz, 30 Hz	1 dB	B.13	116
Filter details	Order	Critical frequency	Minimum attenuation in stopband	Figure	Page
Chebyshev II	5	30 Hz	-20 dB, -40 dB, -60 dB	B.14	117
Chebyshev II	3, 5, 7	30 Hz	-40 dB	B.15	118
Chebyshev II	5	20 Hz, 30 Hz, 40 Hz	-40 dB	B.16	119

Savitzky-Golay filtering

To be able to compare the Savitzky-Golay method with the other filters, combinations of orders and window lengths are determined that are found to have certain cut-off frequencies. The cut-off frequency f_c is defined as the frequency where the amplitude gain first passes -3 dB, or 0.707 (unity) amplitude gain. This is also dependent on the sampling frequency of the data set. A full overview of the used combinations of orders and window lengths, with resulting cut-off frequencies, can be found in table B.4. The regular wave tests were performed a sampling frequency f_s of 1000 Hz, the irregular wave tests with a sampling frequency f_s of 400 Hz. So different window lengths are used to get the same frequency response of the filter for both data sets.

In table B.3 the performed comparisons are displayed. First, the influence of varying cut-off frequency (thus varying window length) with constant filter order is compared, then the influence of varying order for a constant cut-off frequency is compared.

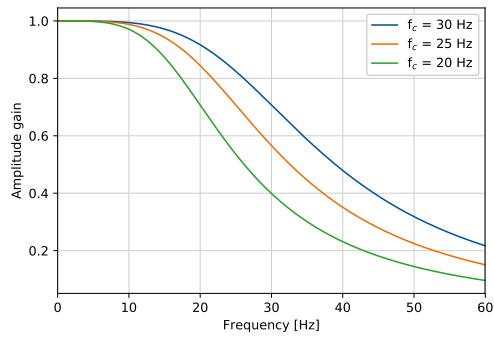
Table B.3: Overview of Savitzky-Golay filter comparisons

Filter details	Cut-off frequencies	Figure	Page
Savitzky-Golay, 3 rd order	10 Hz, 15 Hz, 20 Hz	B.17	120
Savitzky-Golay, 5 th order	10 Hz, 15 Hz, 20 Hz	B.18	121
Savitzky-Golay, 7 th order	10 Hz, 15 Hz, 20 Hz	B.19	122
Filter details	Orders	Figure	Page
Savitzky-Golay, cut-off frequency 10 Hz	1, 3, 5, 7	B.20	123
Savitzky-Golay, cut-off frequency 15 Hz	1, 3, 5, 7	B.21	124
Savitzky-Golay, cut-off frequency 20 Hz	1, 3, 5, 7	B.22	125

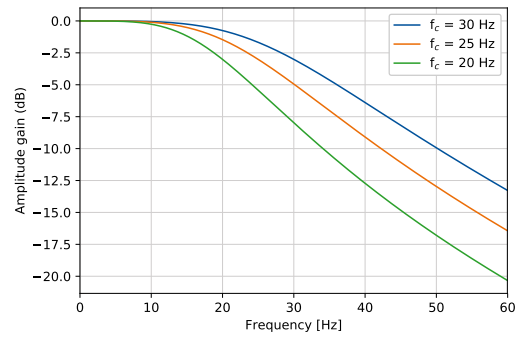
Table B.4: Overview of Savitzky-Golay filter order and window length combinations for cut-off frequencies

Order	Window length					
	$f_c = 10$ Hz		$f_c = 15$ Hz		$f_c = 20$ Hz	
	$f_s = 400$ Hz	$f_s = 1000$ Hz	$f_s = 400$ Hz	$f_s = 1000$ Hz	$f_s = 400$ Hz	$f_s = 1000$ Hz
1	17	45	11	29	9	23
3	43	107	29	71	21	53
5	67	171	45	113	35	85
7	93	235	63	155	47	117

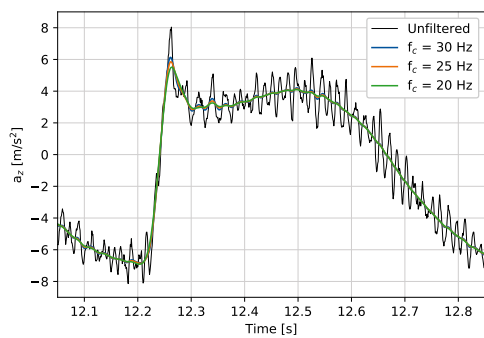
Butterworth filter, 2nd order



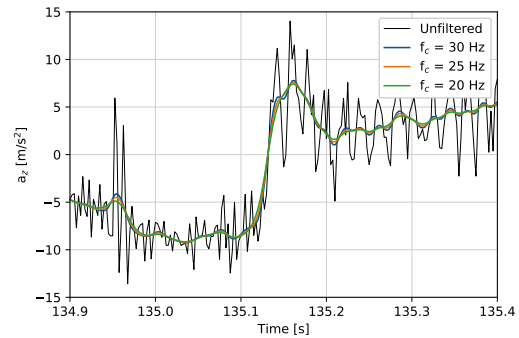
(a) Frequency response



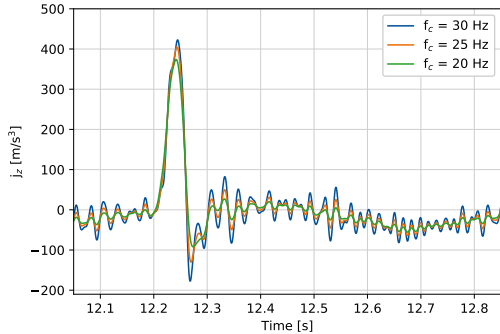
(b) Frequency response (dB)



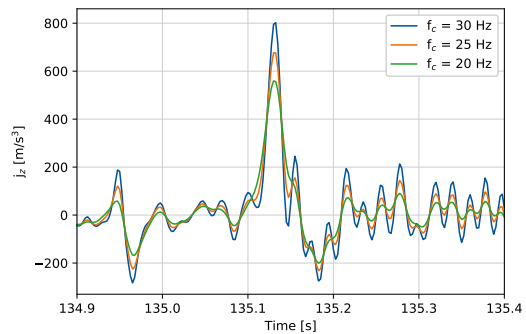
(c) Acceleration regular waves



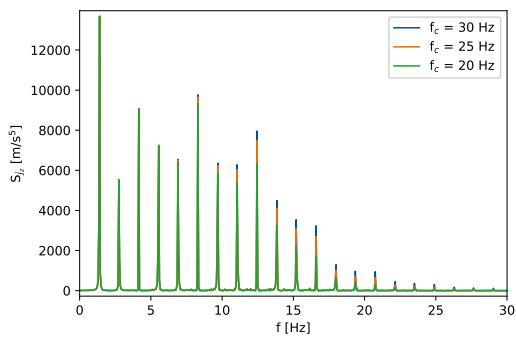
(d) Acceleration irregular waves



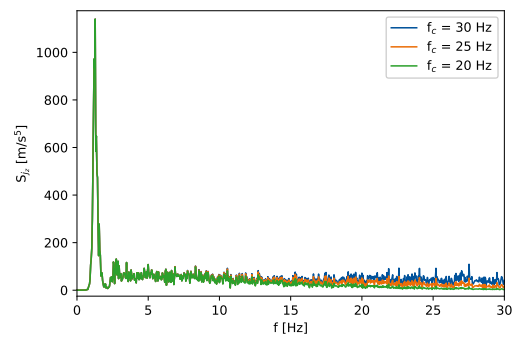
(e) Jerk regular waves



(f) Jerk irregular waves



(g) Energy density spectrum regular waves



(h) Energy density spectrum irregular waves

Figure B.1: Comparison Butterworth filter, 2nd order, cut-off frequencies 20 Hz, 25 Hz, 30 Hz

Butterworth filter, 2nd order

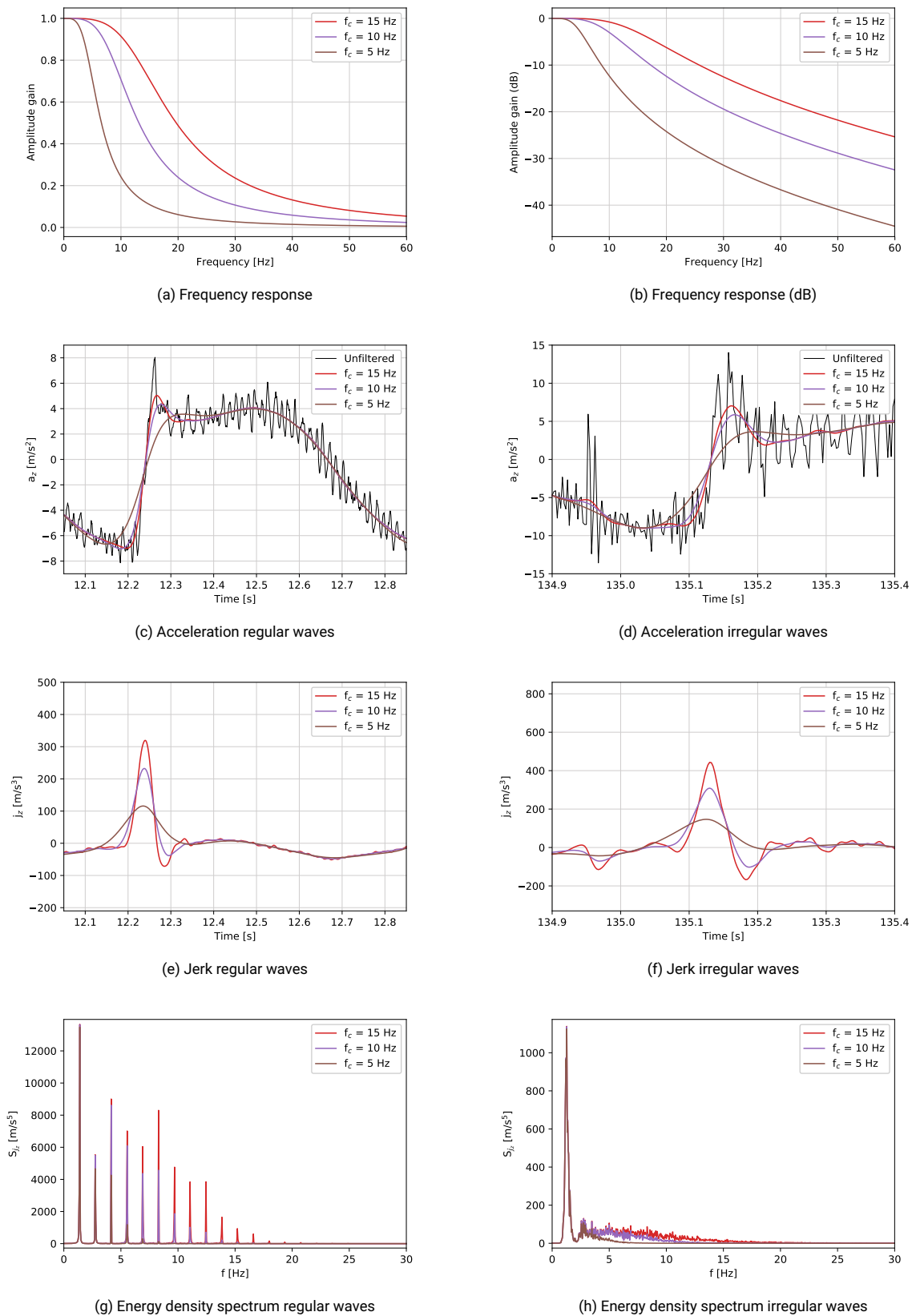
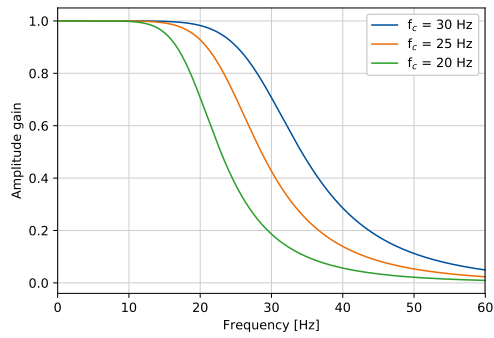
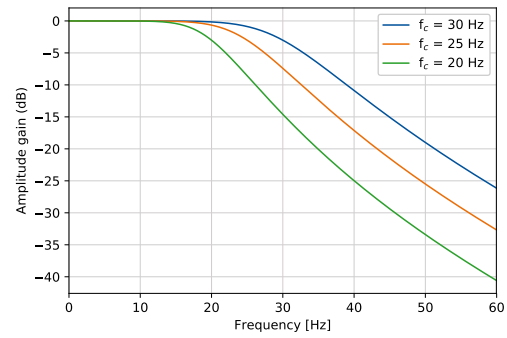


Figure B.2: Comparison Butterworth filter, 2nd order, cut-off frequencies 5 Hz, 10 Hz, 15 Hz

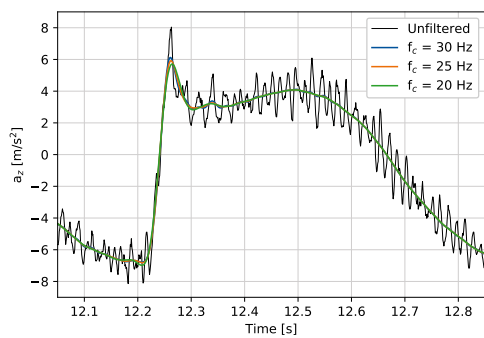
Butterworth filter, 4th order



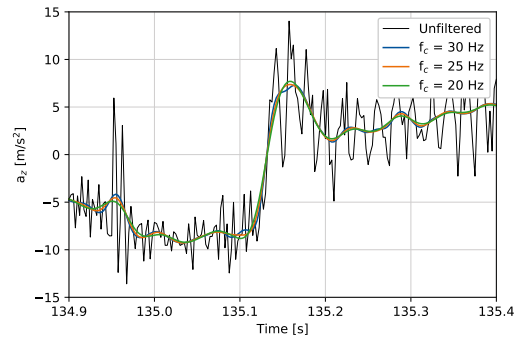
(a) Frequency response



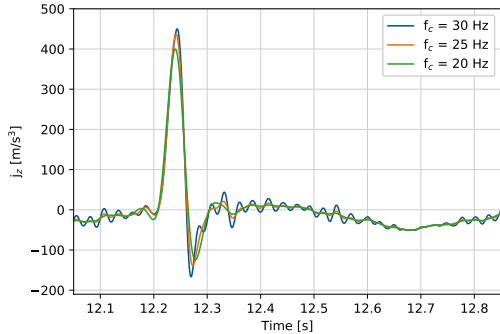
(b) Frequency response (dB)



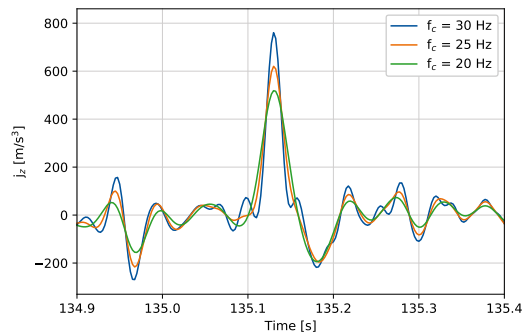
(c) Acceleration regular waves



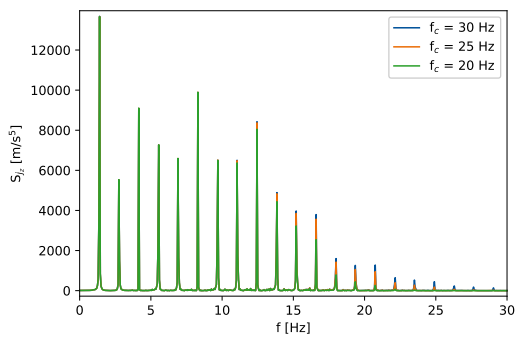
(d) Acceleration irregular waves



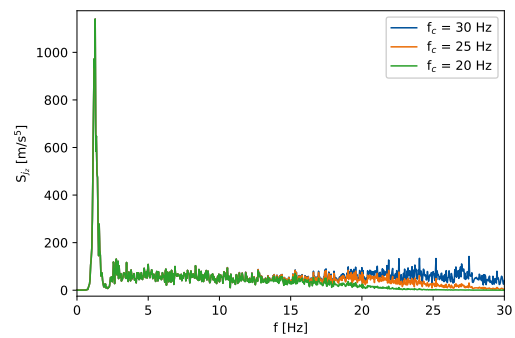
(e) Jerk regular waves



(f) Jerk irregular waves



(g) Energy density spectrum regular waves



(h) Energy density spectrum irregular waves

Figure B.3: Comparison Butterworth filter, 4th order, cut-off frequencies 20 Hz, 25 Hz, 30 Hz

Butterworth filter, 4th order

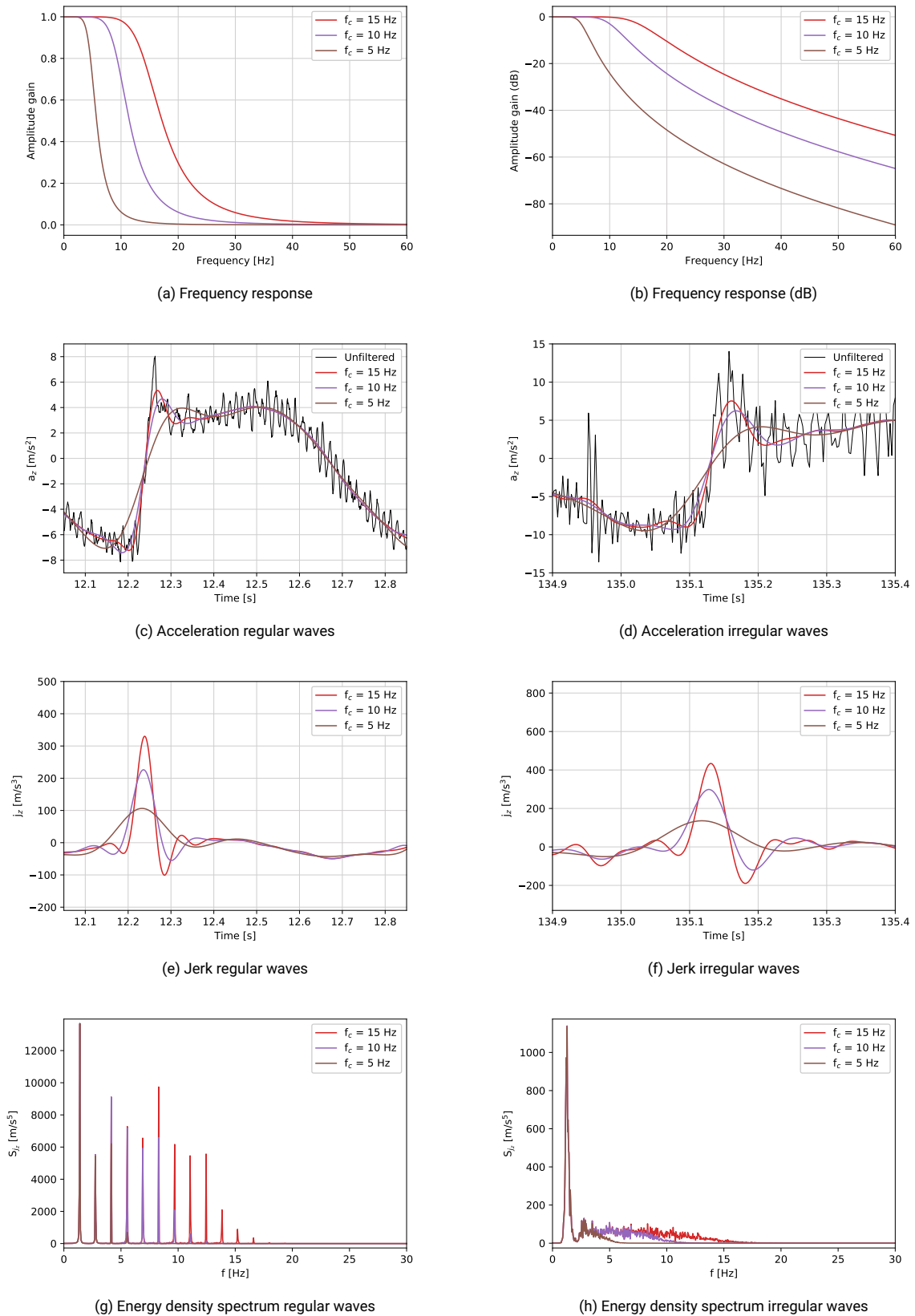
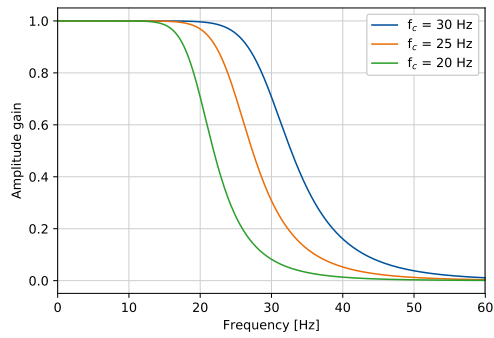
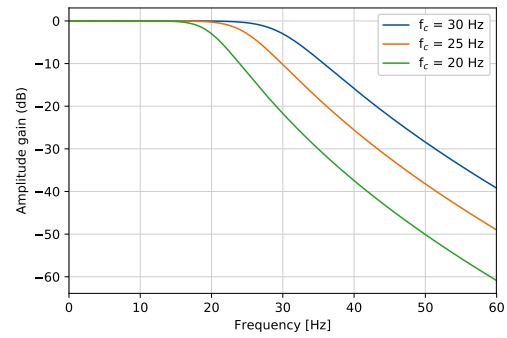


Figure B.4: Comparison Butterworth filter, 4th order, cut-off frequencies 5 Hz, 10 Hz, 15 Hz

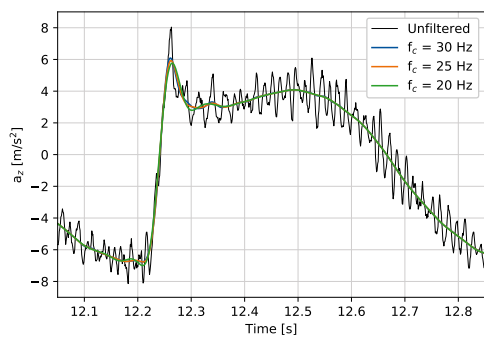
Butterworth filter, 6th order



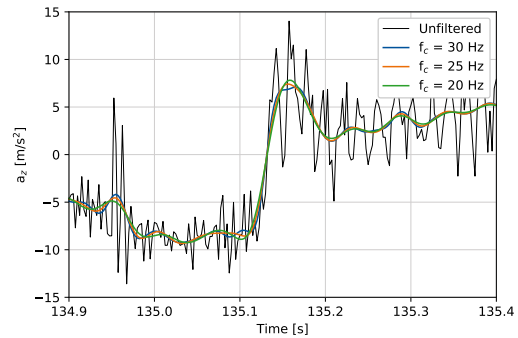
(a) Frequency response



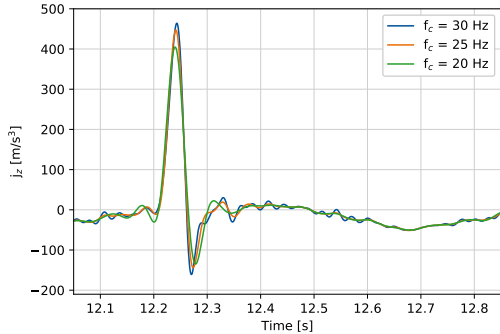
(b) Frequency response (dB)



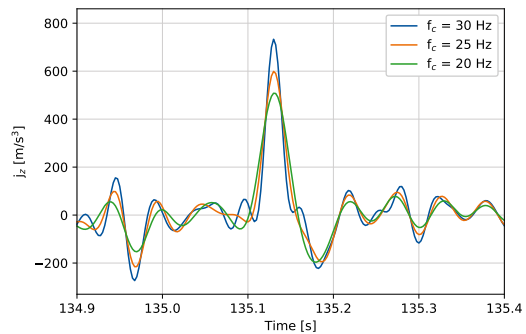
(c) Acceleration regular waves



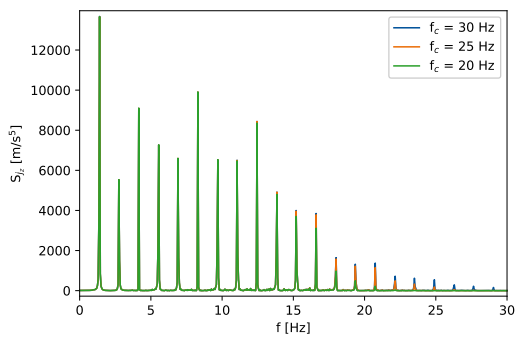
(d) Acceleration irregular waves



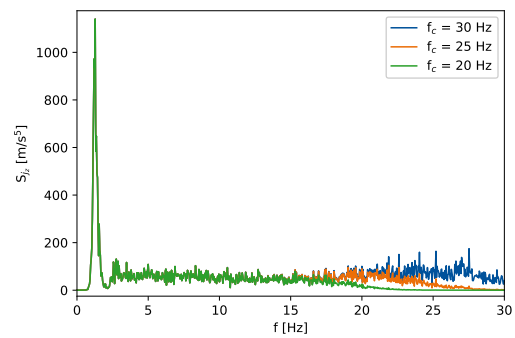
(e) Jerk regular waves



(f) Jerk irregular waves



(g) Energy density spectrum regular waves



(h) Energy density spectrum irregular waves

Figure B.5: Comparison Butterworth filter, 6th order, cut-off frequencies 20 Hz, 25 Hz, 30 Hz

Butterworth filter, 6th order

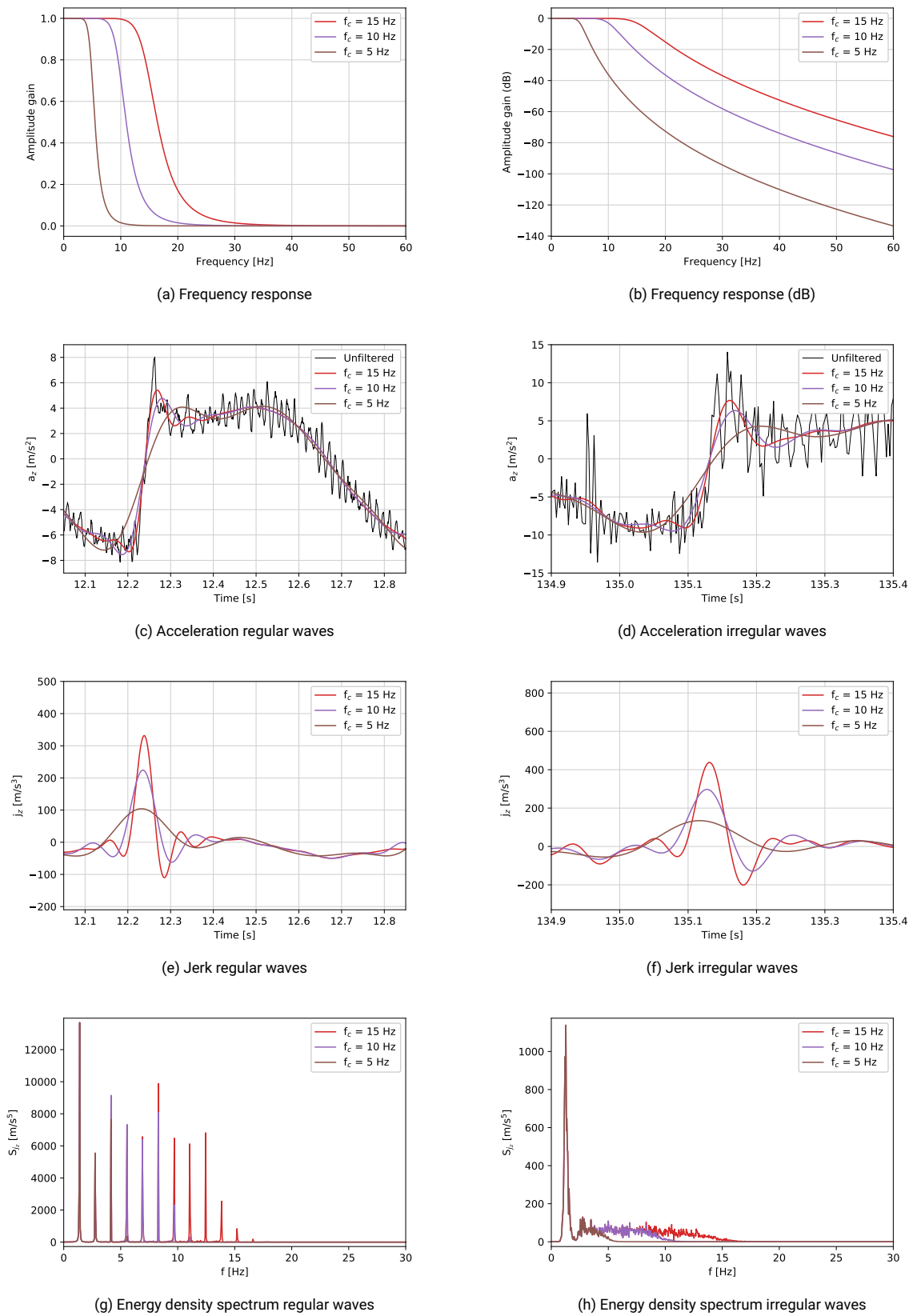
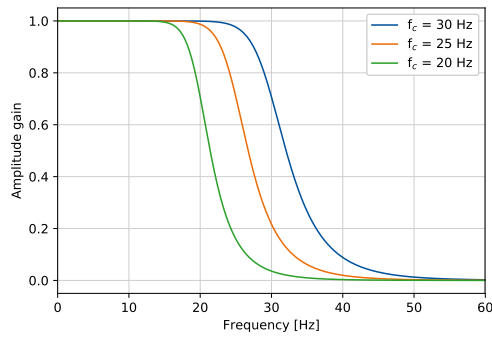
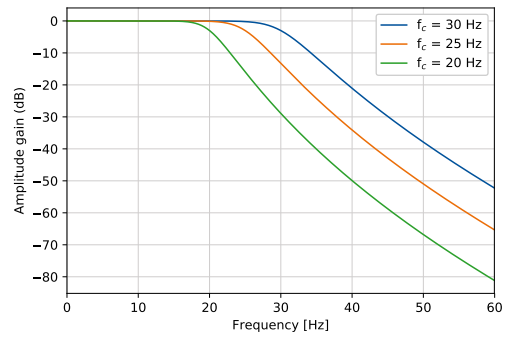


Figure B.6: Comparison Butterworth filter, 6th order, cut-off frequencies 5 Hz, 10 Hz, 15 Hz

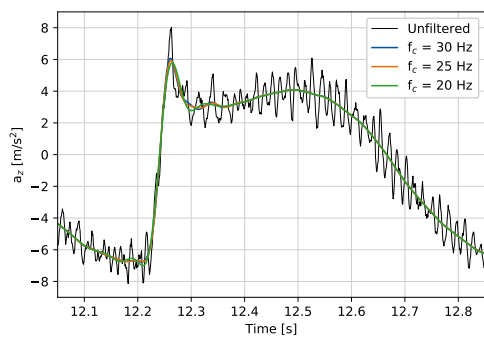
Butterworth filter, 8th order



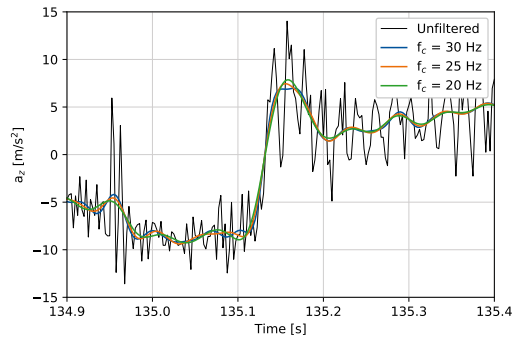
(a) Frequency response



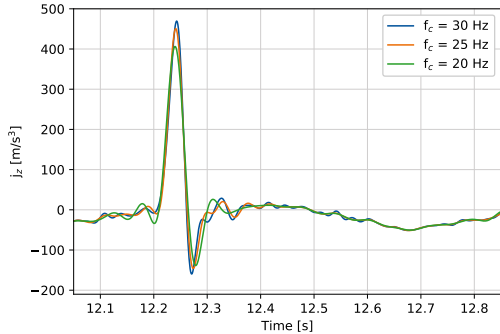
(b) Frequency response (dB)



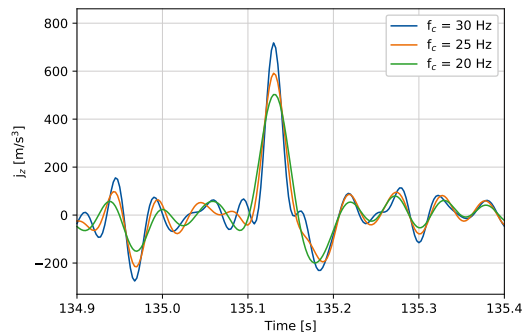
(c) Acceleration regular waves



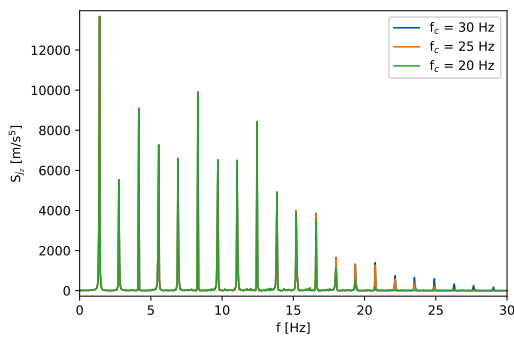
(d) Acceleration irregular waves



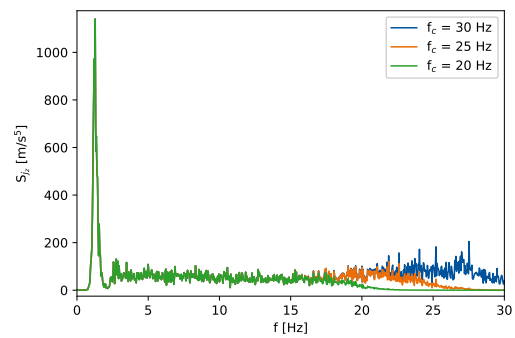
(e) Jerk regular waves



(f) Jerk irregular waves



(g) Energy density spectrum regular waves



(h) Energy density spectrum irregular waves

Figure B.7: Comparison Butterworth filter, 8th order, cut-off frequencies 20 Hz, 25 Hz, 30 Hz

Butterworth filter, 8th order

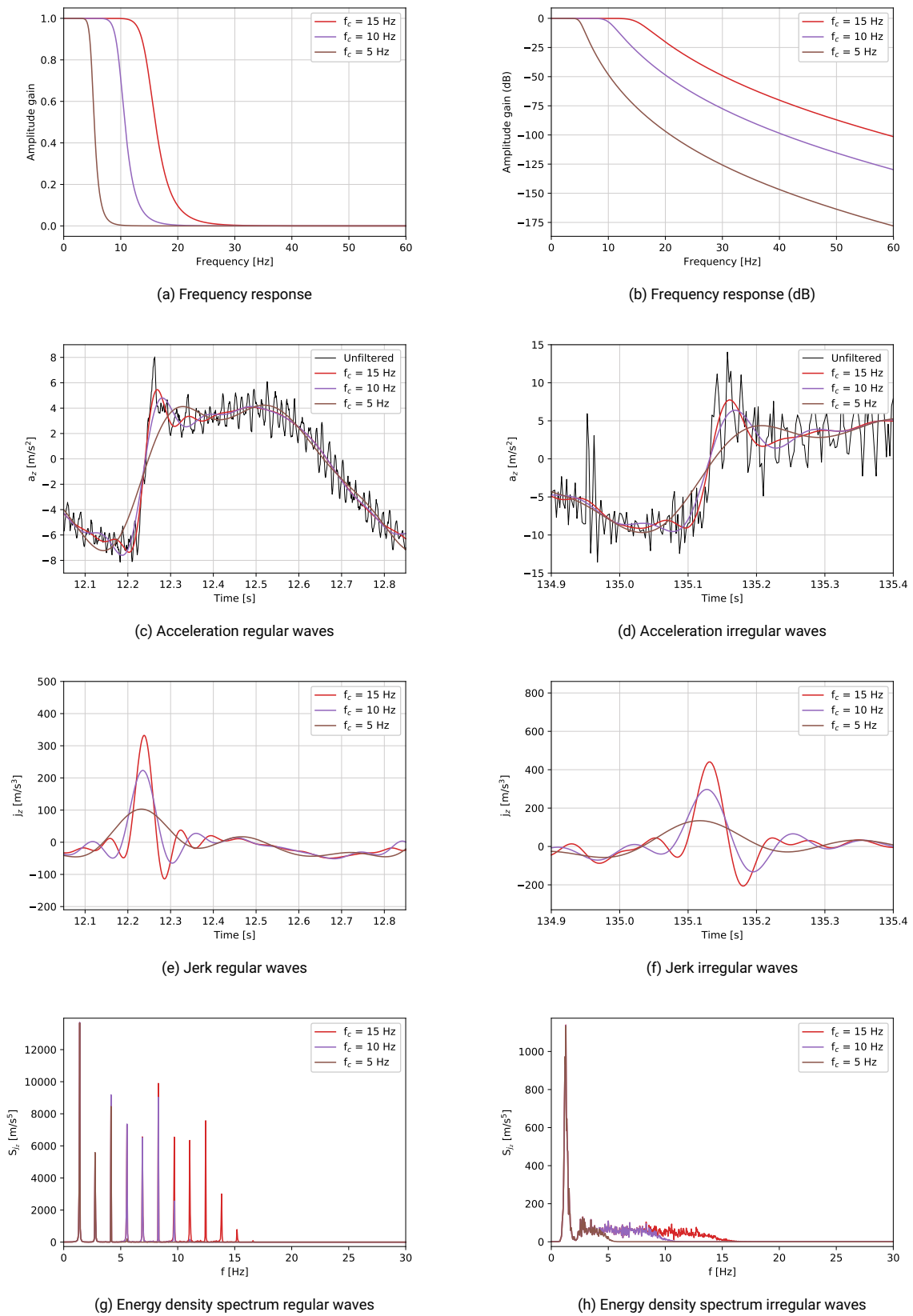
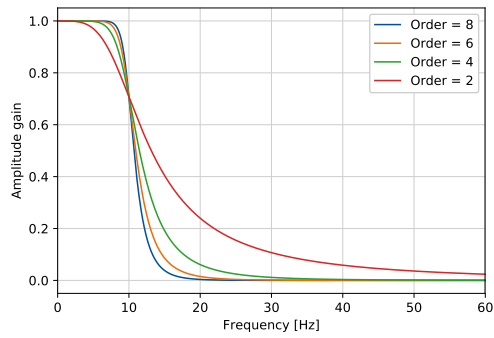
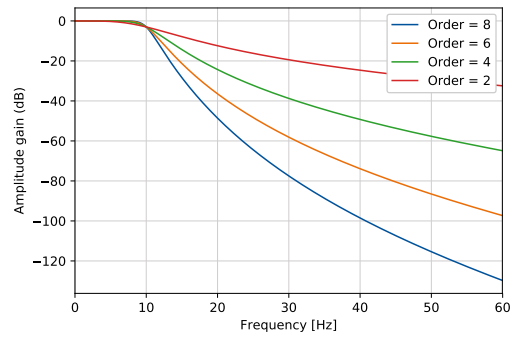


Figure B.8: Comparison Butterworth filter, 8th order, cut-off frequencies 5 Hz, 10 Hz, 15 Hz

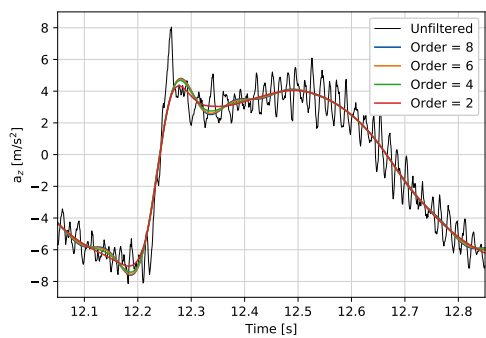
Butterworth filter, cut-off frequency 10 Hz



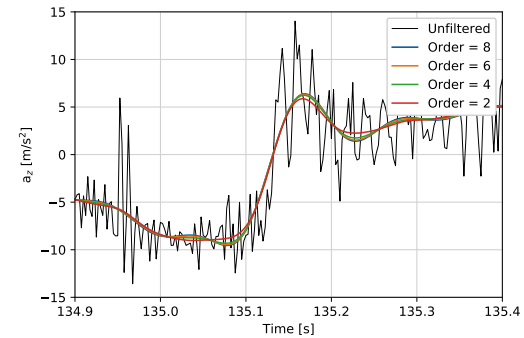
(a) Frequency response



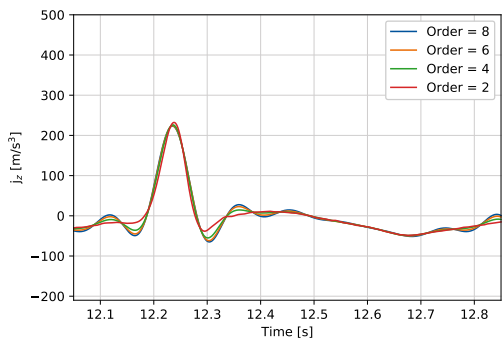
(b) Frequency response (dB)



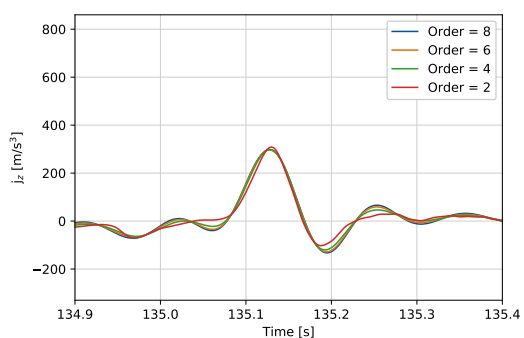
(c) Acceleration regular waves



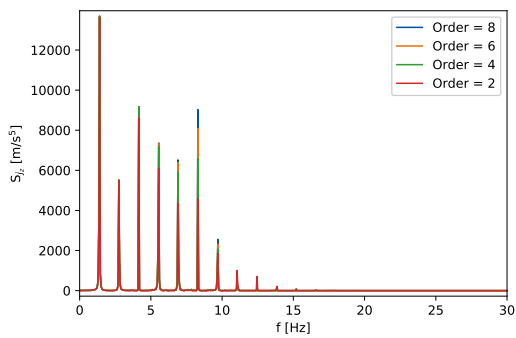
(d) Acceleration irregular waves



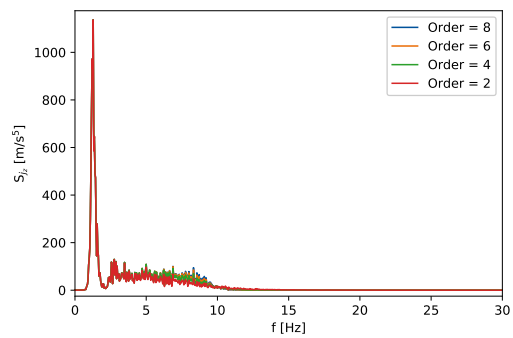
(e) Jerk regular waves



(f) Jerk irregular waves



(g) Energy density spectrum regular waves



(h) Energy density spectrum irregular waves

Figure B.9: Comparison Butterworth filter, 2nd, 4th, 6th, 8th order, cut-off frequency 10 Hz

Butterworth filter, cut-off frequency 20 Hz

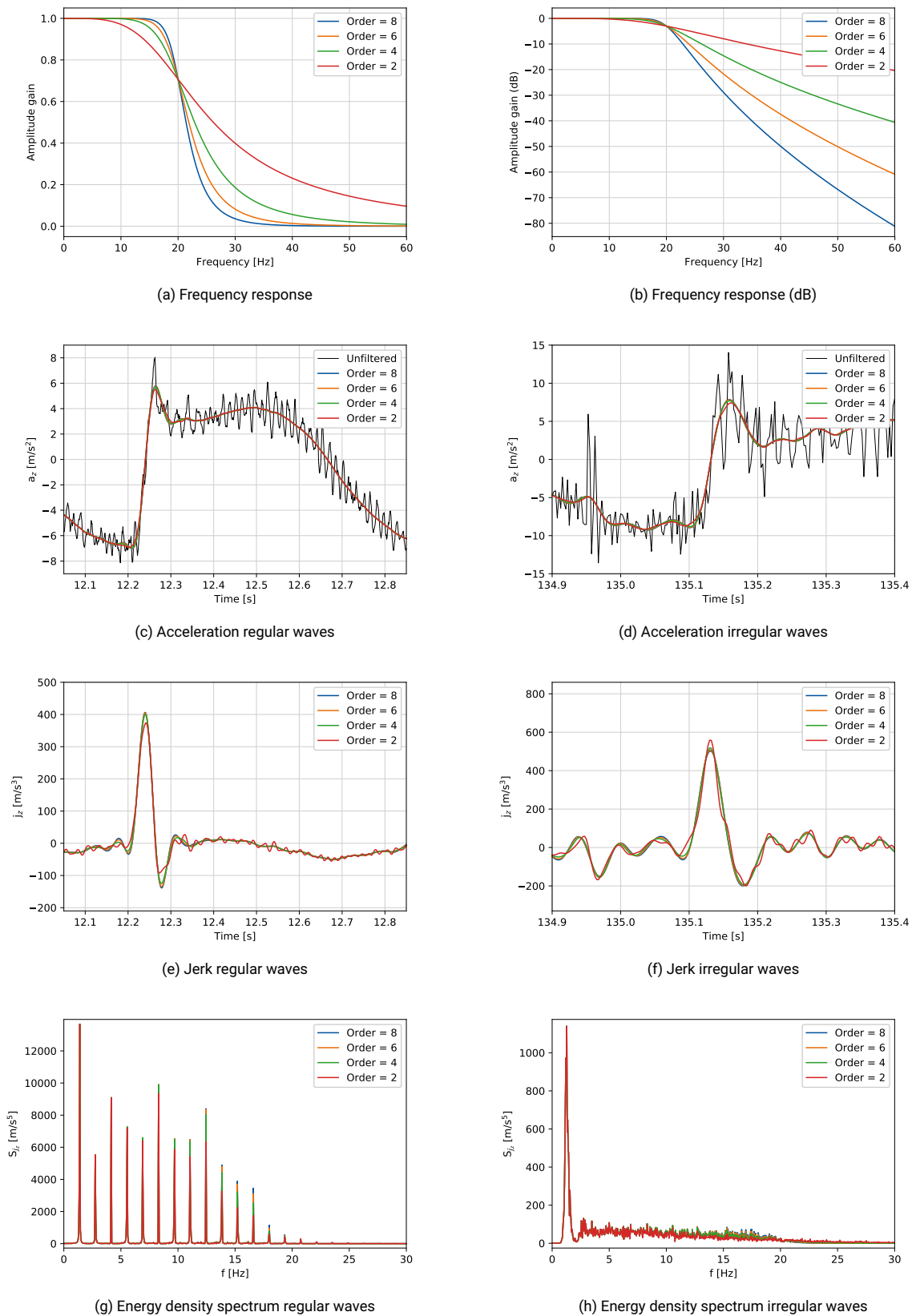


Figure B.10: Comparison Butterworth filter, 2nd, 4th, 6th, 8th order, cut-off frequency 20 Hz

Chebyshev I filter, 5th order, critical frequency 20 Hz

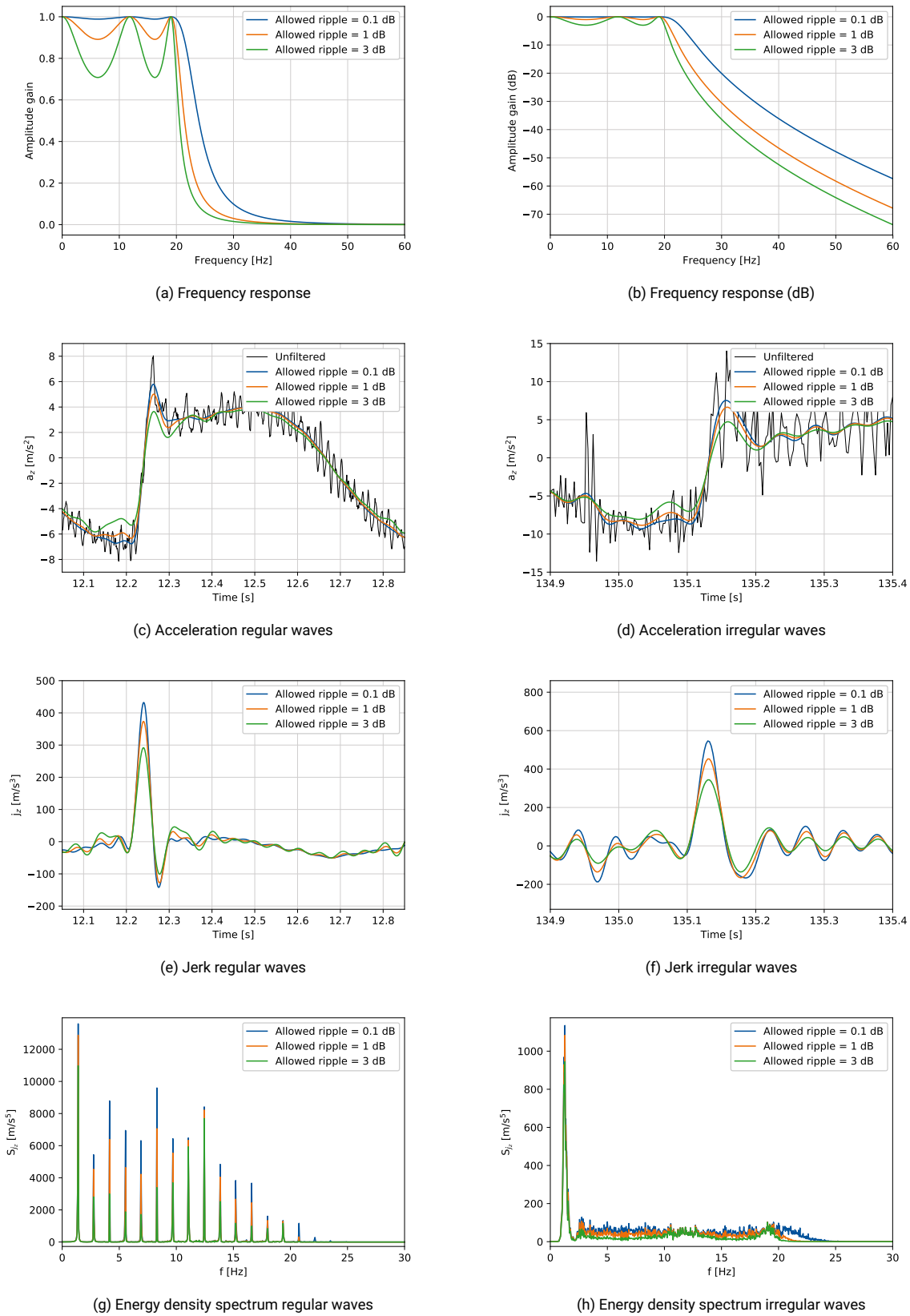


Figure B.11: Comparison Chebyshev I filter, 5th order, critical frequency 20 Hz, allowed ripple 0.1 dB, 1 dB, 3 dB

Chebyshev I filter, critical frequency 20 Hz, allowed ripple 1 dB

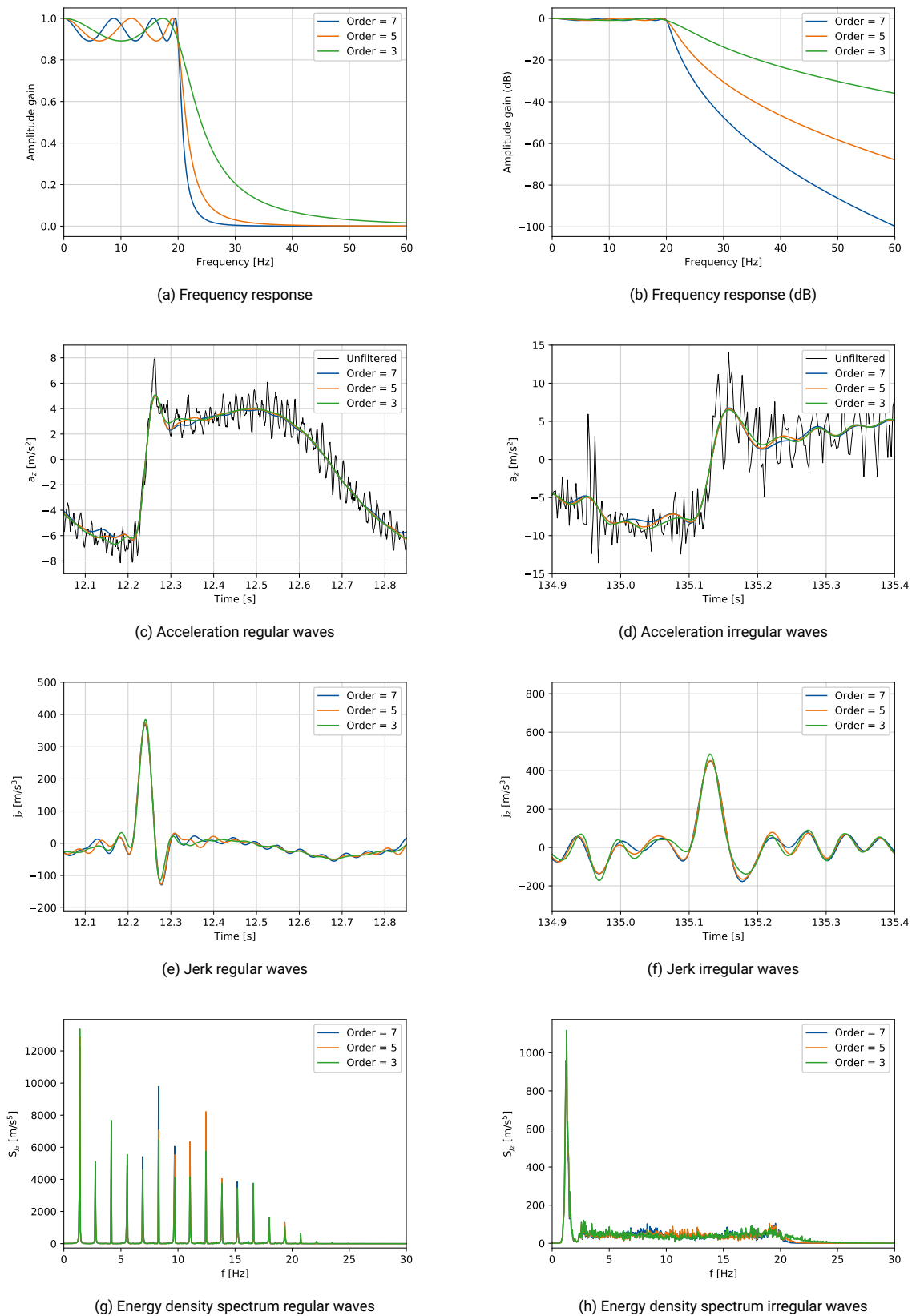


Figure B.12: Comparison Chebyshev I filter, 3rd, 5th, 7th order, critical frequency 20 Hz, allowed ripple 1 dB

Chebyshev I filter, 5th order, allowed ripple 1 dB

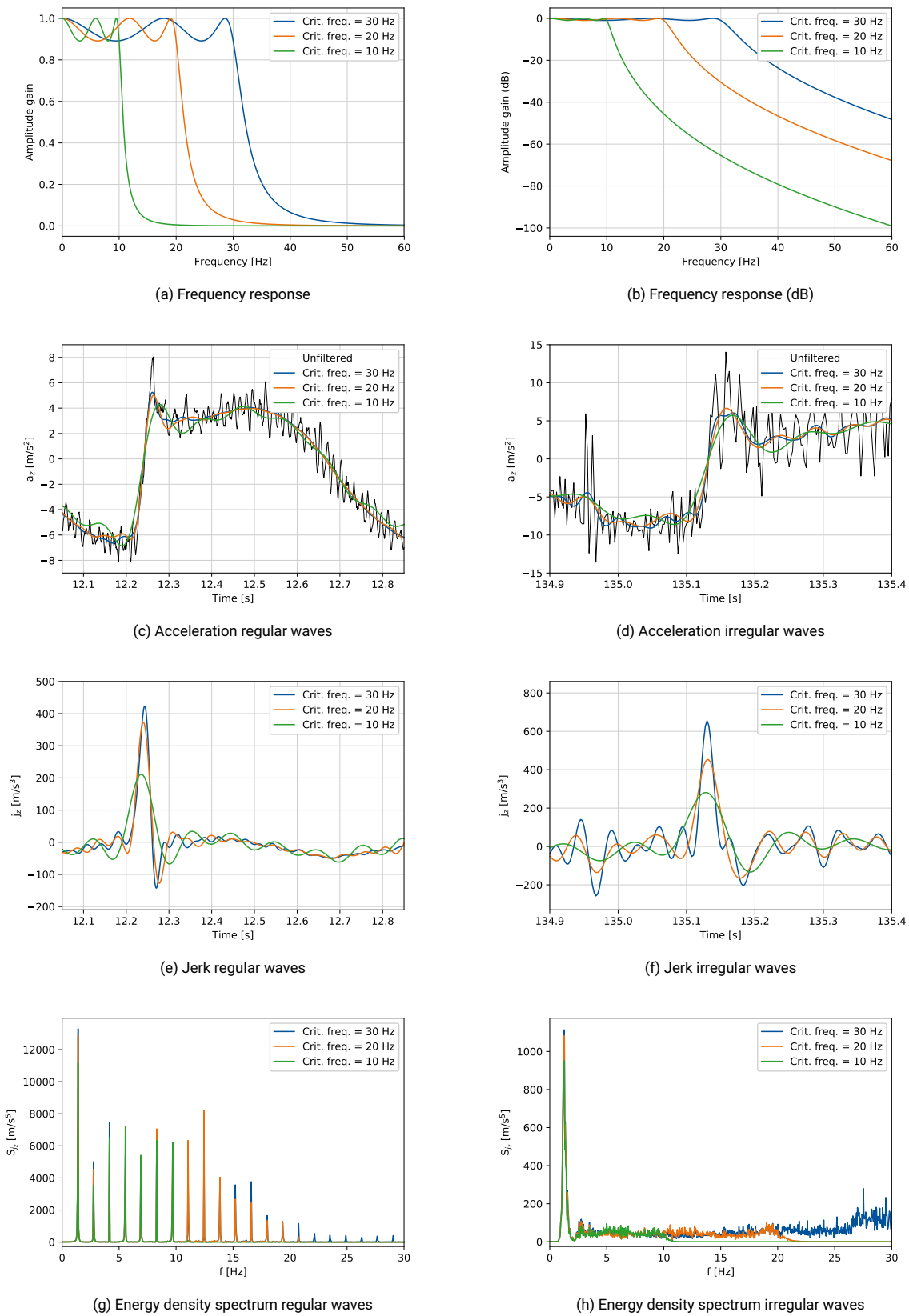


Figure B.13: Comparison Chebyshev I filter, 5th order, critical frequency 10 Hz, 20 Hz, 30 Hz, allowed ripple 1 dB

Chebyshev II filter, 5th order, critical frequency 30 Hz

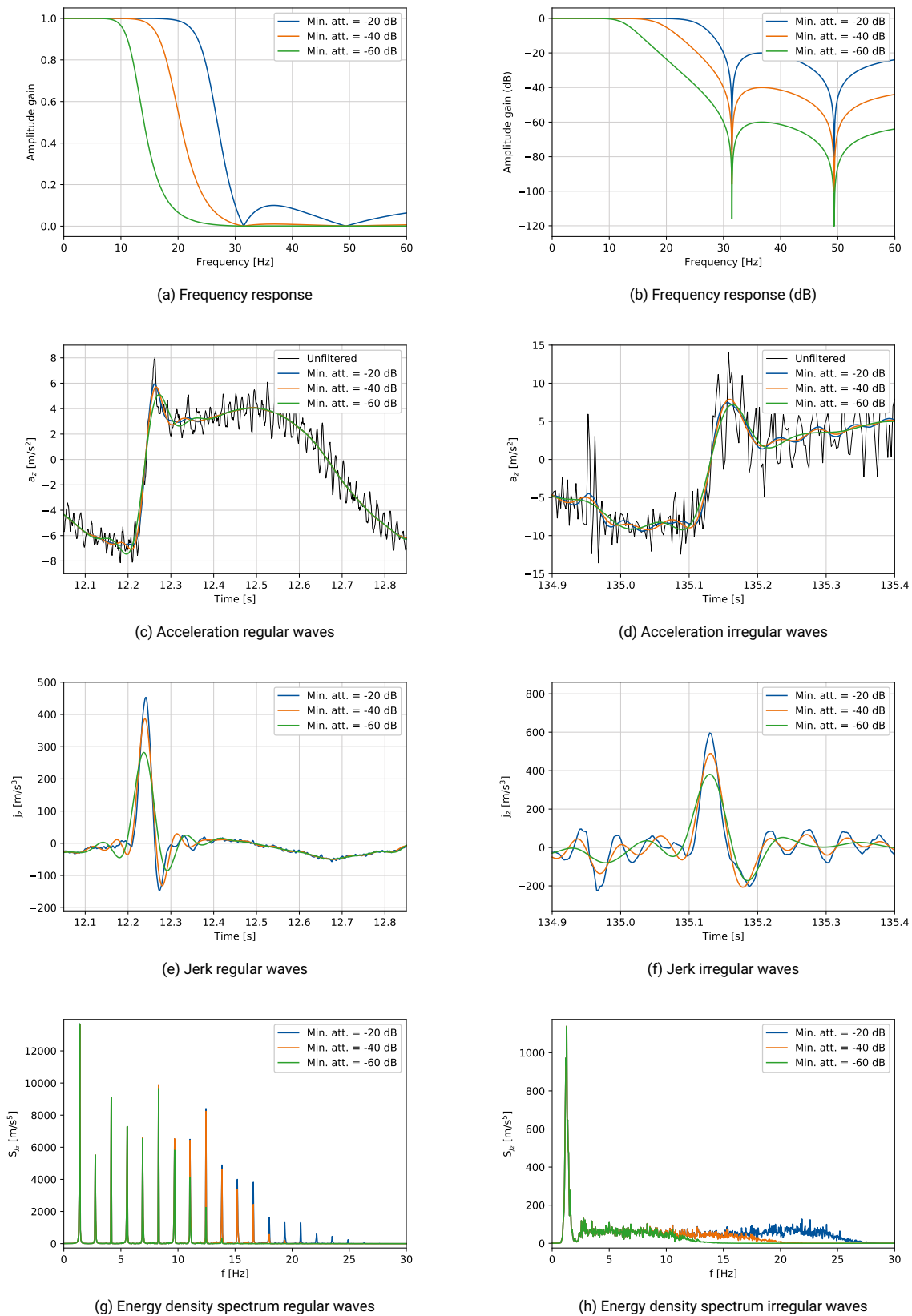


Figure B.14: Comparison Chebyshev II filter, 5th order, critical frequency 30 Hz, minimum attenuation -20 dB, -40 dB, -60 dB

Chebyshev II filter, critical frequency 30 Hz, minimum attenuation -40 dB

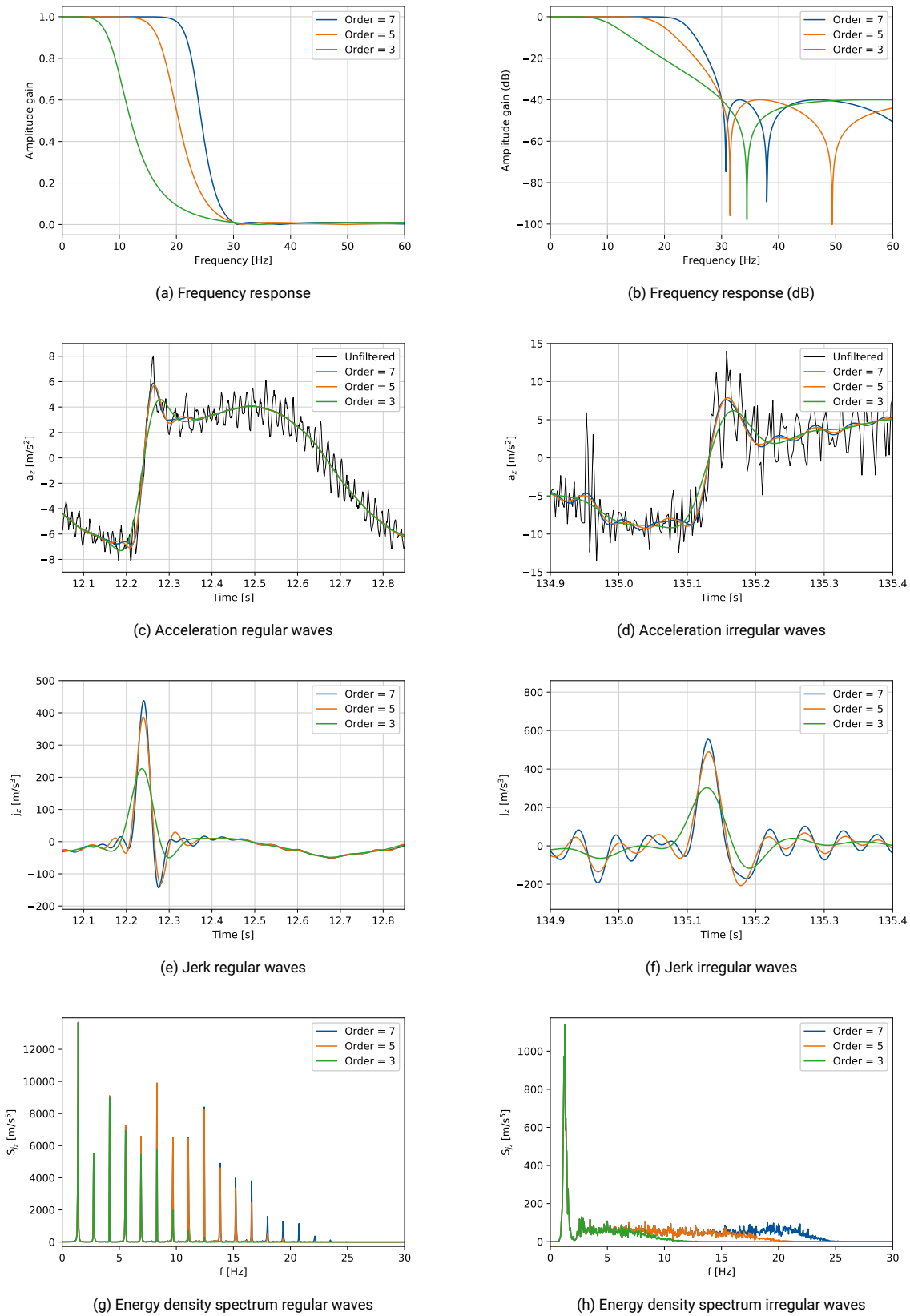


Figure B.15: Comparison Chebyshev II filter, 3rd, 5th, 7th order, critical frequency 30 Hz, minimum attenuation -40 dB

Chebyshev II filter, 5th order, minimum attenuation -40 dB

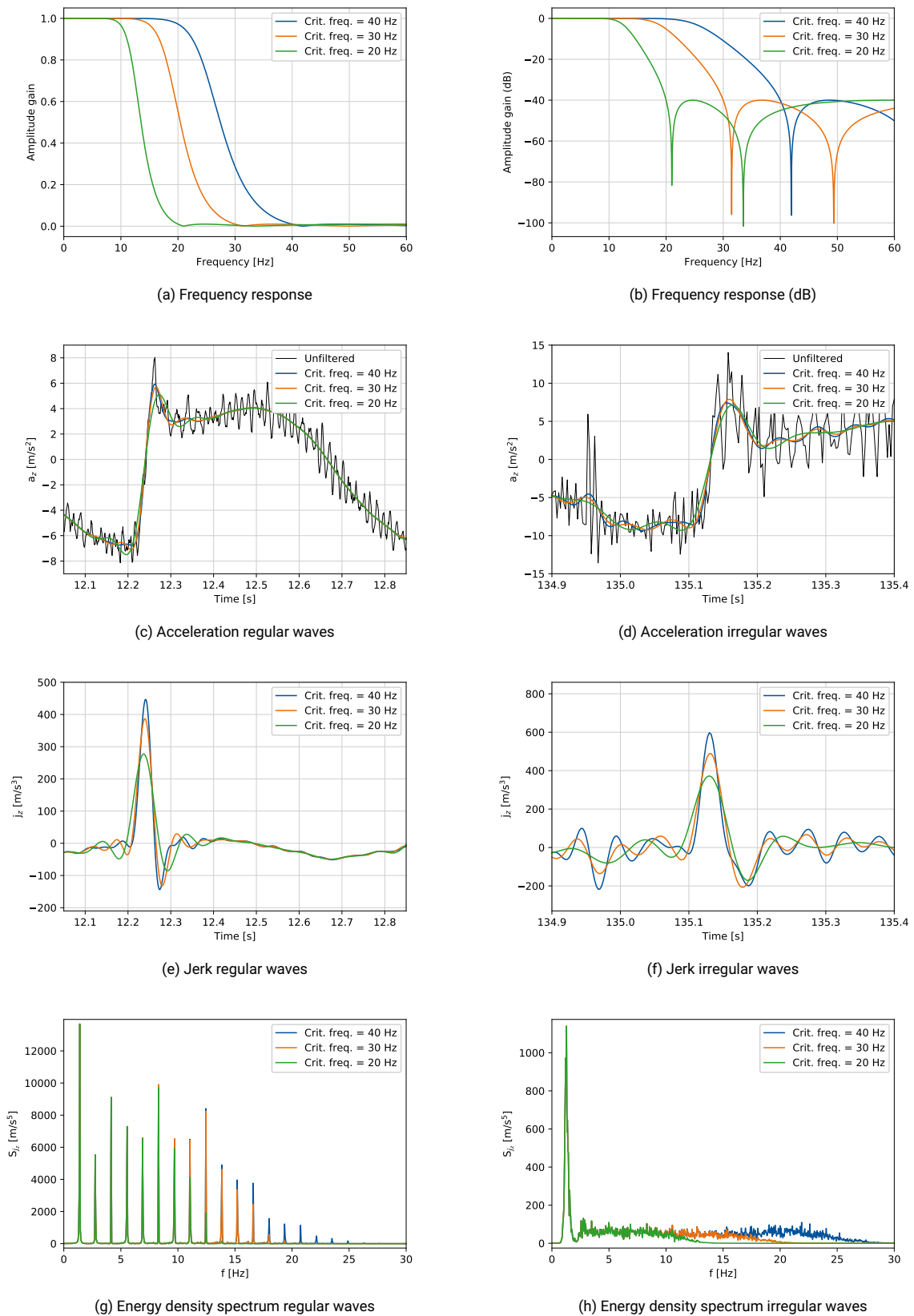


Figure B.16: Comparison Chebyshev II filter, 5th order, critical frequency 20 Hz, 30 Hz, 40 Hz, minimum attenuation -40 dB

Savitzky-Golay filter, 3rd order

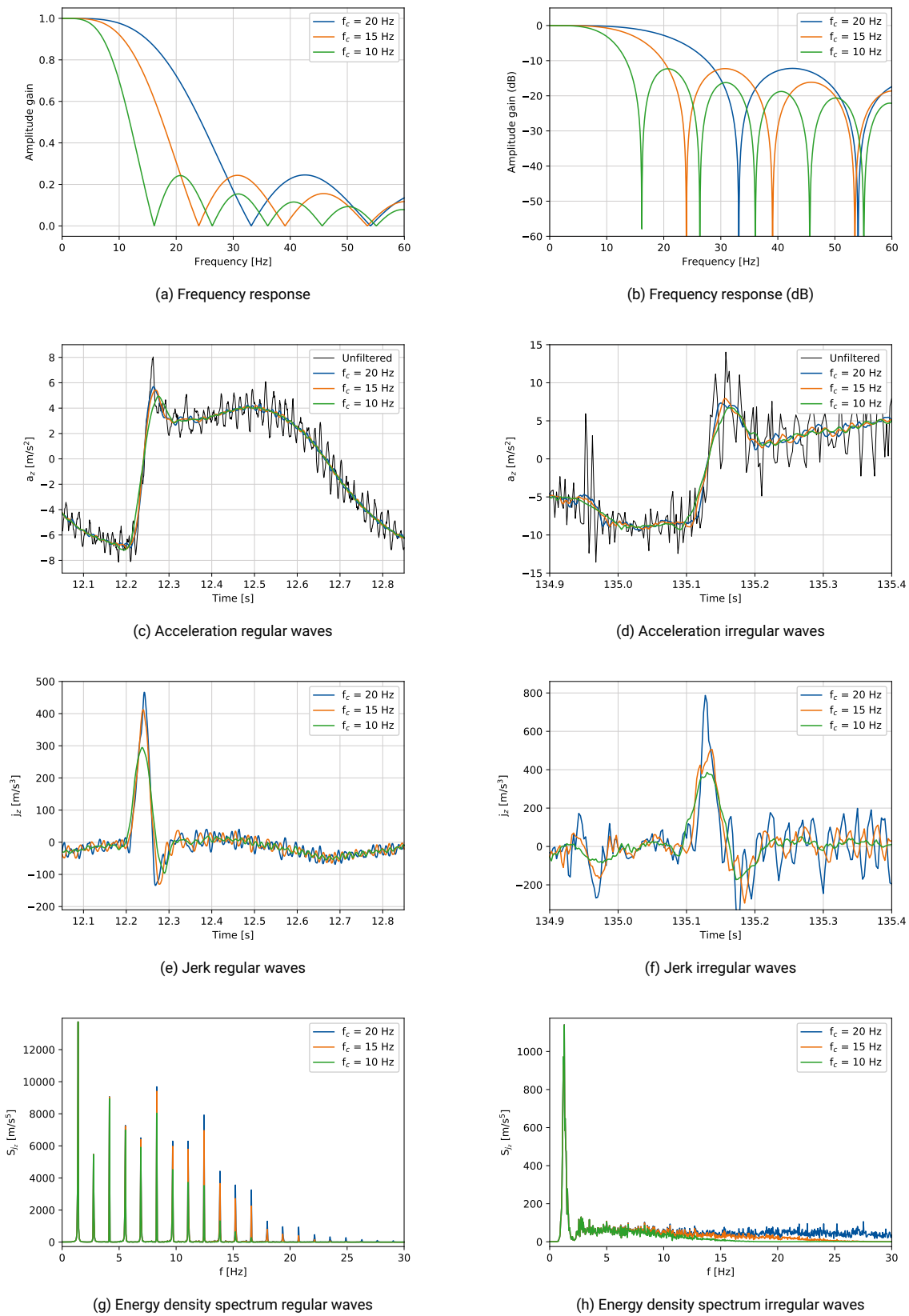


Figure B.17: Comparison Savitzky-Golay filter, 3rd order, cut-off frequencies 10 Hz, 15 Hz, 20 Hz

Savitzky-Golay filter, 5th order

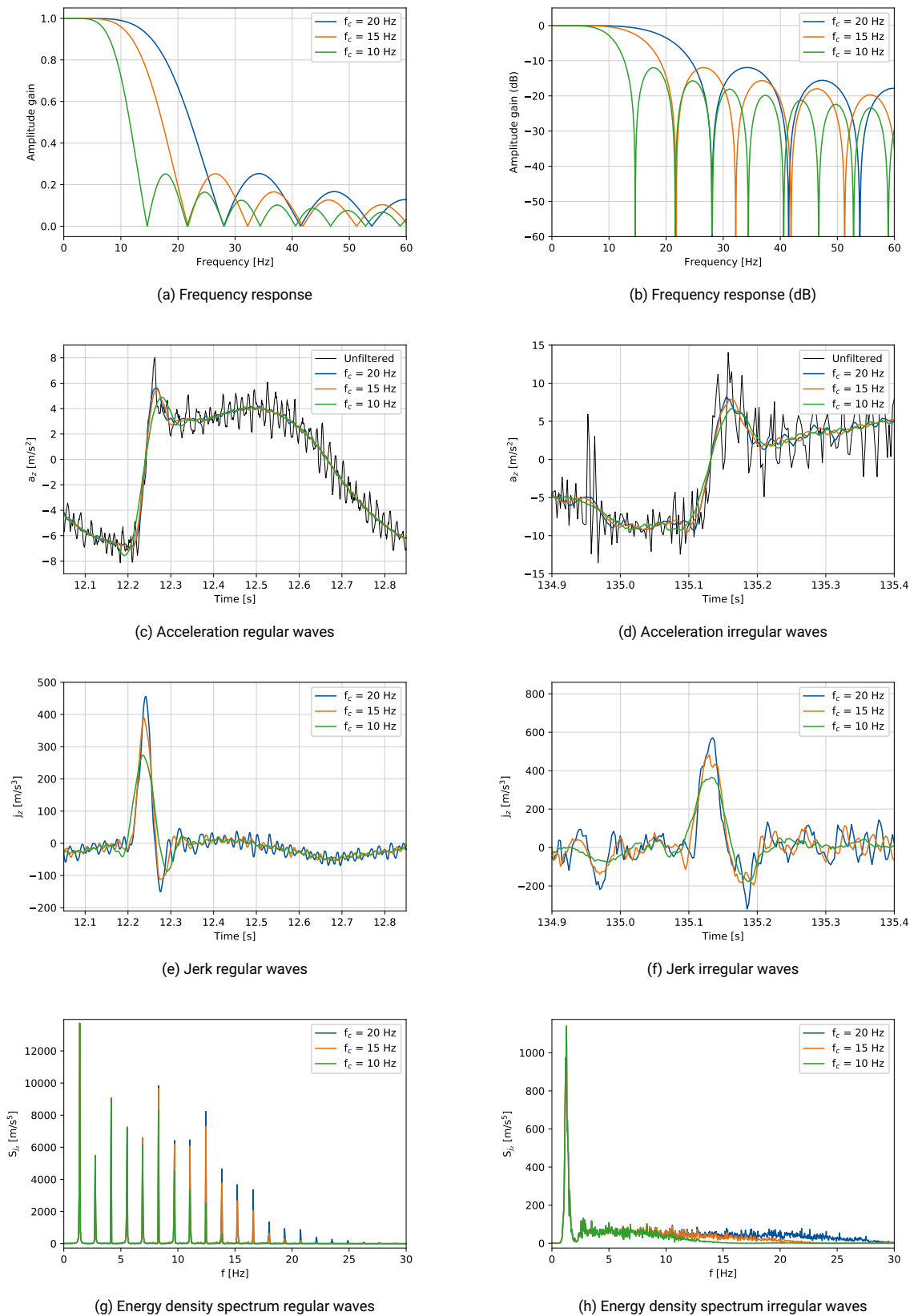


Figure B.18: Comparison Savitzky-Golay filter, 5th order, cut-off frequencies 10 Hz, 15 Hz, 20 Hz

Savitzky-Golay filter, 7th order

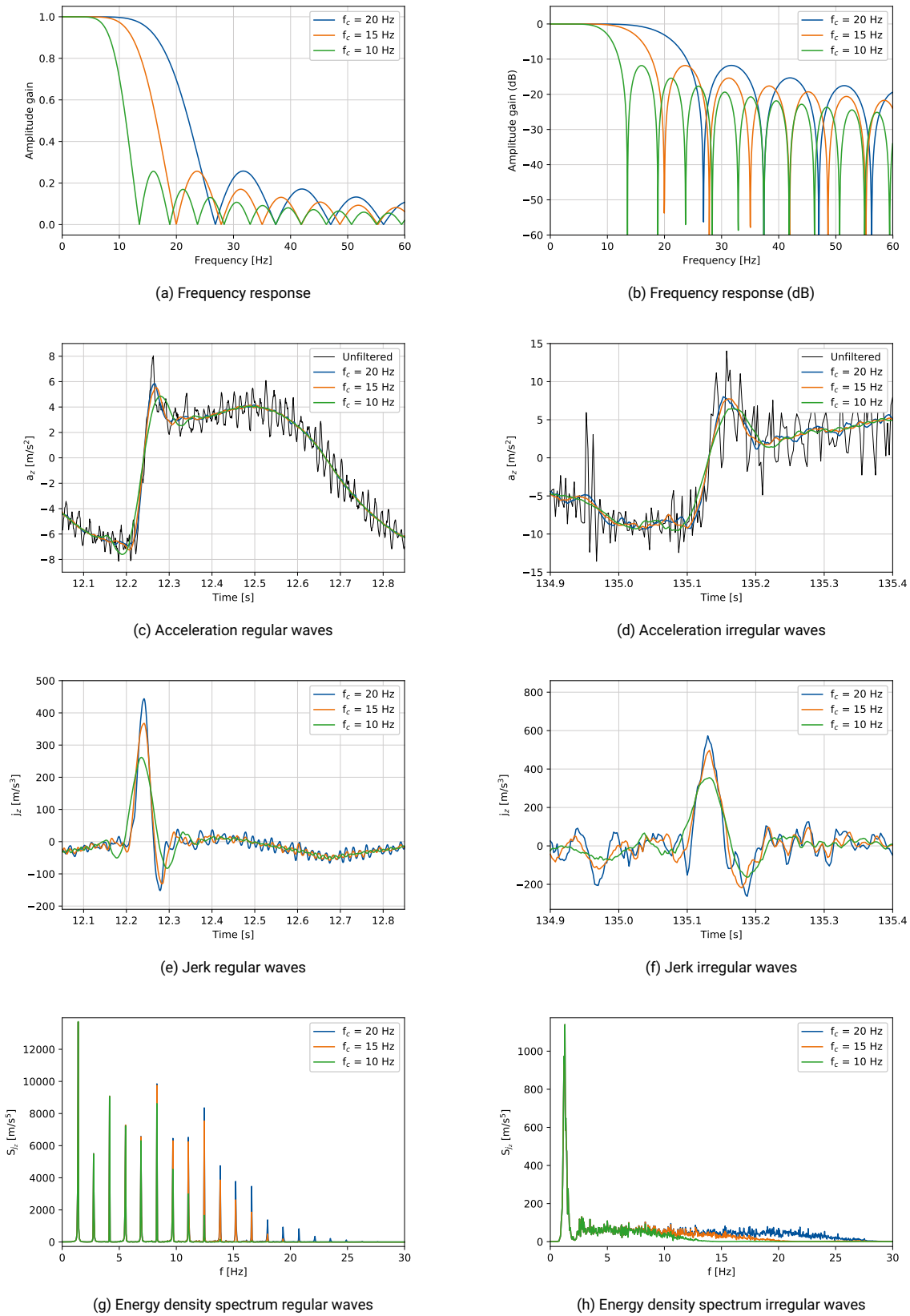


Figure B.19: Comparison Savitzky-Golay filter, 7th order, cut-off frequencies 10 Hz, 15 Hz, 20 Hz

Savitzky-Golay filter, cut-off frequency 10 Hz

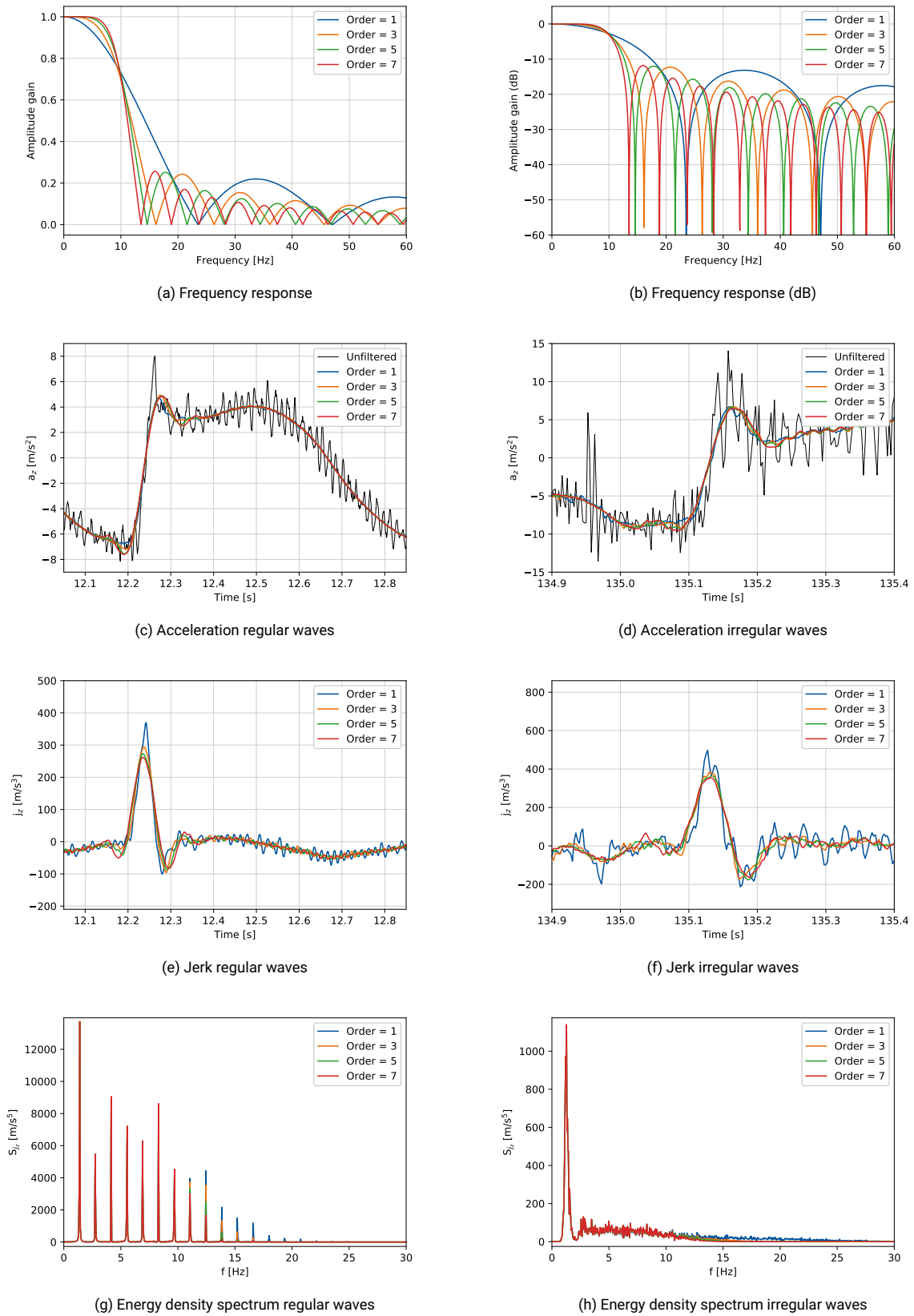


Figure B.20: Comparison Savitzky-Golay filter, 3rd, 5th, 7th order, cut-off frequency 10 Hz

Savitzky-Golay filter, cut-off frequency 15 Hz

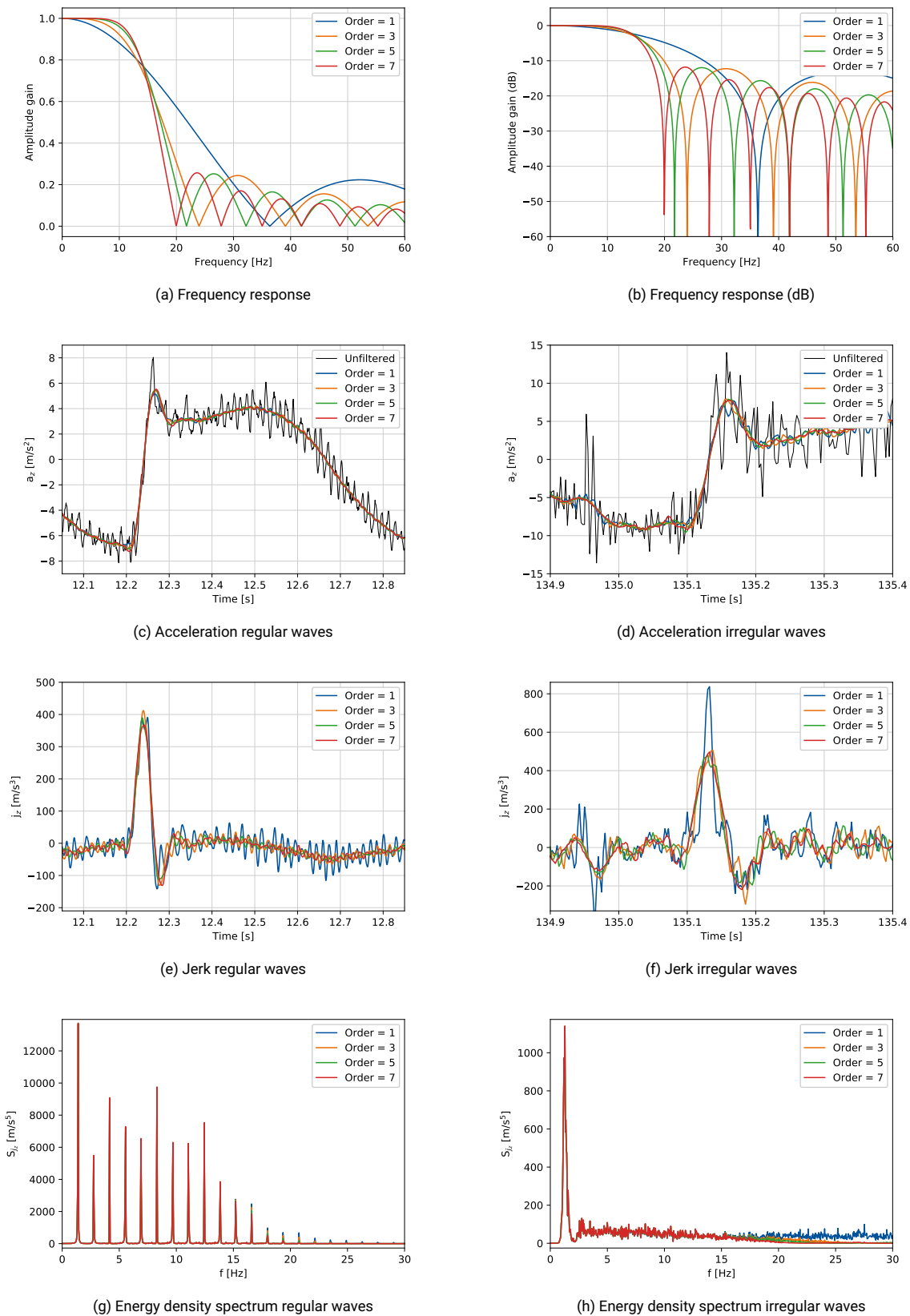


Figure B.21: Comparison Savitzky-Golay filter, 3rd, 5th, 7th order, cut-off frequency 15 Hz

Savitzky-Golay filter, cut-off frequency 20 Hz

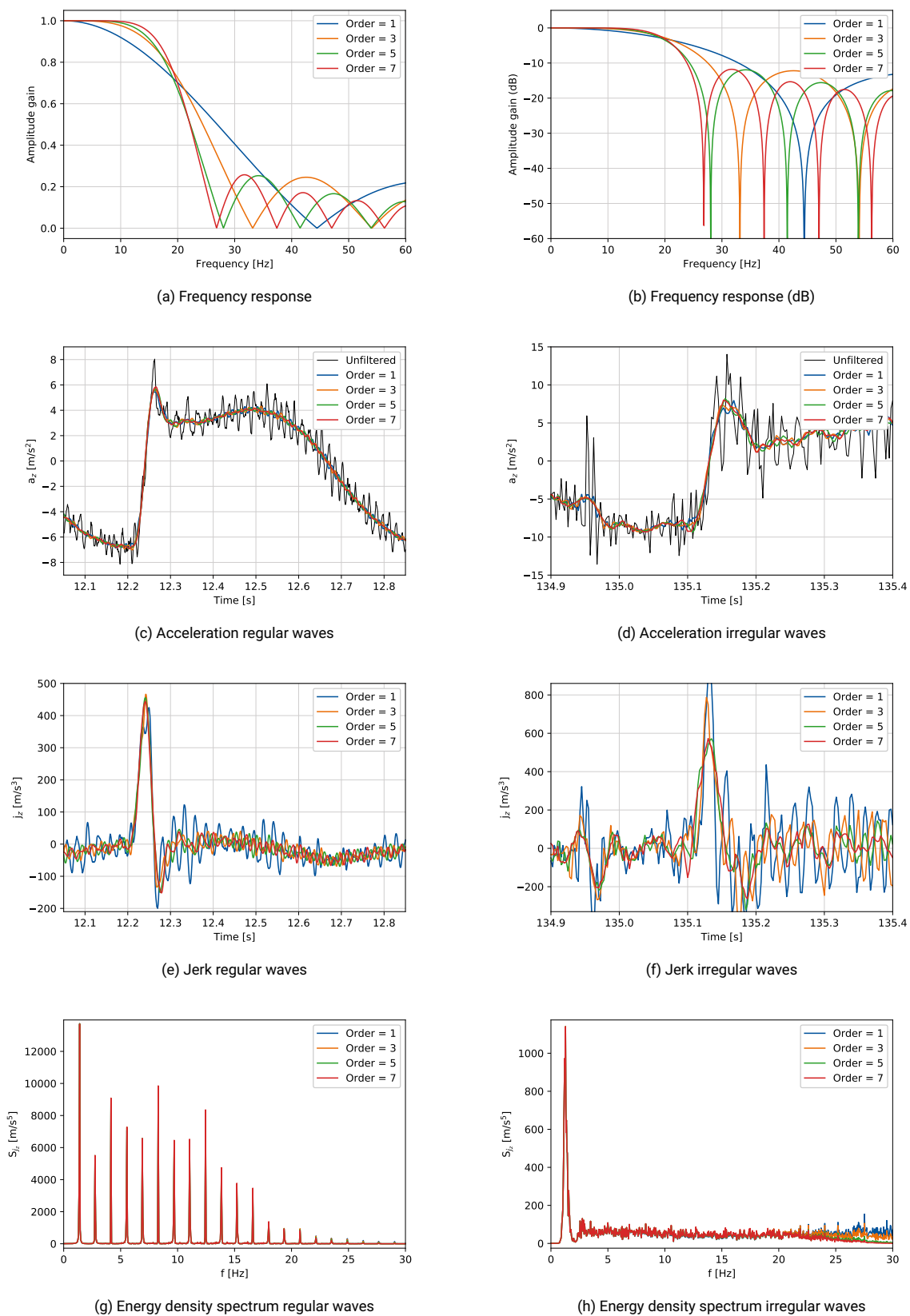


Figure B.22: Comparison Savitzky-Golay filter, 3rd, 5th, 7th order, cut-off frequency 20 Hz

C

Time traces regular waves

In this appendix some time traces of the model tests and calculations are shown to complement the comparisons. The time traces for which heave displacement, velocity, acceleration and jerk are shown can be seen in table C.1. The displacement was also measured, the velocity is obtained from the differentiated displacement signal. In all these time traces it is indicated at what moment the maximum acceleration and maximum jerk occur, to see what the displacement and velocity at that moment is. In the energy density spectra the dotted line indicates the split between first order energy and higher order energy.

Table C.1: Overview of time traces (heave displacement, velocity, acceleration, jerk)

Nr.	Hull [-]	Location [-]	ω [rad/s]	v_s [m/s]	ω_e [rad/s]	κ [-]	ζ_a [mm]	Page
1	ESC	CoG	4.02	2.876	8.76	0.017	32.00	128
2	AXE	CoG	4.02	2.876	8.76	0.017	32.00	129
3	ESC	CoG	4.02	2.876	8.76	0.050	95.00	130
4	AXE	CoG	4.02	2.876	8.76	0.050	95.00	131
5	ESC	Bow	4.02	2.876	8.76	0.017	32.00	132
6	AXE	Bow	4.02	2.876	8.76	0.017	32.00	133
7	ESC	Bow	4.47	2.876	10.33	0.017	26.00	134
8	ESC	Bow	4.47	2.876	10.33	0.033	51.00	135
9	ESC	Bow	4.47	2.876	10.33	0.050	77.00	136
10	AXE	CoG	4.47	2.876	10.33	0.033	51.00	137
11	AXE	CoG	4.02	4.026	10.65	0.033	63.00	138

In table C.2 the time traces for which the heave acceleration and jerk, and pitch acceleration and jerk are plotted can be seen.

Table C.2: Overview of time traces (heave acceleration and jerk, pitch acceleration and jerk)

Nr.	Hull [-]	ω [rad/s]	v_s [m/s]	ω_e [rad/s]	κ [-]	ζ_a [mm]	Page
12	ESC	3.58	2.876	7.34	0.033	80.00	139
13	AXE	3.58	2.876	7.34	0.033	80.00	140

In table C.3 the time traces for which the heave acceleration and jerk, and pitch acceleration and jerk from the RANS CFD calculations and the measurements are plotted can be seen.

Table C.3: Overview of time traces (RANS CFD calculations and measurements)

Nr.	Hull [-]	ω [rad/s]	v_s [m/s]	ω_e [rad/s]	κ [-]	ζ_a [mm]	Page
14	AXE	3.58	2.876	7.34	0.033	80.21	141
15	AXE	4.47	2.876	10.33	0.033	51.33	142
16	AXE	5.37	2.876	13.82	0.033	35.75	143

Time trace 1: ESC, CoG, $v_e = 2.876 \text{ m/s}$, $\omega_e = 8.76 \text{ rad/s}$, $\kappa = 0.017$

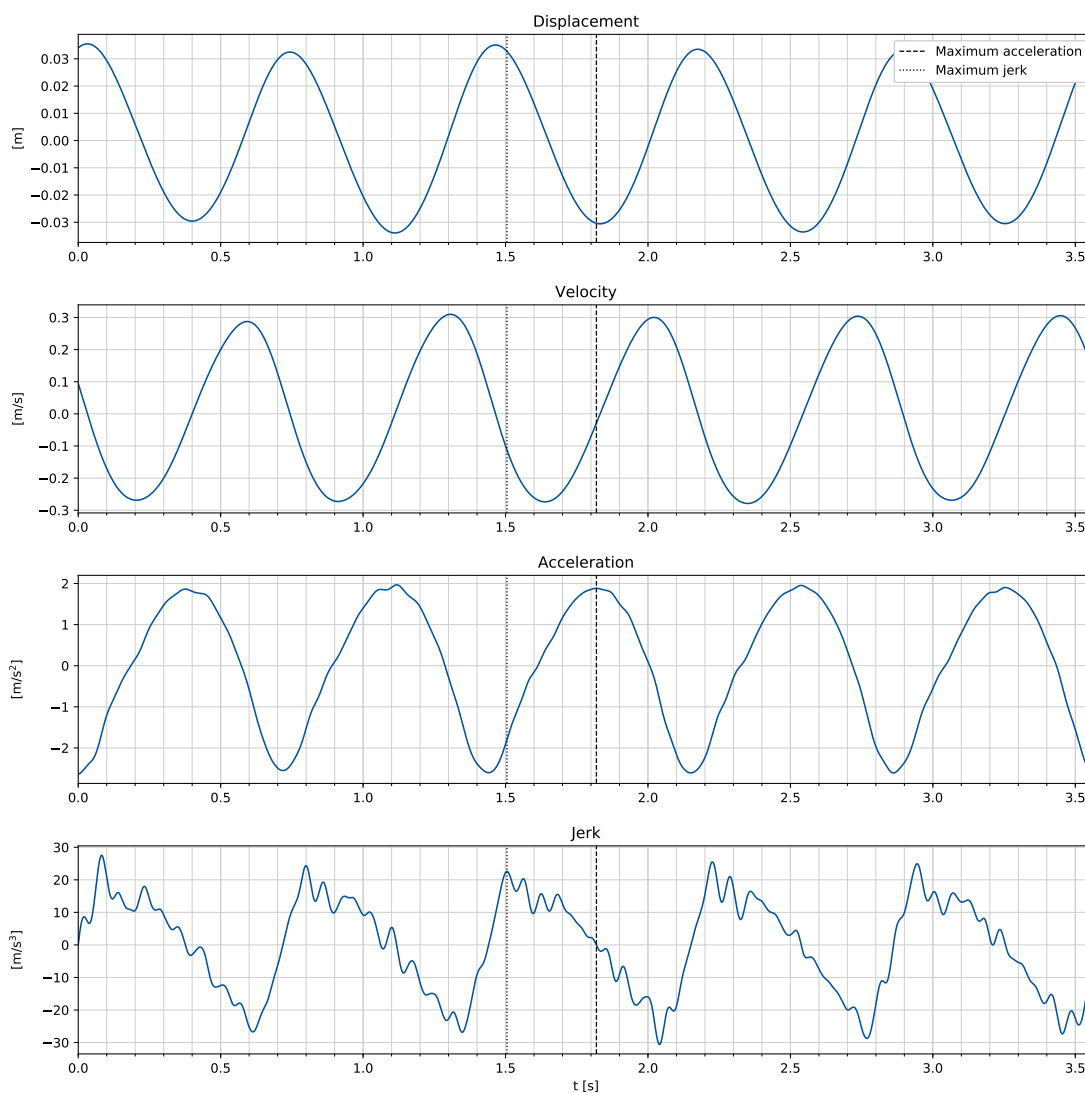


Figure C.1: Time trace 1: heave displacement, velocity, acceleration and jerk

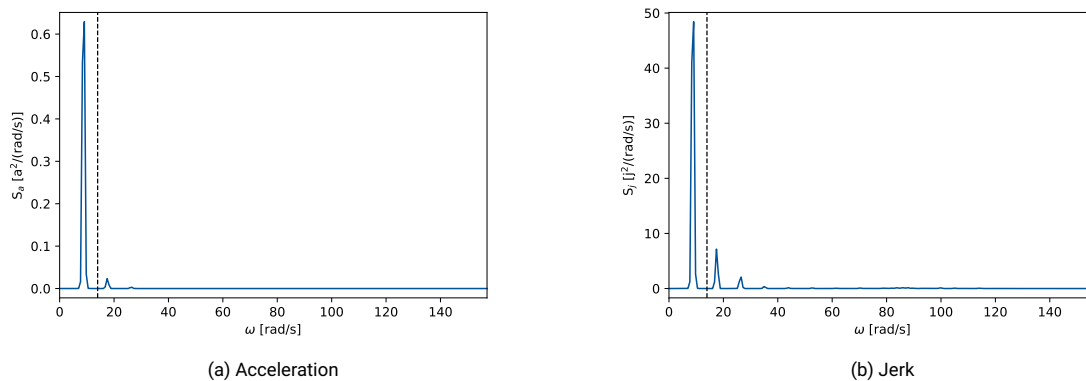


Figure C.2: Energy density spectra of time trace 1

Time trace 2: AXE, CoG, $v_s = 2.876 \text{ m/s}$, $\omega_e = 8.76 \text{ rad/s}$, $\kappa = 0.017$

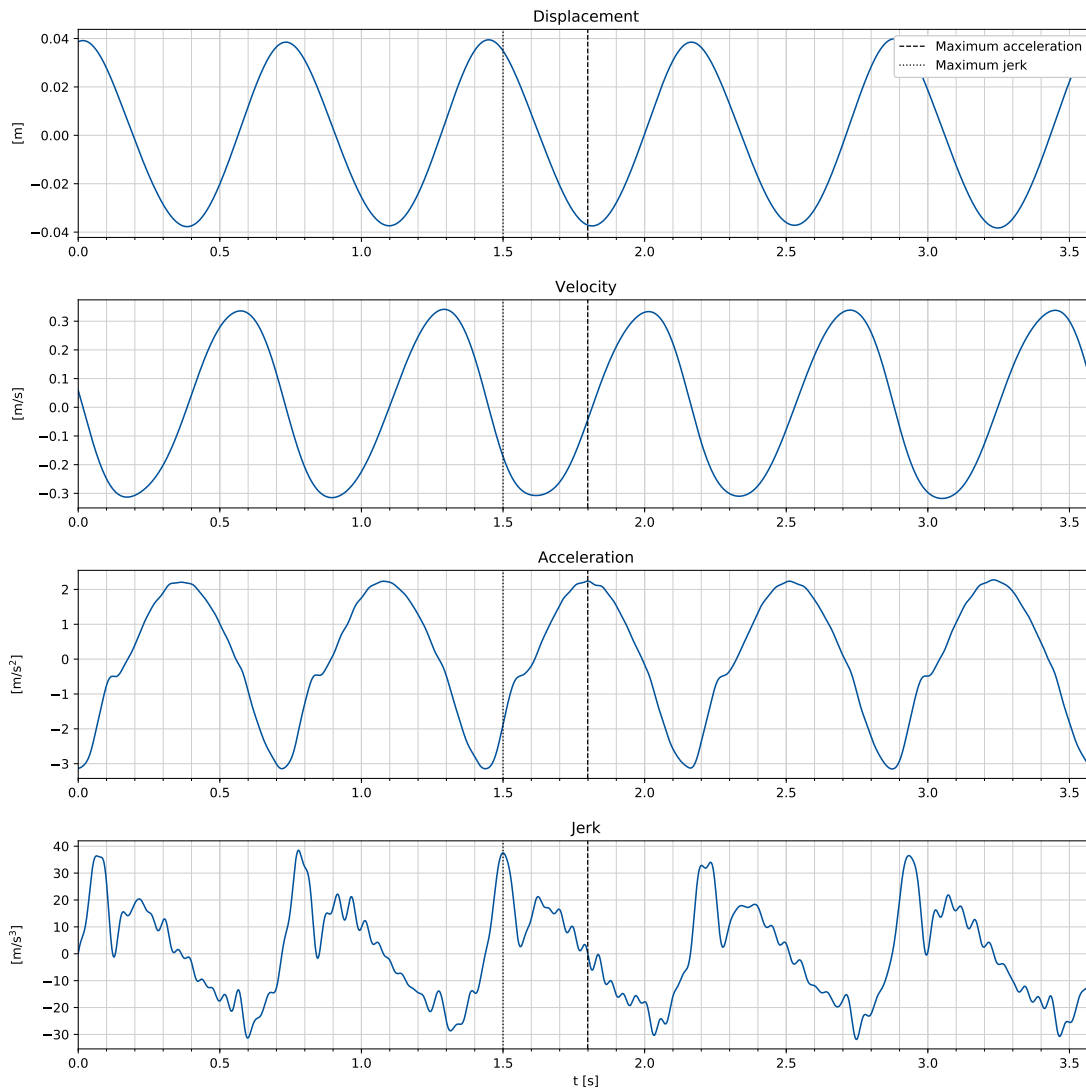


Figure C.3: Time trace 2: vertical displacement, velocity, acceleration and jerk

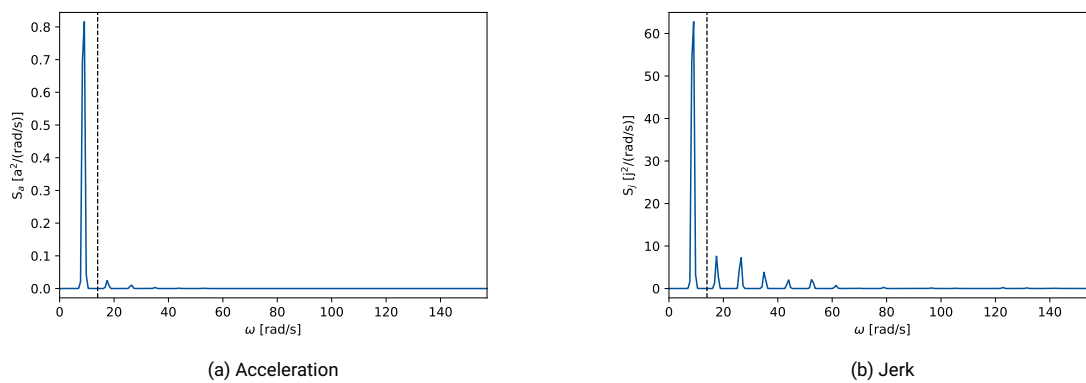


Figure C.4: Energy density spectra of time trace 2

Time trace 3: ESC, CoG, $v_s = 2.876 \text{ m/s}$, $\omega_e = 8.76 \text{ rad/s}$, $\kappa = 0.050$

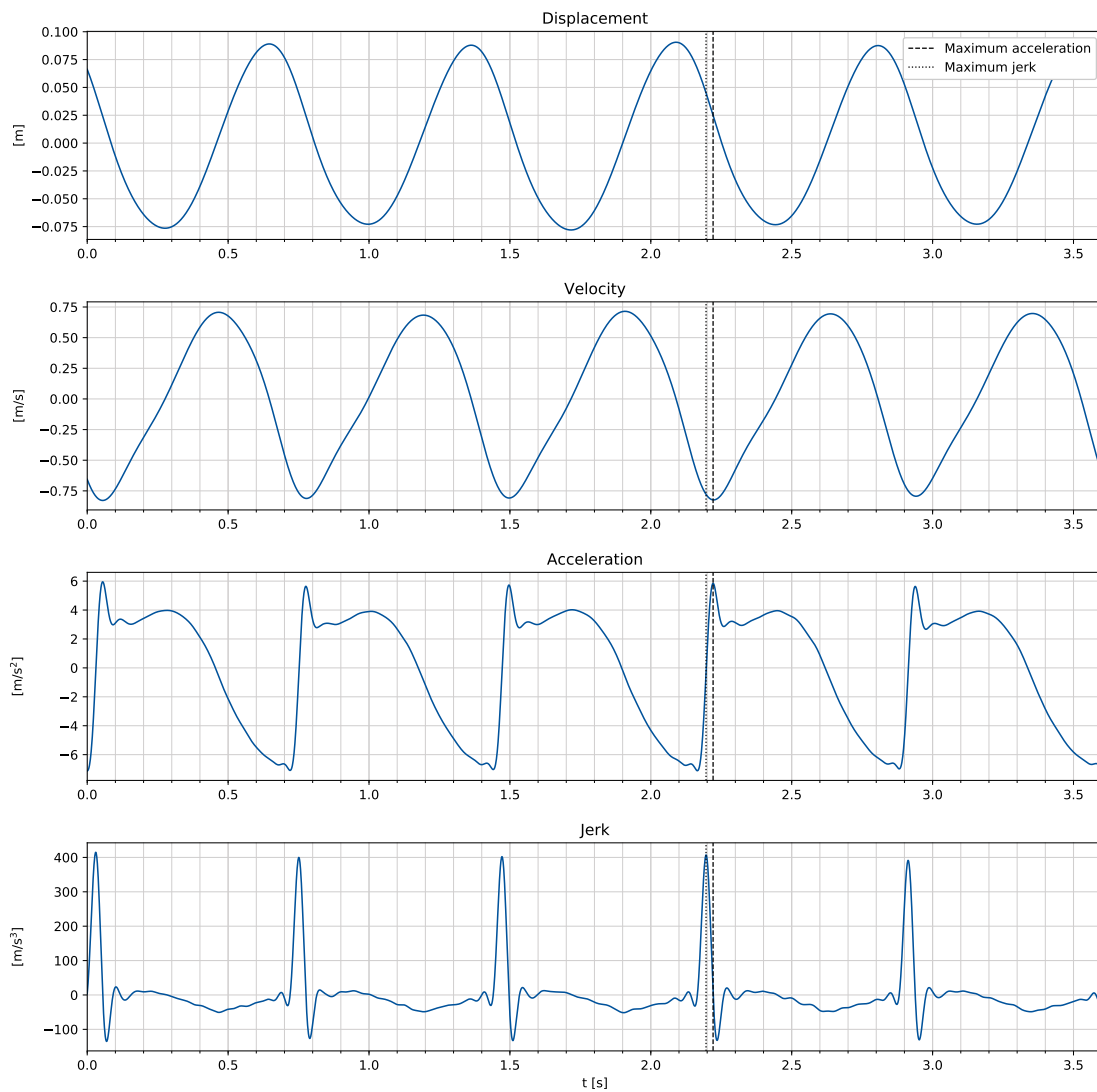


Figure C.5: Time trace 3: vertical displacement, velocity, acceleration and jerk

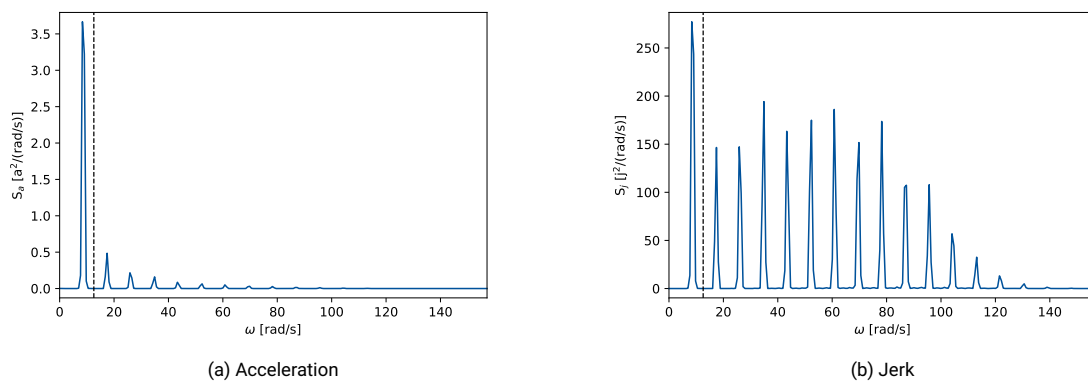


Figure C.6: Energy density spectra of time trace 3

Time trace 4: AXE, CoG, $v_s = 2.876$ m/s, $\omega_e = 8.76$ rad/s, $\kappa = 0.050$

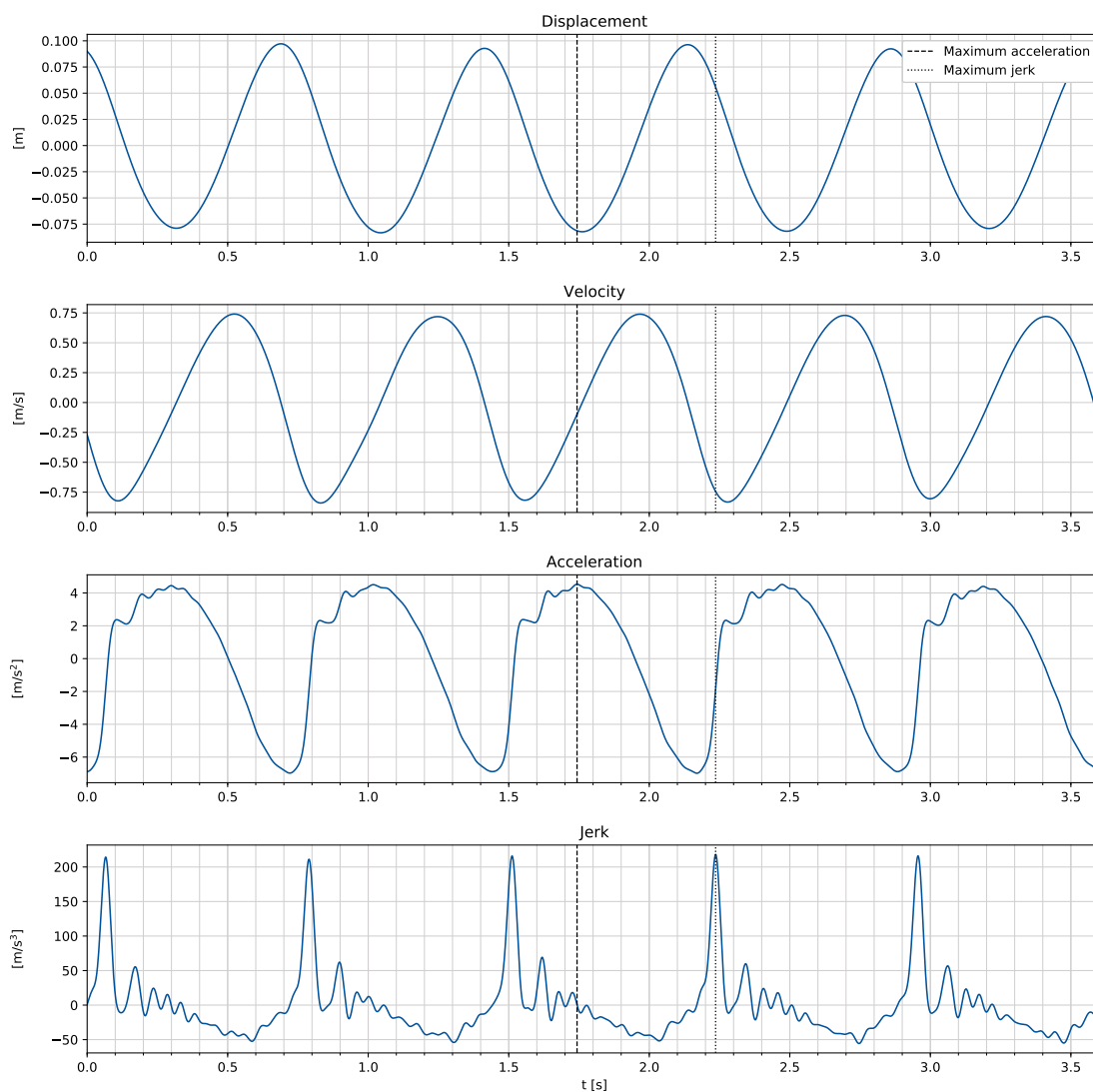


Figure C.7: Time trace 4: vertical displacement, velocity, acceleration and jerk

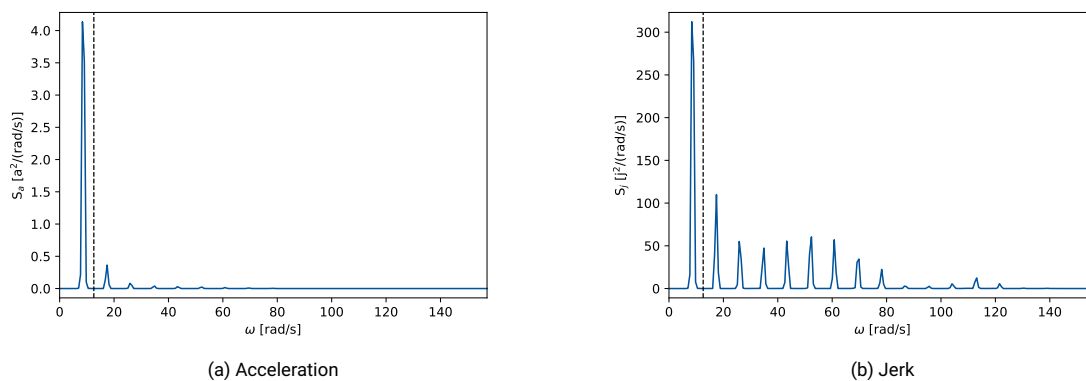


Figure C.8: Energy density spectra of time trace 4

Time trace 5: ESC, bow, $v_e = 2.876$ m/s, $\omega_e = 8.76$ rad/s, $\kappa = 0.017$

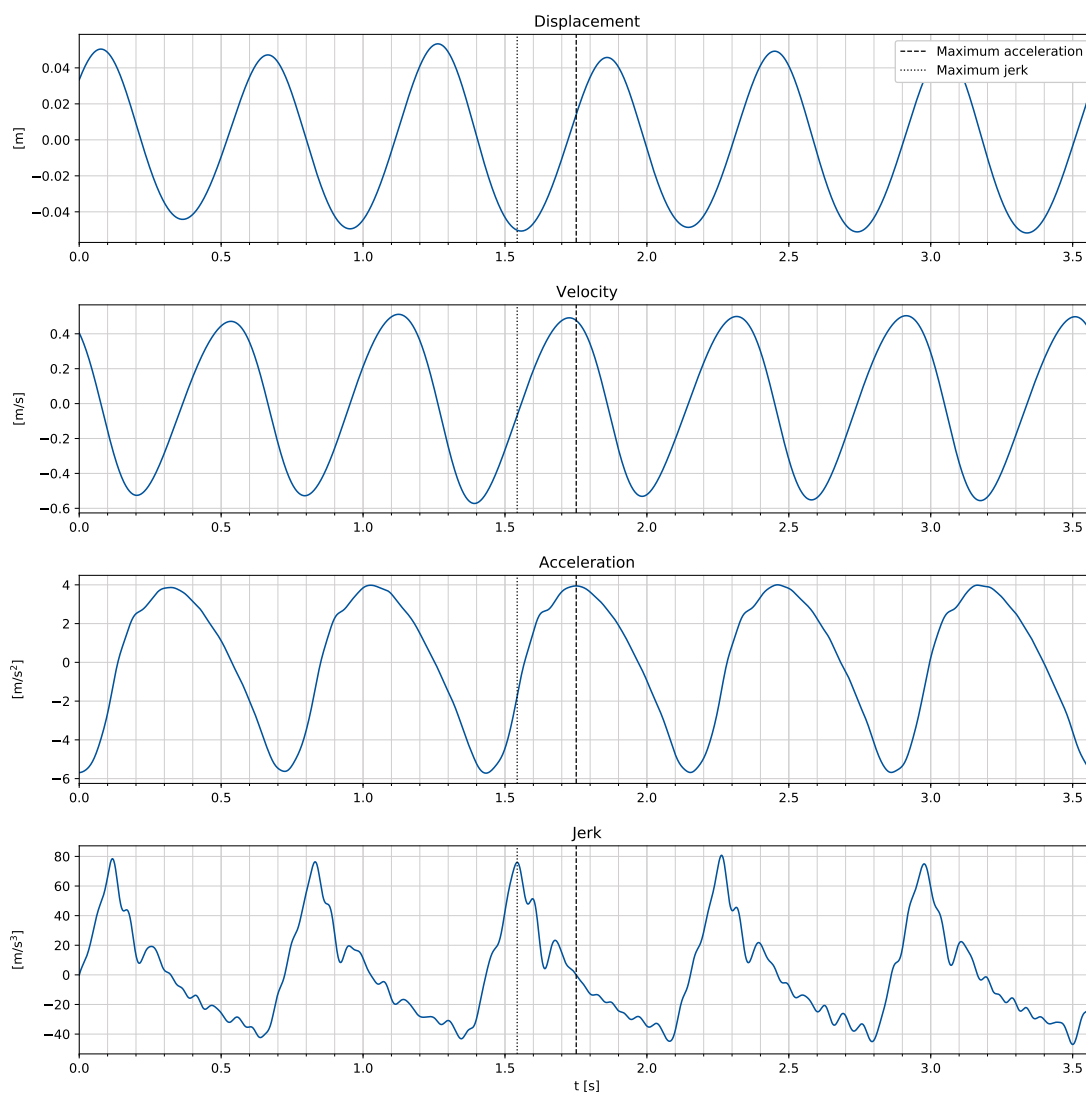


Figure C.9: Time trace 5: vertical displacement, velocity, acceleration and jerk

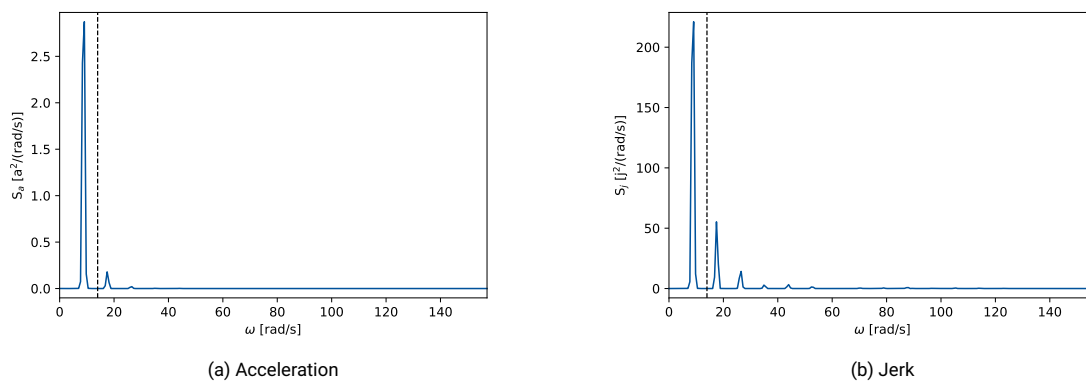


Figure C.10: Energy density spectra of time trace 5

Time trace 6: AXE, bow, $v_s = 2.876$ m/s, $\omega_e = 8.76$ rad/s, $\kappa = 0.017$

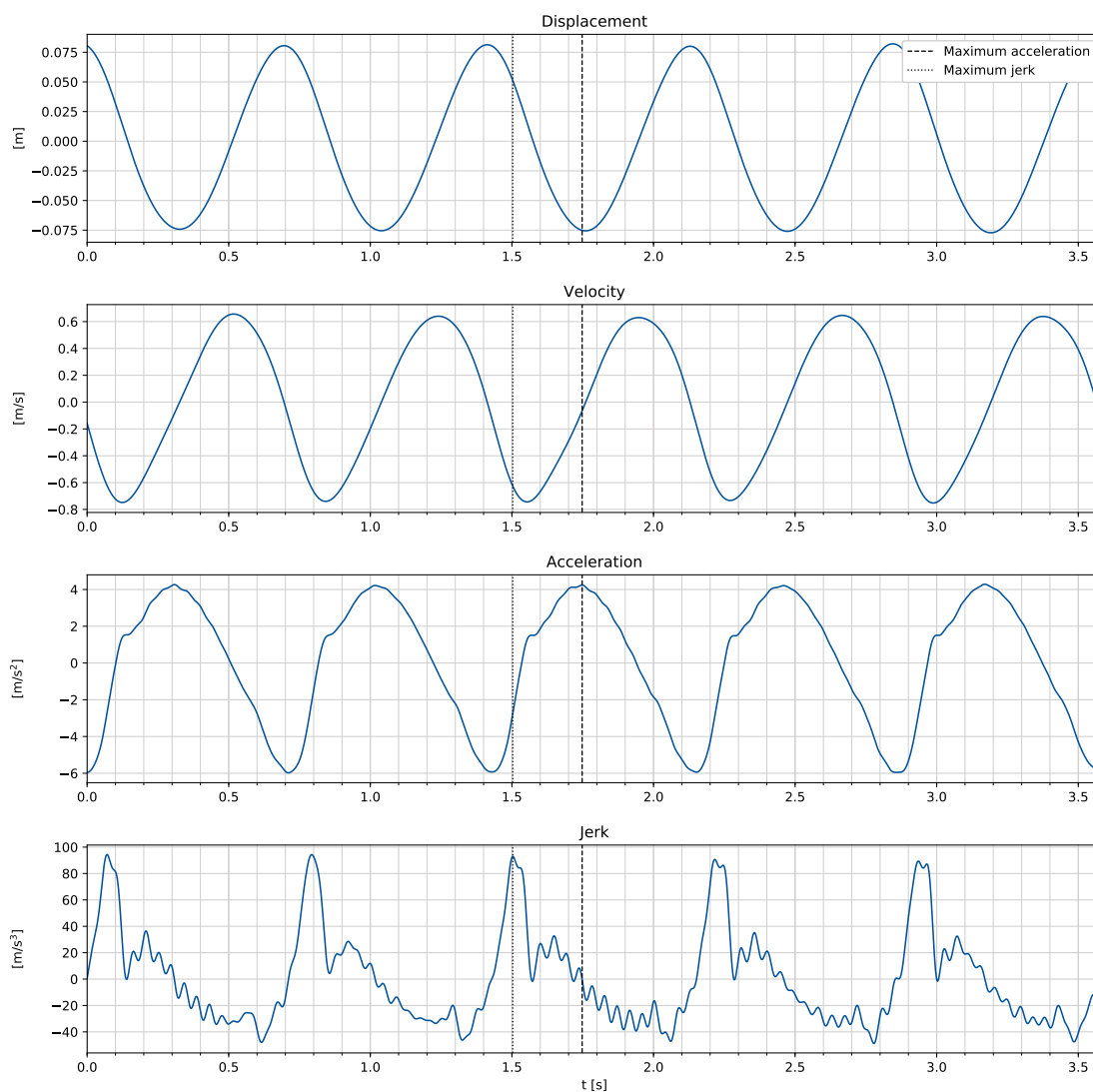


Figure C.11: Time trace 6: vertical displacement, velocity, acceleration and jerk

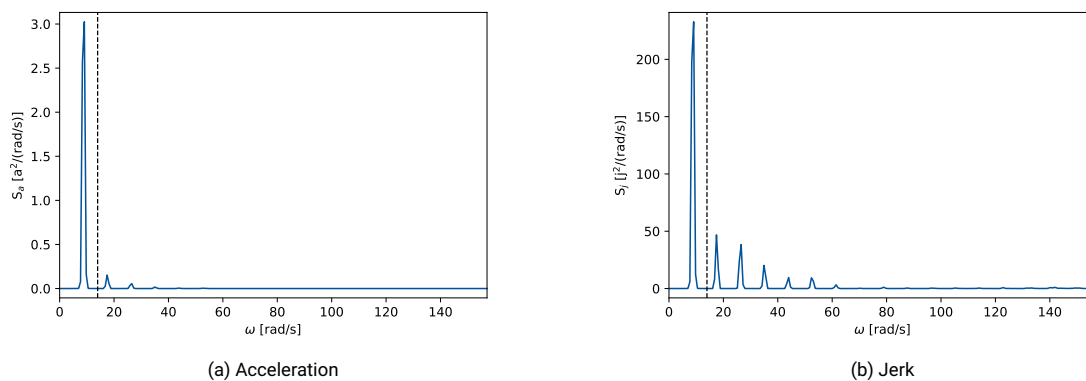


Figure C.12: Energy density spectra of time trace 6

Time trace 7: ESC, bow, $v_s = 2.876$ m/s, $\omega_e = 10.33$ rad/s, $\kappa = 0.017$

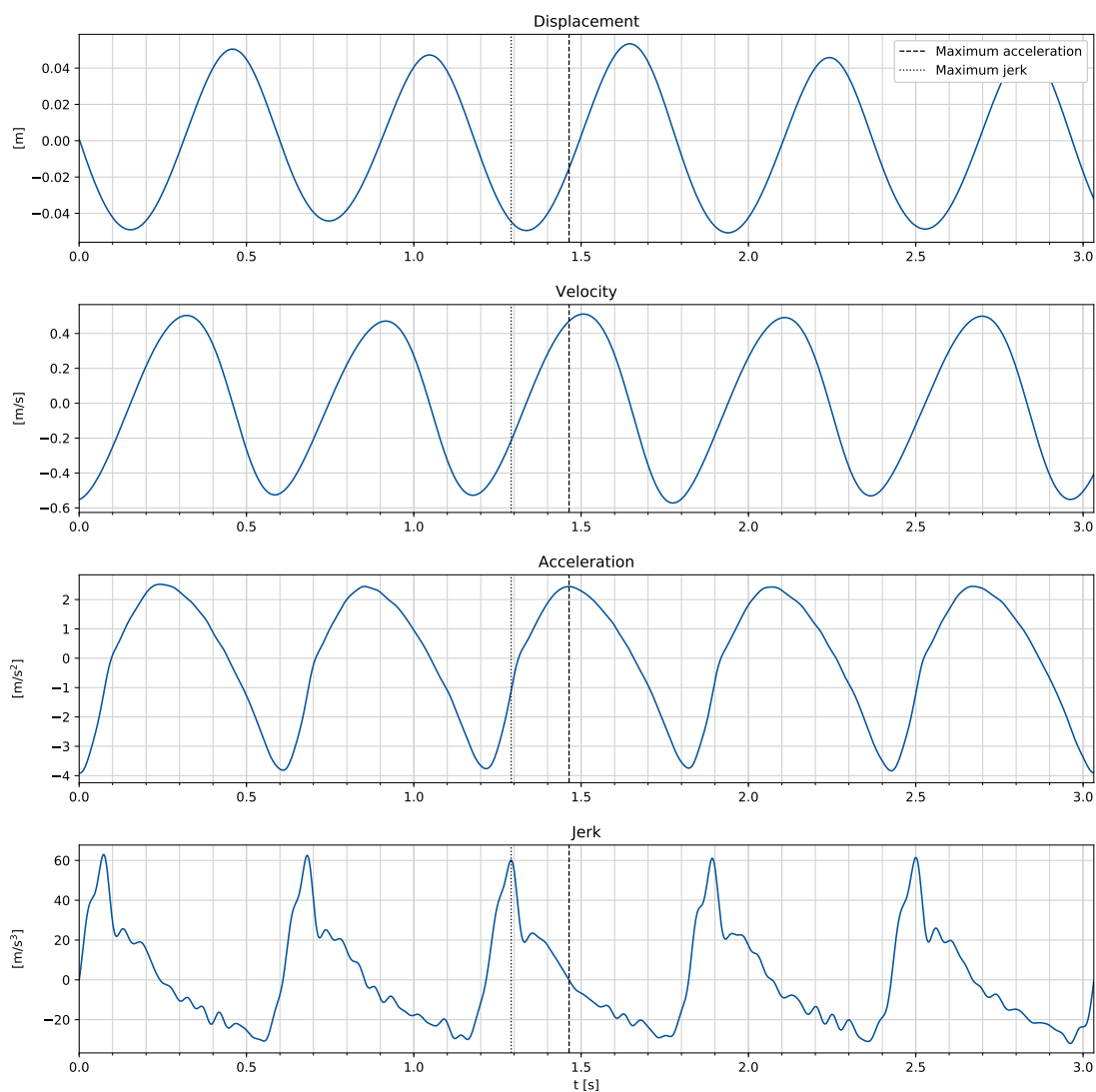


Figure C.13: Time trace 7: vertical displacement, velocity, acceleration and jerk

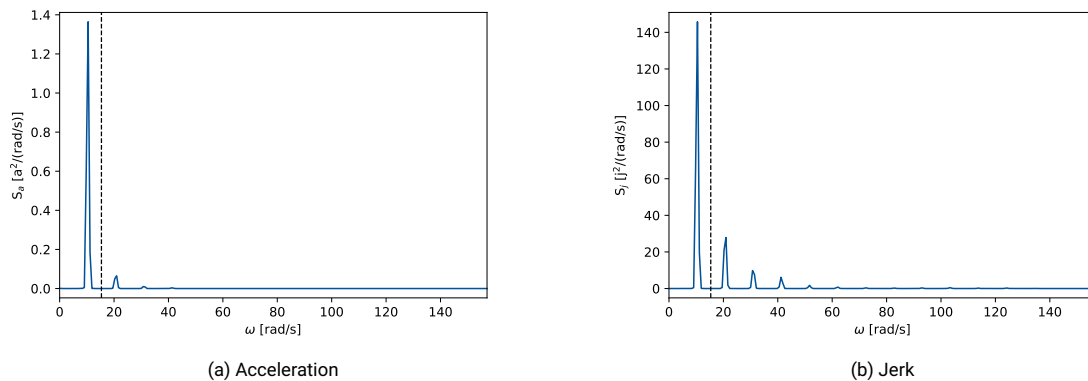


Figure C.14: Energy density spectra of time trace 7

Time trace 8: ESC, bow, $v_e = 2.876$ m/s, $\omega_e = 10.33$ rad/s, $\kappa = 0.033$

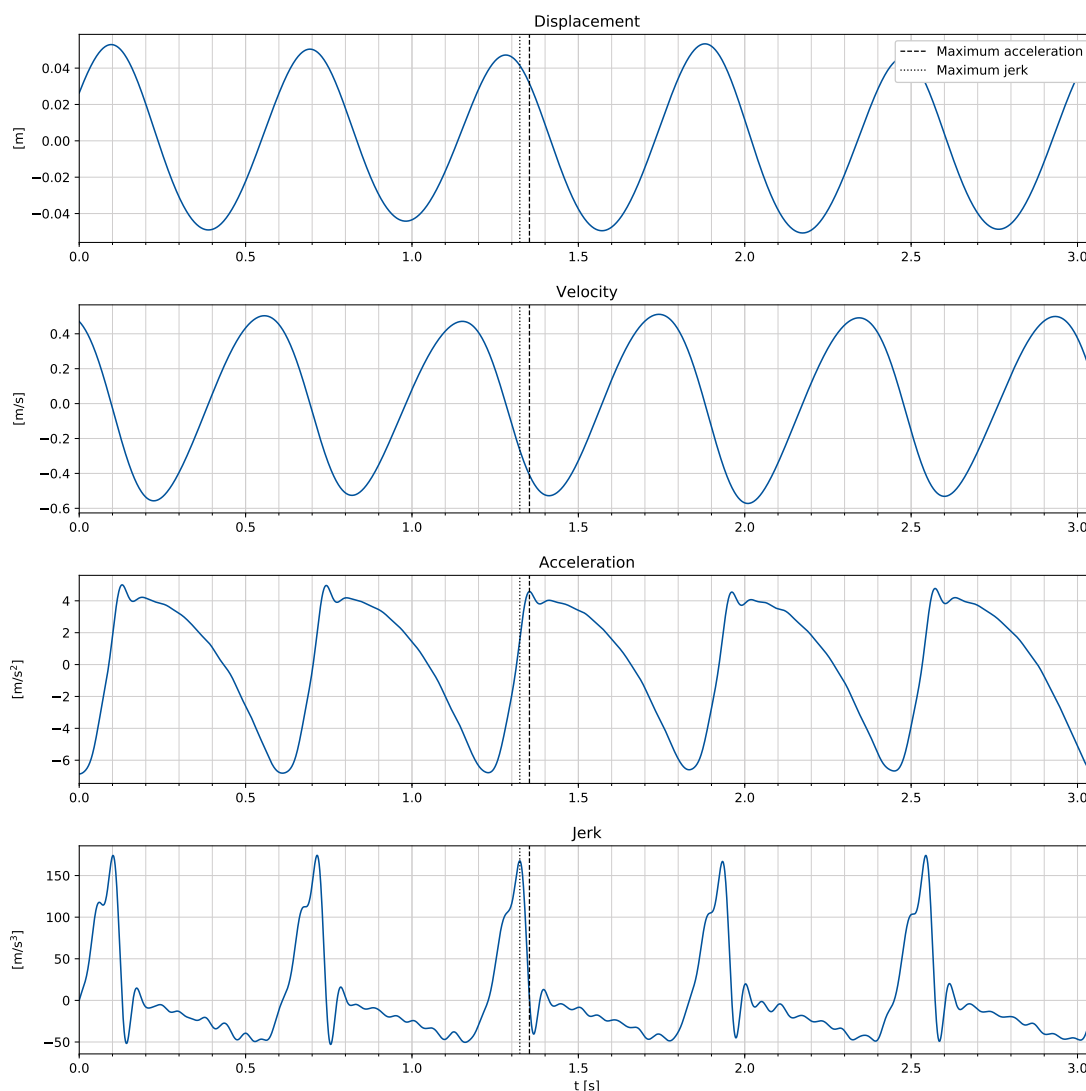


Figure C.15: Time trace 8: vertical displacement, velocity, acceleration and jerk

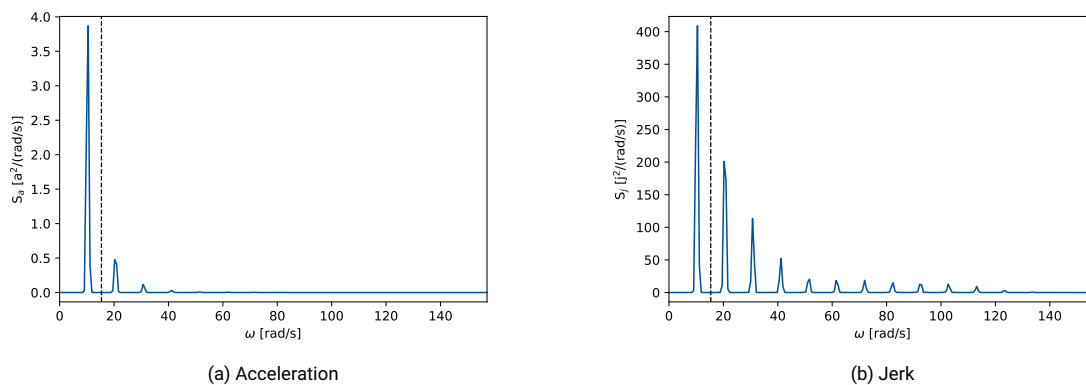


Figure C.16: Energy density spectra of time trace 8

Time trace 9: ESC, bow, $v_e = 2.876$ m/s, $\omega_e = 10.33$ rad/s, $\kappa = 0.050$

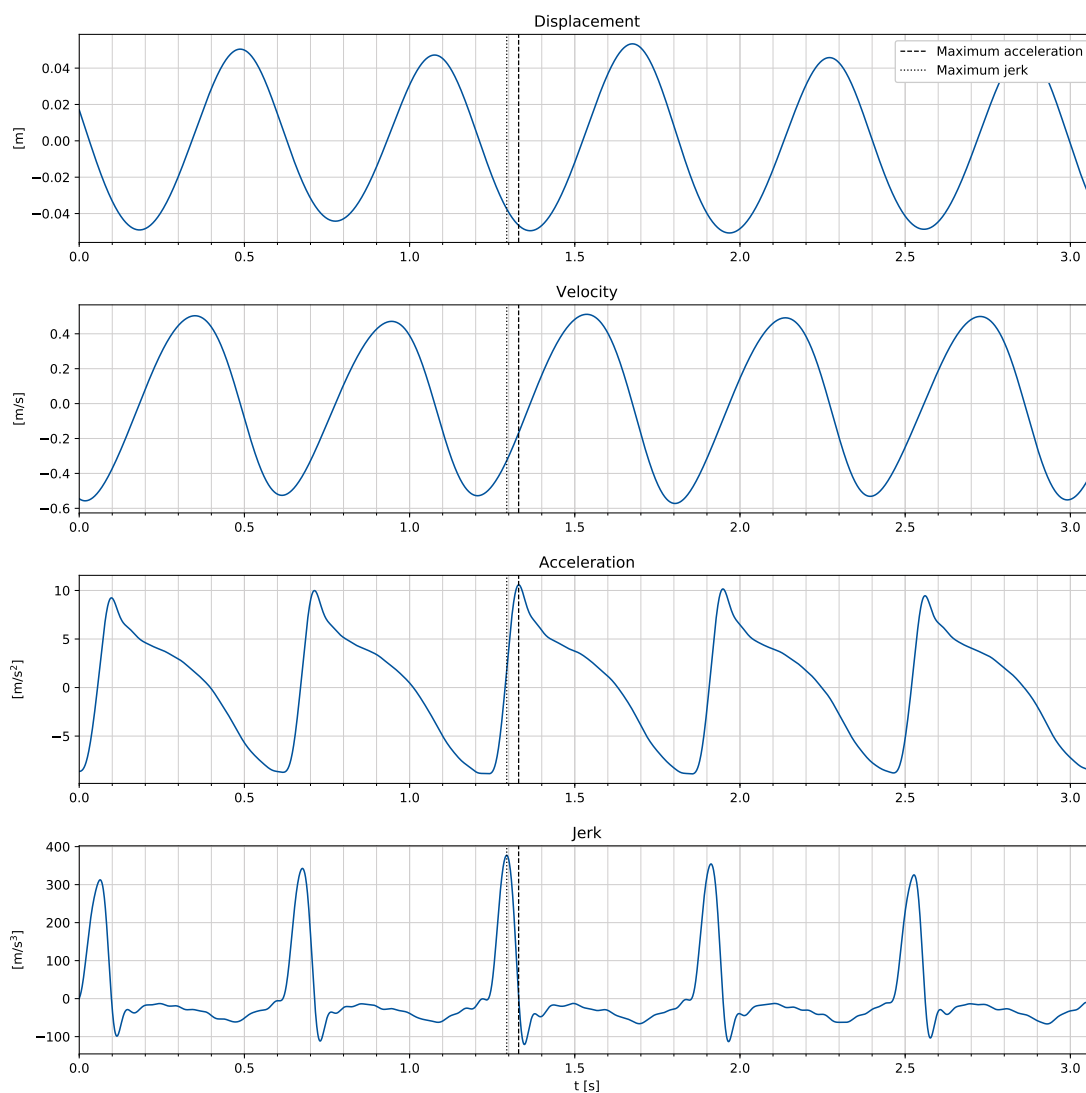


Figure C.17: Time trace 9: vertical displacement, velocity, acceleration and jerk

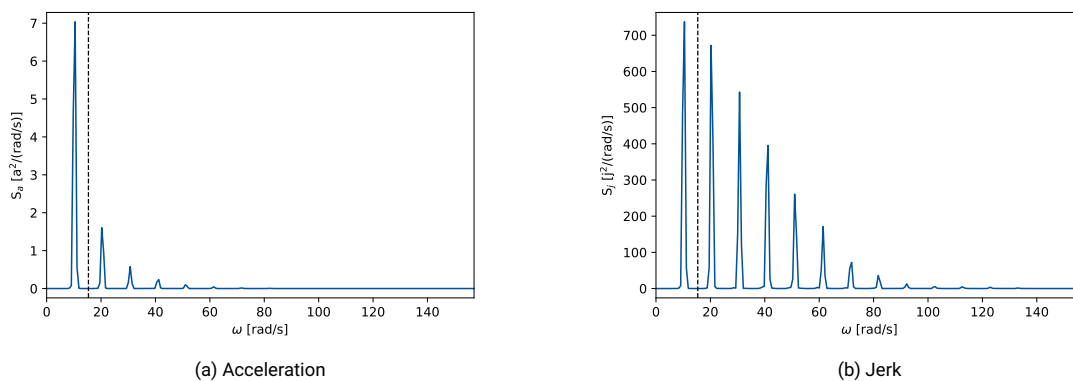


Figure C.18: Energy density spectra of time trace 9

Time trace 10: AXE, CoG, $v_s = 2.876$ m/s, $\omega_e = 10.33$ rad/s, $\kappa = 0.033$

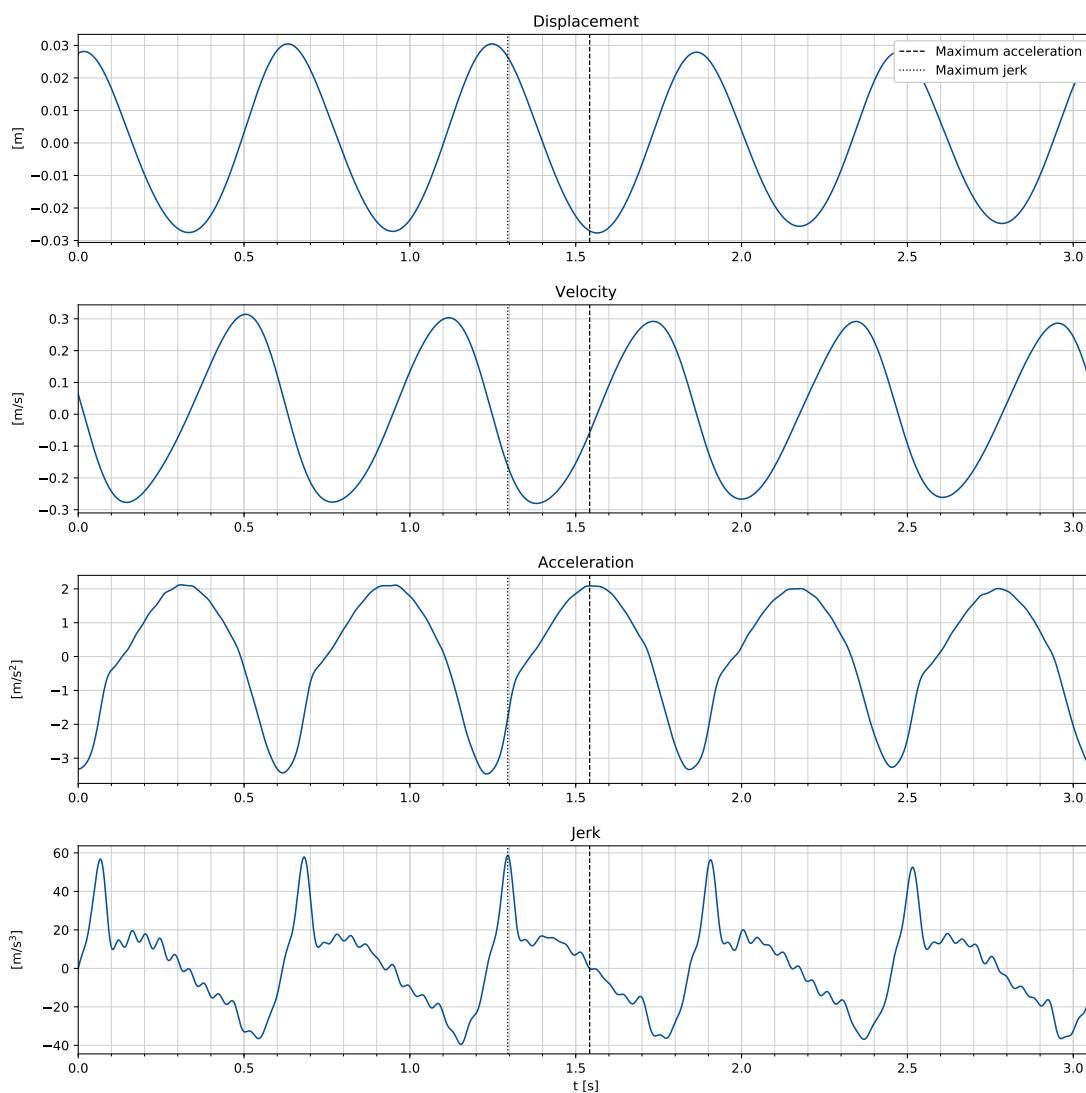


Figure C.19: Time trace 10: vertical displacement, velocity, acceleration and jerk

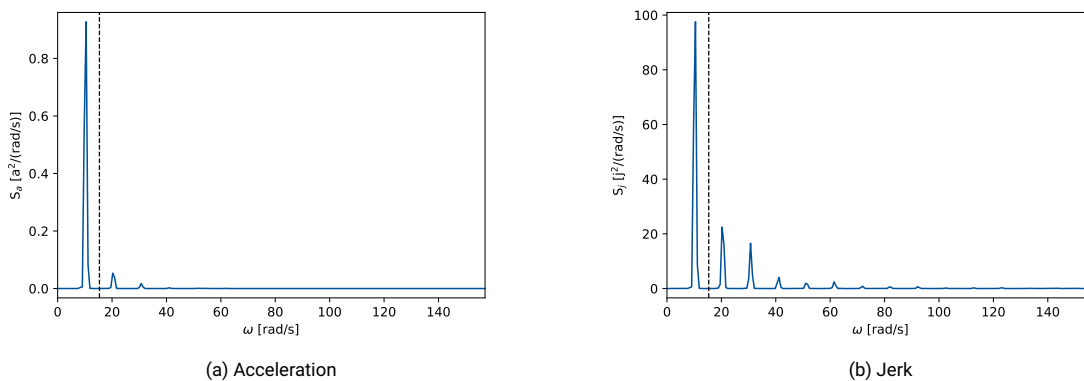


Figure C.20: Energy density spectra of time trace 10

Time trace 11: AXE, CoG, $v_s = 4.026$ m/s, $\omega_e = 10.65$ rad/s, $\kappa = 0.033$

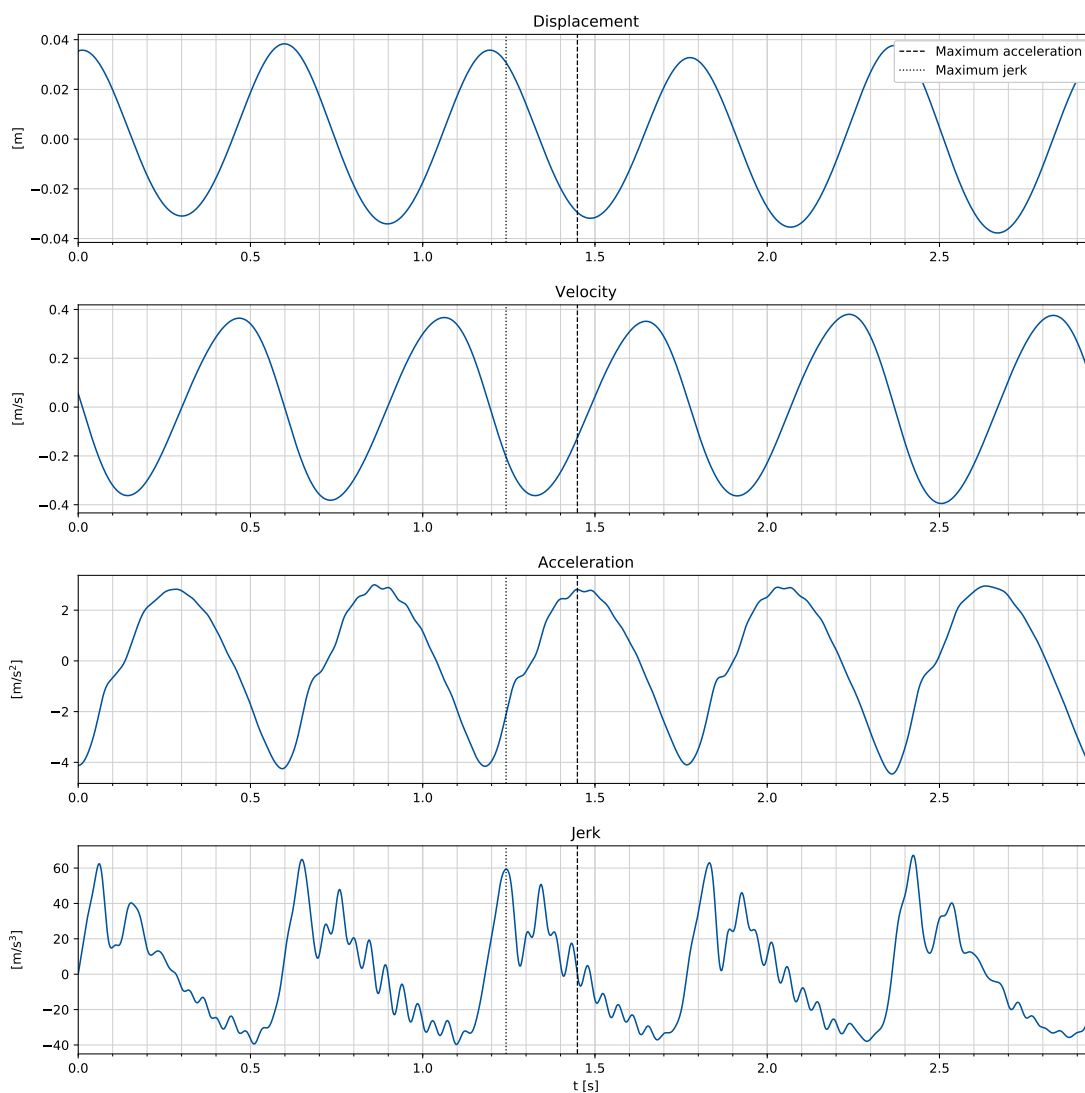


Figure C.21: Time trace 11: vertical displacement, velocity, acceleration and jerk

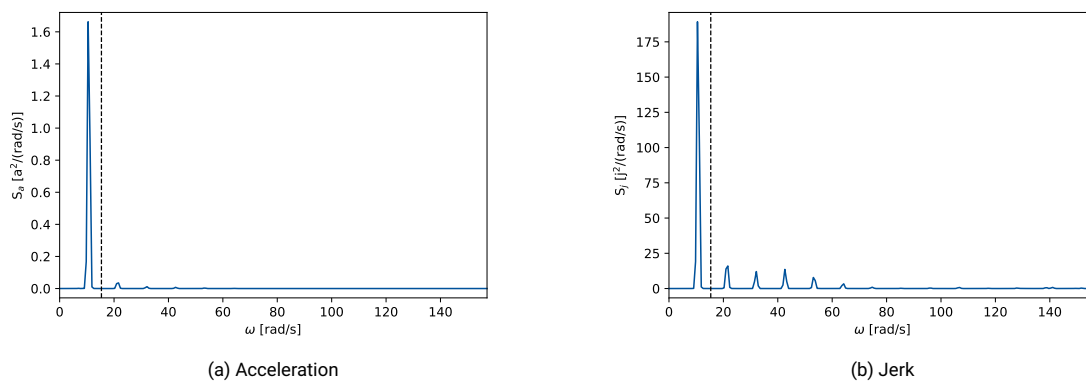


Figure C.22: Energy density spectra of time trace 11

Time trace 12: ESC, $v_s = 2.876$ m/s, $\omega_e = 7.34$ rad/s, $\kappa = 0.033$

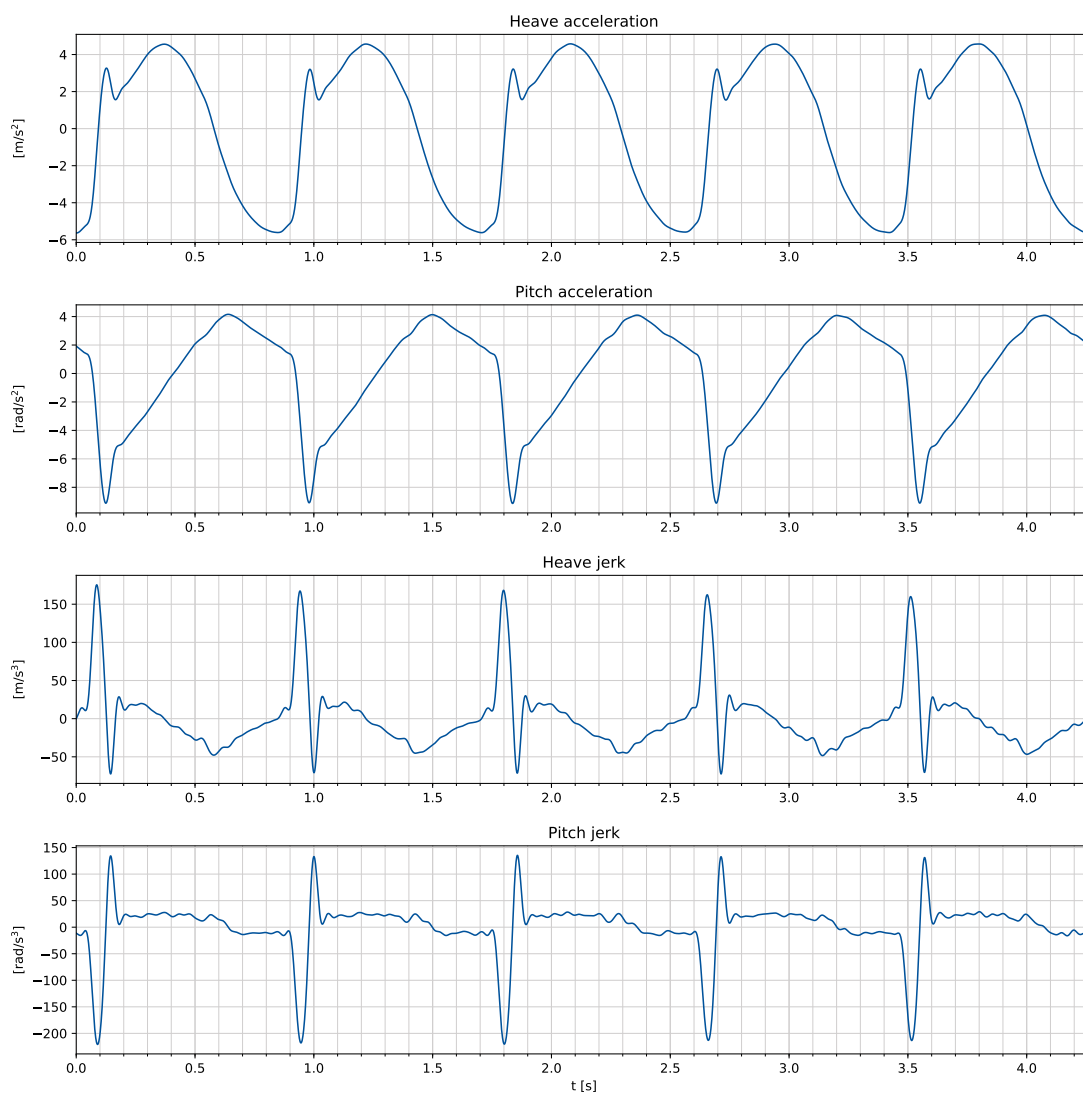


Figure C.23: Time trace 12: heave acceleration and jerk, pitch acceleration and jerk

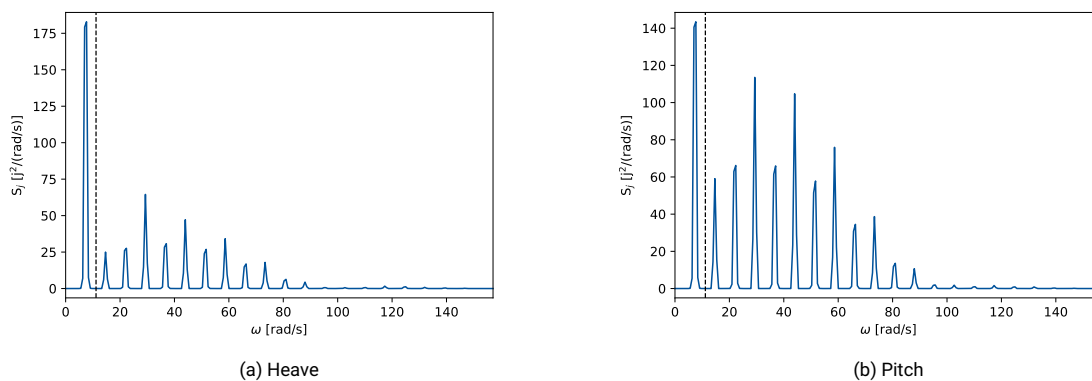


Figure C.24: Energy density spectra jerk of time trace 12

Time trace 13: AXE, $v_s = 2.876$ m/s, $\omega_e = 7.34$ rad/s, $\kappa = 0.033$

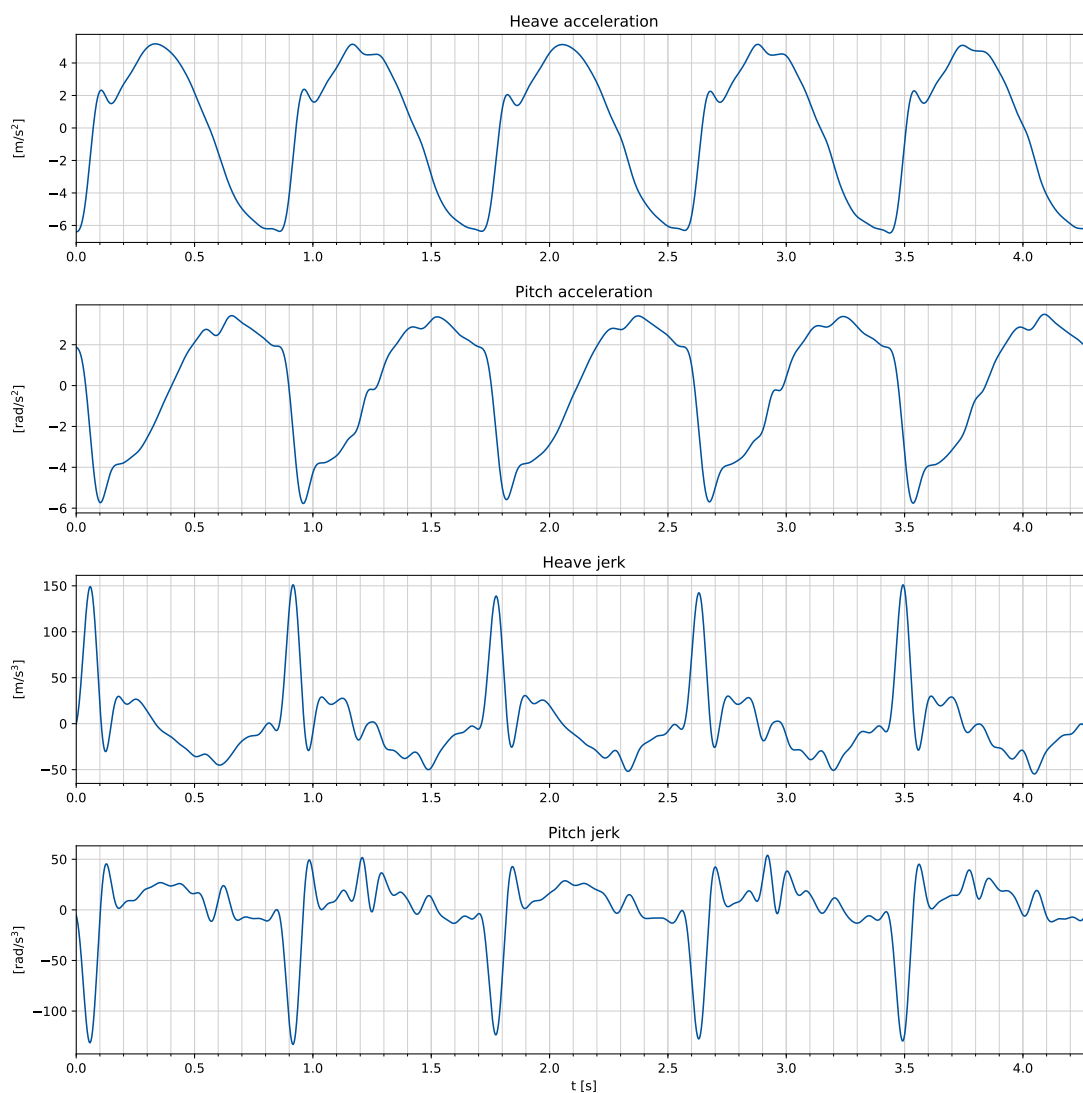


Figure C.25: Time trace 13: heave acceleration and jerk, pitch acceleration and jerk

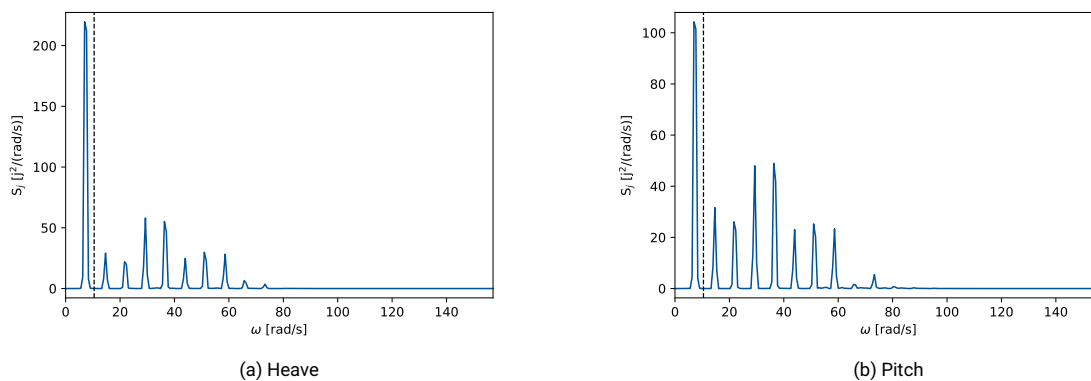


Figure C.26: Energy density spectra jerk of time trace 13

Time trace 14: AXE, $v_s = 2.876$ m/s, $\omega_e = 7.34$ rad/s, $\kappa = 0.033$

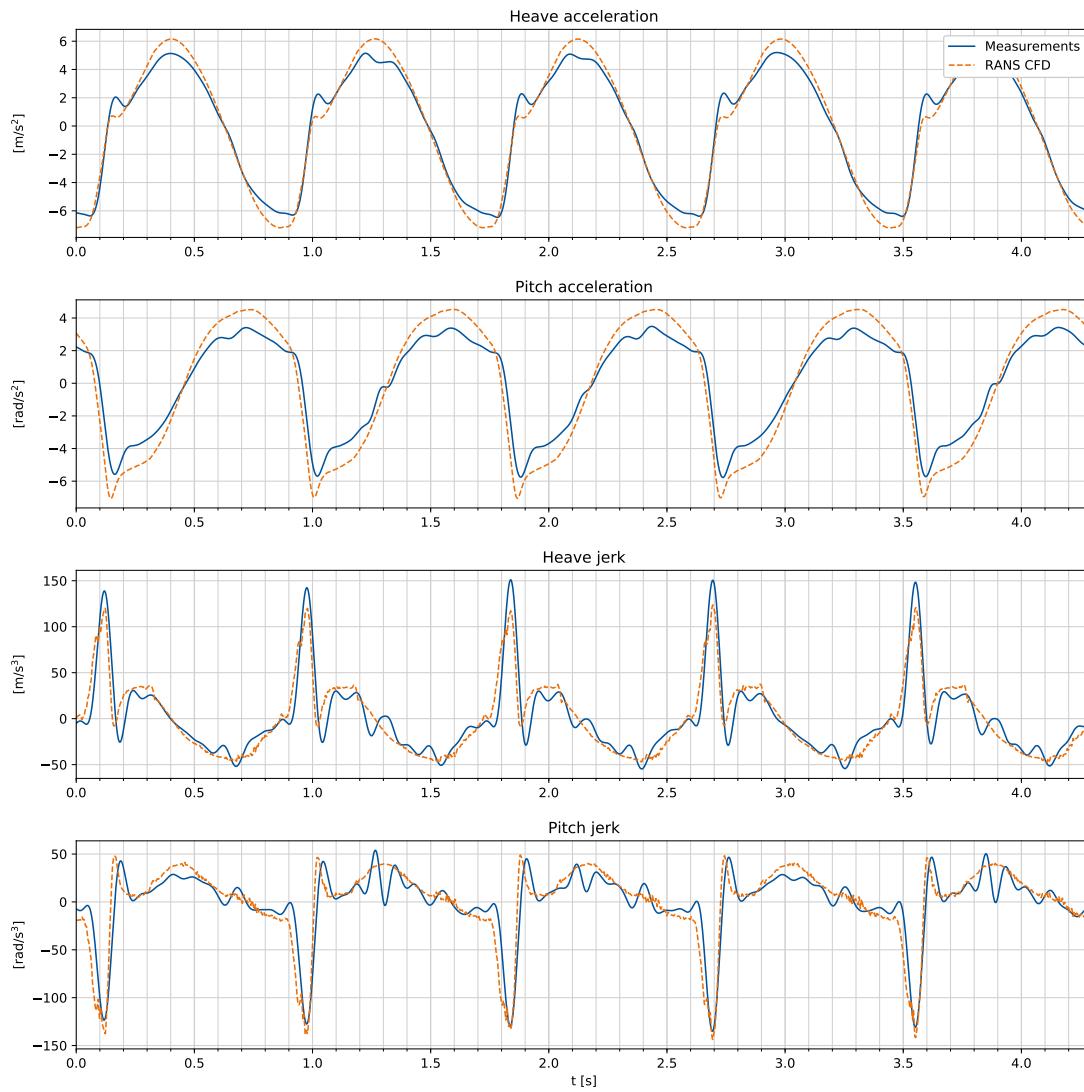


Figure C.27: Time trace 14: RANS CFD calculations and measurements

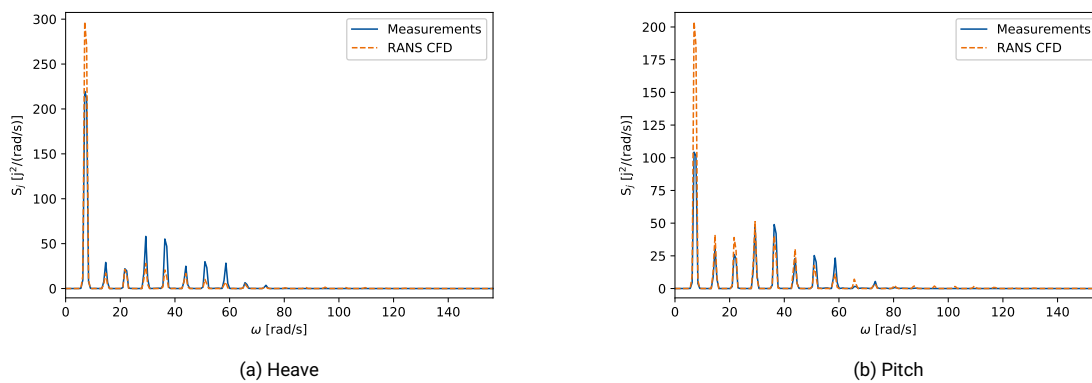


Figure C.28: Energy density spectra jerk of time trace 14

Time trace 15: AXE, $v_e = 2.876$ m/s, $\omega_e = 10.33$ rad/s, $\kappa = 0.033$

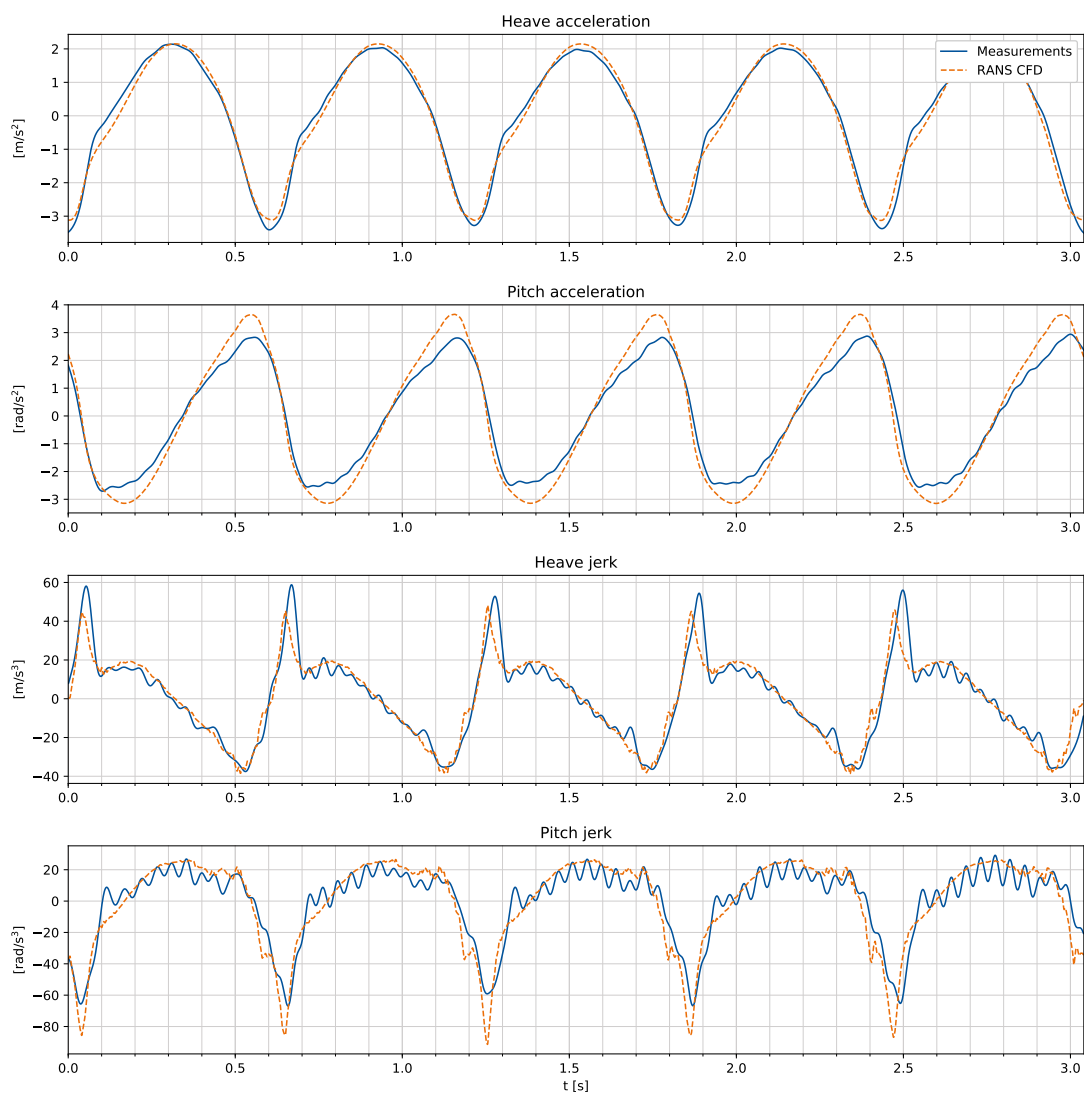


Figure C.29: Time trace 15: RANS CFD calculations and measurements

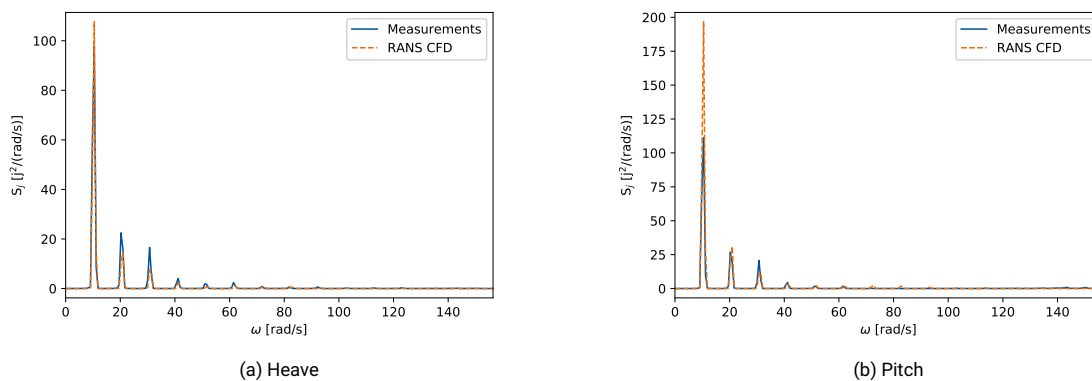


Figure C.30: Energy density spectra jerk of time trace 15

Time trace 16: AXE, $v_s = 2.876$ m/s, $\omega_e = 13.82$ rad/s, $\kappa = 0.033$

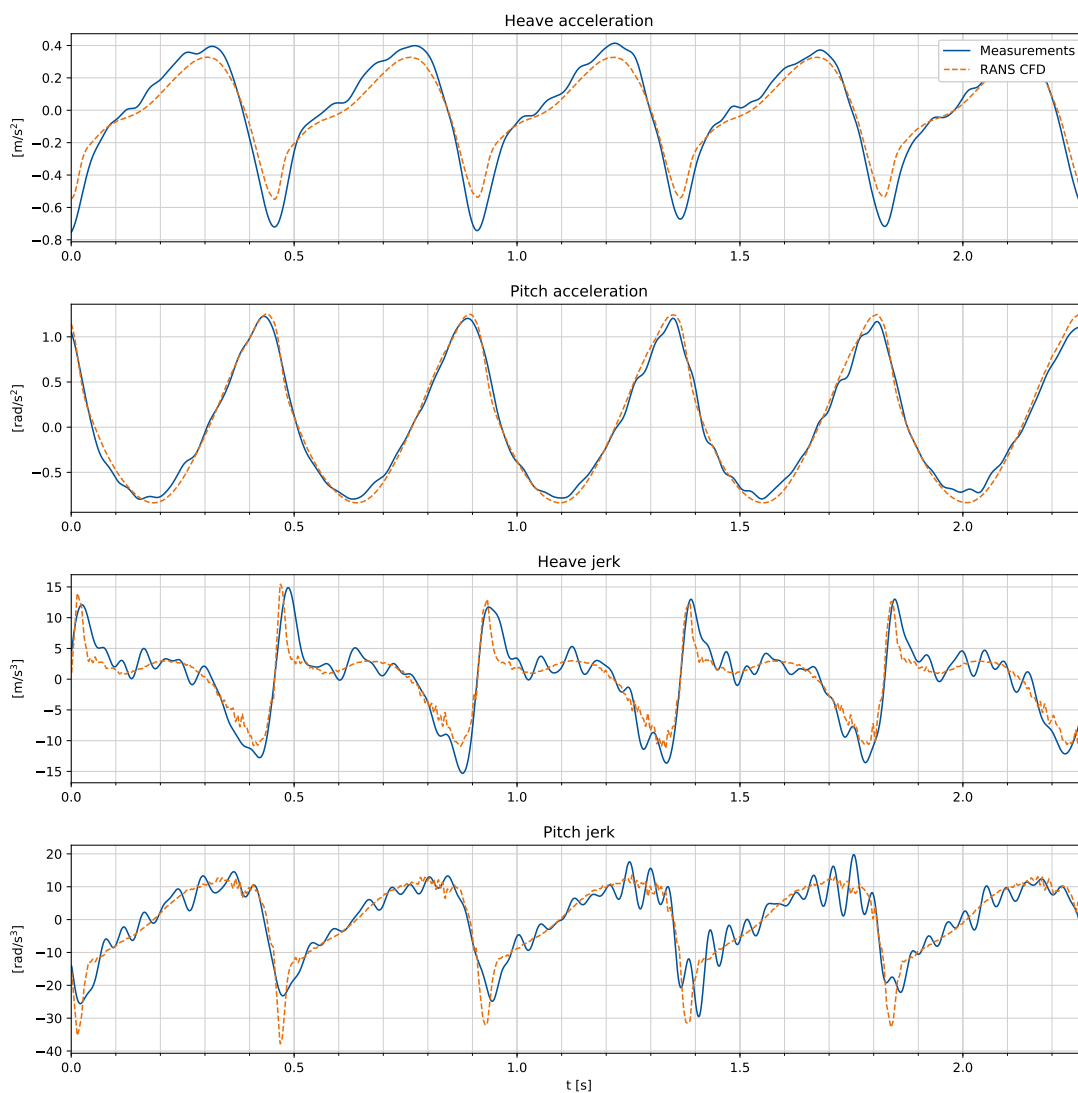


Figure C.31: Time trace 16: RANS CFD calculations and measurements

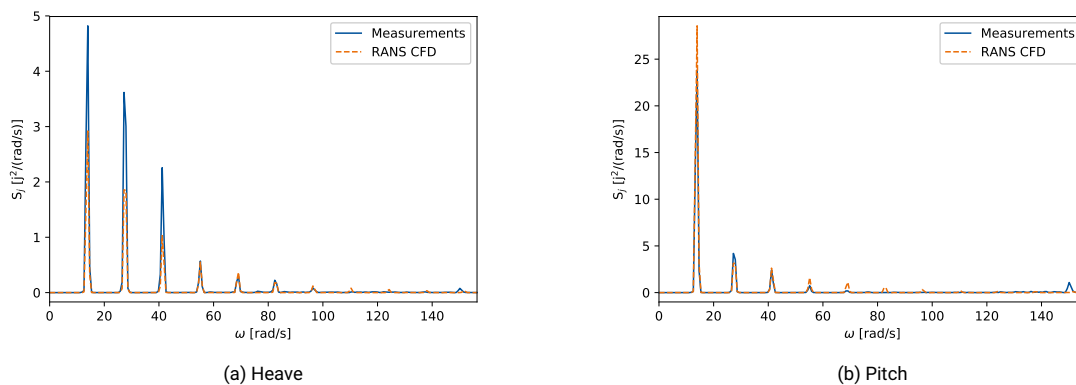


Figure C.32: Energy density spectra jerk of time trace 16